An Exploration of the Relationship between Knee Shape and Kinematics Before and After Total Knee Replacement

Joseph Thomas Lynch

Date of submission – June 2020

A thesis submitted for the degree of

Doctor of Philosophy

of the

Australian National University

i

Statement of Original Work

I, Joseph Lynch, hereby declare that this submission is my own work and that it contains no material previously published or written by another person except where acknowledged in the text. Nor does it contain material that has been accepted for the award of another degree or diploma in any university.

In addition, ethical approval from the ACT Health and ANU Human Ethics Committees were granted for the studies presented in this thesis. Subjects were required to read a subject information document and informed consent was gained prior to data collection.

_____

Signed, Joseph Thomas Lynch

iii

As supervisor of Joseph Lynch's doctoral work, I certify that I consider his thesis

"An Exploration of the Relationship between Knee Shape and Kinematics Before and After Total Knee Replacement" to be suitable for examination.

Signed: _____

Date:_____

Prof Paul N Smith

Medical School

College of Health and Medicine

Australian National University

Acknowledgements

An African proverb says that it takes a village to raise a child. I also believe it takes a village to raise a PhD graduate. There are many people who have helped raise and guide me to the to the point I am at now.

I first need to acknowledge the Australian National University for providing me the opportunity to undertake this thesis. They provided also provided me with a stipend which made this journey possibly.

There are many people who got me to this point of completion when I didn't think I would make it. I would like to thank my primary supervisor, Prof Paul Smith. You gave me the opportunity to work with the team at TORU. Importantly, you trusted us with your patients which allowed us to undertake this ground-breaking research. Thank you for all of your clinical insights you provided throughout this process.

I also need to thank Dr Diana Perriman for her mentorship though this project. She has been a wealth of inspiration and information from the day I decided to undertake this project and continues to be so today. Her constant encouragement provided me reassurance on those days when I didn't think I would ever finish. No matter how busy she was, Diana always made herself available to listen to either a quick 5-minute chat or to provide some more thoughtful insights. Thank you for your unwavering support through every step of this journey.

Thank you, Prof Jennie Scarvell. Your ability to breakdown my seemingly complex web of thoughts into something that was clear and concise always amazes me. I always appreciated

the comments and criticisms you provided me. They made me a better critical thinker and my thesis a better piece of work because of it.

Thank you to both Prof Thor Besier and Dr Marco Schneider from the Auckland Bioengineering Institute at the University of Auckland. Thor, it was an initial conversation with you that introduced many of the concepts used in my thesis. You also provided helpful insights and guidance whenever required. Thank you also for extending an invitation to spend time in your unit during my thesis. While I was only there for a week, the skills I learned were invaluable. Marco, you provided the direction needed to comprehend some of the methods which ended up forming a key aspect of my thesis and I thank you for that. I look forward to collaborating with you both in the future.

Thank you, Prof Mark Pickering for the development of Orthovis, the algorithm and software package that provided the data needed to complete my thesis. We were also lucky enough to have you embedded in TORU for 12 months during a critical time of my thesis which was enormously beneficial for my knowledge.

Thank you to The Trauma and Orthopaedic Research Unit. You have for provided me with a home away from home for the last six years. You give me space to work and distractions when needed. Also working there has broadened my knowledge of orthopaedics in general. Thank you, both Anna and Georgia. You were always there for a chat when I needed a break. A/Prof Rachel Li, thank you for your words of wisdom throughout my PhD journey. I appreciate your honest discussions and look forward to working with you in the future.

To Dr Catherine Galvin, I remember you starting your PhD before me and I was thrilled to watch you complete a magnificent thesis. I think we have worked well together to produce some high-quality research. Thank you for always being up for a coffee/chai in order to

discuss our respective theses. I know that without your friendship this process would not have been as enjoyable.

Thank you, to both Dr John Warmenhoven and Dr Terry Neeman. You both made yourself available for both statistical advice and a friendly catch up whenever needed. Thank you for your patience in explaining the many of the statistical concepts used in this thesis to me numerous times. While I was a bit slow up on the uptake, I think you eventually managed to break through! I look forward to working continuing to work with you in some capacity.

I would like to last thank my family. Firstly, to my wife, Esther: thank you for allowing me the opportunity to take this journey. Your endless support and patience during the hard times has given me the ability to maintain momentum on the days I wanted to stop. Together we have managed to raise three amazing children. You were required to take up much of the parental heavy lifting at times and I am eternally grateful for that. Thank you for always believing in me.

Thank you to my girls, Annabel, Catherine, and Heidi. You are what allowed me to do this project. You focused my mind and gave me the motivation to complete this mammoth task. It has been amazing watching you grow alongside me. In the time I have completed my thesis, you have all learnt to read. write, master bike riding, and perform at dance concerts. I hope we have taught to you to take risks and don't be afraid to try new, and difficult challenges. It is the only way you will learn. I look forward seeing where the world takes you. I love you all

Thank you to Claire and Steve Ede. You are my de facto parents in Australia. You gave Es and I a place to live when we moved back to Canberra and have been so supportive of my journey. You both were willing to help look after the girls, make dinner, repair a flat tire, and do the yard work when we were busy and needed time to focus. This generosity can never be repaid.

To my family back in Canada, thank you for instilling a sense of hard work in me. While I don't get to see as much as I would like, you are all regularly in my thoughts. I am grateful though that we live in an era where we can video chat at any time. This makes the distance apart manageable. Undertaking this thesis has provided me the ability to travel internationally which has allowed me to come home more often than I otherwise would have been able to do.

Finally, thank you to all our participants. You were the lifeblood of this study. Had you not taken time out of your schedules to volunteer to help than this project would not exist. Thank you for agreeing to answer what seemed at times like endless questionnaires, walks up and down the hallway, and climbing up on that box time and time again. I really cherished getting to know you all over the many years this study was ongoing, and I miss seeing you all.

Abstract

The tibiofemoral joint is unique in its design and it is thought that its articular shape is the main driver of biomechanical behaviour. Although the shape of the bony knee is acknowledged to change with osteoarthritis, the specific relationship between shape changes and function is not well understood. Deep flexion, specifically kneeling, is an ideal testing environment for the tibiofemoral joint because it is both a difficult and a desirable activity for people with knee osteoarthritis. Total knee replacement (TKR) is a surgery which attempts to restore the articular shape in order to enhance function. However, the influence of implant design on kneeling kinematics is unclear. This thesis examines the role of knee shape on kneeling kinematics before and following total knee replacement. The four aims of this thesis were to: 1) describe and quantify the main modes of shape variation which distinguish end-stage OA from age- and sex-similar healthy knees; 2) determine whether bony shape can predict deep kneeling kinematics in people with and without OA; 3) examine the published literature to determine whether there are any differences in contact patterns as a function of TKR design; and 4) to prospectively compare the six-degree-of-freedom kneeling kinematics of posterior-stabilised fixed bearing, cruciate-retaining fixed bearing and cruciate retaining rotating platform designs.

Statistical shape modelling identified differences between osteoarthritic and healthy bony knee shape. Specifically: large expansions around the femoral cartilage plate; expansion and depression at the medial tibial border; and an area of corresponding bony expansion on the posterior aspect of the medial femur and tibia. Statistical shape modelling and image registration derived six degree of freedom kinematics were used to test for associations

between knee shape and kneeling kinematics. The kinematic variability was described using bivariate principle component analysis. While we found weak associations between knee shape and kinematics, BMI and group (OA vs Healthy) also predicted kneeling kinematics. This indicates that factors other than bony shape are important in predicting kneeling kinematics. The third study was a systematic review with meta-analyses using quality effects models which characterised the influence of TKR implant design on kneeling contact patterns. The review found posterior stabilised designs were different to cruciate retaining designs, but the heterogeneity was high limiting any firm conclusions. The final study was a prospective randomised clinical trial examining the influence of TKR design on kneeling kinematics. The study found that posterior-stabilised fixed-bearing and cruciate-retaining rotating-platform designs had higher maximal flexion compared to cruciate retaining-fixed bearing designs. Furthermore, the posterior-stabilised fixed-bearing femoral component was more posterior and the cruciate-retaining rotating-platform was in more external femoral rotation throughout flexion. However, there was substantial between-patient variability.

This research breaks new ground around which aspects of bony shape are altered in osteoarthritis and how these shapes, and prosthetic design, influence kneeling kinematics. Furthermore, the methodologies employed in this thesis provide new ways of describing the variability in complex shape and kinematics datasets, which may contribute to the identification of therapeutic efficacy. Knee shape is considered to be an important driver for normal movement. However, the results of this thesis indicate that there are potentially other factors, including soft-tissue properties and patient-specific movement strategies, which might influence the kinematics of deep kneeling. The message for surgeons and other clinicians is that bony shape and TKR design are not the primary drivers of functional performance and that kneeling should be on their radar as an activity to which their patients should aspire.

Table of Contents

List of Figures

List of Tables

Nomenclature

2D	Two Dimensional
3D	Three-Dimensional
Ab/Ad	Abduction-Adduction
AIHW	Australian Institute of Health and Welfare
ANU	Australian National University
AP	Anterior-Posterior
BMI	Body Mass Index
CONSORT	Consolidated Standards of Reporting Trials
BCS	Bi-Cruciate Substituting
bfPCA	Bivariate Functional Principal Component Analysis
CR	Cruciate Retaining
CS	Cruciate Sacrificing
CT	Computed Tomography
DRR	Digitally Reconstructed Radiograph
EF	Extension Facet
FB	Fixed Bearing
FF	Flexion Facet
FFC	Flexion Facet Centre
IE	Internal-External
KL	Kellgren Lawrence Osteoarthritis Severity Scale
ML	Medial-Lateral
MP	Medial Pivot
MRI	Magnetic Resonance Imaging

OA	Osteoarthritis
OARSI	Osteoarthritis Research Society International
OKS	Oxford Knee Score
PCA	Principal Component Analysis
PCL	Posterior Cruciate Ligament
PICKLeS	A prospective imaging study of cruciate retaining, cruciate substituting, and rotating platform TKR, in osteoarthritis and healthy ageing: a randomised control trial #ISRCTN75076749
PROM	Patient Reported Outcome Measure
PS	Posterior Stabilised
ROM	Range of Motion
RP	Rotating Platform
SI	Superior-Inferior
TORU	Trauma and Orthopaedic Research Unit
SSM	Statistical Shape Modelling
VAS pain	Pain Visual Analogue Scale
VAS satisfaction	Satisfaction Visual Analogue Scale
VV	Varus-Valgus

Publications

The work arising from these PhD studies has resulted in the following refereed publications and manuscripts.

Publications:

Lynch JT, Schneider MTY, Perriman DM, Scarvell JM, Pickering MR, Asikuzzaman M, Galvin CR, Besier TF, Smith PN (2019) Statistical shape modelling reveals large and distinct subchondral bony differences in osteoarthritic knees. J Biomech 93:177–184. Included as Chapter four

Lynch, JT., Perriman, DM., Scarvell, JM., Pickering, MR., Warmenhoven, J, Galvin CR, Neeman, T., Besier, TF., Smith, PN. Shape is only a weak predictor of deep knee flexion kinematics in healthy and osteoarthritic knees. Journal of Orthopaedic Research, 2020. 38(10):2250-2261. Included as Chapter five

Lynch, JT., Scarvell, JM., Galvin CR, Smith, PN., Perriman, DM. Influence of total knee replacement design on in-vivo tibiofemoral contact patterns during kneeling: A systematic review and meta-analysis. Knee Surgery, Sports Traumatology, Arthroscopy. 2020. Included as Chapter six

Lynch, JT., Perriman, DM., Scarvell, JM., Pickering, MR., Galvin CR, Neeman, T., Smith, PN. The influence of total knee replacement design on kneeling kinematics: A prospective randomised control trial. Bone and Joint Journal. In Press. Included as Chapter seven

Galvin CR, Perriman DM, **Lynch JT**, Pickering MR, Newman P, Smith PN, Scarvell JM (2019) Age has a minimal effect on knee kinematics: A cross-sectional 3D/2D image-registration study of kneeling. Knee. In Press

Galvin CR, Perriman DM, Newman PM, **Lynch JT**, Smith PN, Scarvell JM (2018) Squatting, lunging and kneeling provided similar kinematic profiles in healthy knees—A systematic review and meta-analysis of the literature on deep knee flexion kinematics. Knee 25:514–530

Scarvell JM, Galvin CR, Perriman DM, **Lynch JT,** van Deursen RWM (2018) Kinematics of knees with osteoarthritis show reduced lateral femoral roll-back and maintain an adducted position. A systematic review of research using medical imaging. J Biomech 75:108–122

Presentations:

Lynch JT, Schneider MTY, Perriman DM, Scarvell JM, Pickering MR, Asikuzzaman M, Galvin CR, Besier TF, Smith PN (2019) Statistical shape modelling reveals large and distinct subchondral bony differences in osteoarthritic knees

- Canberra Area Health Meeting, Canberra 2018
- Australian New Zealand Orthopaedic Research Society, Perth 2018
- World Congress of Biomechanics, Dublin, 2018
- Australian Orthopaedic Association Annual Scientific Meeting, ACT Branch, Canberra, 2018

Lynch, JT., Perriman, DM., Scarvell, JM., Pickering, MR., Warmenhoven, J, Galvin CR, Neeman, T., Besier, TF., Smith, PN. Shape is only a weak predictor of deep knee flexion kinematics in healthy and osteoarthritic knees

- Canberra Area Health Meeting, Canberra 2019

- Australian New Zealand Orthopaedic Research Society, Canberra 2019

- International Combined Orthopaedic Research Societies, Montreal, 2019 POSTER

- International Society of Biomechanics, Calgary, 2019

- Royal Australian College of Surgeons, ACT Scientific Meeting, Canberra 2019

Lynch, JT., Perriman, DM., Scarvell, JM., Pickering, MR., Galvin CR, Smith, PN. The influence of total knee replacement design on kneeling kinematics: A prospective randomised control trial

- Australian Orthopaedic Association Annual Scientific Meeting, ACT Branch, Canberra, 2019

- ANU Medical School HDR Symposium, Canberra, 2019

Awards

- Best Clinical Paper, Canberra Area Health Meeting, Canberra, 2019

- Best Oral Paper, AOA ACT Annual Scientific Meeting 2019

- Vice Chancellors Travel Grant

- International Society of Biomechanics Travel Grant

- Reg Kitchen Scholarship

- Australian Government Research Training Program (AGRTP) Stipend Scholarship, 2017

1 Introduction

The question that this thesis aims to address is "does shape drive function in the healthy, OA and prosthetic knee?" The concept that shape and function are inextricably linked is encapsulated in the maxim attributed to the American architect Louis Sullivan: "Form follows function". In fact, the prose from which this maxim originates is more eloquent and worthy of repetition:

> "Whether it be the sweeping eagle in his flight, or the open apple-blossom, the toiling work-horse, the blithe swan, the branching oak, the winding stream at its base, the drifting clouds, over all the coursing sun, form ever follows function, and this is the law. Where function does not change, form does not change" (Sullivan, 1896)

The concept of form following function in the human body has been variously explored. In the late nineteenth century Wolff developed the concept that bone will adapt to the loads placed upon it (Wolff, 1986). More recently, Pauwels extended this concept by proposing an analytical model to measure these adaptations (Pauwels, 1980). In the musculoskeletal system, both the hip and shoulder's ball and socket design affords us the opportunity for complex movements; and the thumb's morphology provides the hand with the dexterity and strength needed to perform a range of tasks (Ladd et al., 2014). The tibiofemoral joint is unique in its design. While it is inherently unstable due to its small contact area and reduced surface congruence, it is thought that the knee's articular shape is the main driver of biomechanical behaviour (Freeman & Pinskerova, 2005). Although the bony shape of the knee is acknowledged to undergo osteoarthritic changes such as osteophyte development, and joint space narrowing, the relationship between shape changes and function is not well understood. For instance, does a flattening of the medial tibial plateau reduce knee flexion, or impact an accessory movement required for flexion such as axial rotation? Do variations in total knee replacement design provide any kinematic benefit? These are the questions addressed in this thesis.

Deep flexion is an ideal testing environment for the tibiofemoral joint because it is both a difficult and a desirable activity for people with knee dysfunction. The ability to squat and kneel is important for tasks that enhance daily life. High-flexion tasks are those which require more than 120° of flexion (Galvin, 2019; Hemmerich et al., 2006). Specifically, weightbearing deep kneeling is a task which can require up to 165° to achieve (Hefzy et al., 1998). Kneeling is one of the most difficult activities to perform yet also reported as very important. In patients with a TKR, it is the third most important activity, with only sexual activities and stretching rated as more important (Weiss et al., 2002). This is remarkable considering kneeling tasks are only performed in 0.5% of daily life (Huddleston et al., 2009). Kneeling is essential in many Asian and Middle Eastern societies. Muslim and Buddhist religions both require prayer positions which involve deep kneeling (Chokkhanchitchai et al., 2010). Furthermore, many Asian cultures still perform floor kneeling while eating, and during daily living (Kanekasu et al., 2004). In all societies, gardening, cleaning and playing with grandchildren all demand high knee flexion (Rowe et al., 2000).

Knee function is often compromised in knee osteoarthritis. Knee osteoarthritis (OA) is a disease which limits a person's ability to perform high flexion tasks because of reduced pain-free range of motion (Ladd et al., 2014). In Australia in 2018, 2.2 million people were living with osteoarthritis (Australian Institute of Health and Welfare, 2019). These people reported kneeling to be either "very difficult" or "cannot do", which negatively affects their social participation (Theis et al., 2013). Recent World Health Organization reports have addressed the importance of independent living, stating that the goal of rehabilitation is to ensure full participation in all aspects of life (World Health Organization, 2015, 2018). Therefore, deep kneeling is both a compelling activity to study and a useful experimental environment for shape-function studies.

Knee osteoarthritis results in profound structural changes to the bone and to soft tissue structures within and around the joint. Bony shape changes are typically visualized using 2D plain x-ray (Kellgren & Lawrence, 1957) or computed tomography (CT) (Chan et al., 1991).These bony shape changes are used to identify and measure the severity of the disease (van Manen et al., 2012) in association with the history, signs and symptoms (Abhishek & Doherty, 2013). While we know that the shape of OA and healthy knees are different (Barr et al., 2016; Haverkamp et al., 2011; Neogi, 2012; Neogi et al., 2013; Shepstone et al., 2001), we don't yet know which regional anatomic features are the most important when differentiating end-stage OA from healthy or how they impact knee function during activities such as deep kneeling.

The soft tissues of the knee are also affected in knee OA (Loeser et al., 2012). The menisci are typically torn in up to 91% of patients with OA, resulting in increased extrusion and altered joint kinematics (Bhattacharyya et al., 2003; Scholes et al., 2015). Furthermore, intracapsular ligaments are more lax in OA and display degenerative changes, particularly the posterolateral bundle of the ACL (Loeser et al., 2012). Lastly, there is scarring and thickening of the joint capsule (Loeser et al., 2012). Although these soft tissue changes are important, they are not the focus of this thesis.

The knee has complex morphology and the shape of the knee is important to its function. This has led researchers to investigate how shape characteristics influence tibiofemoral kinematics (Clouthier et al., 2019; Iwaki et al., 2000; Martelli & Pinskerova, 2002; Pinskerova et al., 2009; Smoger, 2016). Knee geometry in the sagittal plane has been described as comprising three femoral facets of different function and radii (patella, extension and flexion facets), that interact with a flat medial and convex lateral tibial plateau (Iwaki et al., 2000). Patient-specific variations in these radii have been shown to influence tibiofemoral anterior–posterior translation, internal-external rotation, and the location of the most caudal point on the femur

in early to mid-flexion (Lansdown et al., 2017; Smoger et al., 2015). Other morphological bony features have also been reported to influence function. An increased posterior condylar offset ratio has been associated with greater anterior-posterior translations; and a larger condylar twist-angle has been shown to result in a more externally rotated tibia at heel strike (Hoshino et al., 2012). Recently, combined statistical shape and musculoskeletal modelling revealed that a larger flatter medial tibial plateau was associated with increased external rotation and anterior translation of the femur on the tibia during gait (Clouthier et al., 2019). However, these findings examined shape-function relationships in normal knee cohorts. Far less is understood about the shape-function relationship in pathological groups, particularly those with osteoarthritis. Furthermore, the influence of bony shape on deeper flexion activities has not yet been examined.

Total knee replacement (TKR) aims to restore articular shape and alignment by replacing the osteoarthritic joint surfaces and soft tissues with an artificial prosthesis. The primary aim is to reduce pain and restore good range of movement (Dunbar & Haddad, 2014). While the procedure delivers pain relief and better function to the majority of patients, in up to 20% of cases the outcomes are disappointing (Bourne et al., 2010). Dissatisfied patients report either no change, or increased pain and reduced function (Dunbar, 2001). Reasons for dissatisfaction following knee arthroplasty have been reviewed extensively. Predictors of dissatisfaction include chronic and centrally mediated pain, psychological status that influences coping ability, malalignment and other errors in surgery and, relevant to this thesis, residual loss of function (Dunbar et al., 2013; Harris et al., 2013; Howells et al., 2016; Maratt et al., 2015; Noble et al., 2006; Schnurr et al., 2013). Additionally, dissatisfaction due to loss of function might, in part, be related to altered kinematics and a feeling of instability (Naili et al., 2017). Importantly, joint biomechanics have been associated with joint function and implant longevity (Banks & Hodge, 2004).

The features of a successful outcome after TKR are having a pain free knee with good range of movement (Dunbar & Haddad, 2014). Significant development of modern TKR prostheses design has focused on restoring kinematics in order to achieve high flexion. As such, implant choice is dictated not only by implant survival and surgeon preference, but also kinematic performance (Vertullo et al., 2017). According to the Australian Orthopaedic Association National Joint Replacement Registry, the two most commonly used designs are posterior stabilised (PS) and posterior cruciate retaining (CR) with both having fixed and rotating bearing tibial insert variants (Australian Orthopaedic Association National Joint Replacement Registry (AOANJRR), 2019). A cam and post were designed to facilitate rollback of the femoral condyles on the tibial bearing by replacing the PCL in the PS design. The CR design retains the posterior cruciate ligament (PCL) and relies on the ligament's function to closely mimic native knee femoral rollback in deep flexion (Insall et al., 1982; Victor et al., 2005, 2010). The rotating tibial platform was designed to increase the freedom of the joint by decoupling rotation from flexion while reducing contact stresses on the polyethylene bearing through higher articular conformity and greater tibiofemoral contact area (McEwen et al., 2005; Walker & Sathasivam, 2000). While there are minimal differences between implants in terms of pain, clinical and functional outcomes (Bercik et al., 2013; Jiang et al., 2016; N. Li et al., 2014; Verra et al., 2013), historically, the CR design, overall, has a slightly lower revision rate at 18 years when compared to PS designs (9.5% vs 8.2%) (Australian Orthopaedic Association National Joint Replacement Registry (AOANJRR), 2019). However, in terms of function, the PS design has been reported to confer greater maximal flexion (Verra et al., 2013) which might be beneficial for patients wanting to be able to kneel. Therefore, understanding the kinematic profiles of different TKR designs in vivo might help explain why some patients report dissatisfaction following surgery and whether the shape of the prostheses does indeed dictate function.

1.1. Aims

This thesis aims to:

1. Describe and quantify the main modes of shape variation which distinguish end-stage OA from age- and sex-similar healthy knees.

2. Determine whether bony shape can predict deep-kneeling kinematics in people with and without OA.

3. Systematically review the published literature to determine whether there are any differences in the contact patterns of kneeling as a function of TKR design.

4. Prospectively compare the six-degree-of-freedom kinematics of posterior-stabilised fixed bearing (PS-FB), cruciate-retaining fixed bearing (CR-FB) and cruciate retaining rotating platform (CR-RP) designs during kneeling.

The overall objective of this work is to contribute to the knowledge of how knee shape influences deep kneeling kinematics and the implications for ongoing operative and non-operative treatments.

The results of this thesis are intended to inform clinicians about potential strategies for optimising kneeling before and after total knee replacement.

1.2. Thesis Overview
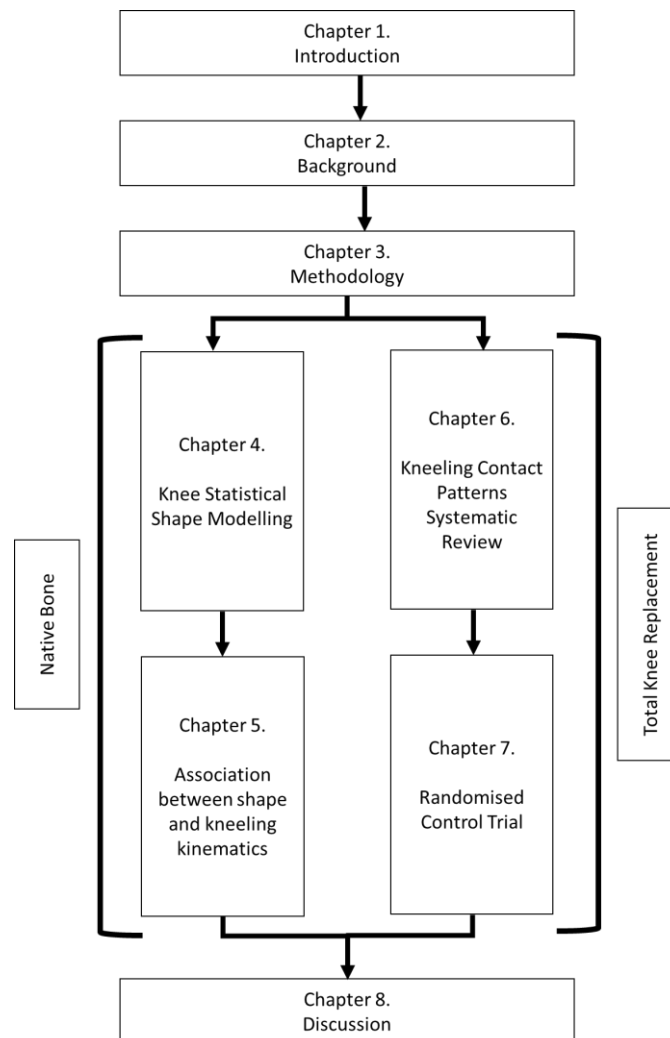
Figure 1-1: Workflow of thesis

This thesis is divided up into seven chapters (Figure 1-1). Chapter two provides an overview of the literature which relates to this thesis. Chapter three will discuss the pertinent methods used to address the aims within this thesis. It describes the participants included and the recruitment timelines. Additionally, it will describe the data collection techniques which are used. Furthermore, this chapter describes the method of how knee shape was quantified using statistical shape modelling. This chapter also gives a detailed description of the technology used to analyse kneeling kinematics. Finally, it describes the important statistical methods used to analyse the data.

Chapter four is a cross-sectional observational study which describes the differences between healthy and end-stage osteoarthritic knee shape. The ability to understand specific shape differences between these two groups will provide clinicians with the ability to understand expected regional shape differences in patients prior to a total knee replacement. Furthermore, understanding the shape features of an osteoarthritic knee will allow us to identify possible regions that explain the altered kinematics of deep kneeling. This study is published in the Journal of Biomechanics (Q1, H-index: 190; Impact Factor: 2.58) (Lynch et al., 2019).

Chapter five is a cross-sectional observational study which aims to use shape features described in chapter three to predict kneeling kinematics. This study will provide insights into the role that knee shape plays in kneeling kinematics which has not yet been addressed. This study is published in the Journal of Orthopaedic Research (Q1, H-index: 148; Impact Factor: 3.14) (Lynch et al., 2020).

Chapter six is a systematic review and meta-analysis that aims to characterise the role that TKR implant design has on kneeling contact patterns. This study reports the data describing the influence of prosthetic TKR design on kneeling kinematics in terms of contact patterns. This study is published in Knee Surgery, Sports Traumatology, Arthroscopy (Q1, H-index: 115; Impact Factor: 3.05) (Lynch et al., 2020).

Chapter seven is a prospective randomised clinical trial examining the differences in kneeling kinematics between three knee replacement designs. This is the first RCT to examine the influence of design on kinematics and will provide insights into the different kinematic patterns that exist between designs. This study has been accepted for publication in The Bone and Joint Journal (Q1, H-index: 171; impact factor: 4.30).

Chapter eight explores the results of the studies included in this thesis and how the findings contribute to the literature. This chapter discusses the implications of the findings and the limitations of the thesis as well as some suggestions for future research.

2 Literature Review

2.1 Knee Anatomy

The knee is one of the largest and most complex joints in the human body. It is comprised of four bones, and it allows movements in six-degrees-of-freedom. The bones which make up the knee are the distal femur, proximal tibia, proximal fibula and patella. Together, these bones create three joints which all form the knee: tibiofemoral, patellofemoral, and tibiofibular joints. This thesis will focus solely on the tibiofemoral joint.

2.1.1 Femur

The distal femur is comprised of asymmetric medial and lateral condyles which are separated posteriorly by an intercondylar notch and anteriorly by the trochlear groove. These condyles form the main articular surface of the femur on the tibia. Sagittaly, both the medial and lateral condyles shaped as cams. The lateral condyle is the more prominent and is broader both in its antero-posterior and transverse diameters (Gray & Carter, 1919). The anterior trochlear groove allows patellar articulation. On both the medial and lateral side of the distal femur, two epicondyles are present which allow ligament attachment and visualisation of the joint line (Gray & Carter, 1919) (Figure 2-1). Superior to the medial epicondyle is the abductor tubercle, which is thought to be another important landmark for referencing the joint line, especially in TKR (Iacono et al., 2014).
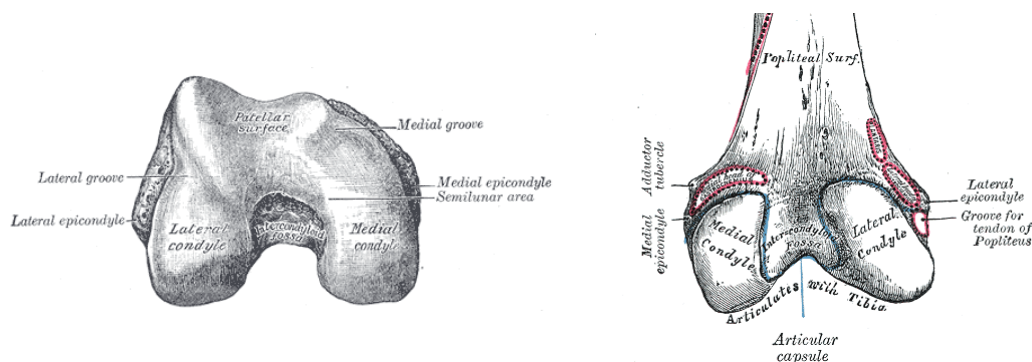
Figure 2-1: Distal femur anatomy (Gray & Carter, 1919)

2.1.2 Tibia

The proximal tibia consists of two asymmetric facets or plateaus. The larger medial facet is oval in shape and is slightly concave from side to side (Figure 2-2). The anterior surface which slopes upwards by an average of 11° and is on average 17 mm in length (Iwaki et al., 2000). The lateral facet is nearly circular, is concave from side to side, but slightly convex near its posterior part. The facets articulate with the femoral condyles. These facets are separated by prominent medial and lateral intercondylar eminences. These separate the intercondylar area into anterior and posterior facets. The anterior facet provides attachment sites for the ACL and anterior meniscal ligaments while the posterior facet provides posterior meniscal attachments and a space for the PCL to pass through and attach further distally on the tibia.
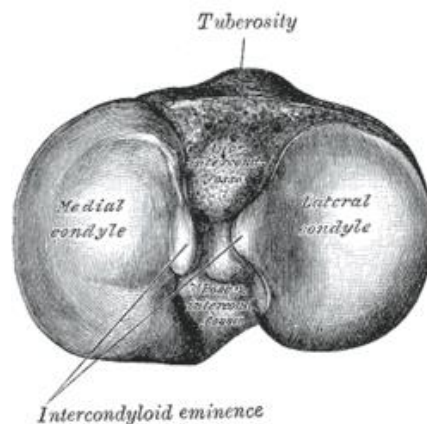
Figure 2-2: Proximal tibia anatomy (Gray & Carter, 1919)

2.2 Morphological Changes in the Knee Secondary to Osteoarthritis

Knee osteoarthritis (OA) is a disease which limits a person's ability to perform many tasks because of reduced pain-free range of motion (Ladd et al., 2014). In Australia in 2018, 2.2 million people were living with osteoarthritis (Australian Institute of Health and Welfare, 2019). The cost of OA was estimated to be more than $2.1 billion in 2015, and by 2030, this

is expect to exceed $2.9 billion (The Royal Australian College of General Practitioners, 2018).

The current understanding of the development of osteoarthritis includes a complex relationship between mechanical, biochemical, cellular and genetic factors. (Chen et al., 2017; Creamer & Hochberg, 1997) OA occurs when the equilibrium between is tissue breakdown and repair disturbed, which can happen if mechanical loads on a joint exceed tolerance levels (Hunter, 2011). OA results in the breakdown of soft tissue within the joint and leads to an abnormal loading response within the subchondral bone (Donell, 2019; Isaacson & Brotto, 2014). Typically, OA presents itself in the medial compartment resulting in osteophyte development, chondral wear, instability, and varus knee alignment. The shape changes are likely a reaction to the altered subchondral loading environment. A number of authors have presented the theory that there is a cyclical relationship where either abnormal stresses or physiological response leads to bone remodelling (shape changes) within the knee resulting in increased joint contract forces and point loading; thereby leading to further abnormal remodelling (Figure 2-3) (Donell, 2019; Guilak, 2011; Mellon & Tanner, 2012).
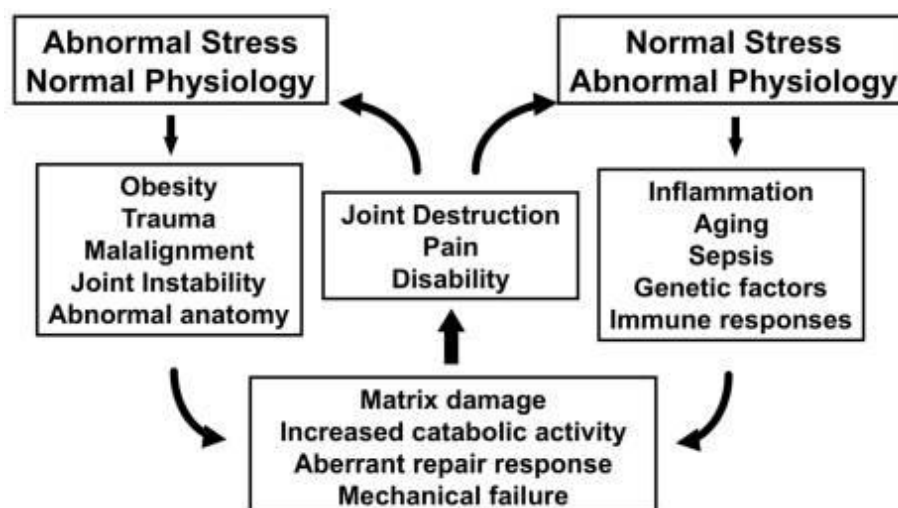
Figure 2-3: Hypothesis for the development and progression of Osteoarthritis. Adapted from Guliak 2011. (Guilak, 2011)

The effects on the shape of the bones, which is the focus of this thesis, include condylar squaring, reduced joint space due to cartilage and meniscal wear, as well as sclerosis and presence of osteophytes (Fairbank, 1948; Kellgren & Lawrence, 1957)**.** The net result of these changes are knee mal-alignment, reduced motion, increased pain and altered knee kinematics (Arthritis Australia, 2014; Australian Commission on Safety and Quality in Health Care, 2017; Scarvell et al., 2018). It has long been believed that altered loading through the knee contributes to the onset and progression of OA; however, how the shape of the knee is associated with the presence or progression of the disease is less appreciated. Fairbank was the first to report morphological changes in a knee with OA in a group of participants who underwent a meniscectomy (Fairbank, 1948). He reported seeing radiographic evidence of condylar flattening, joint space narrowing, and osteophytic ridge formation. Following this initial understanding of osteoarthritic changes, there has been considerable work undertaken to examine what specific features change in OA and if there is the ability to predict who might go on to get OA based on their bony knee morphology (Altman et al., 1986; Dieppe et al., 1993; Felson et al., 2000; Tanamas et al., 2010).

2.2.1   Knee Osteoarthritis Classification Systems

Knee osteoarthritis is a degenerative disease, and as such, bony shape and soft tissue changes occur along a continuum. Therefore, in order to understand where a knee lies on this continuum various classification systems have been developed. There are a number of grading systems which use various imaging modalities such as X-Ray, CT, or MRI with the most common being plain radiograph. Figure 2-4 describes the most common X-ray based scoring system's grading scales (Wright & The MARS Group, 2014).

TABLE II Grading Scales for the Radiographic Osteoarthritis Classification Systems*					
Scale	Grade and Characteristics				
Kellgren-Lawrence	0: No JSN or reactive changes	1: Doubtful JSN, possible osteophytic lipping	2: Definite osteophytes, possible JSN	3: Moderate osteophytes, definite JSN, some sclerosis, possible bone-end deformity	4: Large osteophytes, marked JSN, severe sclerosis, definite bone ends deformity
IKDC	A: No JSN	B: >4 mm joint space; small osteophytes, slight sclerosis, or femoral condyle flattening	C: 2-4 mm joint space	D: <2 mm joint space	
Fairbank	0: Normal	1: Squaring of tibial margin	2: Flattening of femoral condyle, squaring and sclerosis of tibial margin	3: JSN, hypertrophic changes, or both	4: All of the characteristics at left, to a more severe degree
Brandt et al.	0: <25% JSN without secondary features (subchondral sclerosis, geodes, and osteophytes)	1: <25% JSN with secondary features or 25%-50% JSN without secondary features	2: 25%-50% JSN with secondary features or 50%-75% JSN without secondary features	3: 50%-75% JSN with secondary features or >75% JSN without secondary features	4: >75% JSN with secondary features
Ahlbäck	0: Normal	1: JSN† (with or without subchondral sclerosis)	2: Obliteration of joint space	3: Bone defect/loss <5 mm	4: Bone defect and/or loss 5-10 mm
Jäger-Wirth	0: No arthrosis	1: Initial arthrosis, small osteophytes, minimal JSN	2: Moderate arthrosis, about 50% JSN	3: Medium-grade arthrosis	4: Heavy arthrosis

*JSN = joint space narrowing, and IKDC = International Knee Documentation Committee. †Joint space narrowing is <3 mm of the joint space or <50% of the other compartment.

Figure 2-4: Grading scales for different radiographic osteoarthritis classification systems (Wright & The MARS Group, 2014).

The most widely used method is Kellgren and Lawrence system (Kellgren & Lawrence, 1957). This scale, initially proposed in 1957, uses weight bearing anterior-posterior and lateral x-rays to visualise changes in various morphological parameters within the tibiofemoral joint (Figure 2-5). Despite the advent of newer MRI based systems this is still the most commonly used system clinically due to the ease of obtaining radiographs and simple scoring system. However, a recent study from the MARS group found the ICC of the KL scale to be poor at 0.38 (Wright & The MARS Group, 2014). Additional criticisms of this criteria have been that correct application of KL grading is difficult due to the vague and subjective wording of each grade. Furthermore, it is insensitive to change, does not allow for medial or lateral OA (Kohn et al., 2016). In current practice changes are only interpreted in two dimensions at any one time, either by x-ray (Kellgren & Lawrence, 1957), CT (Chan et

al., 1991), or MRI (Hunter et al., 2011) thereby underutilizing their potential for OA

progression and surgical planning. The challenge is to increase the precision of the

classification system for knee OA whilst maintaining, or improving, the clinical utility.

Statistical shape modelling has the ability to detect subtle changes within the bony anatomy

and could therefore be a beneficial addition to classification systems.
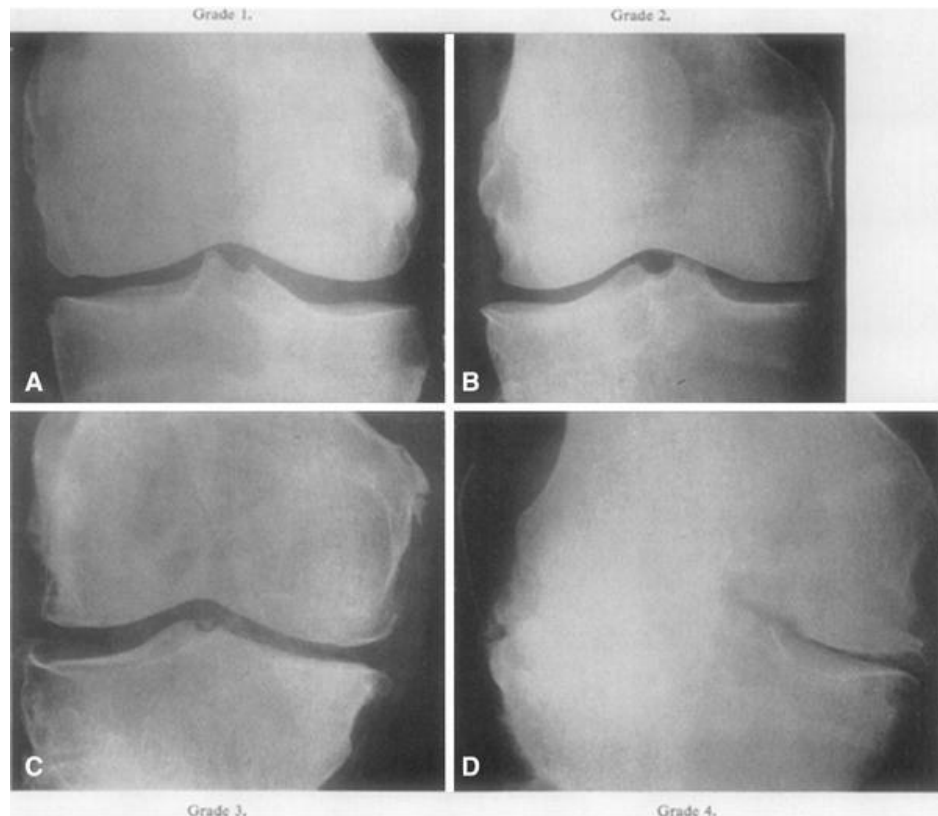
Figure 2-5: Kellgren and Lawrence osteoarthritis classification system
AP radiographs of the knee. A) Representative knee radiograph of KL classification Grade
1; (B) Representative knee radiograph of KL classification Grade 2; C) Representative knee
radiograph of KL classification Grade 3; (D) Representative knee radiograph of KL
classification Grade 4 (Kellgren & Lawrence, 1957)

2.2.2   Distal Femur

Shape changes specific to the osteoarthritic femur have been reported. Modelling 2D coronal

images of the intercondylar notch in a group of excavated skeletons (900AD to 1850)

revealed osteoarthritic notches were generally more symmetrical and the medial edges were

straighter and less concave when compared to non-arthritic (Shepstone et al., 2001). Matsuda compared the condylar geometry in a Japanese group of 30 valgus and 30 varus OA knees as well as 30 healthy participants using radiographs and MRI (Matsuda et al., 2004). They found that the lateral condyle in OA knees with valgus alignment were smaller, but this finding didn't occur to the medial condyles in varus knees. Sex differences have also been reported in a sample of Chinese participants with OA (Yang et al., 2014). Lateral condylar height was significantly greater in males than females while women had smaller mediolateral (ML) /anteroposterior (AP) ratios. Female sex is also an independent risk factor for disabling knee OA (Manninen et al., 1996) but it is unclear whether these relationships are also present in a healthy population as it was not reported in this study.

2.2.3 Proximal Tibia

Specific changes in the tibia have also been studied. The presence of a caudally oriented medial tibial spine was more likely to be associated with early knee cartilage degeneration when compared with osteophytes in other directions (Nakamura et al., 2006). Additionally, Matsuda and colleagues examined anatomic features associated with varus malalignment and found that increased slope of the posterior tibia is a risk factor for knee OA (Matsuda et al., 1999). Differences in posterior tibial slope have been associated with medial and lateral compartment OA (Nunley et al., 2014). OA knees were reported to have a flatter slope (mean 6.8°) whereas patients with lateral uni-compartmental OA had a relatively greater posterior tibial slope (mean 8°). The authors suggest that the posterior tibial slope may be a reaction to disease, with medial disease demonstrating more anterior wear leading to flattening of the slope while lateral disease leads to posterior wear and an increase in the slope. This finding is supported by Weidow *et al.* who reported the same pattern in cartilage wear (Weidow et al., 2002).

One limitation of the relationships in the studies described above is that only individual shape factors were used. These required *a priori* identification, are usually identified on 2D image of single slice projections, are not currently considered in combination, and therefore might not characterize overall knee shape.

2.2.4   Statistical Shape Modelling of the Whole Knee

Changes to the shape of the entire tibiofemoral joint due to osteoarthritis can be assessed using statistical shape modelling (SSM). SSM is a technique that quantifies the variability between a set of similar shapes. SSM uses principal component analysis (PCA), to identify areas of coincident shape variation called modes of variation. This enables the entire geometry within a dataset to be characterized using a small number of principle components.

Osteoarthritic tibiofemoral shape has been examined using a number of different shape modelling techniques including modes of variation and shape vectors. The application of each of these analyses to different populations and datasets has contributed to our current understanding of how knee shape relates to clinical and functional outcomes. Haverkamp *et al.* used statistical shape modelling on 2D AP X-rays and detected differences in the modes of variation between groups of OA and normal knees from a Dutch cohort (Haverkamp et al., 2011). The authors found that an increased knee width, deceased joint space, increased knee extension, and a more elevated lateral tibial plateau were all associated with the presence of OA. However, this study was limited by the use of 2D image data for the shape models as well as the potential for out-of-plane and positioning errors. More recently, Barr *et al.* used normalised shape vectors as a way of examining shape to quantify differences between OA and normal knees (Barr et al., 2016). This technique collapses multiple principle components into one and thereby describes knee shape in terms of difference from the mean shape (Figure 2-6). The authors found that participants undergoing TKR had a knee shape which was further from the mean than non-OA knees with the femur shape being the most different. Therefore,

shape was found to be an important defining feature of OA using this global shape analysis technique. However, other techniques can be used to examine region-specific changes. Using a similar technique, Bowes and colleagues described four year longitudinal changes in bone area in a group of participants who developed OA and those who did not (Bowes et al., 2015). They reported all OA knee compartments showed increased bone area over time compared with non-OA participants. However, they only described compartmental differences, limiting our knowledge of which anatomic features are the most important when differentiating OA from healthy and how much those features change.
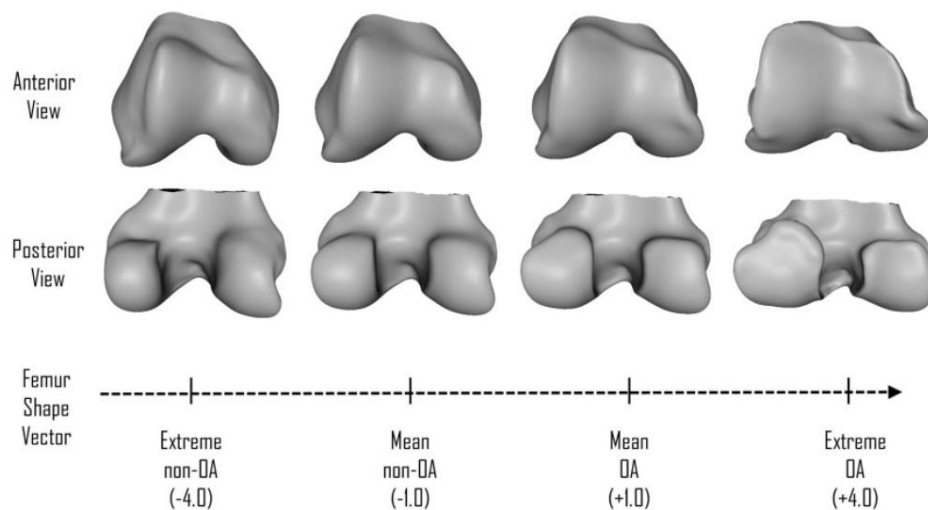
Figure 2-6: Anterior and posterior views shape model reconstruction. The femoral shape vector is scaled to -1 as the mean shape without radiographic OA and +1 with established radiographic OA (Barr et al., 2016).

The examination of modes of variation in knee shape has been used to predict the development of OA. Bredbender *et al*., used statistical shape modelling to determine the modes of variation between knee shapes of 12 females who progressed to OA and 12 females who didn't (Bredbenner et al., 2010). They found that knee shape of patients who progressed to OA differed from those who did not. Specifically, the OA knees were larger in the AP and ML direction while being less high than control tibias except for medial intercondylar

eminence and posterior lateral corner. Additionally, the posterior condylar and the lateral epicondylar regions of the femur were larger in the OA group. This study was crucial because it demonstrated that shape is an important factor in the development of OA. However, the all-female population and small sample make any large population conclusions difficult.

Shape vectors have also been applied to OA knee data to determine if shape is predictive of OA development. Neogi *et al.* (2013), also compared shape data from 178 people who progressed to OA within 12 months with data from 353 participants who did not (Neogi et al., 2013). However, similar to Barr *et al.* they used shape vectors to describe the global shape changes. They found that the knees which progressed to OA had a shape vector which was further from the mean than the knees which did not progress. Therefore, this data supported that of Barr et al. but had the added advantage of predicting OA rather than just describing it. Specifically, after adjusting for baseline Kellgren Lawrence (KL) score, the odds ratio of developing OA within 12 months was 2.9 to 6.4 times higher if a patient had a shape vector which was further from the mean. Both modes of variation and shape vectors have the ability to distinguish between healthy and osteoarthritic knees and predict those knees which will go on to get OA.

2.3   Functional Anatomy

2.3.1   Traditional Measurements

Owing to the complex morphology of the knee, researchers have been interested in understanding its role in kinematics for the last two centuries. Weber and Weber were the first to describe that the condyles rotated on the tibia ''like the wheels of a cart on the road'' and that the flexion axis lay through the centres of the circles (Weber & Weber, 1836). Since then, the understanding of kinematics has largely been characterised by using cadaveric dissections

or medical imaging (CT, MRI, X-Ray). These modalities generally allow for analysis using single slice images in different planes. Studies have tended to focus on sagittal plane motion (flexion-extension) as this is the degree of freedom with the greatest movement and therefore the biggest driver of human propulsion.

Movements of the femoral condyles on the tibial plateau are characterised as having varying lengths and radii (Iwaki et al., 2000; Martelli & Pinskerova, 2002; Pinskerova et al., 2009). The posterior condyles sagittal radii, measured from six cadavers, were on average 22 mm and 21 mm (medial and lateral respectively). Additionally, the articulating portions of the condyles can be divided into three facets. The extension facet (EF) which is when the knee is in 0-20° of flexion, the flexion facet (FF) which occurs between 20-120° of flexion, and the posterior horn facet (PHF) for movements above 120° (Figure 2-7) (Martelli & Pinskerova, 2002; Pinskerova et al., 2009). Interestingly, the PHF does not come into contact with the tibia, as movement occurs only on the posterior horns of the menisci (Pinskerova et al., 2009). The medial condyle was initially subdivided into two separate arcs: an anterior arc associated with extension and a posterior arc associated with flexion. The lateral condyle was described primarily in terms of a flexion facet upon which joint rotation and translation occurred (Figure 2-7). During flexion up to 120°, the medial condyle stays relatively stable on the tibial plateau with the lateral condyle rolling and sliding posteriorly (Hill et al., 2000). In deeper flexion, the medial condyle begins to move posteriorly, up to 8 mm, while the lateral condyles move an additional 5 mm (Pinskerova et al., 2009). This equal movement of the medial and lateral condyles suggest that there is little to no axial rotation during deep flexion (Pinskerova et al., 2009).
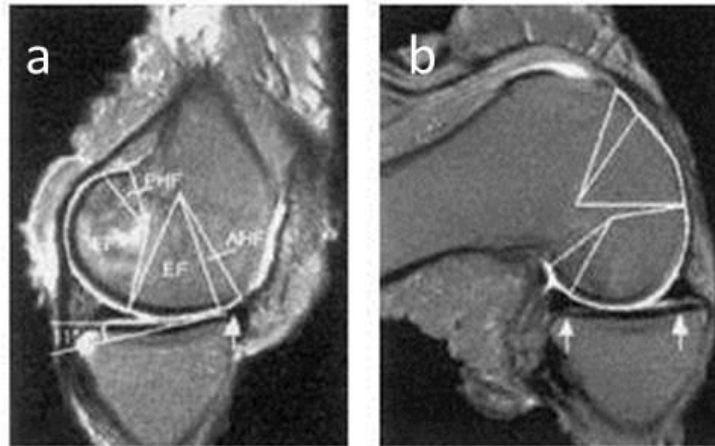
Figure 2-7: Description of flexion facets of medial condyle in a) 0 and b) 120°
of flexion (Martelli & Pinskerova, 2002)

In the coronal view, the joint is curved, and the tibiofemoral surfaces are more congruent

between the inside aspect of the medial condyle and the tibial eminence (Martelli &

Pinskerova, 2002). The flattened inferior aspect of the lateral condyle is less congruent which

is suggestive of increased mobility (Martelli & Pinskerova, 2002). Additionally, the articular

surface of the lateral condyle is slightly longer than its medial counterpart which could

contribute to the varus orientation of the femur (Smith et al., 2003). When the knee flexes into

deep flexion, the lateral condyle moves 2 mm more caudally compared to its position during

mid-flexion (Pinskerova et al., 2009).

The concave shape of the medial tibial plateau and the convex shape of the lateral tibial

plateau allow for complex and asymmetrical movements of the femur on the tibia as seen in

Figure 2-8. These motions have been described as a combination of rolling, sliding and

spinning (Freeman & Pinskerova, 2005; Moschi & Zingoni, 1977; Smith et al., 2003). The

increased congruency of the medial compartment contributes to the constraint of the medial

condyle while also influencing the arc of motion of the lateral condyle around the tibial

eminence (Martelli & Pinskerova, 2002). The medial location of the longitudinal axis results

in greater lateral condyle motion during flexion/extension (Todo et al., 1999). Furthermore,

there is a mismatch between the amount of AP translation between the medial and lateral condyles during flexion which causes internal tibial rotation, commonly referred to as the screw-home mechanism (Masouros et al., 2010).
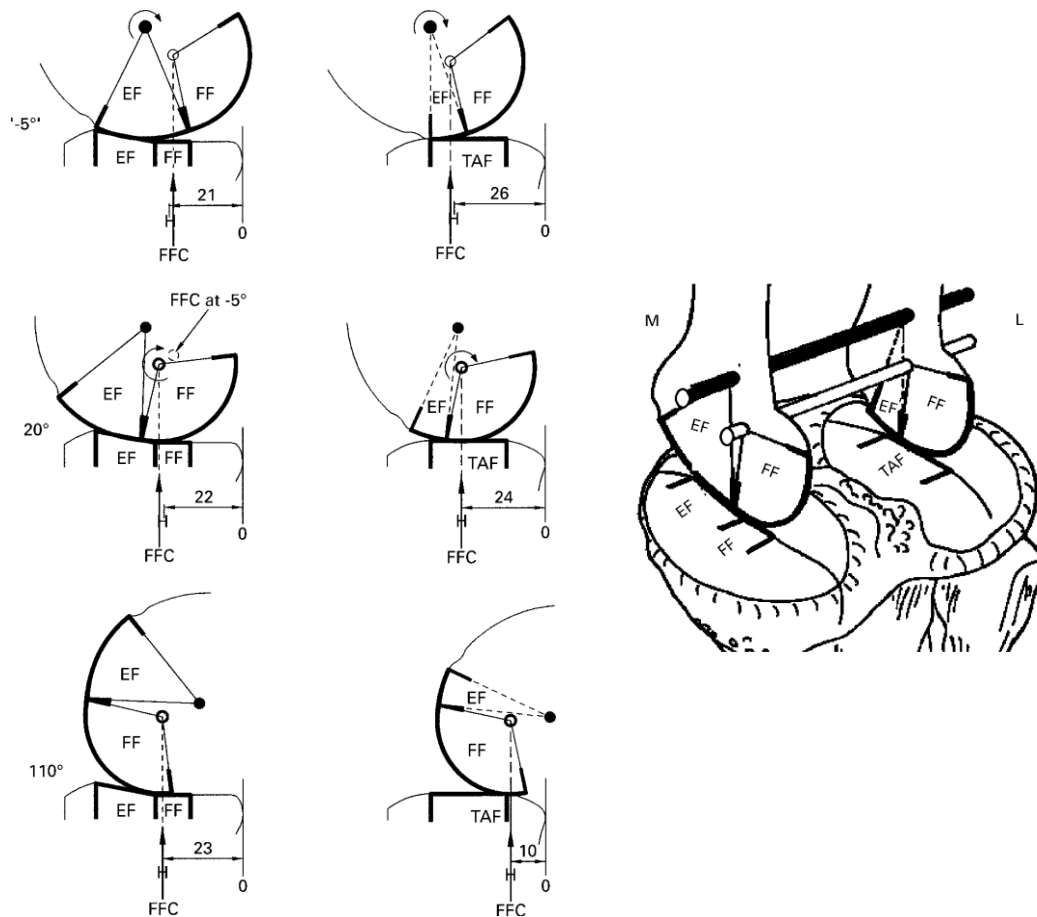
Figure 2-8: Diagrams of sagittal sections of the tibiofemoral joint
Medially (left) and laterally (right) at -5°, 20° and 110° showing different relative positions of femur on tibia. Right image is a reconstructed drawing (Iwaki et al., 2000)

There is evidence that each of these many and varied combinations of shape characteristics might influence kinematics of the knee. Hoshino examined the effect of distal femur bony morphology and translational and rotational kinematics (Figure 2-9). They found moderate correlations for condylar offset ratios (COR) and anterior/posterior tibial translation. The larger the COR, the larger the translation (R^2=0.57, in men only). Additionally, condylar twist angle (CTA) was highly correlated with internal tibial rotation range ($R^2 = 0.81$) in women,

but the correlation was not significant in men (Hoshino et al., 2012). These findings suggest that it is not simply the articulating geometry of the distal condyles that influence knee joint motion but also their relative alignment and shape.

The current single-plane medical imaging modalities (X-Ray, CT or MRI) are used to describe the linear relationship between motion and geometry through subjective inspection. These methods are limited because the results are contingent on the selection of a particular finite set of morphological factors. Statistical shape modelling has the unique capacity to utilize all of the complexity inherent in individual knee shape to detect how subtle geometric changes influence kinematics.
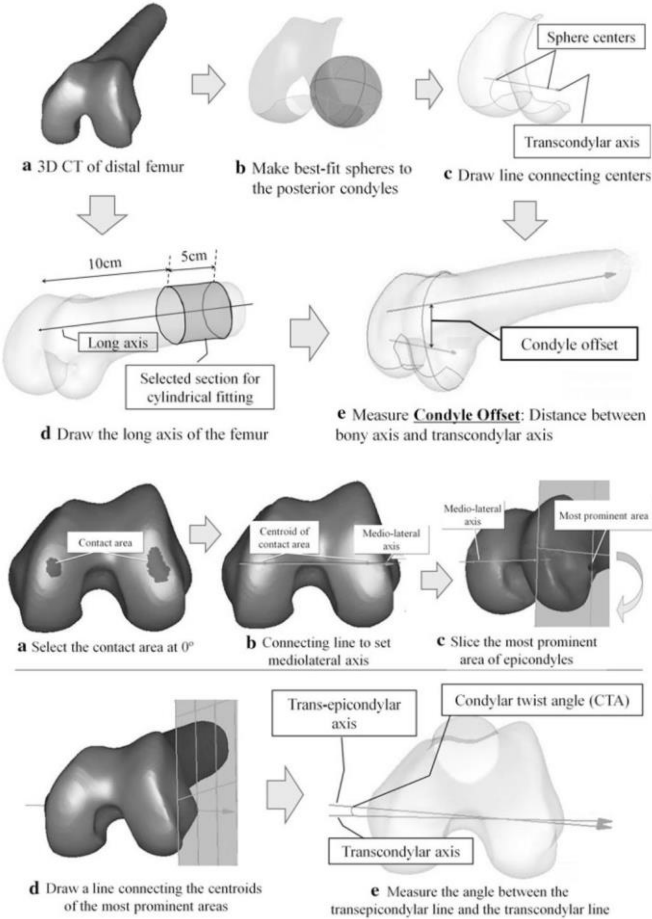
Figure 2-9: Definition of condylar offset (top) and condylar twist angle (bottom) (Hoshino et al., 2012)

2.3.2 Influence of Statistical Shape Modelling on Knee Kinematics

Statistical shape modelling has the ability to provide a more detailed understanding of the relationships between shape and kinematics. While previous work has provided certain insights into the relationships between kinematics and morphological parameters, one major drawback of this approach is that these relationships are typically described from single slice imaging and they also draw conclusions about entire populations from relatively small samples. Additionally, previous work does not consider the shape of the knee as a whole and how a comprehensive set of morphological parameters might interact. Statistical shape modelling has the capacity to analyse the shape of an entire object and can therefore be used to examine how shape relates to different kinematic variables by grouping coincident shape parameters using Principle component analysis (PCA). To date, there are only three papers which have used shape modelling to define these relationships. Smoger *et al*. attempted to identify these relationships in a group of 20 male cadaveric knees. The authors found that 15 principle components were able to explain over 95% of the variation in the data. The first modes described scaling and shape changes in the condylar radii and their influence on tibiofemoral anterior–posterior (AP) translation, internal-external (IE) rotation, and the location of the most caudal point on the femur. Sagittal femoral condyle geometry or J-curve were directly linked to the AP translation and IE rotation kinematics and, ultimately, the location of the most caudal point. Furthermore, using predictive modelling, the authors were able to predict the kinematics and contact patterns based on shape with an accuracy of 1.9 +/- 0.39 mm. Kinematic predictions were better in the medial compartment and in the ML direction. The main limitation of this paper is that these knees are cadaveric with standardised loading applied. It is unknown whether these relationships will hold true *in-vivo*. Recently, a combined statistical shape and musculoskeletal modelling approach was used to examine how simulated gait kinematics were influenced by articular knee shape (Clouthier et

al., 2019). The authors reported that a larger flatter medial tibial plateau was associated with increased external rotation and anterior translation of the femur on the tibia during gait. While the relationships differed slightly to Smoger *et al.*'s work, these findings support the concept of shapes relationship with function in early to mid-flexion activities. However, both approaches do not directly examine the relationship between shape and function in-vivo, limiting real-world applications.

Statistical shape modelling has shown that kinematics is related to shape in a pathological knee group (Lansdown et al., 2017). In a study of ACL-injured and reconstructed knees Lansdown *et al.* found multiple tibial and femoral bone shape features that were associated with abnormal knee kinematics compared to their contralateral limb. Specifically, in extension, increased medial femoral condylar and tibial height, a more spherically shaped medial femoral condyle, and a shorter anterolateral plateau were all associated with a more anterior tibia. In 30° of flexion, a more spherically shaped medial femoral condyle, a shorter medial plateau supero-inferiorly, a longer lateral plateau anteroposteriorly and an increased height of the anteromedial tibial plateau, were all associated with a more anteriorly positioned tibia (Figure 2-10). The main limitation of this paper was that the kinematics were overly simplistic since the measurements were static and achieved under quasi-loading conditions, thereby ignoring the task-dependent nature of kinematics.
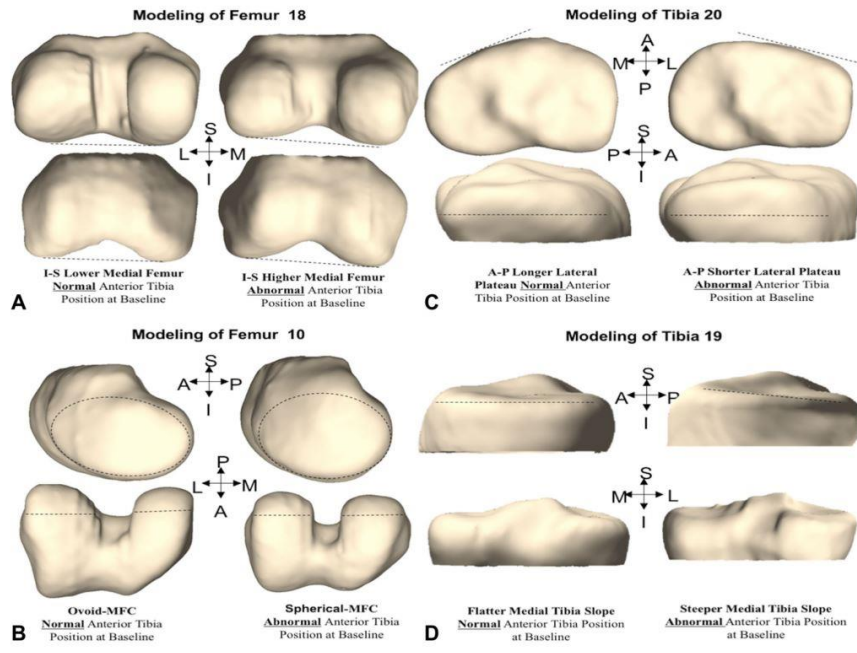
Figure 2-10: Shape modes which were correlated with abnormal kinematics (A) the height of the medial femoral condyle (MFC) (B) the sphericity of the medial femoral condyle; (C) the length of the lateral tibial plateau (D) tibial slope. Taken from Lansdown et al 2017 (Lansdown et al., 2017)

2.3.3 Relationships Between Degree of OA and Kinematics

It has been established that people with osteoarthritis experience both structural and kinematic changes associated with their joint disease (Baert et al., 2012; Mezghani et al., 2017; Nagano et al., 2012; Zeng et al., 2017). Recent work from our group examined osteoarthritic kinematics during deep flexion and found that osteoarthritic knees had reduced range of motion, maintained a more adducted position and showed less posterior translation of the lateral femoral condylar axis when compared to healthy knees. (Galvin, 2019; Scarvell et al., 2018). However, the associations between kinematics and specific osteoarthritic shape changes is less well understood. Understanding these relationships between osteoarthritic severity and joint kinematics is important. Ersoz *et al*. was the first to report correlations between Kellgren Lawrence (K/L) grades and sagittal and rotational ranges of motion ($r = $ -0.361 to -0.553; -0.338 to -0.439, respectively) (Ersoz & Ergun, 2003). Hilfiker *et al.* found

similar results showing negative associations between range of motion and increasing K/L grades after controlling for age, body mass index, social class, sex and comorbidities (Hilfiker et al., 2015). However, their results indicated that pain was also independently associated with lack of extension. Finally, Laxafoss *et al*., in 2013, demonstrated that increasing K/L grade produced a shift towards varus alignment on x-ray at a rate of 0.55°– 0.76° per K/L grade (Laxafoss et al., 2013).

Relationships between OA severity and kinematic variables have also been reported during functional tasks, specifically gait. A systematic review revealed reduced knee flexion and extension when comparing people with moderate and severe OA (Mills et al., 2013). A meta-analysis was not possible due to the heterogeneity of the data. Further gait analyses revealed the variables associated with increasing OA grade were reduced sagittal range of motion in stance phase and increased varus alignment (Nagano et al., 2012). Zeng et al supported these findings reporting a reduction in range of motion (ROM) in all degrees of freedom as OA severity increased (Zeng et al., 2017). Additionally, they reported that the osteoarthritic femur became more medial, anterior and distal with OA progression. Finally, a recent study by Mezghani *et al.* in 2017 used a regression tree analysis to find precise kinematic gait variables that could distinguish between healthy, moderate and severe osteoarthritic knees. They identified sagittal flexion angle, IE rotation ROM during swing phase and varus/valgus ROM during loading phase as the important kinematic variables which distinguished between OA severity (Mezghani et al., 2017).

While a number of studies have focused on global OA progression through K/L grades, fewer studies have examined the associations between the specific morphological features of OA and kinematics. The presence and position of osteophytes are reported to be correlated with ROM (Holla et al., 2011). In addition, features such as, narrowed joint-space, increased density of subchondral bone and enlarged bones are associated with reduced ROM in OA

knee joints (Ozdemir et al., 2006). However, while these associations are significant, the correlations are weak (r between 0.14 and 0.34). While there is some evidence to support the hypothesis that osteoarthritic changes are associated with kinematic changes, because these correlations are only low to moderate and differ between studies the evidence has not been well established. It could be that current measures of both kinematics and shape are not sensitive enough to accurately characterize these relationships.

While prior research has illuminated the possible influence of the shape of the femoral condyles and tibial plateau on joint kinematics (Freeman & Pinskerova, 2005; Pinskerova et al., 2009), there are still significant gaps in our understanding. Three-dimensional modelling has the ability analyse complex shapes, such as the knee, and characterize the information so that it can be interpreted in the context of joint kinematics. In this way, subtle but important pathological changes in the shape of the knee can be related to kinematics. Currently the data which describes the relationship between knee shape and kinematics has been achieved using either cadaveric specimens or simplistic kinematic analyses. There is an opportunity to marry sophisticated statistical shape models with state-of-the-art *in vivo* kinematic analysis to comprehensively describe the relationship between shape and kinematics in health and disease. The presence of patient specific shape changes in osteoarthritic knees are well known. It is also accepted that the kinematics of OA knees are disrupted and variable. However, the relationship between these shape changes and the altered kinematics are not well established. Although there is good evidence linking increased severity of knee OA with abnormal kinematics, there is little known about whether knee shape *per se* is an important predictor of joint kinematics.

2.4 Total Knee Replacement

A number of strategies exist to conservatively manage osteoarthritis. Education, weight loss, muscle strengthening program, bracing, and the use of drugs such as acetaminophen, non-steroidal anti-inflammatories (NSAIDs) are all highly effective tools (McAlindon et al., 2014). However, once these approaches are exhausted, the surgical option is explored, and many patients go on to receive a total knee replacement (TKR). In Australia in 2018, over 56,000 TKR were implanted (Australian Orthopaedic Association National Joint Replacement Registry (AOANJRR), 2019). This was an increase of 1.1% compared to the previous year and these numbers are expected to increase. (Australian Orthopaedic Association National Joint Replacement Registry (AOANJRR), 2019).

The goal of a TKR is to restore articular shape and alignment by replacing the osteoarthritic joint surfaces and soft tissues with an artificial prosthesis. The concept of TKR, can be traced back as far as Themistocles Gluck's 1891 ivory hinged knee (Figure 2-11). However, the modern concept of a condylar design where the osteoarthritic weight bearing articular surfaces of both the distal femur and proximal tibia are removed and replaced with a combination metal components and polyethylene tibial bearing only began in the 1970s with the Insall and Bernstein, Freeman–Swanson and Duocondylar implants (Bonnin et al., 2012). Modern designs generally consist of femoral and tibial metal components and a polyethylene tibial bearing. The femoral implant has two spherical phalanges which extend distally and posteriorly to cover the condyles, and an anterior trochlea groove to allow patellar articulation. The sagittal condylar geometry is designed to have either single (e.g. Scorpio (Stryker) and Vanguard (ZimmerBiomet)); or multiple radii (e.g. Attune (DepuySynthes) and Nexgen (ZimmerBiomet)) where the centre of rotation coincides with the insertion points of the collateral ligaments (Stoddard et al., 2013). The femoral component also varies in terms of frontal plane radii and trochlear groove design (Saffarini et al., 2016; Willing & Kim, 2011).

The tibial baseplate is flat with a keel which affixes to the bone for greater stability and can allow for a fixed or rotating platform bearing. Femoral components are typically made from cobalt chromium alloy. Tibial components are typically made from either cobalt-chromium or titanium. It is designed to allow attachment of a polyethylene bearing to the tibial bearing typically made from an Ultra High Molecular Weight Polyethylene (UHMWPE). While its design is variable, this bearing generally has a flattened or slightly dished medial and lateral groove. These bearings articulate with the femoral component and together they provide the necessary stability and mobility needed for function.
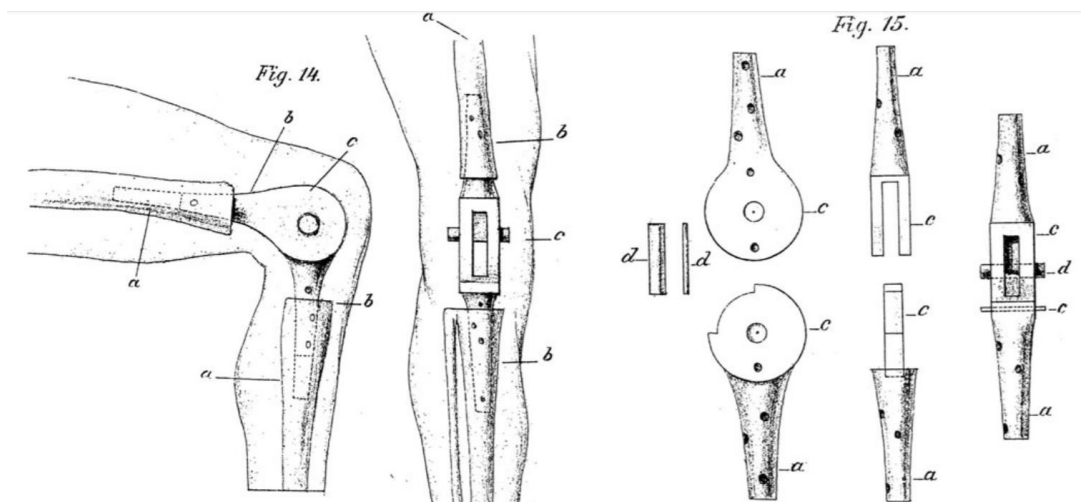
Figure 2-11: Illustrations of ivory hinge joint suggested by Gluck (Gluck, 1891)

There are a number of implant component designs used in TKR surgery. In 2018, 193 different implants were implanted in Australia (Australian Orthopaedic Association National Joint Replacement Registry (AOANJRR), 2019). These designs have varying condylar geometries, tibial slopes, polyethylene characteristics and ligament restraints. However, even with this high heterogeneity, designs can be broken into three broad categories: cruciate retaining (CR) or minimally stabilised; posterior stabilised (or cruciate sacrificing, PS) and medial pivot (or medial stabilised, MP) designs (Australian Orthopaedic Association National Joint Replacement Registry (AOANJRR), 2019). These broad categories of implant design

have arisen from the result of many iterative design changes during the early development of TKR implants (Bonnin et al., 2012). All of these designs include use of either a fixed or mobile bearing (rotating platform), where the latter has an articulating polyethylene tibial component which can either be constrained to a set amount of rotation, or is totally free to rotate relative to the tibial tray. The rotating platform was designed to increase the freedom of the joint by decoupling rotation from flexion, while reducing contact stresses on the polyethylene component through higher articular conformity and greater contact area (McEwen et al., 2005; Walker & Sathasivam, 2000). The CR design retains the posterior cruciate ligament (PCL) and relies on the ligament's function to closely mimic native knee femoral rollback in deep flexion. A cam and post replace the PCL in the PS design, aiming to facilitate rollback of the femoral condyles on the tibial bearing (Insall et al., 1982). In both designs, the mediolateral stability is provided by the collateral ligaments combined with the implant geometry. While there are minimal differences between implants in terms of pain, and clinical outcomes (Bercik et al., 2013; Jiang et al., 2016; N. Li et al., 2014; Verra et al., 2013), the cruciate retaining design has a slightly lower revision rate (Australian Orthopaedic Association National Joint Replacement Registry (AOANJRR), 2019). However, in terms of function, the posterior-stabilised design has been reported to confer greater maximal flexion (Verra et al., 2013) which might be beneficial for patients wanting to kneel.

The goal of TKR surgery is to relieve pain as well as enhance function, range of motion, and joint stability (Medical Advisory Secretariat, 2005). As surgical technique and implant materials have improved, survivorship of the prostheses has increased. The average 18-year survival rate of a TKR is 91.4% (Australian Orthopaedic Association National Joint Replacement Registry (AOANJRR), 2019). The ability to restore walking without pain and limping in more than 90% of cases has led surgeons to offer this operation to younger patients. While in most cases TKR is successful, up to 20% of patients do not have a

completely successful outcome (Bourne et al., 2010). Reasons for lack of satisfaction are: ongoing pain, stiffness, and lack of expected function. (Dunbar & Haddad, 2014; Maratt et al., 2015; Robertsson et al., 2000). However, the functional demands and activity levels of these younger patients have placed increased demands on the prostheses. Kneeling, specifically, is reported as one of the most important yet difficult activities for patients following TKR (Acker et al., 2011; Devers et al., 2011; Weiss et al., 2002). A recent systematic review highlighted the areas of patients' lives which are impacted by kneeling difficulty (Figure 2-12) (Wylde et al., 2019). These tasks vary from activities of daily living to sports and recreation.
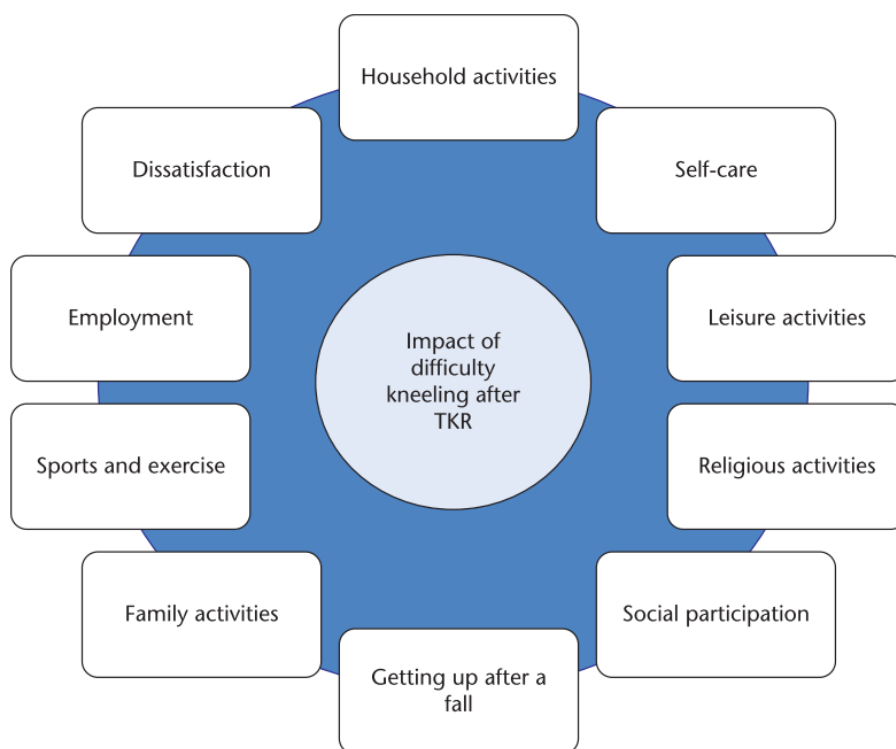
Figure 2-12: Impact of difficulty kneeling after total knee replacement.
Taken from Wylde et al 2019 (Wylde et al., 2019)

The design of modern TKR prostheses have focused on restoring healthy kinematics in order to achieve high flexion. Kinematics features of healthy kneeling include posterior femoral translation, external femoral rotation and increasing valgus while moving into flexion (Galvin

et al., 2019). Therefore, implant choice is dictated not only by implant survival and surgeon preference, but also by kinematic performance (Vertullo et al., 2017). It is therefore crucial to understand the kinematics of different implant designs. However, the debate over which implant to use is still unresolved. A recent systematic review examined the influence of implant design on kinematics during deep flexion (Angerame et al., 2019). The authors found that none of the designs restored normal kinematic patterns and there was high variability within and between designs. However, data was only reported up to 90° of flexion. As many activates require flexion greater than 90°, the influence of implant design is still unclear. A detailed systematic review examining the influence of TKR design on kneeling kinematics can be found in chapter seven.

3 Methodology/Approach

3.1   Study Design

The research contained in this thesis is located within a large randomised controlled trial entitled: A prospective imaging study of cruciate retaining, cruciate substituting, and rotating platform total knee replacement, in osteoarthritis and healthy ageing: a randomised control trial (PICKLeS #ISRCTN75076749). In order to address the aims of this thesis, four studies were nested within the PICKLeS study. These four studies employed three different study designs. Studies one and two utilized cross-sectional observational designs; Study three was a systematic review with meta-analysis; and study four was a prospective randomized clinical trial.

3.1.1   Setting

All of the testing was completed at the Canberra Hospital, which is a 600-bed tertiary teaching hospital located in the Australian Capital Territory. Imaging of participants took place at the Medical Imaging Department of the hospital, while subjective and functional testing occurred at the Trauma and Orthopaedic Research Unit (TORU). This research received ethics approval from the ACT Health Human Research Ethics Committee (ETH.4.11.071) and The Australian National University Ethics Committee (2017/354). All participants provided written informed consent.

3.1.2   Recruitment

Participants with end-stage osteoarthritis (OA) were identified from both the private and public waiting lists of Professor Paul Smith (Supervisor). Healthy control participants were recruited using a combination of posters delivered to the community through community organisations, paper flyers and word of mouth. These participants were a combination of a convenience and snowball sample, not purposively or randomly sampled, and all came from the Canberra region. All possible participants were initially contacted by phone. During this

phone call, the participants were provided with an explanation of the study background, aims and details. If the participant was interested, they were sent the participant information form and the questionnaires. Participants were telephoned three days to a week later and if consent was verbally obtained, they were invited to attend an interview and physical examination at Trauma and Orthopaedic Research Unit. Prior to testing, the participant's understanding of what the study entailed was assessed and an opportunity for clarification and questions provided. If the participant and the researcher were satisfied the consent form was signed.

3.1.3   Participants

Healthy participants were eligible if they were usually active and the test knee was pain-free with no history of injury or arthritis. OA participants were eligible for the study if they required a total knee replacement for osteoarthritis. These participants were first screened clinically with x-ray confirmation of OA by one surgeon (PNS). Table 3-1 lists the inclusion and exclusion criteria for all participants.

Table 3-1: Inclusion and exclusion criteria for the Osteoarthritis (OA)/ Total Knee Replacement (TKR) Group and the Healthy Group.

	Inclusion Criteria	Exclusion Criteria
OA Participants.	• X-ray confirmation of osteoarthritis • On surgical list for total knee replacement	• Isolated lateral compartment osteoarthritis • BMI > 38 • Wholly inactive or severely restricted to the minimum of activities of daily living. • Knee flexion < 90° (can you position your foot under your knee while sitting) • A psychosocial reason not to be able to consent or complete the requirements of the study • Metastatic disease • Pathological fracture • Revision knee replacement • Poor understanding and is unable to provide informed consent • Pregnancy
Healthy participants.	• At least one pain free knee • No history of injury or arthritis	• Poor understanding and unable to provide informed consent • Pregnancy • Metastatic disease

The number of participants recruited relied on the PICKLeS parent study, which required a minimum of 80 healthy participants and 60 participants with OA. One hundred and twenty-three participants, between the ages of 18 and 90, with healthy knees (Figure 3-1) and 124 participants with knee osteoarthritis (Figure 3-2) were initially approached for eligibility. The participant flow for the healthy and OA/TKR cohorts are described in Figure 3-1 and Figure

3-2. Healthy participants under the age of the youngest total knee replacement participant (47 years) were not used in this thesis.
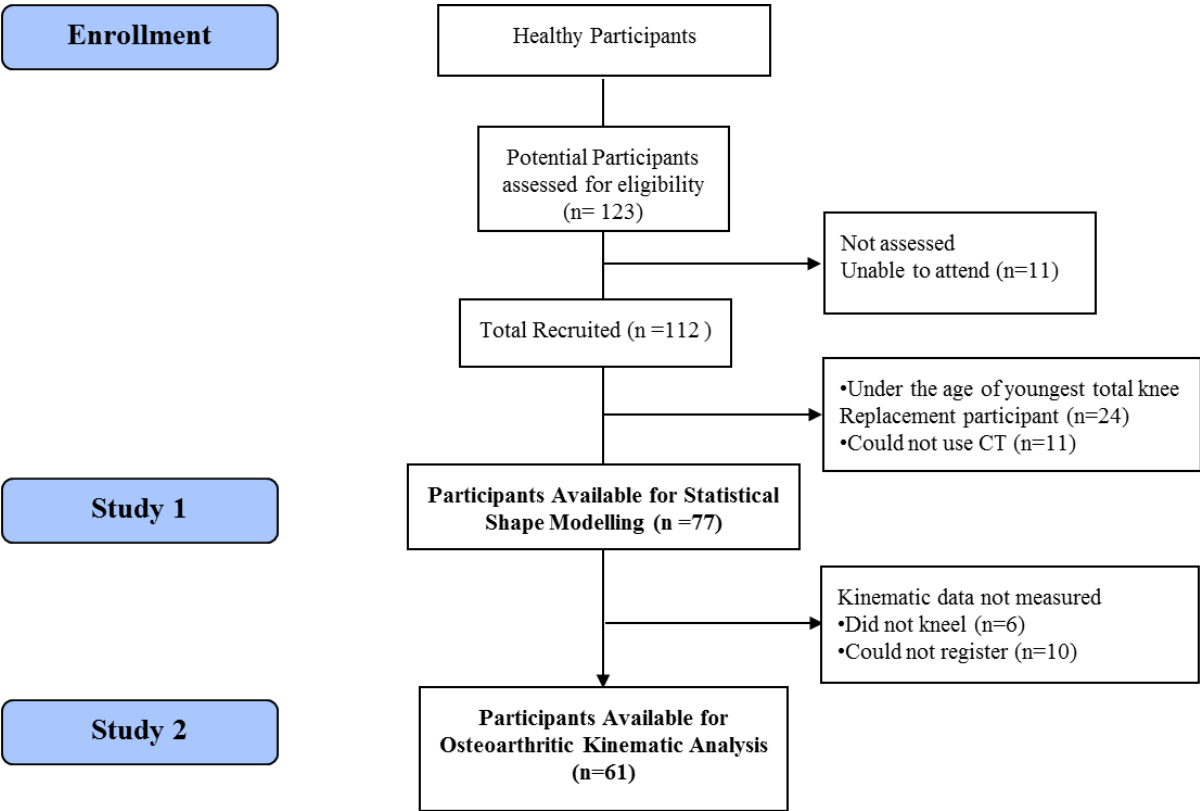
Figure 3-1: Flowchart for healthy participants included in shape modelling studies.

Enrollment

Osteoarthritis/TKR Participants

Potential Participants assessed for eligibility (n= 124)

Excluded (n= 45)
- Cancelled Operation (n= 1)
- Not Interested (n= 13)
- Unavailable for testing (n= 17)
- Did not want to be randomised (n= 7)
- Poor English (n= 2)
- Did not attend initial testing session (n= 3)
- History of Stroke and Parkinson's (n= 1)
- FFD and Valgus >30 degrees (n= 1)

Total Recruited (n = 79)

Could not use CT for Analysis (n=3)

Study 1

Participants Available for Statistical Shape Modelling (n=76)

Could not import Fluoroscopy (n=1)
Could not Register (n=17)

Study 2

Participants Available for Osteoarthritic Kinematic Analysis (n=58)

Randomized Control Trial (n=79)

- Trial implant not used (n=11)

Randomized (n=68)

Cruciate Retaining Fixed Bearing (n= 24)

Cruciate Retaining Rotating Platform (n=23)

Posterior Stabilised Fixed Bearing (n=21)

1 Year Follow-Up

Removed (n = 2)
- Missed 1 year F/U (n=1)
- Declined due to OA in ankles (n=1)

Removed (n = 2)
- Patellar Fracture and Infection (n=1)
- Lost to F/U (n=1)

Removed (n = 0)

Cruciate Retaining Fixed Bearing (n= 22)

Cruciate Retaining Rotating Platform (n=21)

Posterior Stabilised Fixed Bearing (n=21)

2 Year Follow-Up

Removed (n = 2)
- Lost to F/U (n=2)

Removed (n = 3)
- Contralateral knee fracture (n=1)
- THR (n=1)
- Back Surgery (n=1)

Removed (n = 4)
- Loss to F/U (n=3)
- Moved interstate (n=1)

Cruciate Retaining Fixed Bearing (n= 20)

Cruciate Retaining Rotating Platform (n=18)

Posterior Stabilised Fixed Bearing (n=17)

Final Analysis (Study 4)

Cruciate Retaining Fixed Bearing
1 Year (n=2)
2 Year (n=20)

Cruciate Retaining Rotating Platform
1 Year (n=3)
2 year (n=18)

Posterior Stabilised Fixed Bearing
1 Year (n=4)
2 Year (n=17)

Figure 3-2: Flowchart for participants included in the osteoarthritis and total knee replacement group for shape modelling and randomised clinical studies

Participant's testing schedule is reported in Table 3-2. The baseline visit lasted approximately 90 minutes and included consenting, examination, functional testing, self-reported questionnaires, a CT scan and video fluoroscopy. The OA participants then underwent arthroplasty surgery within 4 weeks, and the testing sessions were repeated 12 and 24 months following TKR. The healthy group were only required to attend one session. The period of recruitment and testing was between February 2012 and November 2018.

Table 3-2: Participant Testing Schedule

	Total Knee Replacement	Healthy
Baseline	- Fluoroscopy - CT - Clinical Exam - Functional Tests - Patient Reported Outcomes Measures	- Fluoroscopy - CT - Clinical Exam - Functional Tests - Patient Reported Outcomes Measures
Arthroplasty Surgery		
12 Months Post Surgery	- Fluoroscopy - Clinical Exam - Functional Tests - Patient Reported Outcomes Measures	
24 Months Surgery	- Fluoroscopy - Clinical Exam - Functional Tests - Patient Reported Outcomes Measures	

3.2 Data Collection

3.2.1 Clinical Data Collected

To assess the severity of osteoarthritis and recovery from surgery, a number of clinical and patient-reported measures were collected.

3.2.1.1 Questionnaires

Several patient-reported outcome measures (PROMs) were used in this thesis. These PROMs are questionnaires which measure a patient's self-reported view of their health status, perceived level of impairment, disability, and health-related quality of life. While not used to answer the main aims of the thesis, the questionnaires give an indication about clinical differences between the groups compared in each study. These questionnaires are commonly given to participants at baseline and, if appropriate, at 12- and 24-months follow-up and can allow comparisons of outcomes pre and post procedure or to a control group (Kingsley & Patel, 2017). The Oxford Knee Score (OKS) is a 12-item questionnaire which assesses patient's knee pain and function (Murray et al., 2007). It contains 12 questions, 7 that assess function and 5 that assess pain. It is scored out of 48 points with 0 being the worst and 48, the best. The OKS can assess function and pain for those with OA, and track progress following TKR. The OKS has moderate construct validity when compared to the Knee Society Score, the SF-36, and the Stanford Health Assessment questionnaire (Dawson et al., 1998).

Two Visual Analogue Scales (VAS) were administered: pain and surgical satisfaction. VAS is scored on a linear scale from 0-100 with 100 being the worst outcome. VAS pain is a unidimensional measure of intensity of pain (McCormack et al., 2020). It is widely used and is a recommended method for assessing recovery progression of disease and recovery from surgery (Price et al., 1983). Furthermore, it shown to have good content validity when compared to other similar scoring systems (Cincinnati, Larson, Lysholm) (Garratt et al.,

2004).The VAS satisfaction is a measure related to patient expectations, pain relief, and improvement in function following total knee replacement. (Dunbar & Haddad, 2014; Maratt et al., 2015; Robertsson et al., 2000). This is an important measure of success following total knee replacement (Bryan et al., 2018). The VAS score gives an overall indicator of the perceived success of the TKR surgery. Satisfaction is a multifactorial outcome which is associated with expectations, pain relief, and functional improvement (Bryan et al., 2018). Improved patient satisfaction has shown significant correlation to pain and physical function (Robertsson et al., 2000).

3.2.1.2 Osteoarthritis Grading

Osteoarthritis severity was graded using the Kellgren Lawrence (KL) Score. The KL grade is a 2-dimensional grading system use to describe the severity of knee osteoarthritis (Kellgren & Lawrence, 1957). A score of 0 indicates no osteoarthritis and 4 signifies severe osteoarthritis (Table 3-3). In this study, The KL grade was determined using the AP projection of supine CT scans. Both OA and healthy groups were graded. The scans were graded by 2 pairs of independent assessors. Kendall's W was used to determine the level of agreement. Agreement was excellent; W=0.97, p<0.0005

Table 3-3: Kellgren and Lawrence radiological criteria for assessment of knee osteoarthritis.

Grade 0 None: No features of OA
Grade 1 Doubtful: Minute osteophyte
Grade 2 Minimal: Definite osteophyte, unimpaired joint space
Grade 3 Moderate: Moderate diminution of joint space
Grade 4 Severe: Joint space greatly impaired with sclerosis of subchondral bone

3.2.2 Imaging Data Collection

The remainder of this chapter provides an overview of the main methodologies that were used in this thesis to test the research questions. To test the research question regarding the impact of shape on kinematics, tibiofemoral shape was described using statistical shape modelling. Six degree of freedom knee kinematics were calculated using 2D-3D image registration. To compare post-operative kinematics, three TKR- computer-aided design (CAD) models were registered onto 2D fluoroscopic images. Bivariate functional principal component analyses (bfPCA) were used to describe variability in the kinematics. Full descriptions of these methods follow here.

3.2.2.1 Computed Tomography (CT)

In order to undertake statistical shape modelling, and image registration, a reconstructed 3D image of the knee is required. All participants received a 3D spiral computed tomography (CT) scan of the knee (Toshiba Medical Systems, Ōtawara, Japan) at the baseline visit. The field of view was at least 150 mm above and below the tibiofemoral joint line. Slice thickness was 1 mm with a resolution of 512 x 512 voxels with spatial dimensions 0.625 x 0.625 x 0.5 mm^3 and 16 bits/pixel. The participant was positioned supine with the test knee placed within a specially designed calibration box (Figure 3-4).

3.2.2.2 Segmentation

Segmentation of the CT data to create 3D renderings of the native bone was achieved using bespoke software called Orthovis (Matlab, The Mathworks, Inc., Natick, MA). The femur, tibia, and combined tibia and fibula were segmented from the CT images, to provide 3D volumes for image registration and statistical shape modelling. The CT of the native bone was segmented slice by slice to isolate the bony anatomy of the knee from its soft tissue. Orthovis

semiautomatically segments CT data by first allowing the setting of a global segmentation threshold and isolated pixel connectivity limit to assist with removing artefacts throughout the volume. Next, an adjustable polynomial were fit around the bone of interest to remove all pixels outside it (Figure 3-3). Finally, a digital eraser was used for fine removal or restoration of pixels. Intra- and inter-rater variations of the calculated volumes for the femur were 0.99 and 0.84, and for the tibia 0.98 and 0.77 respectively. These intraclass correlations reflect a root mean squared error of up to 3% which equates to a volumetric difference of 1966 mm^3.
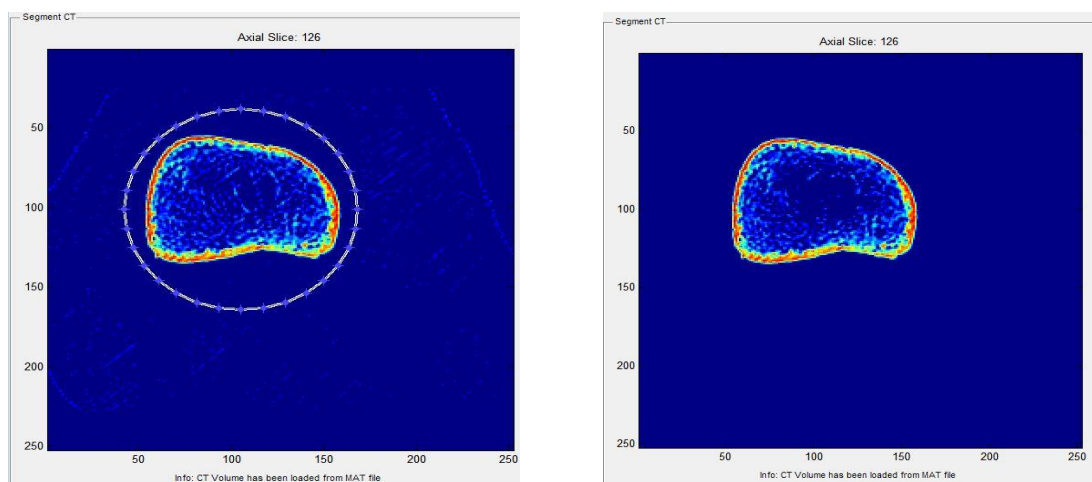
Figure 3-3: An example of Orthovis segmentation of single CT slice of a femur. Left: before segmentation with polynomial fitted around the cortical margin; Right: after removal of the pixels outside the bony cortex

Figure 3-4: Obtaining a CT scan of a participant's knee.

The knee is placed inside the calibration box.

3.2.2.3 Fluoroscopy

In order to analyse knee kinematics, the 3D model needs to be registered frame-by-frame to a dynamic 2D fluoroscopy. To capture movement, a stationary, single-plane, curved panel fluoroscopy (AXIOM-Artis, Siemens) was placed for a sagittal view of the knee. The fluoroscope sampled images at 30Hz with 1024 x 1024-pixel spatial resolution and 12bits/pixel. Distance between the tube source and image intensifier was 1200 mm, with a screen size of 280 mm. The knee of interest was positioned approximately 240 mm from the image intensifier. This position allowed the capture of movements from 0° to approximately 160° (full flexion). Participants were asked to perform a unilateral deep kneeling activity starting with the imaged knee at approximately 90° (upright kneeling), kneeling down to achieve full flexion and returning upright kneeling (Figure 3-5). The foot was not constrained and was free to rotate. The image was optimized in terms of maintaining the tibiofemoral joint within the frame for the whole cycle, at times requiring the fluoroscopic imaging to be repeated up to three times.

A calibration box was also recorded for each participant fluoroscopy event, to provide a mechanism to allow for post-hoc distortion correction of the fluoroscopic images (Figure 3-6). The calibration box has dimensions of 350 mm x 350 mm x 200 mm and contains 1 mm tantalum markers embedded on the anterior and posterior wall of the box. Marker beads were implanted in the Perspex at 20 mm intervals in a grid using a computer driven drill. (Figure 3-6). The box was positioned with the centre of the box the same distance away as the knee had been (240 mm from the image intensifier) (Figure 3-6).
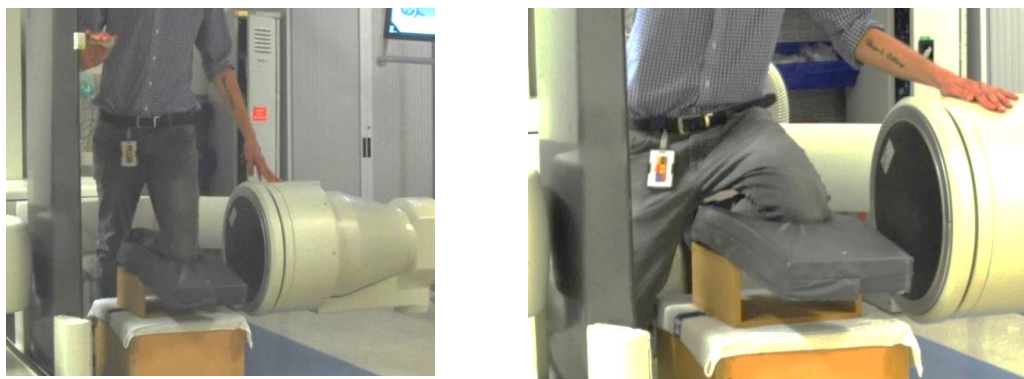
Figure 3-5: Demonstration of kneeling

Left: starting position with flexion at 90; Right: deepest flexion point while kneeling
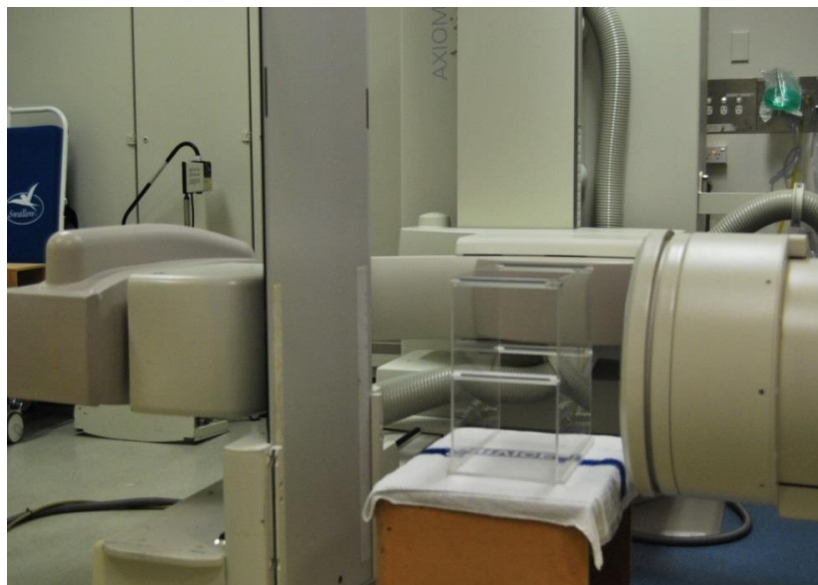
Figure 3-6. Imaging of the calibration box in fluoroscopy

Box positioned with its centre at the same distance from the image intensifier as the knee had been during the kneeling task.

3.3 Statistical Shape Modelling

Historically, joint shape has been characterized using a variety of two-dimensional measures which are typically identified on 2D images (X-Ray) or from single slice projections in three-dimensional scan (MRI, CT) (Dai & Bischoff, 2013; Dargel et al., 2009; Elias et al., 1990; Hoshino et al., 2012; Matsuda et al., 2004; Shepstone et al., 2001). They typically include angles, distances, radii of curvature, areas, and volumes. However, these measures rely on a-priori identification and are not currently considered in combination, and therefore might not characterize overall knee shape. Statistical shape modelling (SSM) is a technique that quantifies the variability between a set of similar shapes. SSM uses principal component analysis (PCA), to identify areas of coincident shape variation called modes of variation. Each shape within a given mode is then assigned principal component (PC) scores or weights. This enables the entire geometry within a dataset to be characterized using a small number of PCs. This dimension reduction is necessary because the number of parameters in a set of shape descriptions are generally too high for efficient or meaningful statistical analysis.

Statistical shape modelling was originally developed by Cootes *et al.* to characterise variability in 2D shapes for computer vision applications (Cootes et al., 1992). Since then, this technique has been applied to 3D anatomical variation (Agricola et al., 2015; Bredbenner et al., 2010; Neogi et al., 2013; Schneider et al., 2018), automatic segmentation (Heimann & Meinzer, 2009), improvements in musculoskeletal modelling (Bahl et al., 2019; Clouthier et al., 2019), relating shape and function (Clouthier et al., 2019; Lansdown et al., 2017; Smoger et al., 2015) and predicting anatomy from sparse geometry (Zhang et al., 2016; Zhang & Besier, 2017).

In this thesis SSM will be used to compare the tibiofemoral shape of people with severe knee OA (pre-TKR) and a non-OA age similar cohort (Chapter four). SSM will also be used to

determine how the shape characteristics of an OA and healthy cohort influence kneeling kinematics (Chapter five).

3.3.1   CT Cropped for Consistent proportions

Shape modelling works best when geometries are proportionally the same size. As such, each tibia and femur were cropped to standard proportions to account for different distal and proximal lengths of the CT obtained, as well as individual participant proportions (Figure 3-7). Using the coronal projection of the CT, the femur was cropped at 1.5 times the distance from the most distal femoral condyle to the adductor tubercle. Using the coronal projection, the tibia was cropped to 1.5 times the distance from the most proximal aspect of the tibial spine to the most inferior point of the superior tibiofibular joint. Corresponding femurs and tibias were recombined using a custom Matlab script to create a tibiofemoral joint for each participant. Variations in alignment were removed by aligning the femoral and tibial meshes so that their axes were orientated at zero degrees of rotation and translation based on the axis for the CT scan set earlier. Finally, all CT's were then smoothed using a Laplacian filter.
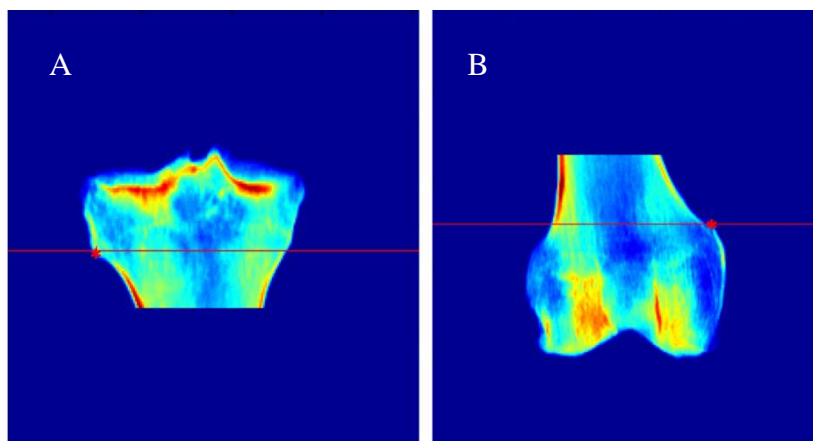
Figure 3-7. Cropping locations for femur and tibia.
A. The tibia was cropped at the superior tibiofibular joint (*) and; B. the femur was cropped at the adductor tubercle (*)

3.3.2 Mesh Generation

The SSM is constructed from a set of tibiofemoral meshes by applying a PCA to a covariance matrix, X, that contains the Cartesian coordinates of a set of nodes in each geometry to be included in the model. Each row in X contains the coordinates for all nodes for a single geometry mesh:

$$\mathbf{X} = \begin{bmatrix} x_{1,1} & y_{1,1} & z_{1,1} & x_{1,2} & y_{1,2} & z_{1,2} & \cdots & x_{1,m} & y_{1,m} & z_{1,m} \\ x_{2,1} & y_{2,1} & z_{2,1} & x_{2,2} & y_{2,2} & z_{2,2} & \cdots & x_{2,m} & y_{2,m} & z_{2,m} \\ \vdots & \vdots & \vdots & \vdots & \vdots & \vdots & \ddots & \vdots & \vdots & \vdots \\ x_{n,1} & y_{n,1} & z_{n,1} & x_{n,2} & y_{n,2} & z_{n,2} & \cdots & x_{n,m} & y_{n,m} & z_{n,m} \end{bmatrix} \quad \text{Equation 1}$$

where *n* is the number of meshes and *m* is the number of nodes in each mesh. Therefore, it is necessary that all meshes within the dataset have the same number of nodes and that these nodes correspond to the same location on each mesh. For meshes with a small number of nodes, it is possible to manually register landmarks on different shapes. For example, in a set of two-dimensional radiographic images of the tibiofemoral joint, one could manually label relevant landmarks in a given order (Figure 3-8).
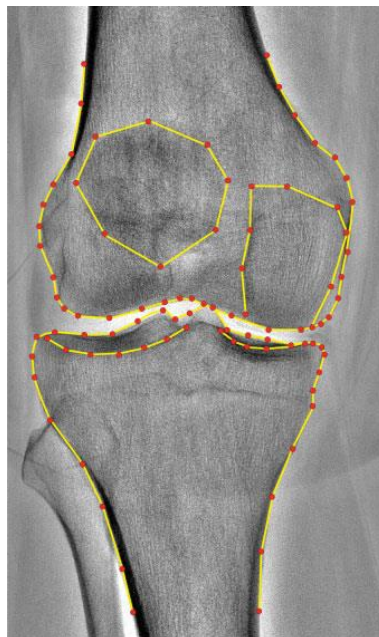
Figure 3-8: Example of simple set of nodal coordinates

Image taken from Haverkamp et al 2011

However, for complex three-dimensional geometries manual labelling is not feasible. A number of techniques have been developed to characterise the geometry of these complex shapes including coherent point drift (Clouthier et al., 2019), piecewise parametric meshes (Zhang et al., 2014), and radial basis functions (Zhang et al., 2018). Radial basis functions (RBF) have the advantage of being meshless which enables the knots, or starting point of the RBF, to be be placed arbitrarily and adaptively to a deformation field. This facilitates increased accuracy of knot placement with each iteration, which isn't feasible in mesh-based registration. Zhang et al. demonstrated good agreement between the target and registered surfaces across features of different complex geometries with fitting errors ranging from 0.37 to 0.99 mm (Zhang et al., 2018).

For this thesis, an initial fitting was performed on a single mesh from one knee in the dataset to create a template. This template was then iteratively fitted with a series of coarse-to-fine fits to all meshes in the dataset, which results in maximum correspondence between meshes.

3.3.3   Alignment

Once nodal correspondence is achieved, all of the meshes within the dataset need to be rigidly aligned to remove similarity-transform variations. These include rotational and translational variations as well as scaling components. Once these are removed only shape variation remains. This is accomplished using a Procrustes analysis which best transforms a group of meshes to align to a target mesh (Gower, 1975). This is accomplished by minimising the least-squared distances between the corresponding nodes (Gower, 1975). A full Procrustes analysis removes all similarity-transform variations while a partial Procrustes analysis retains the isometric scaling component of the shape. A partial Procrustes analysis was used in the

shape models developed in this thesis as size is likely important in understanding differences between groups and likely influences kinematics.

3.3.4   Principal Component Analysis

Dimension reduction is necessary when undertaking shape analysis because the number of parameters generated from a set of shapes is too large for meaningful statistical analysis. Principle component analysis (PCA) is the most common dimension reduction technique for shape analysis (Heimann & Meinzer, 2009). Following rigid alignment, the nodal coordinates are assembled in a covariation matrix centred on the mean mesh coordinates (Equation 1).

A principal component analysis (PCA) is then run on this covariance matrix to create a set of orthogonal principal components or modes of variation and with respective scores which best describe variations of shape within the dataset. The modes are ranked in order of eigenvalues representing principal component variances from largest to smallest in decreasing proportions of variance. PCA allows any shape in the dataset x to be approximated as the sum of the mean shape $\bar{x}$ plus the weighted sum of the principal components ϕ (Equation 2) (Heimann & Meinzer, 2009; Schneider et al., 2015):

$$\mathbf{x} = \bar{\mathbf{x}} + \sum_{i=0}^{n} \boldsymbol{\omega_1} \boldsymbol{\phi_1} \qquad \text{Equation 2}$$

The shape of each bone was described by n principle component (PC) weights, ω, where ω are the amount of variation along an individual principle component; and $'n'$ is the number of principal components needed to explain 90% of the total variation in the population. The PC weights generated by the PCA for each individual's shape, can be extracted for further analyses.

In this thesis, the fitting process, rigid registration and PCAs were repeated using the mean shape as the template. Following this, the fitting process was further refined for individual

shape differences by incorporating PCA fitting using the previous SSM generated from the dataset. In this way, the shape model was optimised by propagating fitting correspondence across the dataset. A final PCA was performed to generate a statistical shape model which generated the PC weights used in subsequent analyses.

3.4   Six Degree of Freedom Kinematics

Image registration with video fluoroscopy is a non-invasive capture method which can track movement of joints in-vivo (Akter et al., 2014a). The goal of image registration is to align two images of the same joint within the same space. One of these images is a three-dimensional (3D) volume either acquired from a CT, MRI or a CAD model. The second is a two-dimensional (2D) video fluoroscopy. Registering the 3D image to the 2D enables the measurement of skeletal kinematics in six degrees of freedom (6DOF). Orthovis for 2D to 3D image registration, was used for the studies contained within this thesis. The Orthovis package is written in Matlab (The Mathworks, Inc., Natick, MA) and uses a combination of 2D single plane fluoroscopy and either 3D CT or a CAD model. Precision of this program was previously reported for in-plane (sagittal) registration as 0.2 mm for translation and 0.3° for rotation, while the out-of-plane precision was 0.9 mm and 0.5° (Akter et al., 2014a; Scarvell et al., 2010).

While video-based motion capture is the most commonly used modality for non-invasive biomechanical analysis, it is much less accurate than image registration. Motion analysis involves multiple video cameras that capture the movement of skin-mounted markers placed on anatomical landmarks. As a result, these systems are subject to errors associated with soft tissue artefact (Peters et al., 2010). A systematic review of 20 studies which quantified soft tissue artefact reported differences of up to 30 mm using these systems compared to a gold

standard (Peters et al., 2010). These differences are both location and task dependent. Soft

tissue artefact is larger in the thigh segment compared to the tibia and during high

acceleration movements (Stagni et al., 2005). Motion analysis involves multiple video

cameras that capture the movement of skin-mounted markers placed on anatomical

landmarks.

3.4.1   Correction of Distortion of Fluoroscopy Images

Prior to image registration, pin cushion distortion, which is a by-product of curved panel

fluoroscopies, needs to be corrected. This was achieved by calibrating the fluoroscopy against

an object with known dimensions; in our case this was a 3D perspex box. The difference

between the distorted calibration box coordinates, as recorded by the fluoroscopy and the

known coordinates were used to determine the coefficients of a polynomial function that was

used to correct the distortion (Figure 3-9).
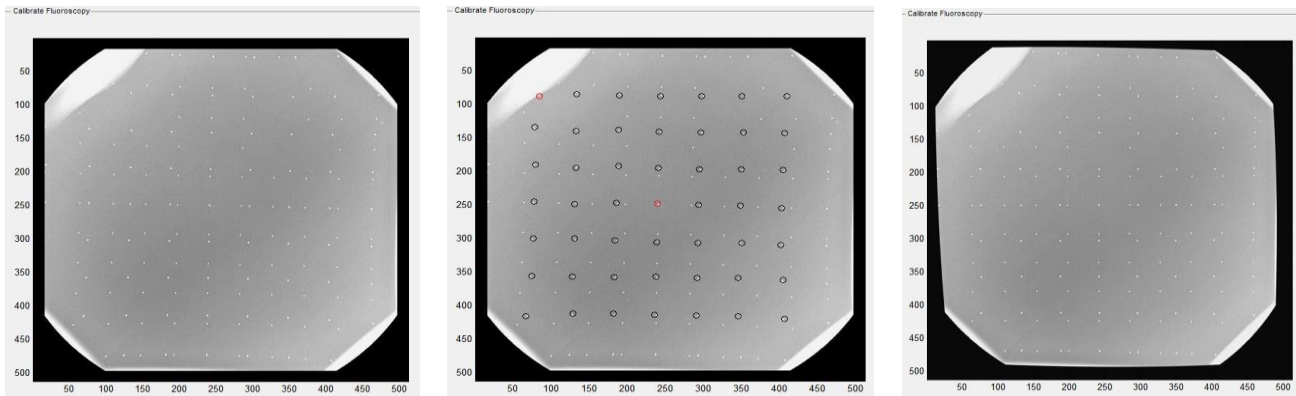
Figure 3-9: Fluoroscopy Calibration

Left: Fluoroscopy image of the calibration box before distortion correction, Middle: Fluoroscopy
image with Orthovis grid overlay, Right: Fluoroscopy image after distortion correction.

3.4.2   Image Registration

Image registration aims to find the best spatial match for the 3D volume (CT or CAD) and

fluoroscopic images. Prior to registration, the 3D volume needs to be converted into a

digitally reconstructed radiograph (DRR) and calibrated. The DRR was calibrated using the

same calibration box used previously. A wrapping function was applied to the 3D volume

which accounts for the conical spread of the X-ray beams from the fluoroscopy source (Figure

3-10). This transform was used to expand parts of the volume that were closer to the X-ray

source and to shrink the parts of the bone that were further away from the source (Scarvell et

al., 2010). Once the DRR was calibrated, it was registered to the fluoroscopic images. This

was achieved using 3 steps: a geometric transform, a similarity measure, and an optimisation

procedure, as follows.
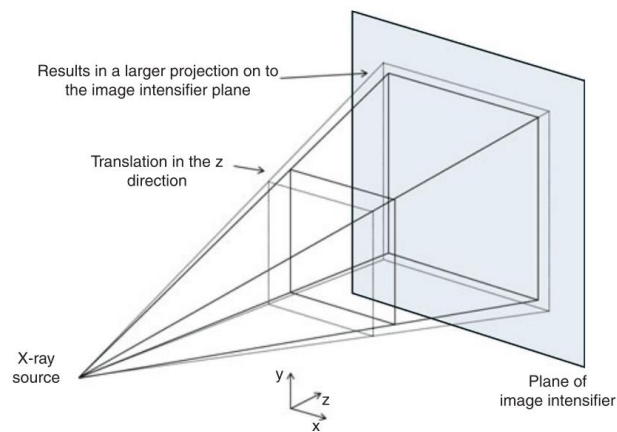
Figure 3-10: Fluoroscopy image projection.

As an object moves closer to the X-ray source it will produce a larger image
at the image intensifier of the fluoroscopy. Image taken from Scarvell et al
2010

3.4.2.1   Geometric Transform

The geometric transform is a 3D rigid-body transformation which aligns the location of

points in the DRR image with the location of points in the fluoroscopic image, correcting

their rotational and translational mismatch (Haque et al., 2014; Muhit et al., 2010;

Scarvell et al., 2010).

3.4.2.2 Similarity Measure

The similarity measure is the algorithm which determines the best fit between the DRR and fluoroscopy. This measure involves a combination of an edge position difference algorithm and sum of conditional variances to improve registration accuracy. The edge position difference algorithm was initially run to quickly estimate the in-plane and out-of-plane parameters (Figure 3-11). The similarity measure was then run on the output of the edge position difference algorithm to produce a more accurate estimate of fit (Saadat et al., 2017).
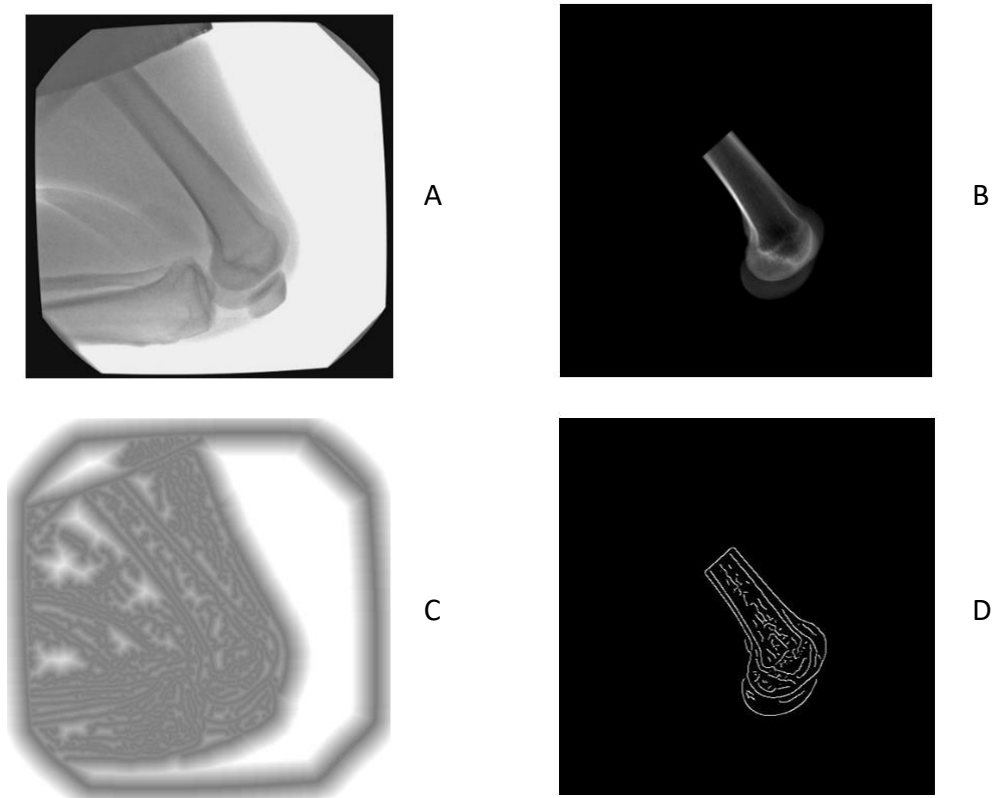
Figure 3-11: The similarity measure for CT and fluoroscopy best fit.
A) An example of a fluoroscopy image; B) 2D projection of a CT image to be registered; C) distance to edge position of the fluoroscopy image; D) The binary edge image of the 2D projection of the CT image. Image taken from Saadat et al. 2017

3.4.2.3 Optimisation procedure

Finally, the optimisation procedure automatically finds the transform which minimises both the edge position difference algorithm and the similarity measure using a gradient-descent method. This method reduces the number of similarity measure calculations. The edge position difference algorithm & sum of conditional variances minimised the number of multiplications required to calculate the similarity measure and therefore increases the speed of the registration while not sacrificing accuracy (Saadat et al., 2017).

This process requires the operator to first manually manipulate the position of the DRR to match the underlying fluoroscopy for size, rotation and alignment. Once initially matched, an initial registration is required. The approximate registration time per frame with the new similarity measure takes approximately 30 seconds to one minute. Following the initial registration, the algorithm uses the most recently registered frame to then automatically registered the current frame These steps are repeated for each fluoroscopy frame for both the femur and tibia. Rotational and translational coordinates were calculated and used to generate six degree of freedom kinematics using the Grood and Suntay referencing system (Grood & Suntay, 1983; Guan et al., 2017).

3.4.2.4 Defining joint coordinate system

In order to describe relative joint alignment and kinematics, a three-dimensional reference system must be applied. We used the Grood and Suntay joint coordinate system (Grood & Suntay, 1983). This system describes the 3D alignment and kinematics by specifying the relative positions of the femur and tibia at each fluoroscopy frame and also the changes in position over time. Relative movements between the femur on the tibia were described by two segment-fixed axes and a mutually orthogonal floating axis. Since its introduction, the Grood and Suntay coordinate system has been recommended by the

International Society of Biomechanics (ISB) in numerous biomechanical studies for a variety of joints (Wu et al., 2002, 2005). The strength of this reference system is its ability to describe biomechanical motion using clinical language. Furthermore, it has advantages over previous systems that used Euler angles for rotational description; as they were dependent on the order of rotations. The Grood & Suntay system are independent of order (Grood & Suntay, 1983).

Axes were set so that the x-axis defined the anterior (+)/ posterior (-) direction, the y-axis defined the proximal (+)/ distal (-) direction and the z-axis defined the lateral (+)/ medial (-) direction. Each segment required two independent orthogonal axes which quantify alignment and motion. These axes needed to be established using anatomical landmarks in the three planes.

3.4.2.5 Joint Coordinate System: Native Bone

Orthogonal frames of reference were established based on individual anatomical locations for each tibia and femur. For the femur, origins were set at the most proximal point of the intercondylar notch (Figure 3-12). The z-axis (superior-inferior, mechanical axis of the femur) was defined by the distal-most aspects of the medial and lateral femoral condyles and a projected line through the femur to the centre of the femoral head (Figure 3-12B). The x-axis (medial/lateral) was orthogonal to the plane defined from a line joining the most posterior aspect of the femoral condyles. The y-axis (anterior/posterior) was perpendicular to both the y and z axes (Grood & Suntay, 1983).

For the tibia, the origins were set at the mid-point of the tibial spines (Figure 3-13). As with the femur, the mechanical axis of the tibia is the longitudinal axis (z). The z-axis (superior/inferior) passed between the two intercondylar eminences (tibial origin) and the centre of the ankle. The x-axis (medial/lateral) was defined by a plane between the centres of

the medial and lateral tibial plateaus, along with the mechanical axis. The y-axis (anterior/posterior) was again, perpendicular to both the y and z axes (Grood & Suntay, 1983).
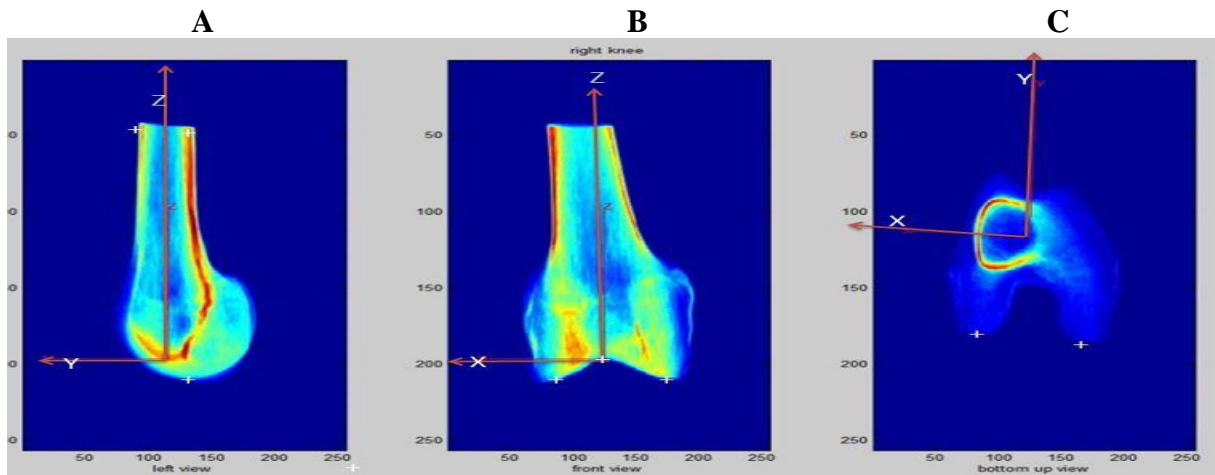
Figure 3-12: Defining femoral axes in the native bone

A) In the sagittal plane; identify three points, the most distal point of the femoral condyle, and the anterior and posterior cortical margins of the femoral shaft. B) In the coronal plane; Identify three points, the most distal points on the right and left femoral condyles and the most proximal point of the intercondylar notch. C) In the transverse plane; identify two points, the most posterior point on the right and left-hand femoral condyle
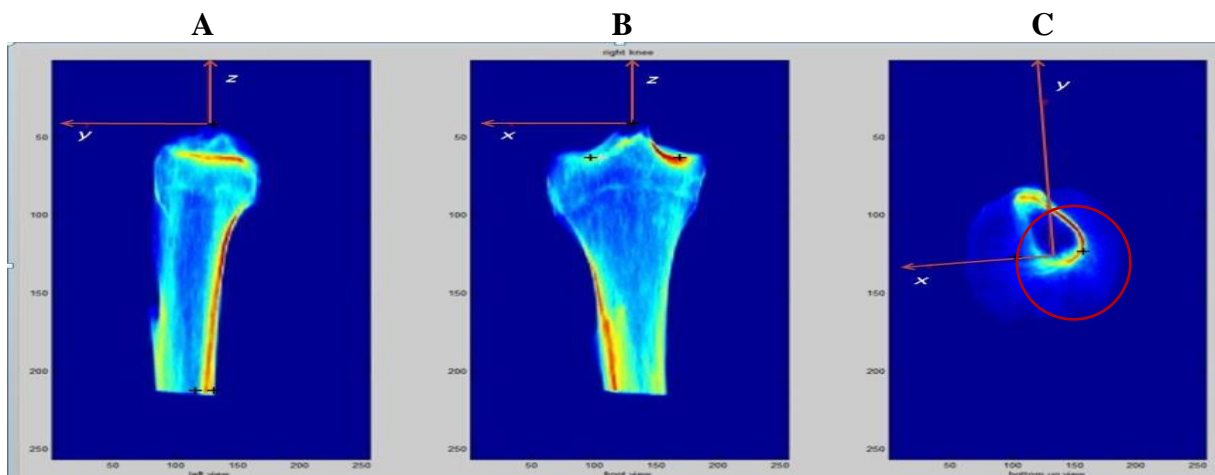
Figure 3-13: Defining the tibial axes in the native bone

A) In the sagittal plane, identify three points, the superior aspect of the intercondylar eminence, and the anterior and posterior margins of the posterior tibial cortex. B) In coronal plane; identify three points, the lowest points of the right and left plateau and the centre of the intercondylar eminence; C) In the transverse plane; identify the line which intersects the

midpoint of the medial and lateral tibial plateau by placing two circles on medial and lateral tibial plateaus.

3.4.2.6   Joint Coordinate System: Total Knee Replacement CAD Model

The origins of the TKR CAD models were established based on geometric locations. The femoral origin was set at the posterior-most point at the mid-point of the intercondylar notch (Figure 3-14). The tibial origin was set at the mediolateral and anterior-posterior mid-point of the tibial baseplate (Figure 3-15) (Guan et al., 2017). Similar to the native knee, the axes were set in order to have the x-axis defining the anterior (+)/ posterior (-) direction, the y-axis defining the lateral (+)/ medial (-) direction and the z-axis defining the proximal (+)/ distal (-) direction. Neutral alignment was defined as no relative angular rotation between the femoral and tibial CAD models
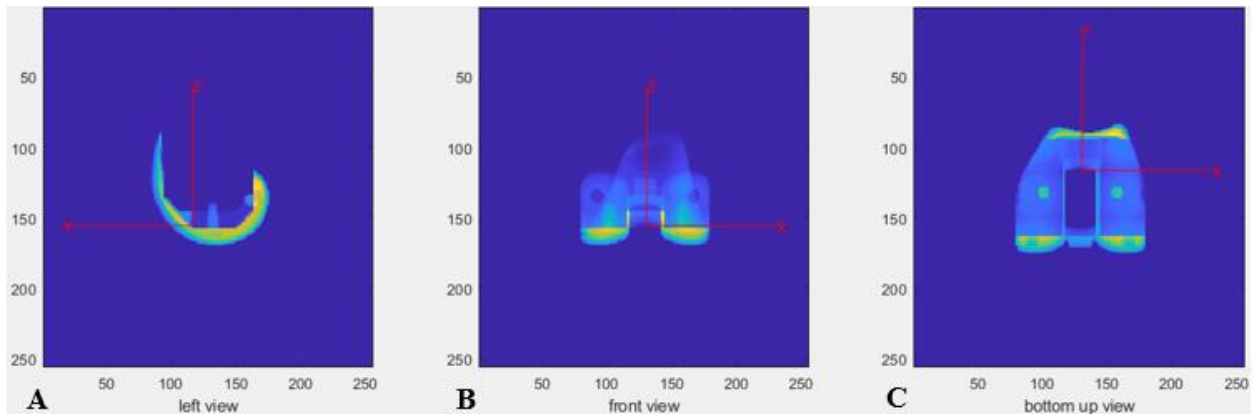
Figure 3-14: Defining the femoral axes in the TKR CAD model

Example of a left Cruciate Retaining CAD model. The origin of the femoral axis system was identified in three planes. A. Sagittal view - The most anterior position of the floor of the femoral component. B. Coronal - At the mid-point of the intercondylar notch. C. Axial - The midpoint of the most anterior point of the intercondylar notch. The x-axis for the femoral component was parallel to the transverse surface of the most anterior point of intercondylar notch. The z-axis was perpendicular to the x-axis. The y-axis was perpendicular to both the x-and z-axes.
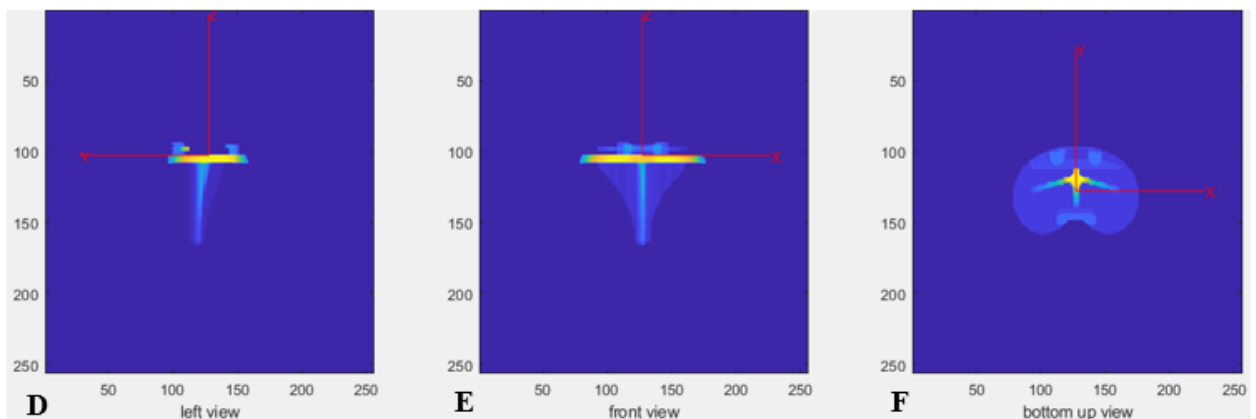
Figure 3-15: Defining the tibial axes in the TKR CAD model

Example of a left rotating platform CAD model. The origin of the tibial axis system was identified in three planes. D. Sagittal view - The anterior-posterior mid-point of the baseplate. E. Coronal – Medial-lateral midpoint of the surface of the tibial baseplate. F. Axial – Top Geometric centre of the tibial baseplate. The x-axis of the tibial component was parallel to the transverse flat surface of the tibial baseplate. The z-axis of the tibial component was perpendicular to the transverse flat surface of the tibial baseplate and the x-axis. The y-axis was perpendicular to both the x-axis and the z-axis.

Positive rotations are defined as flexion, internal femoral rotation (Figure 3-16), and varus rotation (Figure 3-17). Positive femoral translations are in the medial (Figure 3-18), anterior (Figure 3-20), and superior (Figure 3-19) directions.

Internal rotation (+)   **Neutral**   **External rotation (-)**
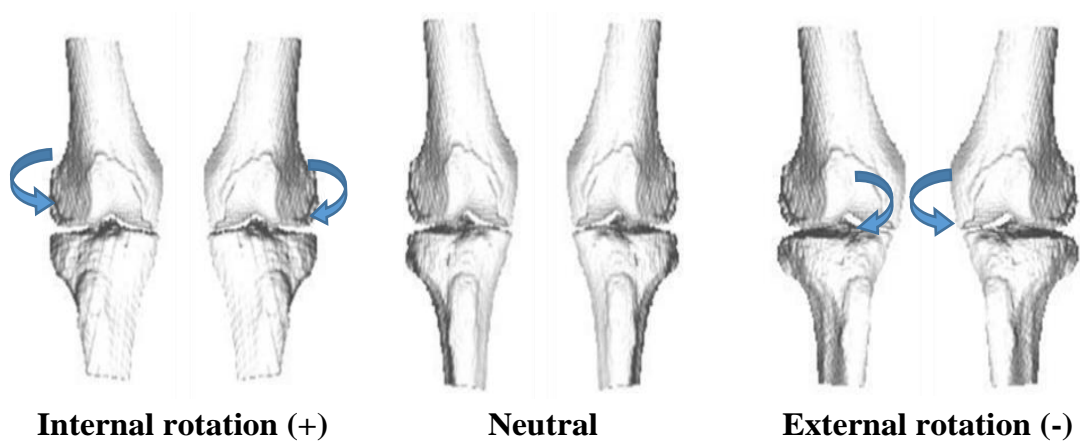
Figure 3-16. Internal/external rotation of the femur <u>relative to the tibia</u>

Adduction/Varus (+)   **Neutral**   **Abduction/Valgus (-)**
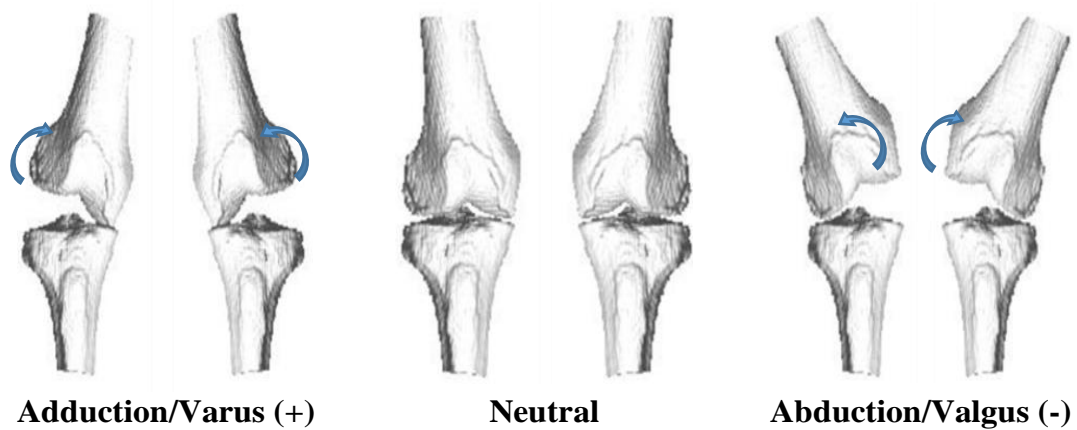
Figure 3-17. Adduction (varus) and abduction (valgus) of the femur <u>relative to the tibia</u>

Medial (+)   **Neutral**   **Lateral (-)**
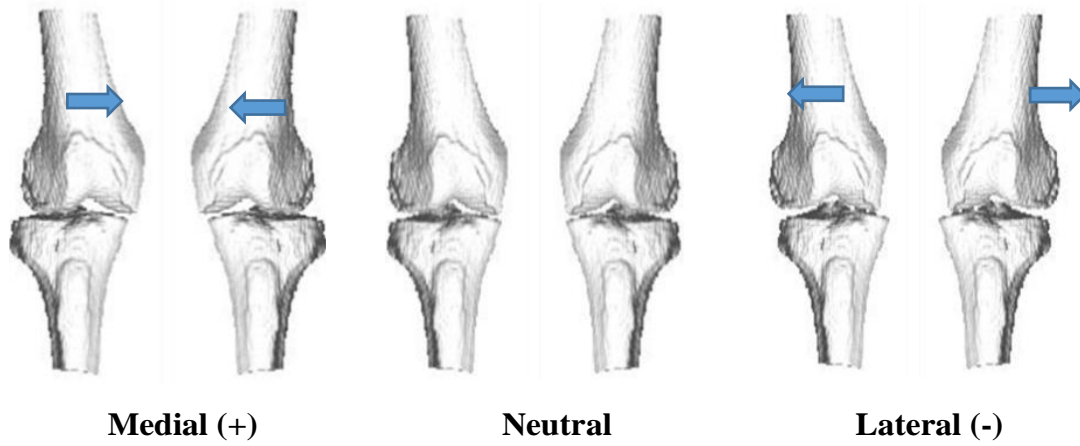
Figure 3-18. Medial/lateral position of femur <u>relative to the tibia</u>

Superior (+)   **Neutral**   **Inferior (-)**

Figure 3-19. Superior/inferior position of femur <u>relative to the tibia</u>

Anterior (+)   **Neutral**   **Posterior (-)**
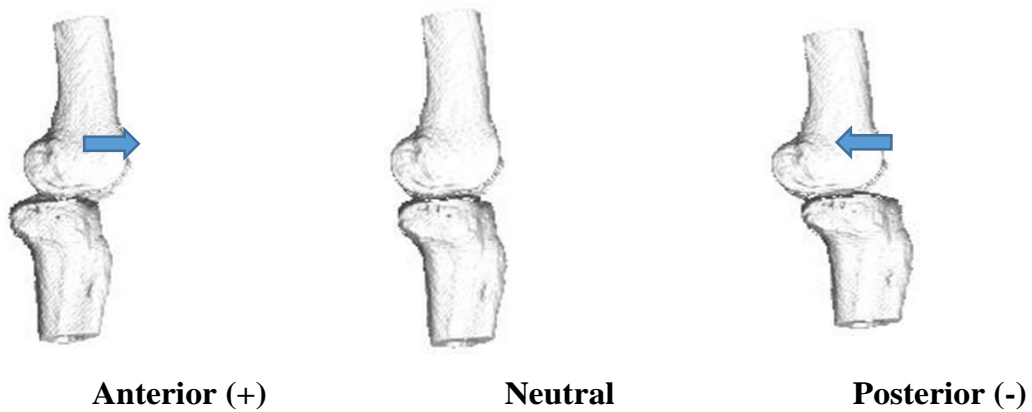
Figure 3-20. Anterior/posterior position of femur <u>relative to the tibia</u>

3.4.3   Kneeling Divided into Kinematic Phases

The kneeling task was divided into two phases: going into and coming out of flexion. Phase 1 (going into flexion) included all datapoints from the start in upright kneeling, starting with the hip above the knee at approximately 90° of flexion and finished at maximum flexion. Phase 2 (coming out of flexion) was the reverse. During the task, some participants did not move smoothly. This resulted in difficulty identifying the transition between phase 1 and phase 2 (Figure 3-21). In order to generate consistent phase endpoints, a phase-identifying algorithm was written in the 'R' statistical package (R Core Team, 2018). Briefly, this algorithm took the first derivative of flexion vs frame (time) and identified the frame number each time the derivative curve crossed zero indicating a change in direction. These points were used to determine the start and end of the phases (Figure 3-22). For this thesis, we are focusing on the 'into flexion' phase.
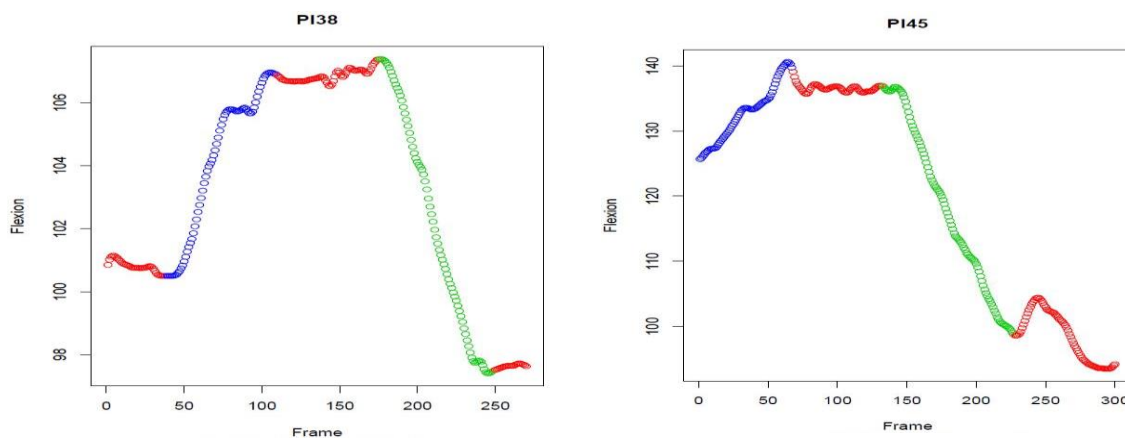
Figure 3-21. Examples from two participants with noisy flexion curves which made phase identification difficult without the phase-identifying algorithm.
Blue line indicates 'into flexion' phase; Green line indicates 'coming out of flexion' phase; red line indicates points outside these phases.
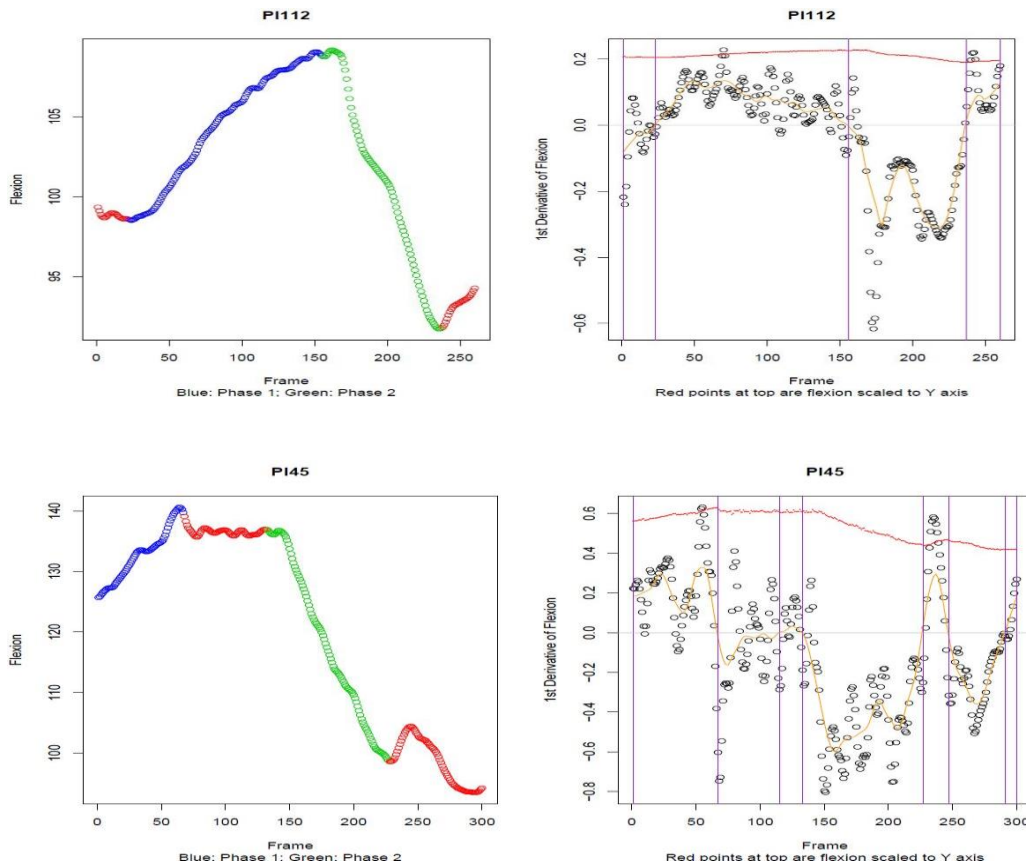
Figure 3-22. Example of phase determination.

Left figures are flexion vs frame. Blue line indicates into flexion phase; Green line indicates out of flexion phase; red line indicates points outside these phases. Right figures represent the 1st differential curve of flexion. Purple lines identify areas where curve crosses zero indicating change in direction.

3.4.4   Functional Data Analysis

Complex biomechanical data are typically described as a time-series or a function of another variable, encapsulating information about an entire movement or activity. Standard analysis techniques for describing and comparing knee kinematics typically focus on pre-defined features such as maxima, minima, specific values, and slopes (Kawashima et al., 2013; Kitagawa et al., 2010; Mochizuki et al., 2013; Zeighami et al., 2017). However, the use of discrete data points fails to describe the entire waveform. Appropriate statistical techniques

are therefore needed to manage these large and complex forms of data, allowing for the integration of biomechanics into applied contexts.

Functional Data Analysis (FDA) can be used to express kinematic waveforms arising from time-series data, as a function which can then be analysed using multivariate data analysis (PCA, t-tests). This has advantages over conventional multivariate statistical models as all data points are represented by functions and are allowed to correlate with each other (Warmenhoven et al., 2019b). Furthermore, FDA has the ability to detect: differences between groups, differences that exist over time, and the magnitude and meaningfulness of these differences (Park et al., 2017; Warmenhoven et al., 2017).

One particular FDA model of interest is bivariate principal component analysis (bfPCA). Similar to traditional principal component analysis, bfPCA uses dimension reduction to characterise the main sources of variability within a dataset (Warmenhoven et al., 2019a). However, this analysis is unique, in that it permits a better understanding of the interaction between different pairings of 6DOF variables (eg. angle vs flexion or displacement vs flexion) for different participants. bfPCA also provides various options for visualisation of differences between individuals for the different kinematic pairings (Warmenhoven et al., 2019a). Each kinematic variable can be displayed independently relative to time, or relative to another variable in the form of angle-angle diagrams (Harrison et al., 2007). It is particularly useful for deep knee flexion where there is not a common end point and therefore cannot be normalised to 100% of cycle which is typically seen in gait analysis (Deluzio & Astephen, 2007; Harding et al., 2012).

To accurately generate a bfPCA model, a number of steps are required. Initially, both variables of interest were temporarily normalised to 100% of the movement cycle in order to give all waveform in the dataset the same amount of data points (Figure 3-23- middle). An

initial moving median filter was passed over both datasets to remove any noisy spikes (Figure 3-23- right). These two sets of curves were then estimated as separate functions containing 100 points using a 4th order B-splines. The B-splines further smooth the curves by adding a roughness penalty to the fitting procedure. The roughness penalty term ensures that the smoothness of each fitted curve was controlled, and this was achieved by minimising the penalised residual sum of squares term.
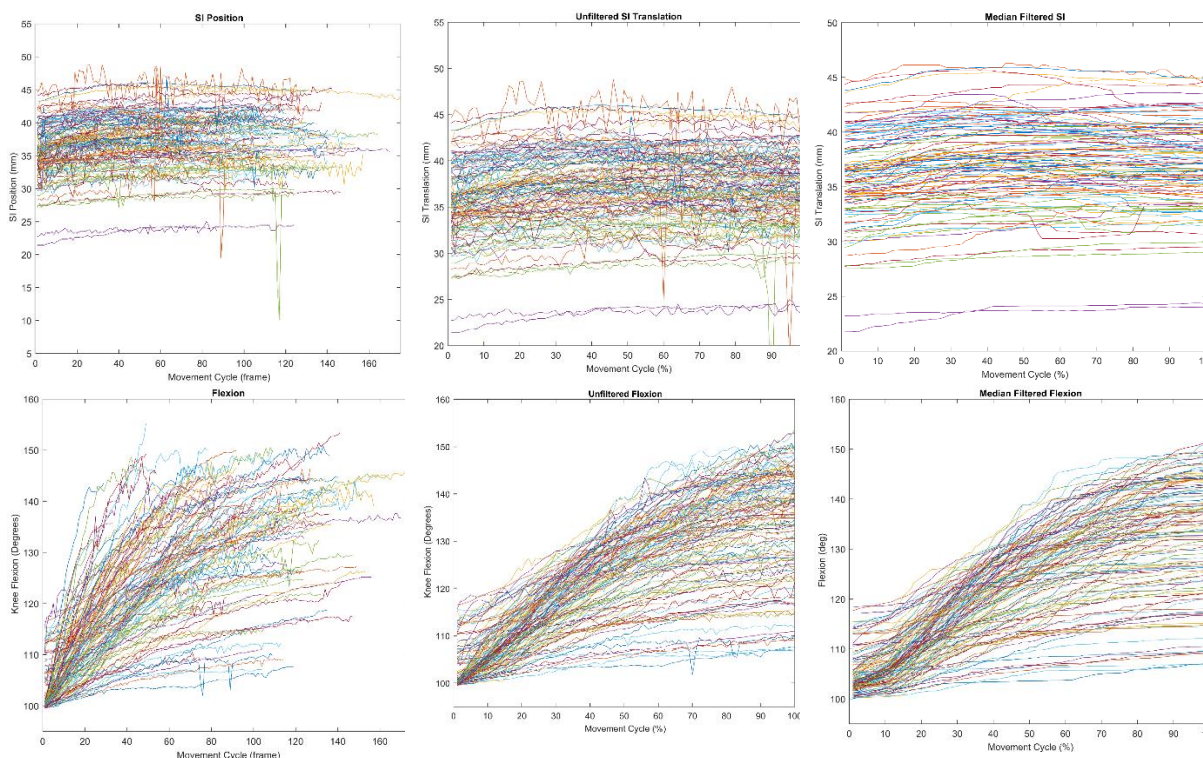
Figure 3-23: Representative kinematic waveforms of kneeling
Superior-inferior position (top) and Flexion (bottom) graphs as a function of time. Left: raw data un-normalised (represented per frame); Middle: raw data normalised to 100% of movement cycle; Right: smoothed with moving medial filter

Once normalisation and smoothing of data has taken place, bivariate functional principal components (*bf*PCs) were calculated by taking the first and second functions and concatenating them into a composite function (Warmenhoven et al., 2019a). A covariance function was then derived for this composite function, with a standard PCA process being applied to this composite function. Similar to conventional PCA, the scores or weights

retained for each bfPC were obtained for each bivariate function. Additionally, the bivariate functions representing each bfPC were reconstructed for visual inspection of the kinematic characteristics and variability. (Figure 3-24). Finally, the exported PC weights can be used with traditional multivariate data analysis statistics including group classifications and random forest regressions.
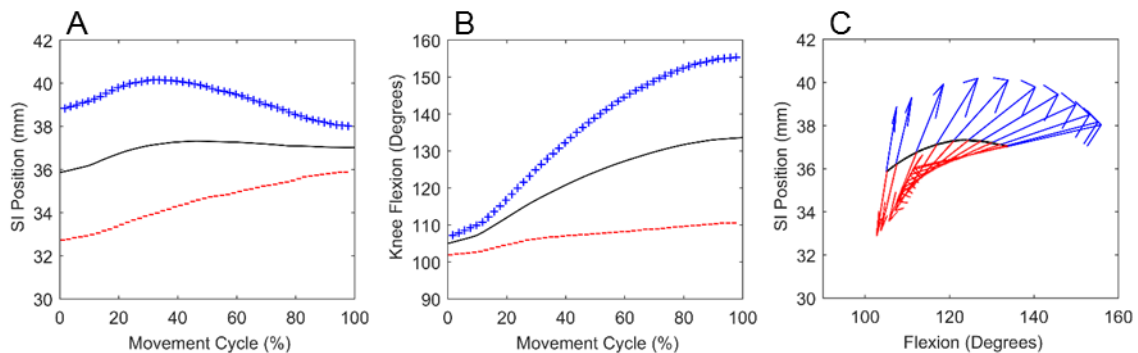
Figure 3-24: Representative bfPCA analysis.

bfPC1 can be visualised with each variable independently (A and B). Here, positive scorers are indicated by the '+' line in blue, and negative scorers the '−' line in red. bfPC1 is also visualised with both variables concurrently (C), where variability in each bfPC is indicated by the direction and size of the arrows away from the mean profile in each graph. In every profile the mean profile is plotted in solid black and the magnitude of the variability within bfPC1 has been scaled using a constant equivalent to +/− 2 SD of the bfPC scores. Note: SI= Superior-Interior translation measured in mm

3.5   Statistical Analysis

Regression analyses were performed to answer the questions posed in this thesis: A logistic regression model estimated the likelihood of bony shape distinguishing between OA and healthy knees (Study one); Random Forest Regression models were used to predict the influence of bony knee shape on kneeling kinematics (Study two) and; linear regression models were developed within a detailed analysis plan to compare the differences in kneeling

kinematics as a function of implant design (Study four). These techniques are described below.

3.5.1 Logistic Regression (Chapter Four)

A binary logistic regression model was used to determine the shape parameters which best discriminated between OA and healthy knees in chapter four. Logistic regression is used to model the probability that a given set of data fall into a certain binary class/group (*i.e.* OA vs healthy). This is accomplished by creating a logit function using maximum likelihood estimation to predict group membership. The model constructed for this study included Group (OA and healthy) as the dependent variable, shape mode as the independent variable and BMI, sex and age as covariates. Shape principal components (modes) were added in a forward stepwise fashion until there was no more statistically significant improvement in the fit of the model. Principal components (modes) which best distinguished between OA and healthy shapes, along with their corresponding coefficients and odds ratios, were reported.

3.5.2 Random Forest Modelling (Chapter Five)

Random forest regression modelling was used to determine which bony shapes could predict kinematics in Chapter five. Random forest regression is a type of supervised machine learning based on multiple decision trees (Breiman, 2001). Each tree was created by selecting a subset of the input parameters and running them through a decision tree to obtain a prediction for each sample. This process was repeated 100 times using different subsets of the data to generate a forest. By using this procedure, called bagging, different trees are assigned different training parameter sets. This process is unbiased as the prediction for each sample is based on trees built on trees which do not contain that sample (out-of-bag error). If a feature has poor predictive ability it will not appear in any nodes of the trees comprising the forest. However, if a feature is highly predictive it will not only appear in several trees, but will also

have a tendency to appear in nodes that are more close to the root. The final predicted regression value is obtained by averaging the regression values of all of the random trees (Breiman, 2001). Predicted values are compared to actual values to determine prediction error.

In this thesis, tibiofemoral shape modes, group, BMI and sex were included as predictors in all the random forest models. Separate models were created to predict the normalised weights for all kinematic bfPCA models as well as maximal flexion. Each model's performance was assessed by partitioning the data into training (70%), validation (15%) and testing (15%) datasets. These percentages were selected to produce a stable model and one that would not overfit the data. The training dataset was used for initial fitting of the parameters in the model. The validation dataset was used for evaluating the fit of the training model and to tune the parameters in the model. Finally, the testing dataset was used to evaluate the final fit of the model. Results for each model were reported in terms of predictor importance, variation explained by the model (R^2), correlations between predicted and actual data, root-mean-squared error (RMSE) and normalised RMSE (NRMSE). NRMSE was defined as RMSE divided by the difference between the maximum and minimum observed values and expressed as a percentage. Finally, associations between important shape predictors and kinematics were visualised using scatterplots with associated R^2 values.

3.5.3   Randomised Clinical Trial Statistical Plan (Chapter Six)

A detailed statistical analysis plan to address the aims of chapter six was completed prior to analysis of the RCT in order that a blinded analysis could be undertaken. An independent statistician (Dr Teresa Neeman PhD) blinded to the group assignments performed all of the analyses. All analyses were carried out using the Intention-to-Treat principle using two year follow-up data where it was available and if not, one-year data were brought forward.

3.5.3.1 Description of Dataset

Each kinematic variable was expressed as a function of knee flexion in 5° increments. This was achieved by calculating the mean of all values within data bins at 90°, 95°, 100°, 105°, 110°, 115°, 120°, 125°, 130°, 135°, 140° of knee flexion. The bins surrounded the flexion value by ±2.5°. For example, data from between 112.5° to 117.5° flexion was used to calculate the mean value of a kinematic variable described at 115° of flexion. The range of each of the kinematic variables was calculated as the difference from the mean 90° value and maximal flexion.

3.5.3.2 Data Extrapolation

There were 36 participants who did not start the kneeling task at 90° of knee flexion and so backward extrapolation of this missing kinematic data was required to have a dataset that could be compared. This was achieved using the travelling salesman problem (TSP) algorithm (Lawler et al., 1985). This algorithm used the kinematic curves with complete data (*i.e.* curves which contained kinematic values starting at 90°) to predict the missing values at 5° flexion intervals for the curves that were missing data. Briefly, the TSP algorithm achieves the most likely interpolation of the missing data by determining the best fit for the data-deficient curve within the dataset. The TSP algorithm essentially orders the curves using least to greatest differences in root-mean-squared errors (RMSE) and then the missing data can be imputed from the curves which are most similar.

A leave-one-out (LOO) cross-validation was performed to assess the ability of the TSP algorithm to predict the kinematic values of a new participant from outside of the training set. In each of the iterations, one curve containing complete data for one participant was left out from the development model. The model, based on the remaining curves, was then used to predict the kinematic values for the left-out participant. Separate TSP algorithms were

performed for each variable. Results for each TSP model, comparing the actual and predicted data, were reported in terms of RMSE for 5 incrementally increasing intervals starting at 90° to 124° (Table 3-4).

Table 3-4: Prediction errors from the Travelling Salesman Problem Algorithm for 5 missing flexion intervals from 90°. Errors are reported as root-mean-square error (RMSE). The number of participants who were missing data in each interval are reported

Flexion Interval Missing (°)	Number of Participants	Abduction-Adduction (°)	Internal-External Rotation (°)	Superior-Inferior Position (mm)	Mediolateral Position (mm)	Anterior-Posterior Position (mm)
5	14	0.30	0.58	0.42	0.33	0.80
10	11	0.35	0.68	0.4	0.42	1.30
15	8	0.40	0.95	0.39	0.63	1.17
20	1	0.48	1.42	0.48	0.75	1.17
25	1	0.64	1.40	0.70	0.87	1.31

3.5.3.3 Baseline and Demographic Data

Continuous baseline demographic data (age, body mass, height, BMI) as well as baseline PROMS (Oxford Knee Score, VAS Pain) were summarised using means and SD for each randomised group. Categorical baseline data (sex, operated side) were summarised using frequencies and percentages within each randomised group. Baseline data were summarised in tabular form.

3.5.3.4 Statistical analysis of Primary and Secondary Outcomes

All analyses were carried out using the statistical software package R v3.6.1 (R Development Core Team, 2019). Mean kinematic ranges for the six degree of freedom (including flexion), kinematics at maximal flexion, VAS Pain, VAS satisfaction and Oxford Knee Scores were compared between the three groups using linear regression models (the *lm* function in R), adjusting for BMI, sex and age. A linear regression is one of the most common statistical

tools available and is used to understand if there is a relationship between two or more variables. Specifically, it is used to determine the strength of a linear relationship between a continuous dependent variable Y (mean kinematic ranges) and one or more independent variables X (group, BMI, age, sex). Based on the results of these models, the adjusted means and confidence intervals were reported. The p-value indicating evidence for overall group differences was reported (*anova* function in R). Post-hoc pairwise comparisons were made to test for difference between group using the Tukey method (*emmeans* function in R).

Average positional kinematics at 10° intervals were compared between the three groups using a mixed effect linear regression (the *lmer* function in the lmerTest package in R), with flexion*Group, BMI, sex and age as fixed effects and subject ID as the random effect. A mixed effect linear regression is an extension of linear regression which allows both fixed and random effects to be modelled. This type of regression is particularly useful when there is non-independence in the data (i.e. repeated measure data). Based on the results of these models, the adjusted means and confidence intervals were reported. The p-value, indicating evidence for overall group differences, was reported (*anova* function in R). We also indicated, where relevant, whether the group effect depended upon the flexion angle (group by flexion interaction). Post-hoc pairwise comparisons were made to test for difference between group using the Tukey method (*emmeans* function in R).

4 Statistical Shape Modelling Reveals Large and Distinct Subchondral Bony Differences in Osteoarthritic Knees

This thesis is submitted as a Thesis by Compilation in accordance with

https://policies.anu.edu.au/ppl/document/ANUP_003405

I declare that the research presented in this Thesis represents original work that I carried out during my candidature at the Australian National University, except for contributions to multi-author papers incorporated in the Thesis where my contributions are specified in this Statement of Contribution.

Title: Statistical shape modelling reveals large and distinct subchondral bony differences in osteoarthritic knees

Authors: Lynch, Joseph T., Schneider, Marco T.Y., Perriman, Diana M., Scarvell, Jennie M., Pickering, Mark R., Asikuzzaman, Md., Galvin, Catherine R., Besier, Thor F., Smith, Paul N.

Publication outlet: Journal of Biomechanics

Current status of paper: Published

Contribution to paper: JTL: research design, acquisition, analysis and interpretation of data, drafting and critically revising the paper; MTYS: interpretation of data, data analysis, drafting and critically revising the paper; DMP: research design, analysis and interpretation of data, critically revising the paper; JMS: research design, analysis and interpretation of data, drafting and critically revising the paper; MA: interpretation of data, data analysis, drafting and critically revising the paper; MRP: research design, analysis and interpretation of data, critically revising the paper; CRG: acquisition, analysis and interpretation of data, drafting and critically revising the paper; TFB: interpretation of data, drafting and critically revising the paper; PNS: research design, interpretation of data, drafting and critically revising the paper. All authors have read and approved the final submitted manuscript.

Senior author or collaborating authors endorsement: _____

Joseph Lynch   25/06/20
Candidate – Print Name   Signature   Date

Paul N Smith   25/06/20
Primary Supervisor – Print Name   Signature   Date

Dr Diana Perriman   25/06/20
Delegated Authority – Print Name   Signature   Date

FIRST STUDY

4.1 Abstract

Knee osteoarthritis (OA) results in changes such as joint space narrowing and osteophyte formation. Radiographic classification systems group patients by the presence or absence of these gross anatomical features but are poorly correlated to function. Statistical-shape modelling (SSM) can detect subtle differences in 3D-bone geometry, providing an opportunity for accurate predictive models. The aim of this study was to describe and quantify the main modes of shape variation which distinguish end-stage OA from healthy knees. Seventy-six patients with OA and 77 control participants received a CT of their knee. 3D models of the joint were created by manual segmentation. A template mesh was fitted to all meshes and rigidly aligned resulting in a set of correspondent meshes. Principal Component Analysis (PCA) was performed to create the SSM. Logistic regression was performed on the PCA weights to distinguish morphological features of the two groups. The first 7 modes of the SSM captured >90% shape variation with 6 modes best distinguishing between OA and healthy knees. OA knees displayed sub-chondral bone expansion particularly in the condyles and posterior medial tibial plateau of up to 10 mm. The model classified the two groups with 95% accuracy, 96% sensitivity, 94% specificity, and 97% AUC. There were distinct features which differentiated OA from healthy knees. Further research will elucidate how magnitude and location of shape changes in the knee influence clinical and functional outcomes.

4.2 Introduction

Osteoarthritis (OA) is a disease that involves the breakdown of cartilage and underlying bone resulting in pain and altered joint dysfunction (Arthritis Australia, 2014; Australian Commission on Safety and Quality in Health Care, 2017). In Australia, OA is estimated to affect 8.1% (over 2 million) of the population and costs Australia over $3.2 billion per year (Arthritis Australia, 2014). The response to this disease has been an increase in total knee replacement (TKR) which, given the projected increase in average population age and obesity, is likely to become financially unsustainable (Abhishek & Doherty, 2013). Outcomes of TKR are variable, with up to 20% of patients reporting dissatisfaction following their operation (Bourne et al., 2010). Therefore, the importance of deepening our understanding of OA and the role of joint replacement versus other interventions in disease progression and amelioration has become more urgent.

Bony knee shape is changed in OA but clinical imaging data is not well correlated with pain and function (Barr et al., 2015). The clinical diagnosis of osteoarthritis can be made from the history, symptoms and signs alone (Abhishek & Doherty, 2013), but the severity of the disease is commonly determined from visualising tissue morphologic changes on imaging (van Manen et al., 2012). Bone is normally imaged with 2D plain x-ray (Kellgren & Lawrence, 1957) or computed tomography (CT) (Chan et al., 1991) while Magnetic Resonance Imaging (MRI) is also used to help clinicians assess soft tissue damage and further understand the degree of disease severity (Hunter et al., 2011). The appearance of an osteoarthritic knee is highly variable with differing amounts of condylar squaring (Fairbank, 1948), tibial flattening and widening (Ding et al., 2007), joint space narrowing, and osteophyte formation (Kellgren & Lawrence, 1957). These changes give each osteoarthritic knee its own unique bony shape. However, people with OA knee present with different levels of pain and functional limitation regardless of their imaging findings (Hunter et al., 2013). It

is probable that simple visual inspection of clinical imaging is insufficient to detect the subtle changes associated with pain and dysfunction. Advancements in both medical imaging and computational modelling allow for analysis of the entire shape of joints in a way that clinical imaging assessments cannot. These techniques offer an avenue for objectively classifying shape due to OA in order to evaluate associations with symptoms and progression.

Statistical Shape Modelling (SSM) precisely characterises complex shapes by grouping coincident shape parameters using Principal Component Analysis (PCA). PCA decomposes shapes into a set of discrete components, or modes, which describes the main ways in which the shape varies across the population (Cootes et al., 1992; Dryden & Mardia, 1998). The modes can then be compared to detect what shape features are different between cohorts (Agricola et al., 2015; Pavlova et al., 2017; Schneider et al., 2015, 2018). Additionally, SSM allows for the analysis of specific associations between regional anatomy and parameters such as kinematics and joint contact mechanics (Schneider et al., 2017), which are known to be affected by OA. This method differs from current clinical measurement strategies because it is not limited by *a priori* assumptions and systems. Instead, the patterns and relationships are permitted to emerge from the data. In this way associations between shape and other important determinants of function and wellness can be interrogated.

Bone shape has been found to differentiate between OA and healthy knees, but 3D regional anatomical differences have not been systematically explored. Research describing changes in the knee using SSM have identified whole joint subchondral bone-shape as a possible biomarker for differentiating between healthy and osteoarthritic knees (Barr et al., 2016; Bredbenner et al., 2010; Haverkamp et al., 2011; Neogi et al., 2013). Bredbenner *et al.* conducted a landmark study using a longitudinal image database which demonstrated that people with OA knees had observable shape characteristics prior to symptom development. These included a slight expansion of the posterior and distal condylar surfaces and spreading

and depression of the tibial plateau. Further, Bredbenner *et al.* quantified the magnitude of these changes using SSM. This study was crucial because it demonstrated that shape is an important factor in the development of OA. Other researchers have proceeded to identify specific shape characteristics of symptomatic OA knees. Specifically, the femur displays widening and flattening of the femoral condyle, expansion around the cartilage plate and narrowing of the intercondylar notch (Barr et al., 2016; Bowes et al., 2015; Neogi et al., 2013). The tibia is described as having an "elevated" lateral plateau, a reduction in the space between tibial spines and increase in bone area most prominent along the perimeter of the bone (Bowes et al., 2015; Haverkamp et al., 2011). Although the tibia has been described as undergoing uniform changes in OA (Barr et al., 2016), these claims are apparently unsubstantiated with actual data. While we know that bony shape differentiates the OA knee from the healthy knee (Barr et al., 2016; Haverkamp et al., 2011; Neogi, 2012; Neogi et al., 2013; Shepstone et al., 2001), we don't yet know which regional anatomic features are the most important when differentiating end-stage OA from healthy. Nor do we know the magnitude of these changes. Therefore, the aim of this study was to describe and quantify the main modes of shape variation which distinguish end-stage OA from age- and sex-similar healthy knees.

4.3 Participants and Methods

4.3.1 Participants

The participants in this study were recruited as part of a larger randomised controlled trial of knee replacement designs with age- and sex-similar healthy control participants (ISRCTN75076749). The OA group included 76 patients who were awaiting TKR for OA. The healthy group (N=77) were included if they were pain free with no history of lower limb

pathology. Participants included 52% and 56% females in the healthy and OA group, respectively and were similar in age (mean 67.6 and 66.8 years, respectively) (Table 4-1). All participants provided written consent and ethics approval was granted by the Australian Capital Territory Health and the Australian National University human research ethics committees.

Table 4-1: Patient Demographics for Statistical Shape Modelling

Participant characteristics	Healthy	Osteoarthritis
N	77	76
Age (years)	67.6 ± 10.81	66.8 ± 9.17
Number of females (%)	40 (52%)	43 (56%)
Left Sided Knees (% L)	36 (47%)	36 (47%)
N by KL Grade: 0-1-2-3-4	35-30-9-3-1	0-0-1-23-52
Height (cm)	167.8 ± 9.73	169.3 ± 9.74
Weight (kg)	70.2 ± 12.78	89.2 ± 19.04
BMI (kg.m^2)	24.9 ± 3.85	31.0 ± 5.37

Note. KL – Kellgren Lawrence grade; BMI – Body Mass Index

4.3.2   Data Collection

Participants received a 3D-spiral CT scan (Toshiba Medical Systems, Ōtawara, Japan) of the knee with a field of view of at least 150mm above and below the tibiofemoral joint line. The OA knees were selected based on which knee was being operated on. If the surgery was a bilateral TKR, then the participant selected their worst knee. The side used in the healthy group was matched to the OA group. Slice thickness was 1mm with a resolution of 512 x 512 voxels with spatial dimensions 0.625 x 0.625 x 0.5mm^3 and 16 bits/pixel.

4.3.3   Image processing

The femur and tibia were isolated from the CT scan images by manual segmentation using custom software (Orthovis v4 Matlab, The Mathworks, Inc., Natick, MA). Manual

segmentation is more precise that automatic because it allows the operator to include

individual features like osteophytes. Intra- and inter-rater variations of the calculated volumes

for the femur were 0.99 and 0.84, and for the tibia 0.98 and 0.77 respectively. Three-

dimensional coordinate systems for the femur and tibia were established using standard

referencing convention defined by Grood and Suntay (Grood & Suntay, 1983). Orthogonal

references frames were established based on individual anatomical locations for each tibia and

femur in the dataset. Origins were set for the femur at the most proximal point of the

intercondylar notch and, for the tibia, at the mid-point of the tibial spines.

Following axis selection, each model was cropped to allow proportional sizing. Using the

anterior/posterior projection of the CT, the femur was cropped at 1.5X the distance from the

distal femoral condyles to the adductor tubercle. The tibia was cropped 1.5X the distance

from the most proximal aspect of the tibial spine to the most inferior point of the superior

tibiofibular joint (Figure 4-1). Corresponding femurs and tibias were recombined using a

custom Matlab script to create a tibiofemoral joint for each participant. The tibia and femur

were not considered separately because of their shape co-dependence. Variations in alignment

were controlled for by aligning the femur and tibial meshes so that their axes were orientated

at zero degrees of rotation and translation. The 3D models were exported as meshed surfaces.

Knee models were down sampled to 30,000 vertices, and smoothed using a Laplacian filter

(MeshLab 2016.12, http://meshlab.sourceforge.net). For consistency, left-side meshes were

mirrored so they appeared as right-sided. These combined tibiofemoral meshes were used in

the SSM for consistency. Meshes from both osteoarthritic and healthy groups were combined

in order to create one SSM.
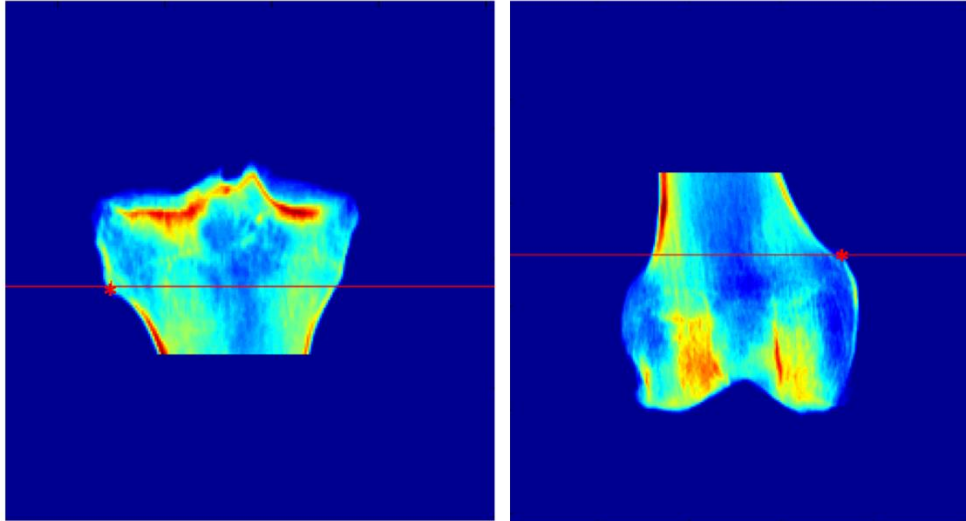
Figure 4-1: Cropping locations for femur and tibia.

The tibia was cropped at the superior tibiofibular joint (*) and the femur was cropped at the adductor tubercle (*)

4.3.4 Statistical Shape Model Generation

The technique implemented for this study was based on previous methods (Schneider et al., 2015; Zhang et al., 2014). Firstly, a template mesh was created using a series of radial basis functions to parameterise the tibiofemoral joint (Zhang et al., 2018). This template was based on a single mesh from one knee in the dataset. This template was iteratively fit with a series of coarse to fine fits to all meshes in the dataset, which resulted in maximum correspondence between meshes. Corresponding meshes were then rigidly aligned, using a partial Procrustes analysis which minimised the least-squared distances of corresponding points (Gower, 1975). This allowed for only the shape and scaling variability to be included in the model.

Principal Component Analysis (PCA) was then run on the nodal coordinates of the aligned meshes to create a shape model. PCA is used for dimension reduction which allows any shape in the dataset x to be approximated as the sum of the mean shape $\bar{x}$ plus the weighted sum of the principal components ϕ (Heimann & Meinzer, 2009; Schneider et al., 2015):

$$x = \bar{x} + \sum_{i=0}^{n} \omega_1 \phi_1$$

Where n is the number of principal components needed to explain 90% of the total variation in the population. Therefore, the shape of each bone was described by n principal component (PC) weights, ω, where ω are the amount of variation along an individual principal component.

Following visual inspection of each mesh to ensure the basic shape was correct, the fitting process was repeated using the mean shape as the template. Following this, the fitting process was further refined for individual shape differences by incorporating PCA fitting using the previous statistical shape model generated from the dataset. In this way, the shape model was optimised by propagating fitting correspondence across the dataset to an RMS error of 0.89 mm. A final PCA was performed to generate a statistical shape model which generated the PC weights used in the subsequent analysis. The tibiofemoral PC weights were extracted for each subject from each shape model for logistic regression. Mode weights were normalised to z-scores for consistency and outliers were truncated to 2.5 SD.

4.3.5   Statistics

Binary logistic regression modelling was used to determine the shape parameters which best discriminated between OA and healthy knees (SPSS v25, SPSS Inc., Chicago, Illinois). The model included BMI, sex and age. The model added principal components in a stepwise fashion until there was no more statistically significant improvement of the fit of the model. Principal components which best distinguished between OA and healthy shapes, along with their corresponding coefficients and odds ratios, were reported. Pointwise distances were calculated and visualised to compare anatomical differences between the reconstructed mean-OA and mean-healthy knees. Furthermore, pointwise distances were also calculated for the

reconstructed principal components which best distinguished between OA and healthy. These differences were reported as plus and minus 2 standard deviations away from the mean shape and expressed in millimetres (mm) and percentages in order to quantify the differences between OA and healthy for the entire population.

The effectiveness of the SSM to distinguish between OA and healthy knees was evaluated using a leave-one-out cross validation to generate area under the receiver operator characteristic (ROC) curve (AUC), with sensitivity, specificity, classification accuracy, and positive and negative likelihood ratio (IBM SPSS Modeller for Windows, version 18.2, IBM Corp., Armonk, N.Y., USA).

4.4 Results

The first seven principal components of the combined end-stage OA and healthy SSM accounted for 90% of the total variance in knee joint morphology (Figure 4-2). The variation explained in the entire model by each mode ranged from 77.04% for mode one to 1.23% for mode 7. As expected, since we did not control for scaling, mode one explained the isometric sizing component of the model (Bredbenner et al., 2010; Schneider et al., 2018).
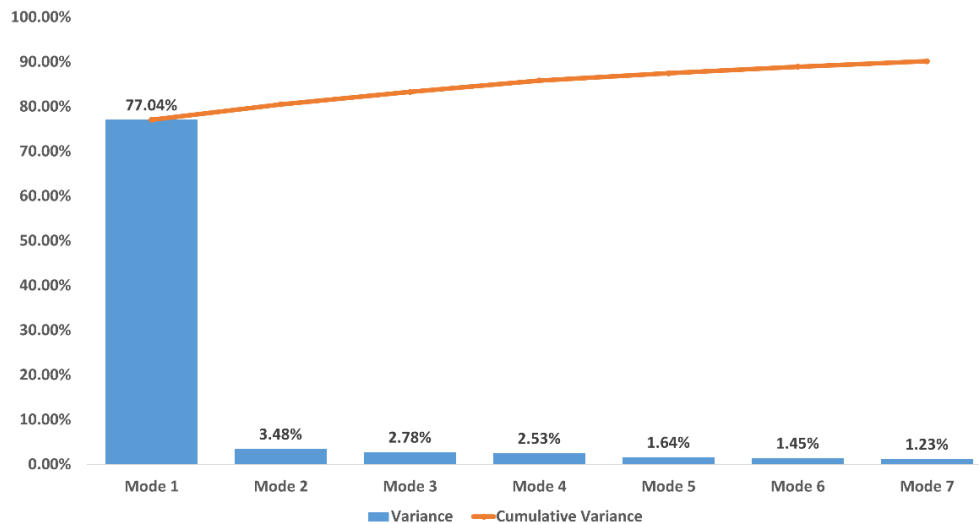
Figure 4-2: Individual and cumulative variation explained by the statistical shape model

Logistic regression results showed that a combination of BMI and 4 modes of variation significantly distinguished between OA and healthy joints (p<0.05). Table 4-2 describes the odds ratios for significant predictors. The model displayed a leave-one-out accuracy of 94.8%, 96.0% sensitivity, 93.7% specificity, 97.0 area under ROC curve, 15.16 positive-likelihood ratio, and 0.04 negative-likelihood ratio.

Table 4-2: Logistic Regression output

Modes of shape variation which significantly differentiate OA from healthy groups

	Mean ± Standard Deviation					
	Healthy (n=77)	OA (n=76)	Coefficient	OR (95% CI)	Sig	Outliers
BMI	24.9 ± 3.85	31.0 ± 5.37	0.42	1.5 (1.1, 2.0)	0.01	5
Mode 1	-0.22 ± 0.92	0.23 ± 1.04	2.39	10.9 (2.2, 53.1)	p<0.001	4
Mode 2	-0.49 ± 0.68	0.49 ± 1.03	6.01	405.8 (14.7, 11205.3)	p<0.001	4
Mode 5	-0.42 ± 0.82	0.43 ± 0.99	4.69	108.9 (7.6, 1554.7)	p<0.001	4
Mode 6	-0.34 ± 0.79	0.34 ± 1.07	4.24	69.2 (5.6, 860.0)	p<0.001	3
Constant	-	-	-9.58	-	0.02	-

Note. OR = odds ratio; CI = confidence interval; Sig = p values of individual predictors

A comparison of the mean differences between OA and healthy knees provided a summary of the modal differences. These included expansion of the femoral cartilage plate extending anteriorly, medially and laterally (Figure 4-3). Posteriorly, there was a large area of bony expansion on the proximal femoral condyle approximately, which equated to an increase of approximately 5 mm (115%) in height compared to healthy knees. On the tibial surface, both medial and lateral plateaus appeared slightly depressed and there was an area of bony expansion on the medial aspect of the tibia extending posteriorly and finishing in a tubercle on the posterior medial plateau which was 3mm larger in the OA knee compared to healthy.
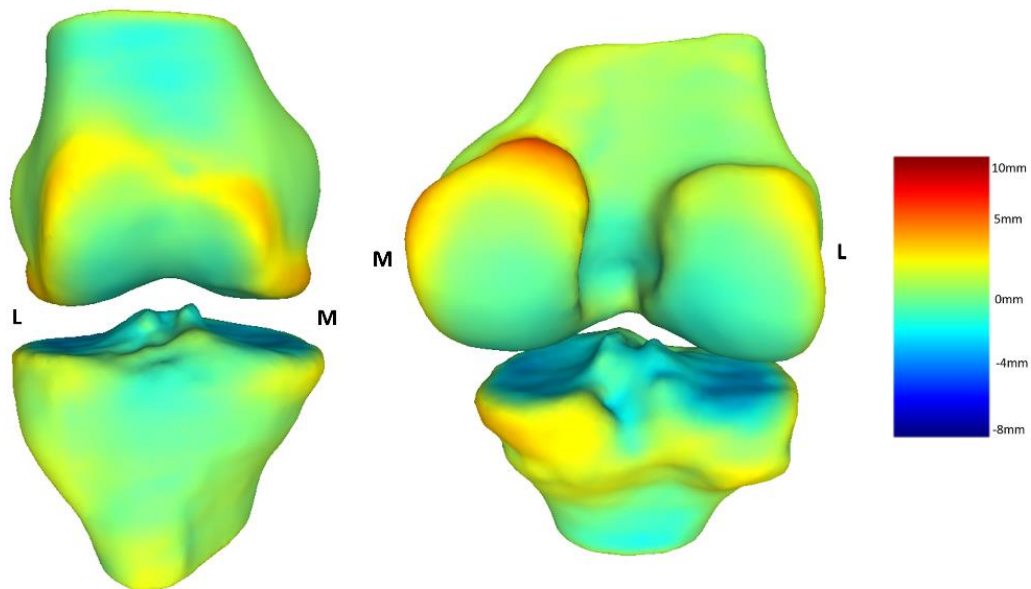
Figure 4-3: Pointwise differences in surface geometry of the reconstructed mean-OA knee relative to mean-healthy knees.
Left: anterior view; right: posterior-superior view. Knees displayed as right sided.
Heat map indicates the extent of the variation in the local anatomy. M= Medial; L= Lateral

Mode 2 described 3.48% of the anatomical variation within the model. Visually, this component represented large regional differences in the anterior femoral cartilage plate

extending posteriorly along the medial and lateral borders (Figure 4-4c). Posteriorly, this mode described an area of bony expansion on the medial condyle resulting in a reduced intercondylar fossa (Figure 4-4d). Tibial differences included expansion of the posterior-medial aspect of the tibial border, causing narrowing of the posterior intercondylar fossa (Figure 4-4b). Finally, mode 2 described a region of expansion within the proximal tibiofibular joint (Figure 4-4a).

Mode 5 explained 1.64% of the anatomical variation and described changes in the height of the tibial plateau and spines (Figure 4-5a); and a region of large bony expansion on the proximal aspect of the posterior medial condyle which differed 10mm from healthy femurs (Figure 4-5b).
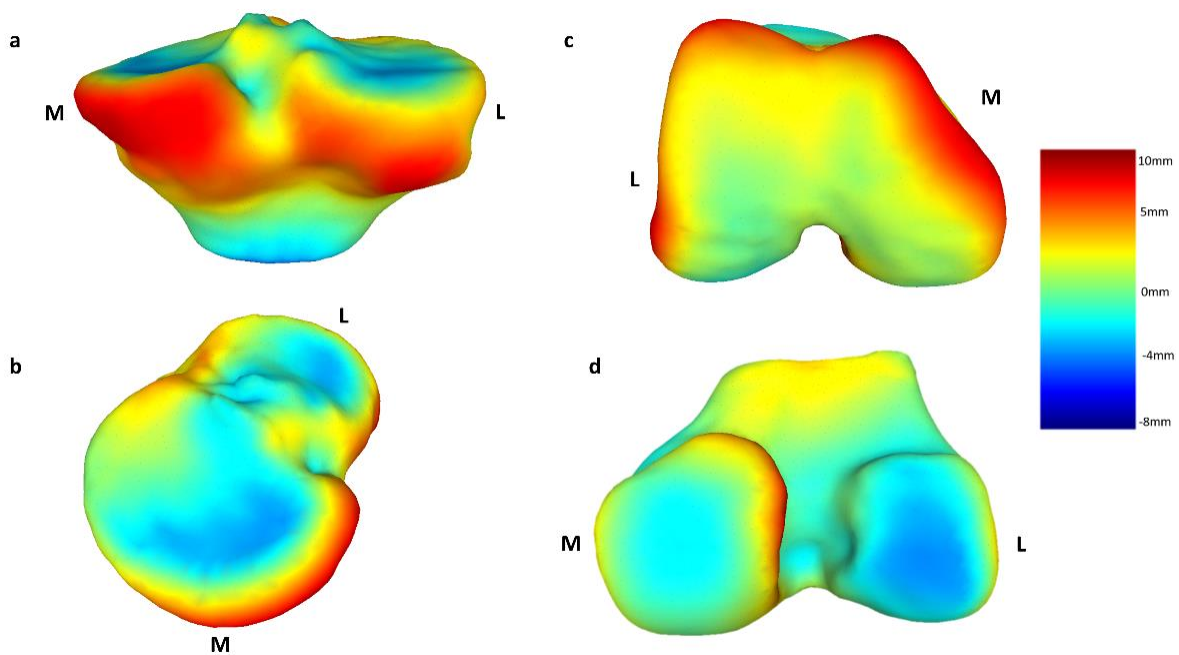
Figure 4-4: Pointwise differences in surface geometry of OA knees relative to healthy knees using mode 2 weightings.
a) posterior view of tibia; b) anterior medial view of tibia; c) femoral articular surface view; d) posterior view of femur. Heat map indicates the extent of the variation in the local anatomy measured at plus and minus two standard deviations away from the mean shape for the population. M= Medial; L= Lateral

Mode 6 (1.45% explained variance) described unique bony shape differences between OA and healthy knees. Specifically, the most prominent feature was a tubercle on the perimeter of the posterior medial tibial plateau (Figure 4-5c). Further differences were detected within the medial femoral cartilage plate and on the medial aspect of the lateral femoral condyle (Figure 4-5d).
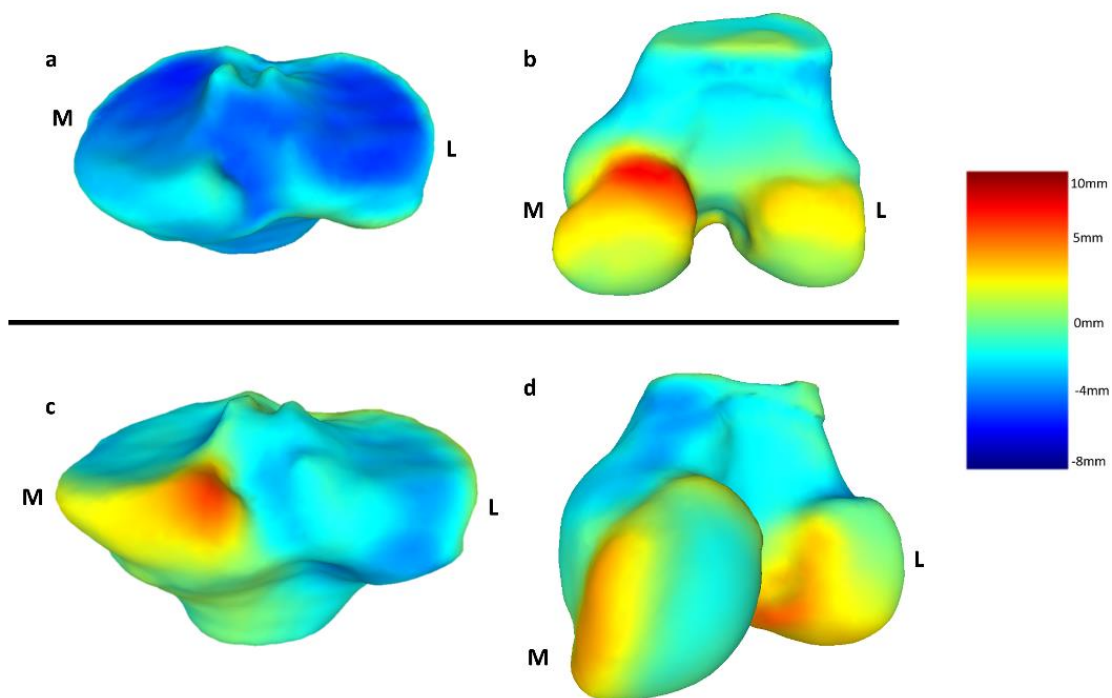
Figure 4-5: Pointwise differences in surface geometry of OA knees relative to healthy knees for mode 5 (upper) and mode 6 (lower).
a) posterior view of tibia; b) posterior femur; c) posterior view of tibia; d) posterior-medial view of femur. Knees displayed as right sided. Heat map indicates the extent of the variation in the local anatomy measured at plus and minus two standard deviations away from the mean shape for the population. M= Medial; L= Lateral

4.5 Discussion

The purpose of this study was to identify unique bony shape features which distinguish between end-stage OA and healthy knees using statistical shape modelling (SSM). This is the first study to quantify the extent of the bony changes which occur in end-stage OA knee. The

main finding was that OA knees displayed bony expansion at the edges of the OA tibial and femoral cartilage plates which were up to 10 mm (190%) larger than healthy controls (Figure 4-4). Furthermore, we found a postero-medial tibial tubercle that was 6 mm (115%) larger than healthy tibias (Figure 4-5c) with a corresponding posterior-medial condylar expansion which was up to 10 mm (190%) larger than healthy femurs (Figure 5b). This may explain the difficulty people with OA knee have in achieving full flexion. Additionally, we found that shape features captured by the model could distinguish between healthy and OA knee shapes with an accuracy of 94.8%. Finally, combining the shape model with logistic regression allowed for the identification of the different shape arrays which characterise OA knees.

There are a number of femoral features which distinguish OA from healthy shapes. These features are regions of bony expansion, with pointwise differences of up to 10 mm (190%), extending throughout the femoral cartilage plate and the femoral borders. Specifically, these changes were the greatest anteriorly, medially, and on the proximal aspect of the posterior-medial condyle. While these changes are similar to those reported in the literature, our study is the first to quantify the potential extent of bony expansion between OA and healthy knees (Barr et al., 2016; Bowes et al., 2015; Neogi et al., 2013). Additionally, there is reduced space within the intercondylar notch which is caused by the expansion of the bone on the medial and lateral condyles of the femur. Several studies have reported similar changes to the intercondylar notch in OA knees noting the increased presence of osteophytes seen on MRI (Chen et al., 2016; Sasho et al., 2017; Shepstone et al., 2001). Flattening of the posterior femoral condyles, particularly the lateral condyle, was observed indicating increased levels of bone remodelling (Matsuda et al., 2004). Therefore, the distal femur in our OA cohort was characterised by significant cartilage plate expansion, a reduced intercondylar notch and flattened condyles.

The tibia demonstrated its own distinct pattern of osteoarthritic changes. Mode 6 describes a large bony tubercle on the posterior-medial plateau of the osteoarthritic tibia which deviates by up to 6 mm (115%) larger than healthy knees. This tubercle has been reported only once previously when Neogi observed it as part of an SSM but did not comment on its significance (Neogi et al., 2013). The fact that it is not commonly reported in relation to OA knee shape is perplexing but may be due to it being occluded on 2D x-ray or missed in MRI slice selection. This tubercle appears to lie under the posterior horn of the medial meniscus. The meniscus is regularly reported as torn in patients undergoing a TKR and the subchondral-bone changes are possibly a result of increased levels of contact stresses which are seen in the medial compartment (Thambyah et al., 2005). Modes 2 and 5 describe changes to the anterior, medial, and posterior borders of the proximal tibia. Previous studies report an overall increase in cross-sectional area of an osteoarthritic tibial plateau (Barr et al., 2014; Wang et al., 2005; Wluka et al., 2005). Our study provides much more specific data and indicates that the expansion is not in the overall size, but is caused by some distinct regional changes.

The parameter within the model which explained the most variation in the SSM was mode 1 and was knee size. Additionally, OA knees were slightly larger than healthy. This finding has been described previously where OA knee size was found to significantly increase over 12 months (Hudelmaier & Wirth, 2016). The authors suggested that increased BMI might be the driver for this increase in knee size. BMI was also a significant distinguishing factor in our model. This was expected due to the fact that the OA group was heavier and increased weight is a known risk factor for knee OA. Although we don't understand the reason for the relative increase in size in the OA group given that osteophytic changes aren't captured in this mode, it is possible that the increase in size is a result of the difference in BMI between the groups.

The interplay between femoral and tibial geometry may play a role in tibiofemoral kinematics (Freeman & Pinskerova, 2005; Pinskerova et al., 2009; Smoger et al., 2015). Osteoarthritis

changes kinematics, specifically femoral roll back and the loss of terminal flexion (Scarvell et al., 2018). There are corresponding areas within the posterior femur and tibia which impinge during deep flexion in normal knees (Yildirim et al., 2007). In OA knees, limited flexion and difficulty kneeling is common (Steultjens et al., 2000). In this study, the bony expansion on the proximal aspect of the posterior medial condyle combined with the tubercle on the posterior medial tibia may be the cause of premature bony contact and loss of deep flexion in OA. Another common kinematic alteration in OA is increased knee varus thrust during gait (Bytyqi et al., 2014; Foroughi et al., 2009). The cartilage plate expansion observed on the medial aspects of the femur and tibia are likely to be associated with varus thrust and the altered loading environment that occurs during OA (Brand & Claes, 1989; Isaacson & Brotto, 2014). The findings of this study will allow the examination of the associations between specific shape changes and functional deficits. These analyses have not previously been performed.

The ability of SSM to discriminate the gross and subtle geometric differences between OA and healthy knees potentially make it an effective predictive and diagnostic tool. Effective clinical decision making with respect to when operative intervention is appropriate is an imprecise art. TKR are increasingly being performed but there is an appetite to exhaust other measures prior to this definitive treatment. SSM offers the opportunity for identification of OA features, monitoring progression, and response to therapies. This concept has been proposed previously by Bredbenner et al. They identified subtle features in knees which proceeded to OA compared to those that didn't (Bredbenner et al., 2010). The features included a slight expansion of the posterior and distal condylar surfaces and spreading and depression of the tibial plateau. We found more tangible and extensive differences, for example expansions of up to 10 mm (190%) around the cartilage plates and the development of tibial tubercle of which was up to 6 mm (115%) in size. These findings may be important

in discriminating between patients who may respond favourably to rehabilitation programs and those who do not. End-stage OA implies awaiting a knee replacement and yet there are non-surgical strategies for ameliorating knee pain in severe OA knee (Skou et al., 2015). Skou et al. demonstrated that 25% of patients removed themselves from the waiting list following a strengthening and education program. It is possible that the 25% did not demonstrate such extensive change in particular features making them more amenable to non-surgical treatment. Clearly this requires further investigation. Therefore, the data presented in this study further advances our understanding about the bony changes that occur in the osteoarthritic knee.

The results of this study should be interpreted in the light of its limitations. The cohorts included were distinctly different. One group had no knee symptoms and the other included people awaiting knee replacement. Although there was variation in terms of Kellgren-Lawrence (KL) grade within each group, the middle grades (2 and 3) were sparsely populated (Table 4-1). Although the polarity of the participants was useful in illustrating the degree of the shape deviation in OA, future studies would benefit from analyzing the shape deviations across the OA spectrum. The healthy group contained 4 participants who had radiographic OA. However, we were interested in the shape of healthy knees versus OA. An interesting future study might be to examine the differences between symptomatic vs healthy OA. We did not include the patella in this study, and it is possible that patella shape may have influenced the shape changes in the trochlear region of the femur. Finally, individual patient-specific osteophytes are likely not included in these analyses due to their heterogeneous nature. Since the SSM captures areas of high variability in descending order, the osteophytes will only appear in the lower order modes where the variation is very small (<1% explained).

In conclusion, the novel contribution of this study lies in the identification and quantification of the changes that occur in knees due to OA. Shape changes in osteoarthritic and healthy

knees were accurately captured and classified with 7 modes of variation. Using logistic regression, unique shape arrays differentiated OA from healthy knees. The shape variation models described may provide a sensitive predictive tool for use in surgical and non-surgical decision making. Further studies will elucidate how the knee shape arrays identified in this study influence the disability related to knee OA.

5 Shape is Only a Weak Predictor of Deep Knee Flexion Kinematics in Healthy and Osteoarthritic Knees

Statement of Contribution

This thesis is submitted as a Thesis by Compilation in accordance with

https://policies.anu.edu.au/ppl/document/ANUP_003405

I declare that the research presented in this Thesis represents original work that I carried out during my candidature at the Australian National University, except for contributions to multi-author papers incorporated in the Thesis where my contributions are specified in this Statement of Contribution.

Title: Shape is only a weak predictor of deep knee flexion kinematics in healthy and osteoarthritic knees
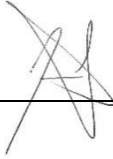
Authors: Lynch, Joseph T., Perriman, Diana M., Scarvell, Jennie M., Pickering, Mark R., Warmenhoven, John., Galvin, Catherine R., Neeman, Teresa., Besier, Thor F., Smith, Paul N

Publication outlet: Journal of Orthopaedic Research

Current status of paper: Published

Contribution to paper: JTL: research design, acquisition, analysis and interpretation of data, drafting and critically revising the paper; DMP: research design, analysis and interpretation of data, critically revising the paper; JMS.: research design, analysis and interpretation of data, drafting and critically revising the paper; MRP: research design, analysis and interpretation of data, critically revising the paper; JW: interpretation of data, drafting and critically revising the paper; C.R.G.: acquisition, analysis and interpretation of data, drafting and critically revising the paper; TFB: interpretation of data, drafting and critically revising the paper; TN: interpretation of data, drafting and critically revising the paper; PNS: research design, interpretation of data, drafting and critically revising the paper. All authors have read and approved the final submitted manuscript.

Senior author or collaborating authors endorsement: _____

Joseph Lynch		25/06/20
Candidate – Print Name	Signature	Date

Endorsed

Paul N Smith		25/06/20
Primary Supervisor – Print Name	Signature	Date

Dr Diana Perriman		25/06/20
Delegated Authority – Print Name	Signature	Date

SECOND STUDY

5.1 Context

This chapter examines the association between the bony shape described in chapter four and kneeling kinematics. The preceding chapter described the shape of the knee using statistical shape modelling and identified some prominent differences between osteoarthritic and healthy knees. Shape of the tibiofemoral joint is known to influence the mechanics of the knee, but little is known about deep flexion activities. Our group recently reported kinematic differences between OA and healthy kneeling (Galvin, 2019). Specifically, Galvin *et al.* reported reduced maximal flexion, reduced anterior-posterior translation and increased superior – inferior position in deep kneeling in OA knees. It is possible that these kinematic differences are the result of altered bony morphology. Specifically, the corresponding regions of bony expansion in the posterior medial aspect of the femur and tibia described in the previous chapter might lead to early impingement which prevent posterior translation and cause levering in the knee as opposed to its typical roll back movement. This chapter seeks to test the association between the shape characteristics described in chapter four and the kinematics of kneeling.

5.2 Abstract

Tibiofemoral shape influences knee kinematics but little is known about the effect of shape on deep knee flexion kinematics. The aim of this study was to examine the association between tibiofemoral joint shape and kinematics during deep kneeling in patients with and without osteoarthritis (OA). Sixty-one healthy participants and 58 patients with end-stage knee OA received a computed tomography (CT) of their knee. Participants completed full flexion kneeling while being imaged using single-plane fluoroscopy. Six-degree-of-freedom kinematics were measured by registering a three- dimensional (3D) static CT onto 2D-dynamic fluoroscopic images. Statistical shape modelling and bivariate functional principal component analysis (bfPCA) were used to describe variability in knee shape and kinematics, respectively. Random-forest- regression models were created to test the ability of shape to predict kinematics controlling for body mass index, sex, and group. The first seven modes of the shape model up to three modes of the bfPCAs captured more than 90% of the variation. The ability of the random forest models to predict kinematics from shape was low, with no more than 50% of the variation being explained in any model. Furthermore, prediction errors were high, ranging between 24.2% and 29.4% of the data. Variations in the bony morphology of the tibiofemoral joint were weakly associated with the kinematics of deep knee flexion. The models only explained a small amount of variation in the data with high error rates indicating that additional predictors need to be identified. These results contribute to the clinical understanding of knee kinematics and potentially the expectations placed on high-flexion total knee replacement design.

5.3 Introduction

Shape of the tibiofemoral joint is known to influence the mechanics of the knee. Sagittal plane geometry has been described as comprising three femoral facets of different function and radii (patella, extension and flexion facets), that interact with a flat medial and convex lateral tibial plateau (Iwaki et al., 2000). Patient-specific variations in these radii influence tibiofemoral anterior–posterior translation, internal-external rotation, and the location of the most caudal point on the femur in early to mid-flexion (Lansdown et al., 2017; Smoger et al., 2015). Independently, an increased posterior condylar offset ratio has been associated with greater anterior-posterior translations; and a larger condylar twist-angle has been shown to result in a more externally rotated tibia at heel strike (Hoshino et al., 2012). Recently, combined statistical shape and musculoskeletal modelling revealed that a larger flatter medial tibial plateau was associated with increased external rotation and anterior translation of the femur on the tibia during gait (Clouthier et al., 2019). However, these findings examined shape-function relationships in normal cohorts. Far less is understood about the shape-function relationship in pathological groups, particularly osteoarthritis.

Osteoarthritis (OA) results in bony shape changes in the knee. Statistical shape modelling has revealed specific and subtle differences between OA and healthy knees. Specifically, the OA distal femoral condyles are wider and flatter, there is expansion of the cartilage plate margins, the intercondylar notch is narrowed, and there is general bony expansion, most notably of the posterior medial condyle (Barr et al., 2016; Lynch et al., 2019; Neogi et al., 2013). Tibial changes include medial plateau flattening and widening, an "elevated" lateral plateau, a reduction in the space between the tibial spines, and an increase in the bony prominence along the medial and posterior perimeter of the plateau (Barr et al., 2015; Lynch et al., 2019). The bony changes seen in OA may contribute to the altered kinematics reported in osteoarthritic patients. Which of these changes is the most important in terms of influence on joint

kinematics is not clear. Furthermore, research to-date has examined shape-function relationships only during gait and early flexion (Clouthier et al., 2019; Lansdown et al., 2017; Smoger et al., 2015). These relationships have not yet been explored in more challenging activities including kneeling and deep flexion.

The ability to achieve full flexion is important for cultural and recreational tasks. Praying, kneeling, gardening and squatting require more than 120° of loaded flexion (Mulholland & Wyss, 2001; Weiss et al., 2002) and individuals with knee OA find these activities to be particularly challenging. People with OA typically have reduced maximal knee flexion and altered kinematic patterns when compared to their healthy counterparts, but these patterns are variable (Scarvell et al., 2018; Steultjens et al., 2000). Deep flexion occurs at the limit of motion, and soft tissue factors are known to influence deep knee flexion kinematics (Kingston & Acker, 2018; Zelle et al., 2007). However, the articular shape is still thought to be important in achieving maximal deep flexion. Indeed, total knee replacement design is predicated on restoring normal shape in order to achieve optimal kinematics (Argenson et al., 2005; Zeller et al., 2017). Therefore, the variability in the kinematics of deep knee flexion might also be the result of altered joint shape.

Optimal analysis of knee kinematics requires capture and comparison of the form as well as the magnitude of the movement being studied. Knee kinematics are complex and typically described as either time series or angle-angle waveforms (Park et al., 2017; Warmenhoven et al., 2019b). However, standard analysis techniques for describing and comparing knee kinematics typically focus on pre-defined features such as maxima, minima, specific values, and slopes (Deluzio & Astephen, 2007; Park et al., 2017). The use of discrete data points neglects the entire waveform. Functional data analysis, functional principal component analysis (*bf*PCA), is an emerging technique which offers the opportunity to quantify the entire

waveform in order to examine the differences between groups (Deluzio & Astephen, 2007; Warmenhoven et al., 2019a).

The aim of this study was to determine whether bony shape can predict deep kneeling kinematics in people with and without OA, using a novel approach combining statistical shape modelling and bfPCA.

5.4 Methods

Level of Evidence: Level 3, case-control study.

5.4.1 Participants

The participants in this study were recruited as part of a larger randomised controlled trial of knee replacement designs with age- and sex-similar healthy control participants (ISRCTN75076749). The OA group included 58 patients who were awaiting TKR for OA. The healthy group included 61 participants who were pain free with no history of lower limb pathology. The OA group had fewer females, higher BMI, higher pain levels and less maximal flexion (Table 5-1). All participants provided written consent and ethics approval was granted by the Australian Capital Territory Health, Australian National University and University of Canberra human research ethics committees.

Table 5-1: Participant Characteristics

Participant characteristics		Healthy	OA
N		61	58
Age (years)		68.6 +/- 9.54	67.5 +/- 9.02
Number of females (%)		34 (56%)	29 (50%)
Left-sided knees (% L)		25 (41%)	30/58 (52%)
N by KL Grade (%)			
	0	30 (49%)	0 (0%)
	1	22 (36%)	0 (0%)
	2	7 (11%)	0 (0%)
	3	1 (2%)	15 (26%)
	4	1 (2%)	43 (74%)
Height (cm)		168.9 +/- 9.74	168.8 +/- 9.53
Weight (kg)		70.8 +/- 13.63	88.1 +/- 17.02
BMI (kg.m^{-2})		24.7 +/- 3.98	30.9 +/- 5.3
Pain (VAS, /100)		2 ± 4	48+/- 26
Max Flexion (°)		142.8 +/-5.45	125.9 +/- 10.31

5.4.2   Data Collection

All participants received a 3D spiral computed tomography (CT) scan of the knee (Toshiba Medical Systems, Ōtawara, Japan) with a field of view of at least 150 mm above and below the tibiofemoral joint line, acquired in supine. Slice thickness was 0.5 mm with a resolution of 512 x 512 voxels with spatial dimensions 0.625 x 0.625 x 0.5 mm^3 and 16 bits/pixel.

Participants were then asked to perform a unilateral deep kneeling activity starting with the knee at approximately 90° until full flexion was achieved (Figure 5-1). Movement was recorded using a single-plane fluoroscopy placed for a sagittal view of the knee, sampling images at 30Hz with 1024x1024-pixel spatial resolution and 12bits/pixel. All participants wore lead garments to protect their organs.
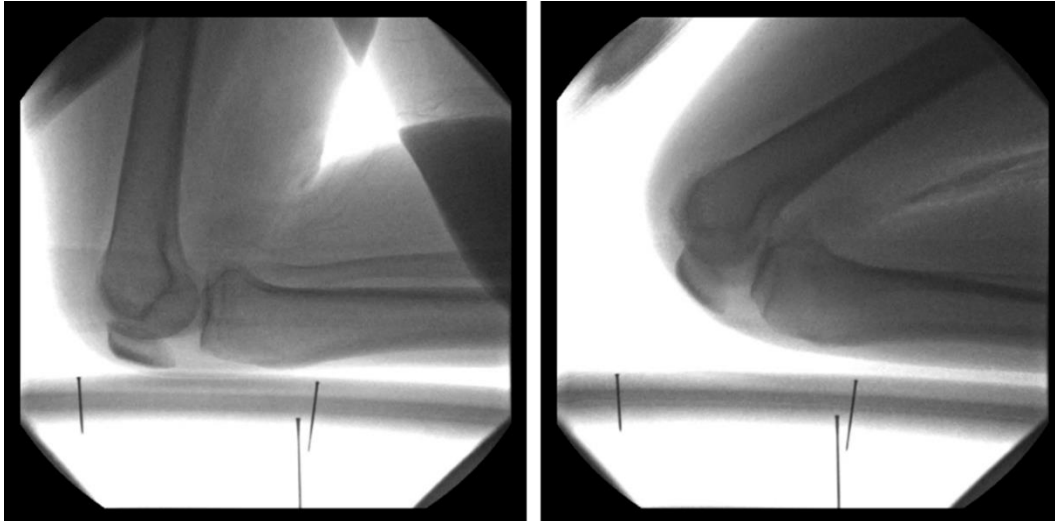
Figure 5-1: Example fluoroscopy of deep kneeling, a) starting position, b) maximal flexion

5.4.3 Image processing

The femur, tibia, and tibia with fibula were manually segmented from the CT scan images using custom software (Orthovis v4 UNSW Canberra; in MATLAB R2018a, Mathworks, Inc., Natick, MA). Three-dimensional coordinate systems for both the femur and tibia were established using the referencing convention defined by Grood and Suntay (Grood & Suntay, 1983). Orthogonal reference frames were established based on individual anatomical locations for all tibias and femurs in the dataset. Origins were set for the femur at the most proximal point of the intercondylar notch and, for the tibia, at the mid-point of the tibial spines(Scarvell et al., 2019).

5.4.4 Kinematics

Kinematics were calculated by a 2D-to-3D image registration algorithm using bespoke software (Orthovis, UNSW, Canberra (Akter et al., 2014b)). Orthovis precision was previously reported for in-plane (sagittal) registration as 0.2mm for translation and 0.3° for rotation, while the out-of-plane precision was 0.9mm and 0.5° (Akter et al., 2014b).

Briefly, the registration aimed to find the best image match between the 3D CT in the 2D fluoroscopy space. This achieved using a number of steps:

1. Segmented CTs were converted into a 2D digital reconstructed radiograph and imported into the 2D fluoroscopy space

2. Fluoroscopy distortion was corrected using a calibration box

3. CTs were matched frame by frame to fluoroscopic images using gradient decent and similarity measures.

4. This process was done first with the femur, second with the tibia and fibula, and finally with just the tibia.

5. Six degree of freedom kinematics were then exported for analysis

5.4.5   Statistical Shape Model Generation

Statistical shape modelling (SSM) was performed using the technique described previously (Lynch et al., 2019; Zhang et al., 2014). An overview of the SSM process is described in Figure 5-2. Following setting of the axes, each model was cropped to standard proportions. Using the coronal projection of the CT, the femur was cropped at 1.5X the distance from the most distal femoral condyle to the adductor tubercle. Using the coronal projection, the tibia was cropped to 1.5X the distance from the most proximal aspect of the tibial spine to the most inferior point of the superior tibiofibular joint. Corresponding femurs and tibias were recombined using a custom Matlab script to create a tibiofemoral joint for each participant. Variations in alignment were removed by aligning the femur and tibial meshes so that their axes were orientated at zero degrees of rotation and translation.
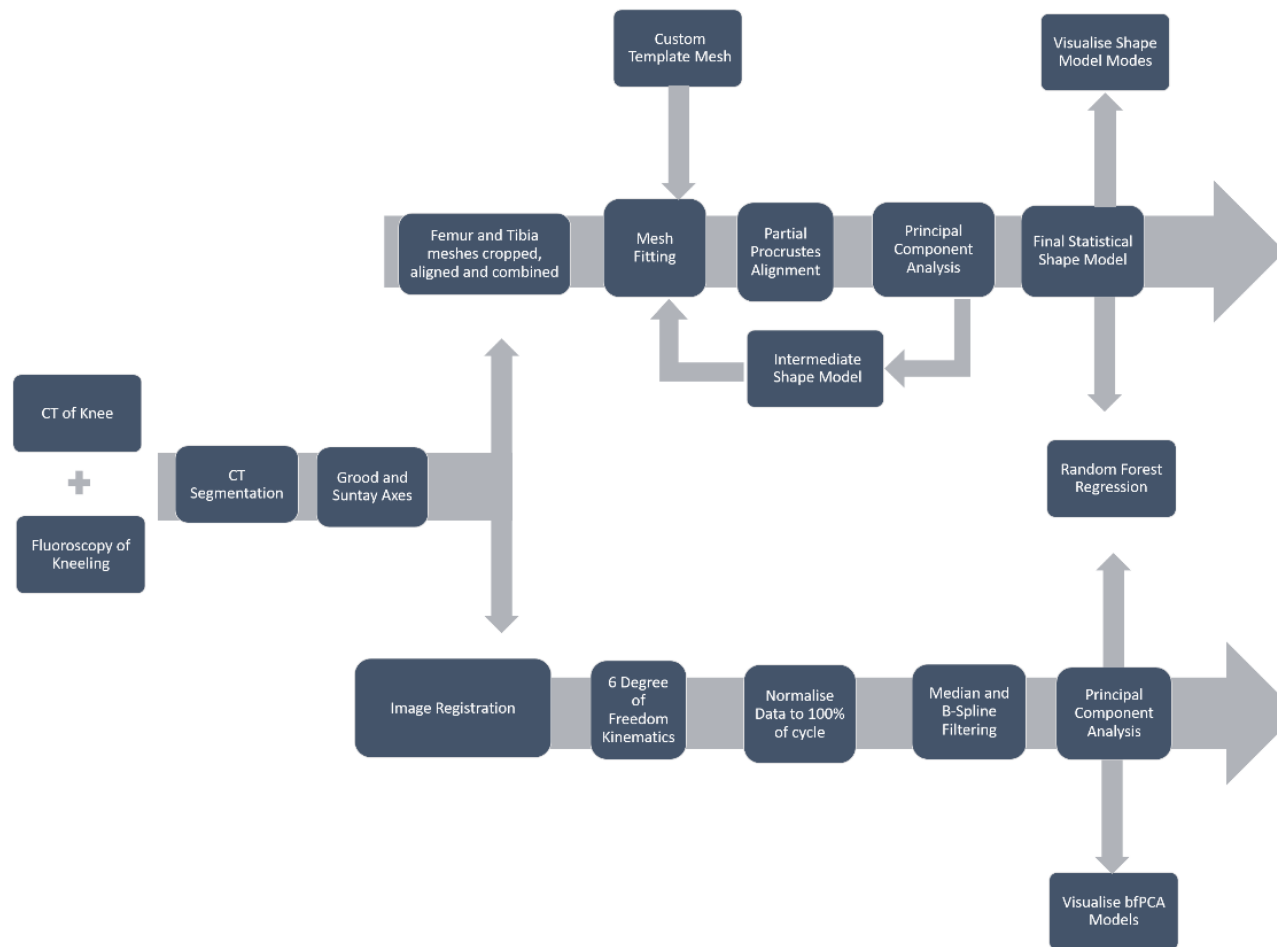
Figure 5-2: Workflow overview of the methods employed in this study.

Top arm described statistical shape modelling. The bottom arm describes how kinematics were calculated using image registration and bivariate function PCA

5.4.6   Mesh Fitting

The 3D models were exported as meshed surfaces. Knee models were down-sampled to 30,000 vertices and smoothed using a Laplacian filter (MeshLab 2016.12, http://meshlab. sourceforge.net). For consistency, left knee meshes were mirrored so they appeared as right-sided, thus all knees were analysed as 'right knees'. A template mesh was created using a series of radial basis functions to parameterise the tibiofemoral joint. This template was based on a single mesh from one knee in the dataset. This template was iteratively fitted with a series of coarse-to-fine fits to all meshes in the dataset, which resulted in maximum correspondence between meshes. Corresponding meshes were then rigidly aligned, using a partial Procrustes analysis which minimised the least squared distances of corresponding points (Gower, 1975). This allowed for only the shape variability to be included in the model.

Principal component analysis (PCA) was then run on the nodal coordinates of the aligned meshes to create a shape model. PCA is used for dimension reduction which allows any shape in the dataset x to be approximated as the sum of the mean shape $\bar{x}$ plus the weighted sum of the principal components ϕ (Heimann & Meinzer, 2009).

$$x = \bar{x} + \sum_{i=1}^{n} \omega_i \phi_i$$

The shape of each bone was described by n principal component (PC) weights, ω, where ω are the amount of variation along an individual principal component. $'n'$ is the number of principal components needed to explain 90% of the total variation in the population.

The fitting process was then repeated using the mean shape as the template. Following this, the fitting process was further refined for individual shape differences by incorporating PCA fitting using the previous SSM generated from the dataset. In this way, the shape model was optimised by propagating fitting correspondence across the dataset. A final PCA was

performed on the nodal coordinates to generate a statistical shape model which determined the principal component weights used in the subsequent analysis. One model was created which contained both OA and healthy knees. The principal components, or modes, which accounted for 90% of accumulated variance were retained and their respective weights were extracted for analyses.

5.4.7   Bivariate Functional Principal Component Analysis

Bivariate functional PCA (bfPCA) was used to describe the variability within the kinematic data. Similarly to SSM, bfPCA decomposes variability of kinematic data into a set of basis functions which can be reconstructed and visualised. To perform bfPCA, kinematic data were truncated so that all time-series started at $100°$ of flexion (to normalise starting position prior to analysis). A bivariate functional PCA was undertaken using the technique previously described by Warmenhoven et al (Warmenhoven et al., 2019a). Briefly, the six degree of freedom knee kinematic data were interpreted as five kinematic variables relative to flexion (i.e. Anterior/Posterior (AP), Mediolateral (ML), and Superior/Inferior (SI) translations and Internal/External (IE) and Abduction/Adduction (Ab/Add) rotations). Initially, both flexion and the other kinematic variables were normalised to 100% of the movement cycle. A 21st order moving median filter was passed over both datasets to remove noisy spikes (Figure 3-24). These two sets of curves were then estimated as functions using 100 4th order B-splines. The B-splines further smoothed the curves by adding a roughness penalty to the fitting procedure. The roughness penalty term was controlled using a smoothing parameter and was achieved by minimising the penalised residual sum of squares term.

Once normalisation and smoothing of individual data had taken place, bivariate functional principal components (*bf*PCs) were calculated by taking the first and second parameter functions and concatenating them into a composite (bivariate) function (Warmenhoven et al., 2019a). A covariance function was then estimated and a standard PCA applied. The *bf*PCA

modes which accounted for 90% of accumulated variance were retained and their respective weights were extracted for analyses. *bf*PCA weights were normalised to z-scores for consistency. Finally, bivariate functions representing each *bf*PCA were reconstructed and plotted for visual inspection of each remaining degree of freedom. (Figure 5-3).
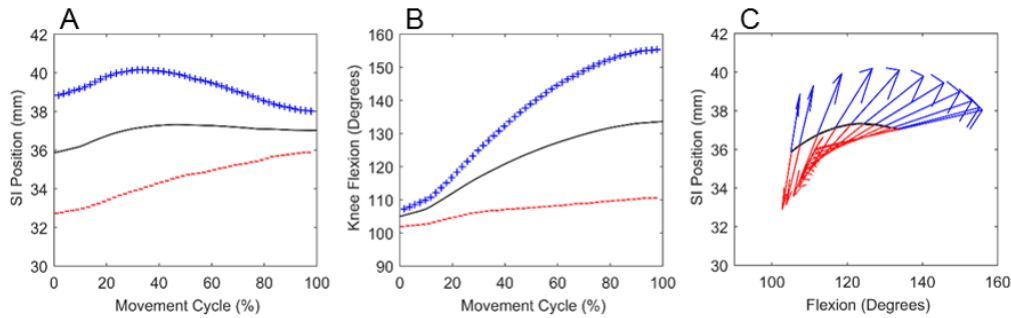
Figure 5-3: Representative bfPCA analysis, for example flexion and superior-inferior translation (mm).

*bf*PC1 can be visualised with each variable independently (A and B). Here, positive scorers are indicated by the '+' line in blue, and negative scorers the '–' line in red. *bf*PC1 is also visualised with both variables concurrently (C), where variability in each *bf*PC is indicated by the direction of the arrows away from the mean profile in each graph. In every profile the mean profile is plotted in solid black and the magnitude of the variability within *bf*PC1 has been scaled using a constant equivalent to +/– 2 SD of the *bf*PC scores. Note: SI= Superior-Interior translation measured in mm

5.4.8   Statistics

Random forest regression modelling was used to determine which bony shapes could predict kinematics using SPSS Modeler 16.0 (IBM Corp). Random Forest regression is a type of supervised machine learning based on multiple decision trees (Breiman, 2001). Each tree was created by selecting a subset of the input parameters and running them through a decision tree to obtain a prediction for each sample. This process was repeated 100 times using different subsets of the data to generate a forest. By this procedure, called bagging, different trees have

different training parameter sets. This process is unbiased as the prediction for each sample is based on trees built on trees which do not contain that sample (out-of-bag error). If a feature has poor predictive ability it will not appear in any nodes of the trees comprising the forest. However, if a feature is highly predictive it will not only appear in several trees but will also have a tendency to appear in nodes that are closer to the root. The final predicted regression value is obtained by averaging the regression values of all of the random trees (Breiman, 2001). Predicted values are compared to actual values to determine prediction error.

In this study, tibiofemoral shape modes, group, BMI and sex were included as predictors in all the random forest models. Separate models were created to predict the normalised weights for all kinematic *bfPCA* models as well as maximal flexion. Each model's performance was assessed by partitioning the data into training (70%), validation (15%) and testing (15%) datasets. These percentages were selected to produce a stable model and one that would not overfit the data. The training dataset is used for initial fitting of the parameters in the model. The validation dataset is used for evaluating the fit of the training model and to tune the parameters in the model. Finally, the testing dataset is used to evaluate the final fit of the model. Results for each model were reported in terms of predictor importance, variation explained by the model (R^2), correlations between predicted and actual data, root-mean-squared error (RMSE) and normalised RMSE (NRMSE). NRMSE was defined as RMSE divided by the difference between the maximum and minimum observed values, expressed as a percentage. Finally, associations between important shape predictors and kinematics were visualised using scatterplots with associated R^2 values.

5.5 Results

5.5.1 Statistical Shape Model

The first seven principal component modes of the statistical shape model (SSM) comprising both the OA and healthy groups, accounted for 90.4% of the total variance in tibiofemoral joint shape (Table 5-2). Mode one explained 77.6% of the total variation and represented the isometric size of the knee.

Table 5-2: Variation explained by each mode of the statistical shape model (SSM).

Mode	1	2	3	4	5	6	7	Cumulative Variation
Tibiofemoral SSM	77.6%	3.5%	2.7%	1.9%	1.8%	1.6%	1.3%	90.4%

5.5.2 Bivariate Functional PCA

Up to three PCs of the kinematic *bf*PCAs explained 90% of the accumulated variance for all four models (Table 5-3). Medial-Lateral translation was excluded from analysis due to high within patient variability in the data.

Table 5-3: Variation explained by each principal component (PC) of the four kinematic bfPCA models.

bfPC	bfPC1	bfPC2	bfPC3	Cumulative Variation
Internal-External rotation	62.1%	27.0%	5.7%	94.8%
Superior-Inferior translation	73.6%	17.7%	N/A	91.3%
Ab/Adduction	77.6%	12.3%	N/A	90.0%
Anterior-Posterior translation	82.1%	9.8%	N/A	92.0%

5.5.3 Random Forest Models

Maximal flexion, the first principal component for all bfPCAs and the second principal component for superior-inferior position were all able to be predicted from the random forest models. Maximal flexion, which was modelled separately, resulted in an R^2 of 0.477. The variance explained by the other kinematic models are reported in Table 5-4.

Table 5-4: Variance explained (R^2) for each kinematic random forest regression model

(Negative values indicate no predictive ability of the model).

Kinematic Models	PC1	PC2	PC3
Internal-External rotation	0.45	-0.32	-0.31
Superior-Inferior translation	0.52	0.11	N/A
Ab/Adduction	0.48	-0.12	N/A
Anterior-Posterior translation	0.43	-0.14	N/A

The first principal component for all bfPCA kinematic models captured variability in maximal flexion (Figure 5-4 and Figure 5-5). Additionally, bfPC1 captured variability in the start and end positions for the superior-inferior and ab/adduction models (Figure 5-4). Furthermore, bfPC1 for the anterior-posterior and internal-external rotation models, captured variability at the end of range which was a function of the variability of maximal flexion (Figure 5-5).
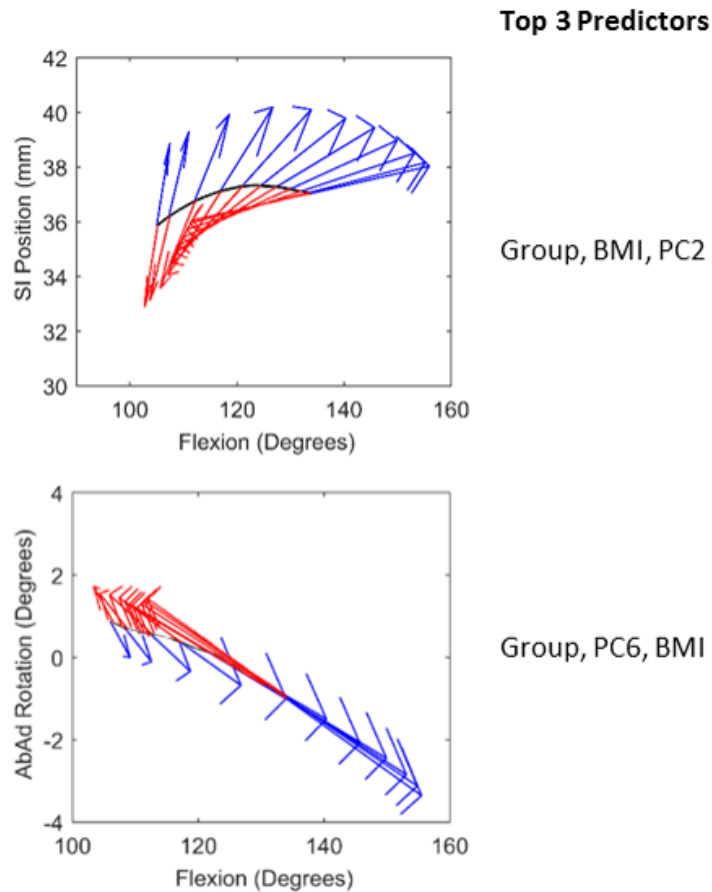
Figure 5-4: Kinematic variations for the first principal component of (top) Superior-Inferior position and (bottom) Ab/Adduction displayed as a function of flexion. Black line is the mean curve; Blue arrows indicate the changes in kinematic pattern at +2SD away from mean (more healthy); Red arrows indicate the changes in kinematic pattern at -2SD away from mean. Features captured in Superior-Inferior position include change in Maximal Flexion, and Superior-Inferior position throughout flexion. Features captured in ab/adduction include change in maximal flexion and ab/adduction angle throughout flexion. Top 3 random forest predictors for each PC are included
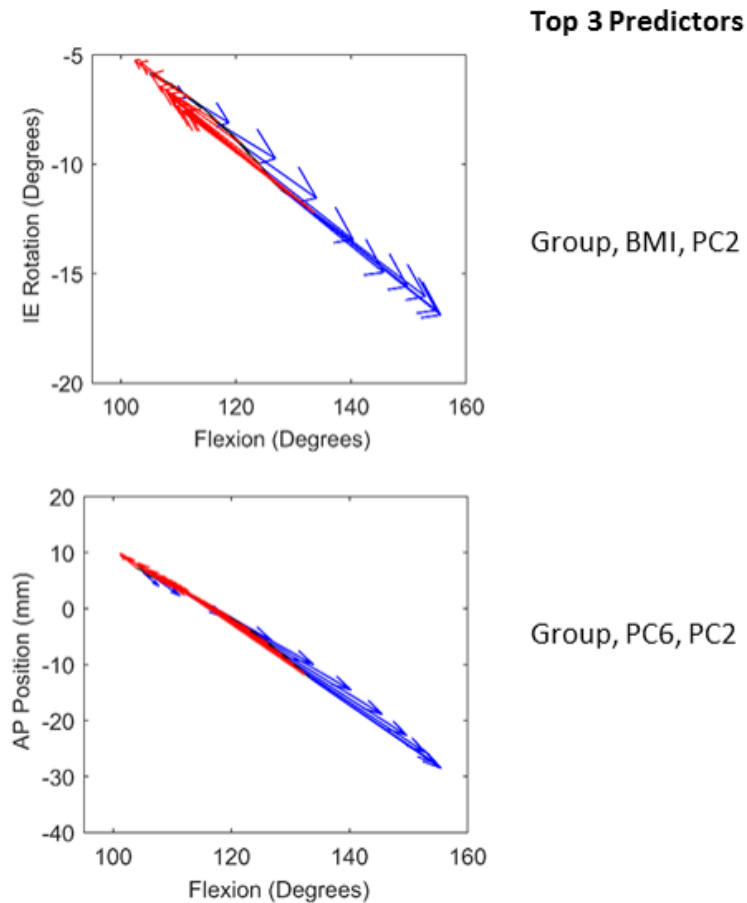
Figure 5-5: Kinematic variations for the first principal component of (top) Internal-External (IE) rotation and (bottom) Anterior-Posterior (AP) position displayed as a function of flexion.

Black line is the mean curve; Blue arrows indicate the changes in kinematic pattern at +2SD away from mean; Red arrows indicate the changes in kinematic pattern at -2SD away from mean. Features captured in IE rotation include reduced rotation angle as a result of reduced maximal flexion. Features captured in AP position include reduced posterior translation as a result of reduced maximal flexion. Top 3 random forest predictors for each PC are included

The striking finding of this study was that shape was a poor predictor of kneeling kinematics with no more than 50% of the kinematic variation being explained by shape in any model. Prediction errors in the validation set were high, ranging between 18.6% and 33.8% of the data (Table 5-5). The random forest model which predicted Superior-Inferior bfPC2 was particularly weak, with less than 12% of the variance explained and large differences between training, validation, and testing partitions (Table 5-5).

The predictors which best predicted maximal flexion and kinematic bfPCA's were a combination of group (OA vs Healthy), BMI and either shape modes 2 or 6 (Figure 5-6 and Figure 5-7). Shape alone could only explain up to 28% of the variation in any of the kinematic data (Figure 5-8).

Table 5-5: Results of random forest regressions models.

	Variation Explained	Training (n=84) 70%					Validation (n=16) 15%					Testing (n=19) 15%				
		Min Error	Max Error	R	RMSE	NRMSE	Min Error	Max Error	R	RMSE	NRMSE	Min Error	Max Error	R	RMSE	NRMSE
Max Flexion (°)	0.48	-14.59	19.19	0.86	6.48	13.49%	-8.07	15.61	0.78	6.02	24.22%	-12.62	9.61	0.77	6.40	25.76%
Internal-External Rotation PC1	0.45	-1.29	1.25	0.84	0.59	15.06%	-0.40	1.65	0.73	0.58	25.92%	-1.55	1.28	0.53	0.65	29.30%
Super-Inferior Position PC1	0.52	-1.40	1.45	0.85	0.65	17.11%	-1.03	1.46	0.66	0.60	29.35%	-1.31	1.66	0.60	0.71	18.64%
Superior Inferior Position PC2	0.11	-1.42	1.36	0.68	0.77	19.98%	-0.44	1.59	0.55	0.80	23.29%	-1.26	1.20	0.10	0.92	33.80%
Ab/Adduction PC1	0.48	-1.42	1.36	0.80	0.65	17.23%	-0.44	1.59	0.75	0.60	27.37%	-1.26	1.20	0.53	0.58	26.87%
Anterior-Posterior PC1	0.43	-1.49	1.40	0.79	0.67	16.16%	-0.63	1.44	0.75	0.59	26.26%	-1.45	1.26	0.46	0.60	26.48%

Note: PC= Principal Component; R= correlation coefficient; RMSE = root mean squared error; NRMSE = normalised root mean squared error which was normalised to total range Max flexion reported in degrees; PC's reported a z-scores
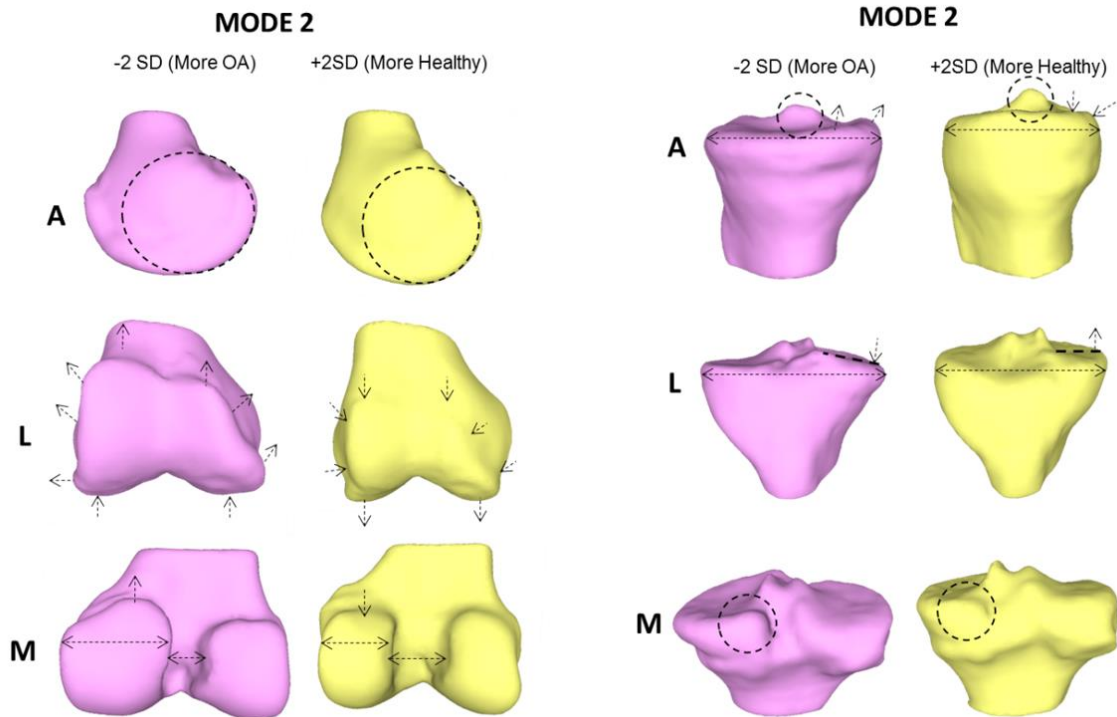
Figure 5-6: Shape variations captured within the second mode of the statistical shape model perturbed by plus and minus two standard deviations away from the mean shape. M = Medial; L=Lateral; A=Anterior
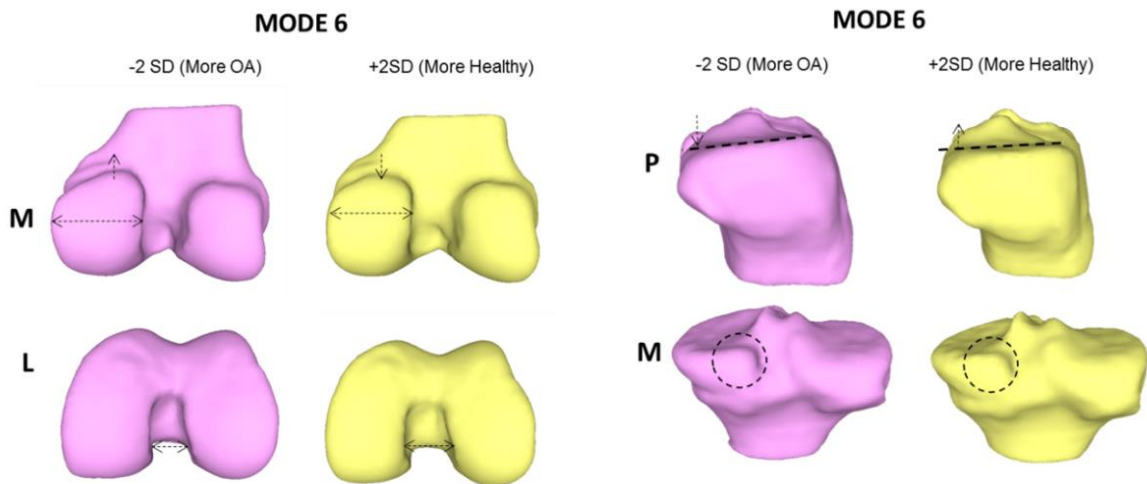
Figure 5-7: Shape variations captured within the sixth mode of the statistical shape model perturbed by plus and minus two standard deviations away from the mean shape. M = Medial; L=Lateral; A=Anterior; P=Posterior
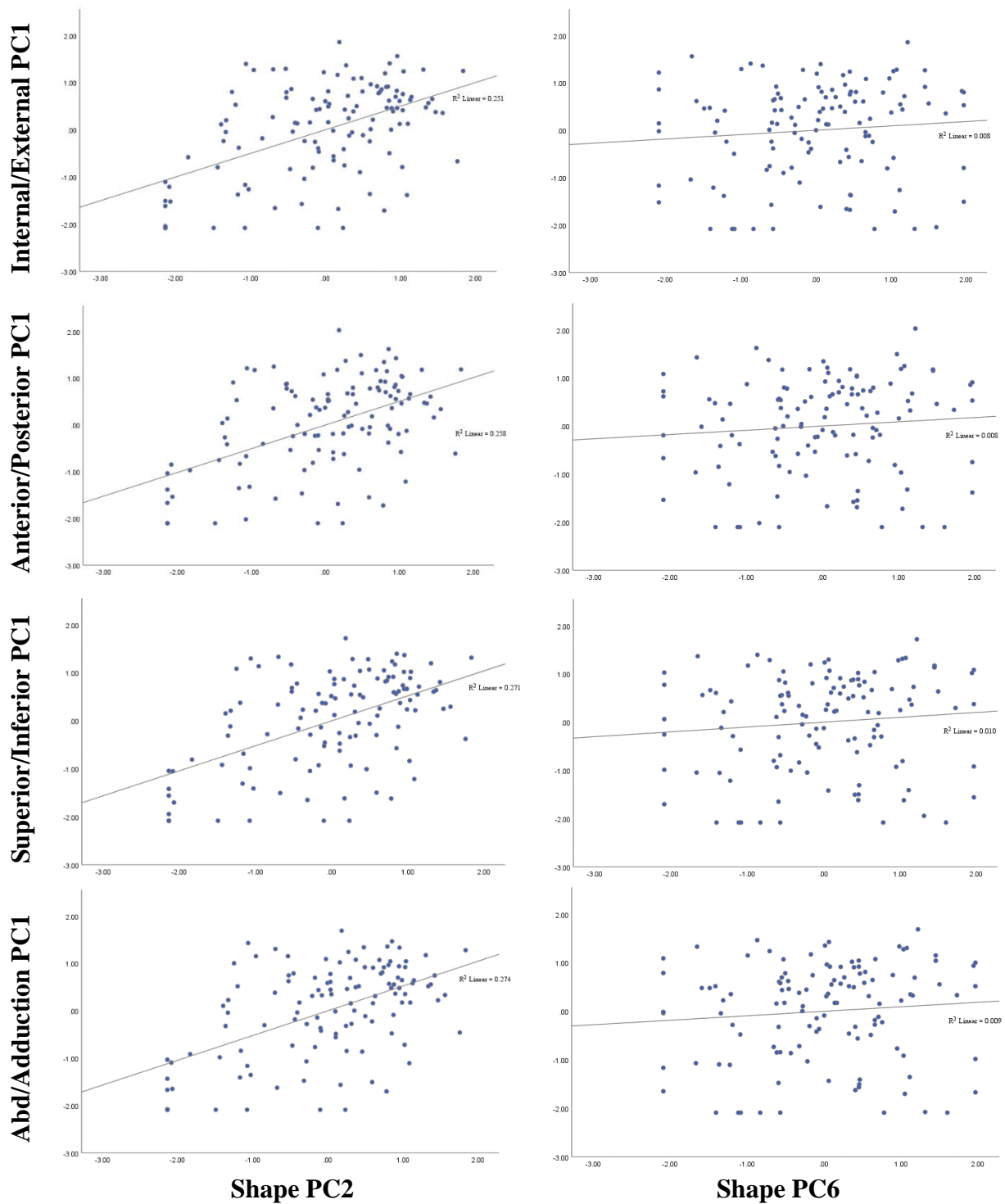
Figure 5-8: Scatterplots of shape modes of variation compared with kinematic principal components which appeared in Random Forest Regression. Variance explained within each plot is reported as R^2

Femoral shape features captured within mode 2 described bony expansions along the cartilage plate and posterior-medial condyle, flattening of the distal condyles, reduced intercondylar

space and changes in the condylar radii. Tibial features included bony expansions posterior-medial tibia plateau, changes in spine heights and alterations in the coronal slope (Figure 5-6). Features in mode 6 included large bony expansions on the posterior-medial femur and tibia, reduced intercondylar space, and alterations to the posterior tibial slope (Figure 5-7).

5.6 Discussion

The purpose of this study was to examine whether changes in bony shape could explain the alterations in kinematics of deep kneeling in patients with OA as compared to a normal cohort. The main finding of this study was that variations in tibiofemoral joint bony shape were only weakly associated with the kinematics of deep knee flexion. While the shape features contained in the 2nd and 6th shape modes had predictive ability, group and BMI were more important. Even so, these variables only explained a small amount of the variation in the models, with high error rates, indicating that other predictors must be more important.

Most of the variability in the kinematics observed in this study were primarily seen at maximum flexion and the start and end positions of the other degrees of freedom. This variability was easily seen in the first PC of each bfPCA. While this study didn't specifically aim to examine the differences between OA and healthy kinematics using bfPCA, the random forest models could detect different kinematic patterns between the two groups. Functional PCA has shown the ability to detect differences between healthy and OA kinematics during gait (Deluzio & Astephen, 2007; Deluzio et al., 1997; Harding et al., 2012), but this was the first study to use PCA to detect differences during deep kneeling .

Our results indicate that features other than bony morphology are important for predicting deep knee flexion kinematics. The lack of relationship between shape and kinematics detected in this study was surprising given the associations between shape and function reported

previously (Clouthier et al., 2019; Lansdown et al., 2017; Smoger et al., 2015). However, these studies focused on early to mid-flexion tasks which do not stress soft tissue structures like end of range knee flexion activities do (Rodríguez-Merchán & Oussedik, 2015). Pinskerova et al. have speculated that impingement of the posterior horn of the medial meniscus might limit flexion (Pinskerova et al., 2009). The patients in our study were required to flex their knee as far as possible in a loaded position which likely resulted in the impingement of the posterior structures of the knee, particularly the menisci. The menisci are impinged during deep flexion as they move posteriorly off the posterior tibial plateau to create a pseudo joint surface (Liao et al., 2017). A recent FEA knee modelling study highlighted the importance of including posterior soft tissue structures in a model to achieve accurate kinematic predictions (Beidokhti et al., 2018). Furthermore, they reported that resection of posterior soft tissue structures resulted in a change of knee joint kinematics in early to mid-flexion but did not describe deep flexion.

In this study, group was an important kinematic predictor in all of the random forest models. Group defined OA and healthy participants and this finding suggests that their kinematics were different. Differences between OA and healthy deep flexion kinematics have been supported in the literature (Scarvell et al., 2018). Specifically, maximal flexion is commonly reported to be reduced in OA knees when compared to healthy (Steultjens et al., 2000). In osteoarthritis the soft tissues of the knee are affected in a number of ways (Loeser et al., 2012). The menisci are typically torn, resulting increased medial extrusion and altered joint mechanics (Scholes et al., 2015). Furthermore, intracapsular ligaments are more lax in OA and display degenerative changes, particularly the posterolateral bundle of the ACL (Loeser et al., 2012). Lastly, there is scarring and thickening of the joint capsule (Loeser et al., 2012). Therefore, the soft tissue changes that accompany the bony shape changes seen in OA may all contribute to the kinematics which have previously been observed in the OA knee.

In this study, BMI was a predictor of kinematics in all of the random forest models. Increased BMI has been reported to restrict maximal flexion in non-pathological, OA and post TKR populations (Jeong et al., 2018; Liao et al., 2017). Earlier thigh-calf contact as a result of soft tissue opposition alters mechanics at maximal knee flexion during kneeling (Zelle et al., 2007, 2009). Early thigh-calf opposition produces a first class lever effect at the knee with the pivot around the tissues opposing (Galvin et al., 2018). Additionally, increased BMI is negatively associated with changes in accessory moments, and rotations in during gait (Harding et al., 2012; J.-S. Li et al., 2017). Specifically, Harding et al. compared gait biomechanics in a group of OA and healthy participants and found that BMI affects gait kinematics and kinetics independently of OA. Therefore, while our OA group had a higher BMI than the healthy group, BMI is likely to have been an independent predictor of kinematics.

Although shape was not a strong predictor of kinematics there were shapes which emerged as more important than others. The shape variations contained in the 2nd and 6th mode which corresponded to enlargement of the posteromedial femur and tibial plateau, with flattening and reduced sphericity of the femoral condyles, were most associated with deep kneeling kinematics. Previously, osteophyte formation and increased Kellgren-Lawrence grade, which is a measure of OA severity derived from x-rays, has been negatively associated with flexion range of movement (Ersoz & Ergun, 2003; Hilfiker et al., 2015). Furthermore, flattening and reduced sphericity of the femoral condyles, have been reported to influence superior-inferior position throughout flexion (Baka et al., 2011; Lansdown et al., 2017; Smoger et al., 2015). Furthermore, a recent systematic review by Scarvell *et al*. reported OA knees to have reduced AP translations, maintain a more anterior position and have reduced axial rotations (Scarvell et al., 2018). Therefore, although the influence of shape was not strong in our models, there are some shape parameters which appear to be more important than others.

That tibiofemoral shape can produce normal kinematics is an underlying assumption of knee replacement design. The geometry of total knee replacement prostheses have been designed to reproduce normal knee kinematics (Andriacchi et al., 2003; Victor & Bellemans, 2006). Recently, the high flexion knee has been a goal for component manufacturers. While a number of high flexion prosthesis designs exist, they all essentially promote enhanced rollback of the femur in order to reduce posterior impingement of the posterior rim of the tibial plateau against the femur (Coughlin et al., 2007; Parrette et al., 2011). However, while high flexion designs have improved kinematic outcomes in some patients, these results have not been consistently demonstrated indicating that kinematics are likely driven by factors other than articular shape (Chaudhry & Goyal, 2019; Jain et al., 2013; Kim et al., 2018). The results of this study support the premise that bony knee shape is not the primary factor determining high flexion knee kinematics.

The results of this study should be interpreted in the light of its limitations. Individual patient-specific osteophytes were possibly eliminated from these analyses due to their heterogeneous nature. Since the SSM captures areas of high variability in descending order, the osteophytes will only appear in the lower order modes where the variation is very small (<1% explained) It is possible that some of these osteophytes will affect the kinematic patterns in deep flexion. Also, we did not include the patella in this study and it is possible that patella shape may have influenced the shape changes in the trochlear region of the femur. We set out to explore the relationships between shape and kinematics, so other factors that influence kinematics such as pain, muscle function, and altered loading patterns were not captured in this study. Future research could extend to explore the influence of these factors.

5.7 Conclusion

In conclusion, variation in the bony shape of the tibiofemoral joint was only weakly predictive of kinematics. Knee shape is considered to be an important driver for normal movement; however, the results of this study indicate that there are potentially other factors, including soft-tissue properties, which might be more influential for the kinematics of deep kneeling. These results have implications for the clinical understanding of the drivers of knee kinematics and in particular the expectations placed on high flexion total knee replacement design.

6   Influence of Component Design on In-vivo Tibiofemoral Contact Patterns During Kneeling after Total Knee Arthroplasty: A Systematic Review and Meta-analysis.

<div align="center">**Statement of Contribution**</div>

This thesis is submitted as a Thesis by Compilation in accordance with

https://policies.anu.edu.au/ppl/document/ANUP_003405

I declare that the research presented in this Thesis represents original work that I carried out during my candidature at the Australian National University, except for contributions to multi-author papers incorporated in the Thesis where my contributions are specified in this Statement of Contribution.

Title: Influence of component design on in-vivo tibiofemoral contact patterns during kneeling after total knee arthroplasty: A systematic review and meta-analysis.

Authors: Joseph T Lynch, Jennie M Scarvell, Catherine R Galvin, Paul N Smith, Diana M Perriman

Publication outlet: Knee Surgery, Sports Traumatology, Arthroscopy

Current status of paper: *Published*

Contribution to paper: JTL conceived the study and participated in its design, reviewed articles for inclusion and quality, performed meta-analysis and drafted the manuscript. JMS participated in the study design, reviewed articles for inclusion and quality and participated in drafting the manuscript. CRG participated in drafting the manuscript. PNS participated in the study design and participated in drafting the manuscript. DMP participated in the study design, reviewed articles for inclusion and quality, and participated in drafting the manuscript. All authors read and approved the final manuscript.

Senior author or collaborating authors endorsement: _____

Joseph Lynch		25/06/20
Candidate – Print Name	Signature	Date

Endorsed

Paul N Smith		25/06/20
Primary Supervisor – Print Name	Signature	Date

Dr Diana Perriman		25/06/20
Delegated Authority – Print Name	Signature	Date

THIRD STUDY

6.1 Context

The previous study provided some insights into how kneeling kinematics are minimally influenced by bony knee shape in healthy and osteoarthritic participants. Non-operative treatment for OA aims to manage pain while restoring joint function (The Royal Australian College of General Practitioners, 2018). For those patients whose sever pain and dysfunction persist, the definitive treatment for OA is a total knee replacement. This procedure involves the removal of the arthritic weight bearing surfaces of the knee and replacing them with prosthetic components. While there are many different implant choices for surgeons to select when performing this surgery, the perfect implant has not yet been identified. Factors which have been reported to influence implant choice are surgeon preference, survivorship and more recently, kinematic performance (Vertullo et al., 2017). Many groups have examined the kinematics of different knee replacement designs, but the sample sizes are small. We sought to gain a better understanding of the effect of different knee prosthetic designs using a systematic review and meta-analysis. For this chapter, we used contact patterns as our kinematic measure. Contact patterns are related to the position of the medial and lateral femoral component relative to the tibial surface. They can be measured either as the closest point between the femoral and tibial surfaces or as the lowest point on each femoral condyle relative to the transverse plane of the tibial base plate.

6.2 Abstract

Modern TKR prostheses are designed to restore healthy kinematics including high flexion. Kneeling is a demanding high flexion activity. There have been many studies of kneeling kinematics using a plethora of implant designs but no comprehensive comparisons. Visualization of contact patterns allows for quantification and comparison of knee kinematics. The aim of this systematic review was to determine whether there are any differences in the kinematics of kneeling as a function of TKR design. A search of the published literature identified 26 articles which were assessed for methodologic quality using the MINORS instrument. Contact patterns for different implant designs were compared at 90° and maximal flexion using quality-effects meta-analysis models. Twenty-five different implants using six designs were reported. Most of the included studies had small sample sizes, were non-consecutive, and did not have a direct comparison group. Only posterior-stabilized fixed-bearing and cruciate-retaining fixed-bearing designs had data for more than 200 participants. Meta-analyses revealed that bicruciate-stabilised fixed-bearing designs appeared to achieve more flexion and the cruciate-retaining rotating-platform design achieved the least, but both included single studies only. All designs demonstrated posterior-femoral translation and external rotation in kneeling but, posterior-stabilised designs were more posterior at maximal flexion when compared to cruciate-retaining. However, the heterogeneity of the mean estimates was substantial, therefore firm conclusions about relative behaviour cannot be drawn.: The high heterogeneity may be due to a combination of variability in the kneeling activity and variations in implant geometry within each design category. There remains a need for a high quality prospective comparative studies to directly compare designs using a common method.

6.3 Introduction

Being able to kneel is reported to be one of the most important activities that fails to meet the expectations of patients after total knee replacement (TKR) (Scott et al., 2012). In TKR, high flexion is an important indicator of success, and considerable effort has been applied to achieving normal kinematic behaviour in TKR designs. Although there are several kneeling variations, they all require up to 165° of flexion which is greater than other high flexion activities (Hefzy et al., 1998; Mulholland & Wyss, 2001). In order to achieve deep flexion, the native femur externally rotates and translates posteriorly on the tibia (Galvin et al., 2018, 2019). Contact patterns enable easy visualisation and quantification of tibiofemoral kinematics. In addition, they make it possible to infer kinematic characteristics such as roll/glide, sheer and instability, and may be important indicators of the potential risk of implant damage and wear (Dennis et al., 1996; Walker & Hajek, 1972).

Modern TKR prosthesis design has focussed on restoring kinematics in order to achieve high flexion. Implant choice is dictated by implant survival, surgeon preference, and kinematic performance (Vertullo et al., 2017). In 2018, Australian surgeons used 193 different femoral and tibial prosthesis combinations (Australian Orthopaedic Association National Joint Replacement Registry (AOANJRR), 2019). These designs can generally be classified into: cruciate sacrificing + posterior stabilised (PS), posterior cruciate retaining (CR), bi-cruciate sacrificing (CS) or bi-cruciate stabilising (BCS), and all can have either fixed bearing (FB) or rotating platform (RP) tibial inserts. However, the CR and PS designs accounted for 91% of those used (Australian Orthopaedic Association National Joint Replacement Registry (AOANJRR), 2019).The CR design retains the posterior cruciate ligament (PCL) and relies on it to achieve femoral rollback in deep flexion. In the PS design a cam and post replace the PCL, which facilitates rollback of the femoral condyles on the tibial bearing. The CS design uses condylar and tibial geometry to drive motion and deliver stability. Finally, the BCS

design uses both an anterior and a posterior a cam and post. The kneeling kinematics of these prosthetic designs have been frequently described, but the individual study cohorts have been small (Delport et al., 2006; Incavo et al., 2004; Watanabe et al., 2013). Therefore, the influence of implant design on kneeling kinematics is still uncertain.

The purpose of this systematic review was to determine whether there are any differences in the kinematics of kneeling as a function of TKR design. Specifically, this review aimed to compare the differences in medial and lateral tibial compartment, anterior and posterior contact patterns at 90° kneeling and kneeling at maximal flexion. It was hypothesised that the PS design would facilitate relatively greater flexion in deep kneeling through enhanced femoral rollback.

6.4 Methods

6.4.1 Literature Search Strategy

This systematic review was registered with the International Prospective Register of Systematic Reviews (Prospero CRD42017064828). An initial search for studies was completed in May 2019 with a final search run in March 2020. The databases included Ovid Medline, Ovid EMBASE, Pubmed, Scopus, Web of Science and The Cochrane Library. The following search strategy was built in Embase and replicated for all other databases using their thesaurus for appropriate terms, for full text studies published in English:

1. Arthroplasty, Replacement, Knee
2. tka or tkr or total knee replacement or total knee arthroplasty
3. contact pattern* OR contact point* OR contact position* OR contact location*
4. kneel*
5. .\Knee Prosthesis
6. 1 or 2 or 5
7. 3 and 4
8. 6 AND 7

These electronic searches were supplemented by cross-checking citations and reference lists of the relevant published studies. Details of all studies returned from the searches were compiled, and duplicates were removed. The remaining studies were screened by title and abstract using inclusion and exclusion criteria (Table 6-1). These selection criteria were chosen to allow comparison of findings between studies with minimal influence of confounding factors. Studies were screened for inclusion by three reviewers (JTL, JMS, DMP) with a provision for disagreement to be resolved by consensus.

6.4.2   Assessment of Methodological Quality

Two independent reviewers undertook the quality assessment (JTL and DMP) and assessed methodological quality using the MINORS checklist (Methodological Index for Non-randomized Studies) (Table 6-2) (Slim et al., 2003). MINORS is a validated scoring tool for assessment of internal and external validity for non-randomized studies (Slim et al., 2003). The items are scored 0 (not reported), 1 (reported but inadequate) or 2 (reported and adequate). Scores are added and total scores converted to a percentage of the maximal possible score. Consensus was employed to resolve any disagreements.

Table 6-1: Inclusion/Exclusion Criteria

Inclusion	Exclusion
• Meta-analyses, systematic reviews, randomised controlled trials, observational studies (cohort and case controlled), conference proceedings,	• Book chapters, case studies and anecdotal reports
• In-vivo measurements	• In-Vitro Studies
• Patients received a total knee replacement for	• Joints other than the knee
• Weight-bearing kneeling task	• Patellofemoral only studies
• Reported medial and lateral compartment contact patterns	• Non-Total Knee Replacement
	• Studies of soft tissue
	• Knee kinetics data only reported
	• Studies that discuss only component wear
	• Studies which only use modelling or simulations.
	• Intraoperative measurements only
	• Motion analysis using skin markers only
	• Methodological studies
	• Not flexion past 90°
	• No contact point data presented

Table 6-2: Methodological Index for Non-randomized Studies (MINORS) Checklist (Slim et al., 2003)

Methodological items for non-randomized studies

1. **A clearly stated aim:** the question addressed should be precise and relevant in the light of available literature
2. **Inclusion of consecutive patients**: all patients potentially fit for inclusion (satisfying the criteria for inclusion) have been included in the study during the study period (no exclusion or details about the reasons for exclusion)
3. **Prospective collection of data**: data were collected according to a protocol established before the beginning of the study
4. **Endpoints appropriate to the aim of the study**: unambiguous explanation of the criteria used to evaluate the main outcome which should be in accordance with the question addressed by the study. Also, the endpoints should be assessed on an intention-to-treat basis.
5. **Unbiased assessment of the study endpoint**: blind evaluation of objective endpoints and double-blind evaluation of subjective endpoints. Otherwise the reasons for not blinding should be stated
6. **Follow-up period appropriate to the aim of the study**: the follow-up should be sufficiently long to allow the assessment of the main endpoint and possible adverse events
7. **Loss to follow up less than 5%:** all patients should be included in the follow up. Otherwise, the proportion lost to follow up should not exceed the proportion experiencing the major endpoint
8. **Prospective calculation of the study size**: information of the size of detectable difference of interest with a calculation of 95% confidence interval, according to the expected incidence of the outcome event, and information about the level for statistical significance and estimates of power when comparing the outcomes

Additional criteria in the case of comparative study

9. **An adequate control group**: having a gold standard diagnostic test or therapeutic intervention recognized as the optimal intervention according to the available published data
10. **Contemporary groups**: control and studied group should be managed during the same time period (no historical comparison)
11. **Baseline equivalence of groups**: the groups should be similar regarding the criteria other than the studied endpoints. Absence of confounding factors that could bias the interpretation of the results
12. **Adequate statistical analyses**: whether the statistics were in accordance with the type of study with calculation of confidence intervals or relative risk

6.4.3 Data Extraction

Participant information, implant details, outcome measures, and results were extracted and compiled in the summary of included studies (Table 4). Data extracted included maximal flexion angle and anterior-posterior contact patterns for both the medial and lateral compartments at 90° kneeling and kneeling at maximal flexion. Mean data and variability were extracted from the published tables or the graphs using Webplot digitiser (https://automeris.io/WebPlotDigitizer/). Where possible, when data were expressed as a percentage, the values were calculated back to mm. Data were reported as a distance from the centre of the tibial baseplate.

6.4.4 Data Analysis

Implants were categorised in to eight possible designs including fixed bearing and rotating platform variants of: cruciate retaining, posterior stabilised, cruciate sacrificing, or bi-cruciate stabilised. Where sufficient, extracted data were pooled into implant categories to enable meta-analysis. Meta-analyses using a quality effects (QE) model were run to determine the pooled means of maximal flexion angle, medial and lateral compartment contact patterns at 90° kneeling and kneeling at maximal flexion for each implant design. The advantage of the quality effects meta-analysis is that it allows for normalisation of individual studies' inverse variance weights based on the additional variance contribution from internal study biases (Doi et al., 2015). This method is different from the usual random redistribution of weights seen with a random effects model. In this way, selection bias is not introduced by excluding studies based on quality, but studies of more inferior quality have less effect on the results of the meta-analysis than those of higher quality.

Because most of the included studies did not have comparator groups, their pooled means and associated 95% confidence intervals were calculated by entering pseudo-comparison group data of zero for all measurement and variation data. In this way the data represented in the

forest plots reflected the translation and rotation data described for each cohort. The weighted

mean differences (WMD) were calculated for maximal flexion angle, medial and lateral

contact patterns (kneeling at 90° and maximal flexion), and lateral to medial compartment

differences (kneeling at 90° and maximal flexion). Only studies which reported contact

patterns in mm were included in the meta-analyses. All analyses were carried out using

MetaXL version 1.1 (EpiGear International; Wilston, Queensland, Australia). Heterogeneity

of contact pattern data, for each implant design, were evaluated using I^2 tests where 0% to

40%: might not be important; 30% to 60%: may represent moderate heterogeneity; 50% to

90%: may represent substantial heterogeneity; 75% to 100%: considerable heterogeneity

(Higgins et al., 2019). A sensitivity analysis was also performed to determine how differences

in kneeling strategy influenced the weighted means for the contact patterns and maximal

flexion by subtracting the studies that used bilateral kneeling from the total cohorts.

Comparison between implant designs was made by visualising the estimated means and

associated confidence intervals. Inferential statistics comparing different meta-analyses are

not possible.

6.5   Results

6.5.1   Data Extraction

The electronic search strategy identified 119 studies, of which 26 studies were included in the

review (Figure 6-1) (Barnes et al., 2011; Coughlin et al., 2007; Delport et al., 2006; Gamada

et al., 2008; Ginsel et al., 2009; Hamai et al., 2008; Hanson et al., 2007; Howell et al., 2013,

2009; Incavo et al., 2004; Kanekasu et al., 2004; Kuroyanagi et al., 2012; Mahoney et al.,

2009; Mikashima et al., 2010; Moonot et al., 2009; Moro-oka et al., 2007; Nakamura et al.,

2009; Nakamura et al., 2014, 2015; Niki et al., 2013; Okamoto et al., 2011; Scott et al., 2016;

Tanaka et al., 2011; Watanabe et al., 2015; Watanabe et al., 2013, 2016).
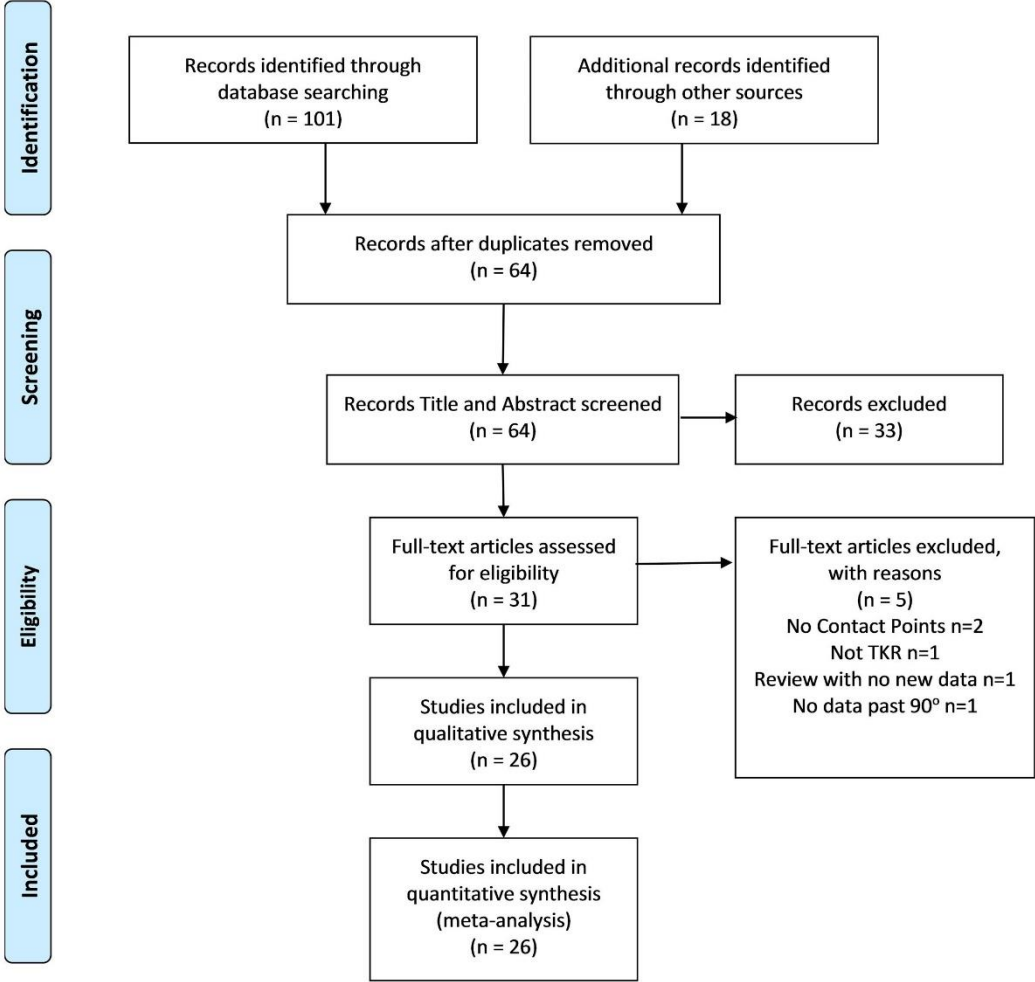
Figure 6-1: Consort Flow Diagram of study identification and screening for final
inclusion.

6.5.2   Study Characteristics

Table 6-3 describes the study characteristics. 26 studies described 41 cohorts and 797 TKRs

from 638 patients. Only posterior-stabilized fixed-bearing and cruciate-retaining fixed-bearing

designs had data for more than 200 participants. On average, there were 19 TKRs per study

group. There were 25 different implants used and six unique implant designs. Unilateral kneeling onto a padded box with the contralateral leg on the ground was most common (n=21).

Table 6-3: Summary of implant designs included in the review

	Number of studies	Number of cohorts	Number of TKRs
Fixed Bearing, PS	7	13	247
Rotating Platform, PS	3	5	50
Fixed Bearing, CR	11	14	243
Rotating Platform, CR	1	2	16
Fixed Bearing, CS	5	6	145
Fixed Bearing, BCS	1	1	25

Note: PS - cruciate sacrificing + posterior stabilised; CR - Posterior cruciate retaining; CS - cruciate sacrificing; BCS – Bi-Cruciate Substituting

6.5.3   Quality and Risk of Bias within Studies

Non-comparative and comparative studies had similar MINORS scores of 64% and 67%, respectively (Table 6-4). Strengths included clearly stated aims, prospectively collected data and appropriately selected end-points. Weaknesses included not reporting prospective power calculations, and non-inclusion of consecutive patients.

6.5.4   Study Data

Study characteristics and kinematic data are included in Table 6-5 and Table 6-6, respectively. One of the 26 studies did not report contact patterns at 90° or maximal flexion (Kanekasu et al., 2004). Only 24 of 26 studies reported contact patterns in mm from the centre of the baseplate and two as a percentage of the distance from the centre (Barnes et al., 2011; Coughlin et al., 2007). All studies generated the contact patterns by registering a computer model of the implant to either a fluoroscopy (n=9) or lateral x-rays (n=17). Kneeling contact patterns were extracted at 90° flexion in 20 cohorts, and maximal flexion in 34 cohorts.

Maximal flexion angle was reported in 38 cohorts (Table 6-6). The sensitivity analysis for

bilateral versus unilateral kneeling revealed that the maximal flexion angle was not different

after Niki *et al.* was removed (Figure 6-2) (Barnes et al., 2011; Coughlin et al., 2007; Niki et

al., 2013). Niki *et al.* included only high flexion patients who were not representative. No

bilateral kneeling data were available for a sensitivity analysis of medial and lateral contact

patterns.

Table 6-4: Quality assessment of included studies according to the Methodological Index for Non-randomized Studies (MINORS) checklist. Each category is scored out of a maximum of 2

			Non-Randomised Studies							Additional criteria in the case of comparative study				
Author	Aim	Consecutive patient	Prospective collection of data	Appropriate endpoints	Unbiased endpoint assessment	Appropriate follow-up	Loss to follow up < 5%	Prospective sample size calculation	Adequate control group	Contemporary group	Baseline group equivalence	Adequate statistical analyses	Score	Percentage
Barnes 2011	2	2	2	2	0	1	-	0	2	0	2	1	14/22	0.64
Coughlin 2007	0	0	2	2	0	2	-	0	2	0	2	2	12/22	0.55
Delport 2006	2	0	2	2	0	2	-	0	2	2	0	1	11/22	0.50
Gamada 2008	2	2	2	2	1	2	2	0	2	2	2	2	21/24	0.88
Ginsel 2009	2	0	2	2	0	1	-	0	-	-	-	-	7/14	0.50
Hamai 2008	2	1	2	2	0	2	-	0	2	0	1	2	14/22	0.64
Hanson 2007	2	0	2	2	0	2	-	0	-	-	-	-	8/14	0.57
Howell 2009	1	1	0	2	0	2	-	0	-	-	-	-	6/14	0.43
Howell 2013	2	2	2	2	0	2	2	2	-	-	-	-	14/16	0.88
Incavo 2004	2	0	2	2	0	2	-	0	2	0	2	2	14/22	0.64
Kanekasu 2004	2	2	2	2	0	2	-	0	-	-	-	-	10/14	0.71
Kuroyanagi 2012	2	2	2	2	0	2	-	0	-	-	-	-	10/14	0.71
Mahoney 2009	2	0	2	2	0	2	-	0	-	-	-	-	8/14	0.57
Mikashima 2010	2	0	2	2	0	2	-	0	2	2	1	1	14/22	0.64
Moonot 2009	2	0	2	2	0	2	-	0	-	-	-	-	8/14	0.57
Moro-oka 2007	2	0	2	2	0	2	-	0	1	2	1	2	14/22	0.64

Nakamura 2009	2	0	2	2	0	2	-	0	-	-	-	-	8/14	0.57
Nakamura 2014	2	0	2	2	0	2	-	0	-	-	-	-	8/14	0.57
Nakamura 2015	2	0	2	2	0	2	-	0	-	-	-	-	8/14	0.57
Niki 2013	2	2	2	2	0	2	2	0	2	2	2	1	19/24	0.79
Okamoto 2011	2	0	2	2	0	2	-	0	2	2	2	2	16/22	0.73
Scott 2016	2	0	2	2	0	2	-	0	-	-	-	-	8/14	0.57
Tanaka 2011	2	2	2	2	0	2	2	2	-	-	-	-	16/18	0.89
Watanabe 2013	2	2	2	2	0	2	0	0	2	2	2	2	18/24	0.75
Watanabe 2015	2	1	2	2	0	2	-	2	-	-	-	-	11/14	0.79
Watanabe 2016	2	0	2	2	0	2	-	2	2	1	2	1	16/22	0.73

Table 6-5: Study Characteristics.

All measures are reported as mean ± SD. Values reported in brackets are ranges.'-' indicates there was no data reported

PS - Cruciate sacrificing + posterior stabilised; CR - Posterior cruciate retaining; CS - Cruciate sacrificing; BCS – Bi-Cruciate Substituting; FB – Fixed Bearing;

RP – Rotating Platform; ^{O} – Degrees; mm - millimetres

Study	Study design (Level of Evidence)	Number of TKRs (patients)	Implant Name	Design	Other Characteristics	Alignment	Age	Follow-up Time	Clinical Rating
Incavo 2004	Retrospective case-control study (IV)	10 (9)	Scorpio, Stryker	FB, CR		Mechanical	68.5±6.10	21.3±12.7	KSS: 91.9 (85–100)
		10 (9)		FB, PS			68.5±6.10		
Kanekasu 2004	Retrospective case series (IV)	18 (12)	Scorpio Superflex, Stryker	FB, PS		Mechanical	-	>3 months	International Knee Society scores (IKS) 99 (97–100)
Delport 2006	Retrospective case-control study (IV)	11 (11)	Performance, Biomet	FB, CR		Mechanical	66 years (53 to 76)	16 months (12 to 24)	'well performing'
		10 (10)		FB, PS					
		10 (10)		RP, PS					
Coughlin 2007	Retrospective case-control study (IV)	11 (7)	Scorpio, Stryker	FB, PS	Standard Tibial Bearing	Mechanical	59-75	50±32months	KSS>85
		11 (8)	Scorpio High Flex, Stryker	FB, PS	High Flexion Tibial Bearing		59-82	23+/55months	
Hanson 2007	Retrospective case series (IV)	22 (16)	Legacy Knee- Posterior Stabilized High Flex, Zimmer	FB, PS		Mechanical	70.9 ± 5.2	minimum 6 months	'Well-Functioning'
Moro-oka 2007	Prospective case-control Study (III)	5 (12)	Natural-Knee, Zimmer	FB, CR	PCL retained	Mechanical	-	72 (54–96) months	KSS: 88 (86–89)
		9 (12)	N2C, Zimmer	FB, CR	ACL and PCL retained		-	71 (4–84) months	KSS: 87 (85–89)
Gamada 2008	Prospective RCT (II)	8 (8)	TC-PLUS SB Solution, Smith & Nephew	RP, CR	Blocks Balancing	Mechanical	71.0 ± 8.4;	10.3±3.1	KSS: 90.5 ± 5.9
		8 (8)		RP, CR	Spreader Balancing		72.2 ± 6.7	11.3 ± 2.3	KSS: 93.5 ± 1.8
Hamai 2008	Retrospective case-control study (IV)	10 (8)	Foundation Knee, DJO Global	FB, CR	Flat Tibial Bearing	Mechanical	71.6	17.3months	KSS Knee 91.4; KSS Function 80.6
		10 (7)	Nexgen LPS, Zimmer	FB, PS	Conforming Tibial Bearing		72.6		
Ginsel 2009	Retrospective case series (IV)	20 (16)	3D Knee System, DJO Global	FB, CR		Mechanical	69 (43-84)	6-12months	KSS>180
Howell 2009	Retrospective case series (IV)	35 (35)	Vanguard, Biomet	FB, CR	Kinematic Alignment	Kinematic	67 ± 9.8 years (53-92y)	4 ± 1.3 months	KSS: 93 (75-100); OKS: 37 (22-48)

Author	Study Type	N (n)	Implant	Bearing	Notes	Alignment	Age	Follow-up	Outcome
Mahoney 2009	Retrospective case series (IV)	20 (15)	ScorpioFlex, Stryker	FB, PS		Mechanical	76.3 (44-90 years)	min 6 months	KSS: minimum Knee 100; Function 80
Moonot 2009	Retrospective case series (IV)	15 (13)	MRK, Finsbury Orthopaedics	FB, CS	Medial Pivot	Mechanical	75 ± 7	17 ± 4 months	KSS: Knee 95 ± 3; Function 99 ± 2
Nakamura 2009	Retrospective case series (IV)	20 (20)	NexGen LPS, FlexMobile	RP, PS		Mechanical	77 (70-84)	minimum 1 year	HSS: 91 (86-97)
Mikashima 2010	Retrospective case-control study	10 (9)	Foundation Knee, DJO Global	FB, CR		Mechanical	66 ± 7	minimum 12 months	KSS: 95 ± 2
		10 (9)	3D Knee System, DJO Global	FB, CR	ACL Substituting		68 ± 5		KSS: 90 ± 7
Barnes 2011	Retrospective case-control study (IV)	9 (9)	Advance, Wright Medical	FB, CS	Medial Pivot	Mechanical	-	5 months (3-8)	Successful
		9 (9)		FB, CR	Double High Tibial Bearing		-	9 months (6-13)	Successful
Okamoto 2011	Retrospective case-control study (IV)	10 (10)	Duracon, Stryker	FB, CR	Bilateral	Mechanical	74	83 months	KSS: 182
		10 (10)	Triathlon, Stryker	FB, PS (n=2); FB CR (n=8)				33 months	KSS: 187
Tanaka 2011	Prospective Longitudinal cohort study (III)	20 (20)	NexGen LPS Flex Mobile, Zimmer	RP, PS / RP, PS / RP, PS		Mechanical	77 years (70–84 years)	3m / 6m / 12m	HSS: 91 (86–97)
Kuroyanagi 2012	Retrospective case series (IV)	25 (21)	Journey BCS, Smith & Nephew	FB, BCS		Mechanical	63 (43-73)	minimum 12 months	well aligned and functioning (KSS: 85±12)
Watanabe 2013	Prospective case-control study (III)	27 (27)	3D Knee System, DJO Global	FB, CR	PCL retained	Mechanical	76±6	18 ± 5 months	-
		29 (29)		FB, CS	PCL Sacrificed		76±6	19 ± 5 months	-
Niki 2013	Retrospective case series (IV)	29 (23)	NexGen LPS Flex, Zimmer	FB, PS		Mechanical	71.4 (53-84)	55 months	KSS: 94.7 (83 to 100)
Howell 2013	Retrospective case-control study (IV)	69 (66)	Vanguard, Biomet Triathlon, Stryker	FB, CR	Kinematic Alignment	Kinematic	65 ±11.4	6 months	Oxford: 42 ± 4.8 (28–48) KSS Function: 93 ± 6.1 (70–100)
Nakamura 2014	Retrospective case-control study (IV)	10	Bi-Surface Knee System, Kyocera Medical	FB, CS	Flat Tibial Bearing	Mechanical	75.4 ± 8.3	41±35 months	judged clinically successful by their surgeons; no ligamentous laxity or pain
		44			Dish Tibial Bearing		75.4 ± 8.3		
Nakamura 2015	Retrospective case series (IV)	22 (18)	Bi-Surface Knee System, Kyocera Medical	FB, CS	Ball and socket type implant	Mechanical	74.7 ± 9.8	74.7 ± 9.8 months	KSS: 98.7 ± 2.3

Watanabe 2015	Retrospective case series (IV)	44 (34)	NexGen LPS Flex, Zimmer	FB, PS		Mechanical	71±7	Minimum 2 year	KSS: Knee 94±5; Function 75±16
Watanabe 2016	Retrospective case-control study (IV)	31 (19)	Actiyas, Kyocera Medical	FB, PS		Mechanical	74 ± 4	2.4 year ± 0.5	KSS: Knee 45 ± 10; Function 50 ± 17
		31 (24)	NexGen LPS-Flex, Zimmer	FB, PS			73 ± 5	2.5 year ±0.4	KSS: Knee 40 ± 11; Function 48 ± 11
Scott 2016	Retrospective case series (IV)	16 (15)	GMK Sphere, Metacta	FB, CS	Medial Pivot	Mechanical	-	10.25 months (6 to 19)	KSS Knee: 86 (80-90); Function: 89 (80-100)

Table 6-6: Summary of Kinematic data extracted.

All kinematics measures are reported as mean ± SD. Brackets are ranges. "-" indicates there was no data reported

PS - Cruciate sacrificing + posterior stabilised; CR - Posterior cruciate retaining; CS - Cruciate sacrificing; BCS – Bi-Cruciate Substituting; FB – Fixed Bearing; RP – Rotating Platform; O – Degrees; mm - millimetres

Study	Number of TKRs (patients)	Design	Other Characteristics	Kneeling Description	Contact Point Measurement	Type of Imaging	Maximal Flexion Angle	Medial Compartment		Lateral Compartment	
								90º	Maximal Flexion	90º	Maximal Flexion
Incavo 2004	10 (9)	FB, CR		Unilateral kneeling on a padded bench supporting the tibial tubercle from the knee to just proximal to the ankle.	measured in mm from centre of tibial baseplate	Lateral x-rays	110 ± 10	0.2 ± 3	-6 ± 4	1 ± 4	-6 ± 3
	10 (9)	FB, PS					111 ± 8	4 ± 4	-5 ± 4	2 ± 6	-5 ± 4
Kanekasu 2004	18 (12)	FB, PS		Unilateral kneeling. Shin placed on a padded bench 30 cm high with the foot hanging freely from the edge. Standing on contralateral leg. Bar in front for support	measured in mm from centre of tibial baseplate	Fluoroscopy	139 (125–155)	-	-	-	-
Delport 2006	11 (11)	FB, CR		-	measured in mm from centre of tibial baseplate	Lateral x-rays	105.41 ± 7.84	Cannot Extract Values	Cannot Extract Values	Cannot Extract Values	Cannot Extract Values
	10 (10)	FB, PS					109.62 ± 16.84	Cannot Extract Values	Cannot Extract Values	Cannot Extract Values	Cannot Extract Values
	10 (10)	RP, PS					94.29 ± 19.28	Cannot Extract Values	Cannot Extract Values	Cannot Extract Values	Cannot Extract Values
Coughlin 2007	11 (7)	FB, PS	Standard	Bilateral kneeling with a pad under the tibia tubercle with the knee	Normalised to anterior-posterior and medio-lateral size. Distance measured from centre of tibial baseplate	Lateral x-rays	118 ± 8	-22 ± 9	-48 ± 10	-25 ± 9	-51 ± 12
	11 (8)	FB, PS	High Flexion				125 ± 6	-21 ± 14	-56 ± 12	-19 ± 12	-59 ± 10
Hanson 2007	22 (16)	FB, PS		Unilateral kneeling on padded riser. Contralateral leg placed dorsal to the midline with slight hip flexion	measured in mm from centre of tibial baseplate	Fluoroscopy	128 ± 7	-	−7.3 ± 6.6	-	−14.1 ± 2.3
Moro-oka 2007	5 (12)	FB, CR	PCL retained	Unilateral kneeling on a padded stool. Contralateral leg on floor	measured in cm from centre of tibial baseplate	Fluoroscopy	109 ± 13	-	-0.1 ± 0.3	-	-0.3 ± 0.6
	9 (12)	FB, CR	ACL and PCL retained				104 ± 16	-	-0.2 ± 0.3	-	0.7 ± 0.3
Gamada 2008	8 (8)	RP, CR	Blocks Balancing	Unilateral kneeling on a padded bench	measured in mm from centre of tibial baseplate	Fluoroscopy	102 ± 12.8	-	-2.7 ± 12.2	-	-10.5 ± 11.4
	8 (8)	RP, CR	Spreader Balancing				107.9 ± 10.1	-	-1.8 ± 8.2	-	-11.1 ± 11.8

Study	N (n)	Type	Implant	Activity	Measurement	Imaging	Flexion			
Hamai 2008	10 (8)	FB, CR	Flat	Unilateral kneeling. Shin placed on a box with the ankle joint extended. Contralateral leg in front	measured in mm from centre of tibial baseplate	Lateral x-rays	all > 120°	4.2 ± 3.6	-	4.8 ± 3.3	-
	10 (7)	FB, PS	Conforming				all > 120°	-3.7 ± 3.2	-	-10.5 ± 3.3	-
Ginsel 2009	20 (16)	FB, CR		Unilateral kneeling on a padded chair. Standing on contralateral leg behind	measured in mm from centre of tibial baseplate	Fluoroscopy	131 ± 13	-	-2 ± 4	-	-10 ± 4
Howell 2009	35 (35)	FB, CR	Kinematic Alignment	Unilateral kneeling on stool; contralateral leg standing on floor	measured in mm from centre of tibial baseplate	Lateral x-rays	116 ± 9.6	3.8 ± 3.3	4.5 ± 3.3	−6.9 ± 5.5	−9.6 ± 5.7
Mahoney 2009	20 (15)	FB, PS		Unilateral kneeling on padded bench; contralateral leg standing on floor	measured in cm from centre of tibial baseplate	Lateral x-rays	129.9 ± 7.22	-	-1.19 ± 0.18	-	-1.4 ± 0.18
Moonot 2009	15 (13)	FB, CS	Medial Pivot Knee	Unilateral kneeling. Shin on a padded stool 30 cm high with the foot hanging freely from the edge	measured in mm from centre of tibial baseplate	Fluoroscopy	119 (101 – 139)	-1 ± 2	-	4 ± 2	-
Nakamura 2009	20 (20)	RP, PS		Unilateral kneeling. Shin on a padded bench 30 cm high with the foot hanging freely	measured in mm from centre of tibial baseplate	Lateral x-rays	124 ± 17.22	-0.1 ± 2.7	-6.7 ± 2.1	-0.7 ± 2.4	-11.8 ± 4.8
Mikashima 2010	10 (9)	FB, CR		Unilateral partial weight-bearing kneeling on padded box at 90° and kneeling at maximal flexion. Contralateral leg standing on floor	measured in mm from centre of tibial baseplate	Lateral x-rays	113 ± 11	1 ± 2	1 ± 3	-4 ± 3	-5 ± 3
	10 (9)	FB, CR	ACL Substituting				123 ± 13	7 ± 5	5 ± 8	-4 ± 5	-7 ± 7
Barnes 2011	9 (9)	FB, CS	Medial Pivot	bilateral kneeling on padded stool supporting the anterior aspect of the leg from tibial tubercle to just proximal to the ankle	Normalised to AP size. Distance measured from centre of tibial baseplate	Lateral x-rays	108 ± 4.7	50.5 ± 12.8	-15.6 ± 6.9	19.6 ± 24.2	−12.4 ± 11.7
	9 (9)	FB, CR	Double High				116 ± 12.4	15.7 ± 25.2	-28.8 ± 20.2	1.7 ± 17.9	-30.8 ± 14.5
Okamoto 2011	10 (10)	FB, CR		Unilateral kneeling. Shin on a padded bench 30 cm high with the foot hanging freely from the edge. Standing on contralateral leg. Bar in front for support	measured in mm from centre of tibial baseplate	Fluoroscopy	119 ± 13	-	-11 ± 6	-	-17 ± 6
	10 (10)	FB, PS (n=2), FB CR (n=8)	Bilateral				120 ± 9	-	Cannot extract separate patterns	-	Cannot extract separate patterns
Tanaka 2011		RP, PS		Unilateral kneeling. Shin on a padded bench 30 cm high with the foot hanging freely from the edge. Standing on contralateral leg. Bar in front for support	measured in mm from centre of tibial baseplate	Lateral x-rays	123.7 ± 12.9	2.7 (−3.1 to 7.5)	-3.8 (−12.5 to 6.3)	-0.3 (−4.5 to 6.2)	-6.2 (−14.0 to 0.5)
	20 (20)	RP, PS					128.6 ± 13.4	2.6 (−3.1 to 7.5)	-5.7 (-12.8 to 4.4)	-1.6 (-6.2 to 3.8)	-8 (17.4 to 0.7)
		RP, PS					129.7 ± 18.3	1.6 (−4.0 to 9.2)	-4.7 (-10.8 to 3.8)	-2.7 (16.8 to 3.5)	-11.6 (-28.5 to -3.3)
Kuroyanagi 2012	25 (21)	FB, BCS		Unilateral kneeling activity on a padded bench with the contralateral foot on the floor	measured in mm from centre of tibial baseplate	Fluoroscopy	128 ± 11	-	-10 ± 3	-	-20 ± 3
Watanabe 2013	27 (27)	FB, CR	PCL retained	Unilateral Kneeling. Shin placed on 5cm pad atop a 15–35cm box with their foot hanging freely	measured in mm from centre of tibial baseplate	Lateral x-rays	115 ± 14	-2 ± 3	-3 ± 4	-4 ± 3	-7 ± 3
	29 (29)	FB, CS	PCL Sacrificed				122 ± 10	-1.7 ± -2.5	2 ± 4	-6.8 ± 1.9	-4 ± 3

Study	N (knees)	Type	Design	Position	Measurement	Imaging					
Niki 2013	29 (23)	FB, PS		Bilateral seiza-sitting position	measured in mm from centre of tibial baseplate	Lateral x-rays	148 ± 8.0	-	Cannot Extract Values	-	Cannot Extract Values
Howell 2013	69 (66)	FB, CR	Kinematic Alignment	Unilateral kneeling on a padded stool with the opposite leg behind them and out of the field of view	measured in mm from centre of tibial baseplate	Lateral x-rays	119 ± 8	2.1 ± 4.2	0.7 ± 4.5	2.5 ± 4.5	-6.5 ± 4.6
Nakamura 2014	10	FB, CS	Flat Tibial Insert	Unilateral kneeling on a 30cm padded bench with the contralateral foot on the floor	measured in mm from centre of tibial baseplate	Lateral x-rays	144 ± 10.3	-	-8.2 ± 5	-	-14.5 ± 2.8
	44		Dish Tibial Insert				138.7 ± 12.6	-	-8.9 ± 4.7	-	-14.8 ± 3.2
Nakamura 2015	22 (18)	FB, CS	Ball and socket	Unilateral kneeling on a 30cm padded bench with the contralateral foot on the floor	measured in mm from centre of tibial baseplate	Lateral x-rays	115.6 ± 22.5	-	-8.3 ± 3.4	-	-14.3 ± 2.9
Watanabe 2015	44 (34)	FB, PS		Unilateral kneeling. Shin on a padded 15 to 35 cm box with their foot hanging freely. Contralateral leg standing on floor	measured in mm from centre of tibial baseplate	Lateral x-rays	123 ± 14	-	-5 ± 4	-	-9 ± 4
Watanabe 2016	31 (19)	FB, PS		Unilateral kneeling. Shin on a padded 15 to 35 cm box with their foot hanging freely. Contralateral leg standing on floor	measured in mm from centre of tibial baseplate	Lateral x-rays	121 ± 10	-7 ± 2	-6 ± 2	-8 ± 2.3	-11 ± 2
	31 (24)	FB, PS					114 ± 9.2	0 ± 2.1	-5 ± 3.5	-4 ± 2.9	-10 ± 2.2
Scott 2016	16 (15)	FB, CS	Medial Pivot	-	measured in mm from centre of tibial baseplate	Lateral x-rays	117 ± 14	-	1 ± 4	-	-6 ± 4

6.5.5 Meta-analysis Findings

There were differences in the estimated weighted means for maximal flexion angle between implant designs (Figure 6-2). The BCS-FB design appeared to achieve greater flexion than both the CR designs; and the CR-RP design achieved less flexion than the PS-FB and BCS-FB designs. Additionally, there were no differences in the contact patterns at 90° (Figure 6-3). However, medial and lateral contact patterns for PS-FB and PS-RP were more posterior compared to CR-FB at maximal flexion (Figure 6-4). For all implant groups the medial and lateral contact patterns demonstrated posterior translation when moving from 90° to maximal flexion (Figure 6-5). Furthermore, at maximal flexion, all groups displayed more posterior translation laterally than medially. Thus, all implants demonstrated slightly more external femoral rotation (equivalent to internal tibial rotation) at maximal flexion compared to 90°. The meta-analysis could not detect any differences in rotation (Figure 6-5). The heterogeneity of the mean estimates (I^2) was substantial, meaning that it was difficult to be certain about the differences that emerged from these analyses.
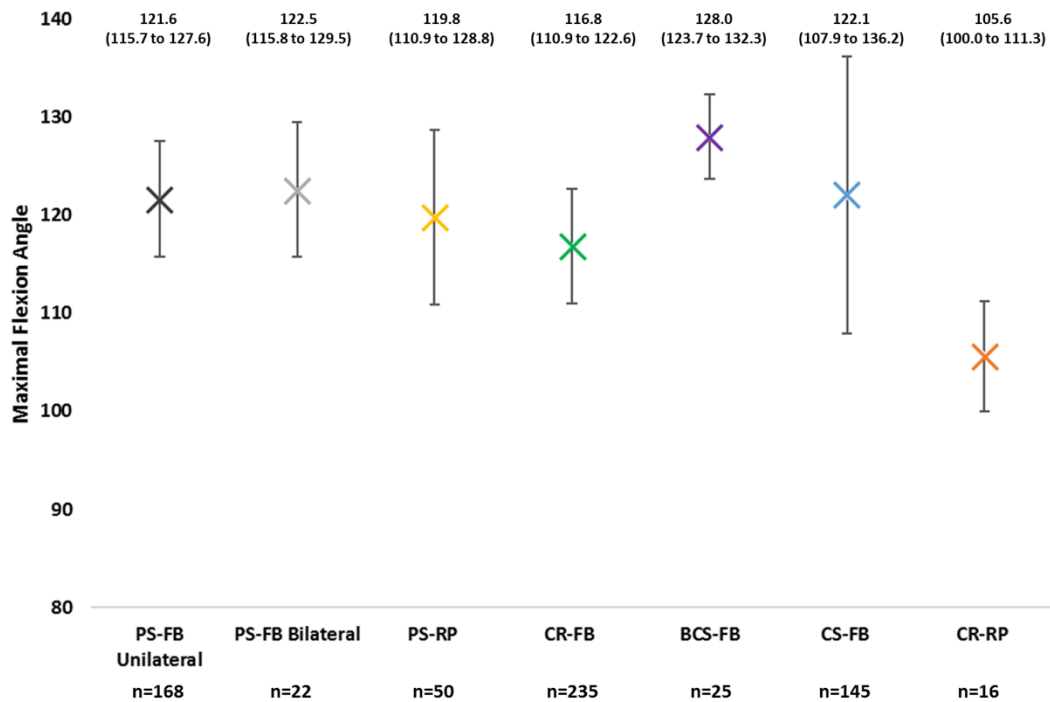
Figure 6-2: Estimates of maximal flexion angle means and 95% confidence intervals derived from quality effects models

PSFB - Cruciate sacrificing + posterior stabilised + fixed bearing; PSRP - Cruciate sacrificing + posterior stabilised + rotating platform; CRFB - Posterior cruciate retaining + fixed bearing; CSFB - Cruciate sacrificing + fixed bearing; CRRP - Cruciate retaining + rotating platform; BCSFB – Bi-cruciate substituting + fixed bearing; N= number of implants within each implant group. Unilateral – Unilateral kneeling strategy; bilateral – bilateral kneeling strategy. Only PSFB had data for bilateral kneeling. This figure does not include data from Niki et al. because data was subjected to significant selection bias (Niki et al., 2013)
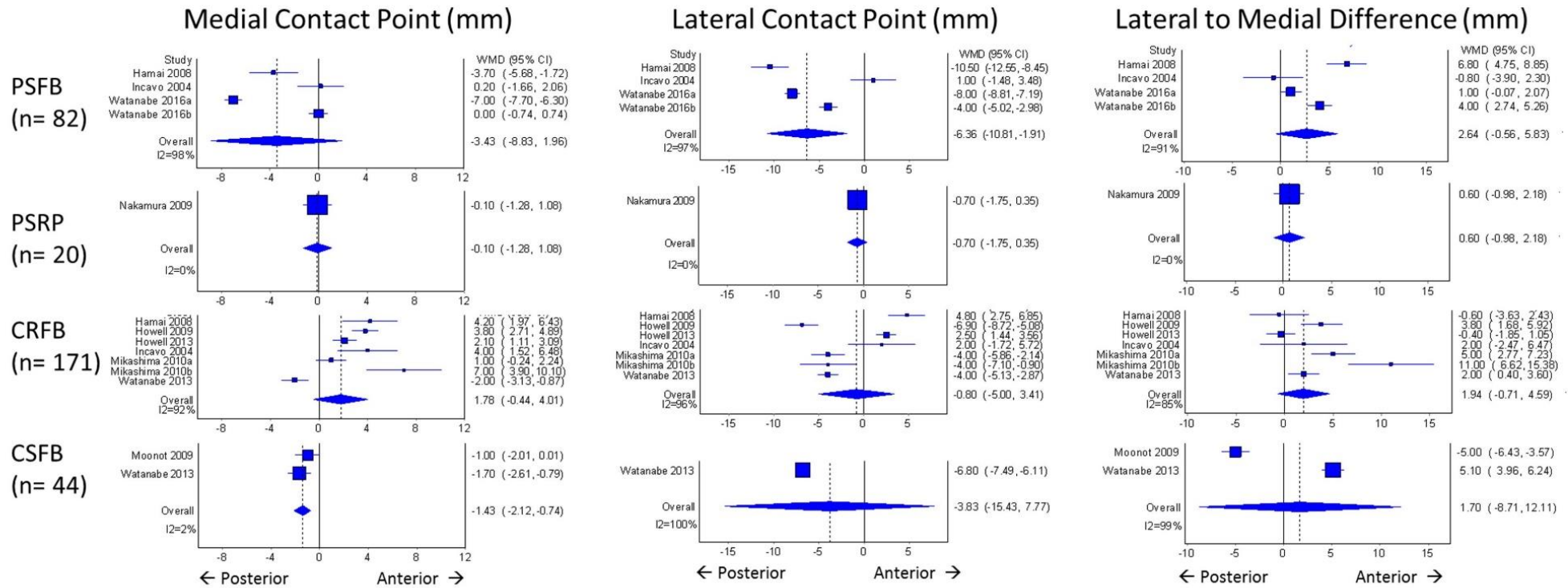
Figure 6-3: Estimated means and 95% confidence intervals for medial and lateral compartment contact patterns at 90° as derived from quality effects models. Means are reported as mm away from the centre of the tibial baseplate. Positive values indicate anterior to the centre and negative values are posterior to the centre. Note: PSFB - Cruciate sacrificing + posterior stabilised + fixed bearing; PSRP - Cruciate sacrificing + posterior stabilised + rotating platform; CRFB - Posterior cruciate retaining + fixed bearing; CSFB - Cruciate sacrificing + fixed bearing; CSRP - Cruciate sacrificing + rotating platform
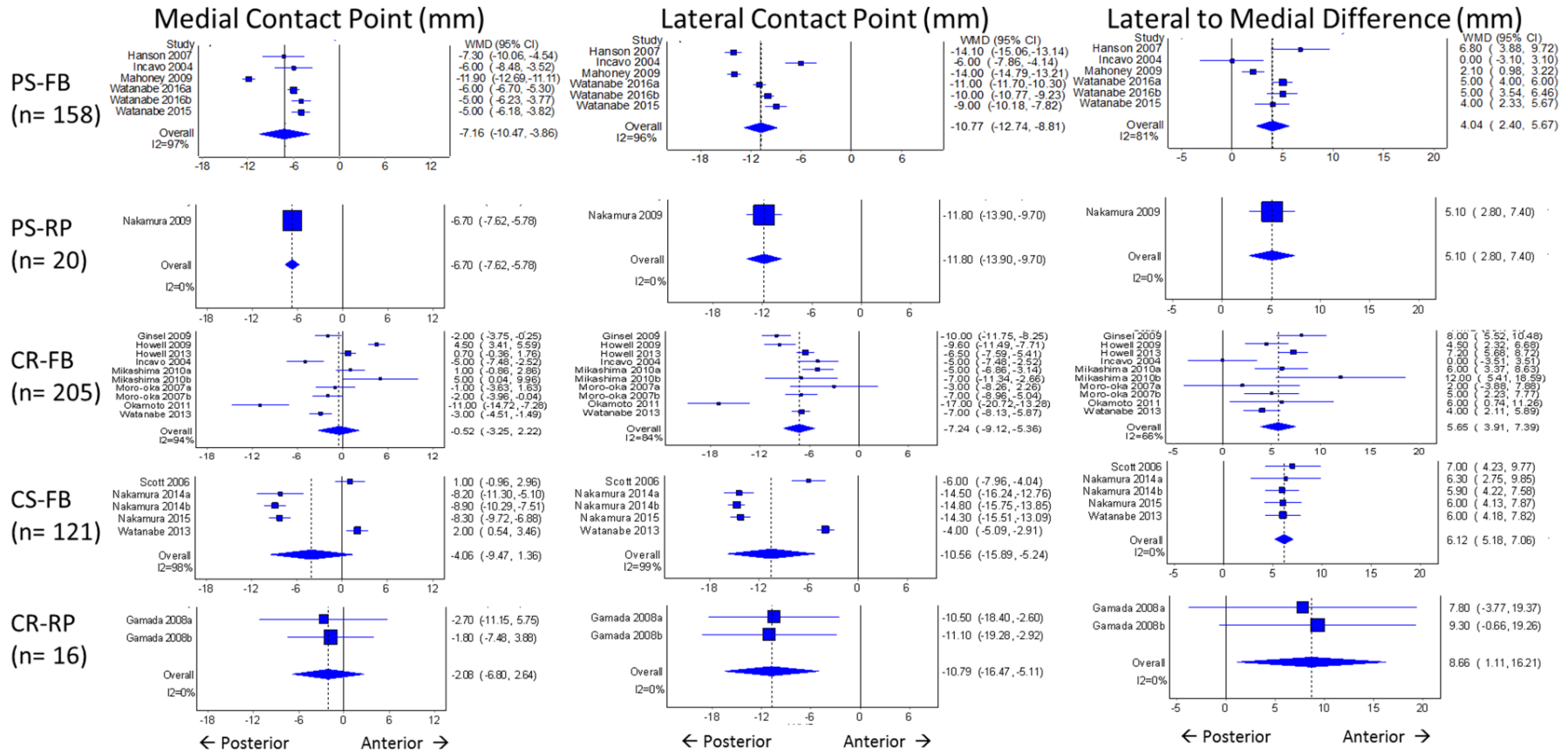
Figure 6-4: Estimated means and 95% confidence intervals for medial and lateral compartment contact points at maximal flexion resulting from a quality effects models.

Means are reported as mm away from the centre of the tibial baseplate Positive values indicate anterior to the centre and negative values are posterior to the centre. Note: PS-FB - Posterior stabilised + fixed bearing; PS-RP - Posterior stabilised + rotating platform; CR-FB - Cruciate retaining + fixed bearing; CS-FB - Cruciate sacrificing + fixed bearing; CR-RP - Cruciate retaining + rotating platform
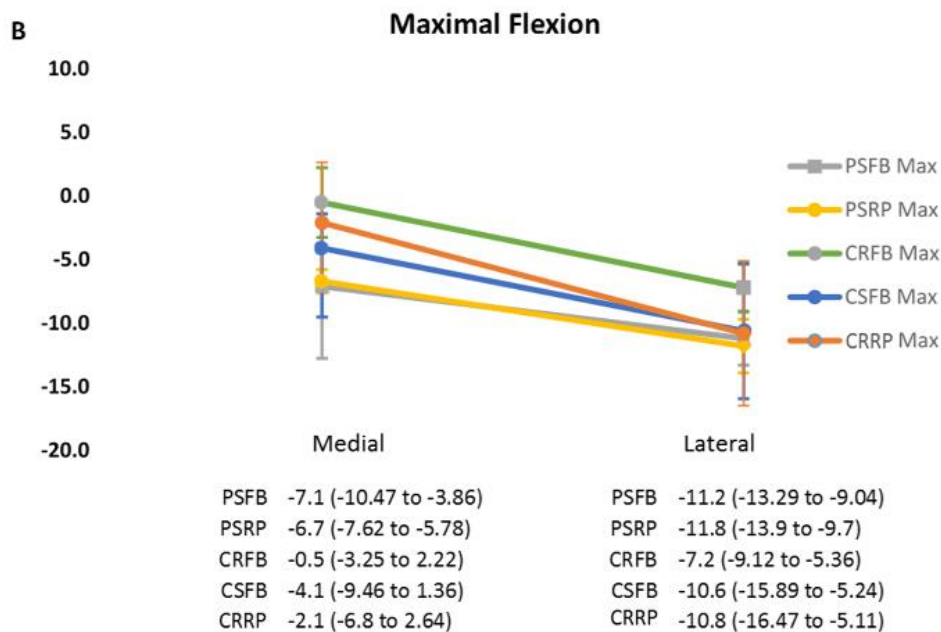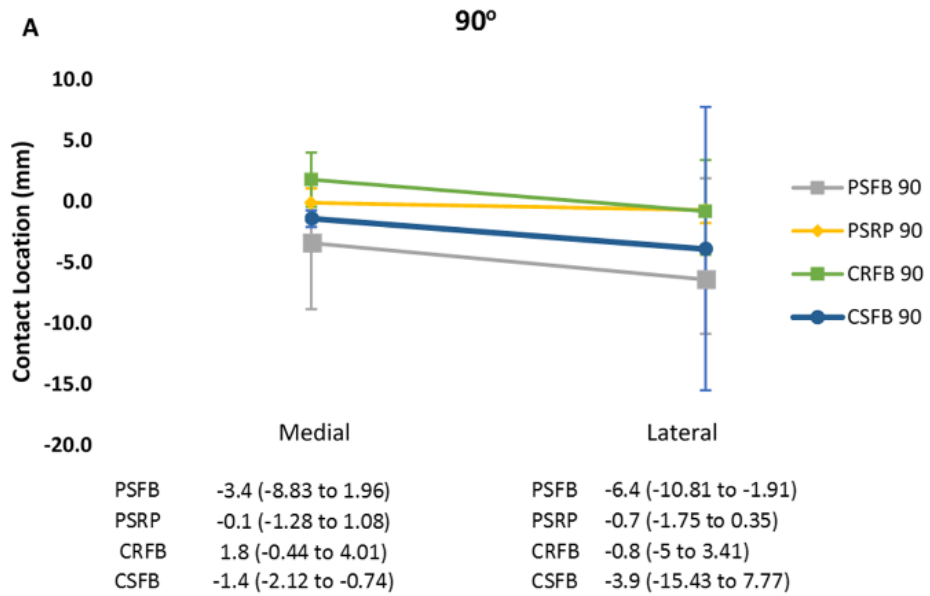
Figure 6-5: Summary of estimated weighted means with associated 95% confidence intervals for medial and lateral compartment contact patterns

A) 90° and B) maximal flexion where a more positive location indicates more anterior. The posterior stabilised designs start and finish more posterior and the cruciate retaining designs are relatively more anterior.

Note: PSFB - Bi-cruciate sacrificing + posterior stabilised + fixed bearing; PSRP - Bi-cruciate sacrificing + posterior stabilised + rotating platform; CRFB - Posterior cruciate sacrificing + fixed bearing; CSFB - Bi-cruciate sacrificing + fixed bearing; CSRP - Bi-cruciate sacrificing + rotating platform

6.6 Discussion

The most important findings of this study were that the femoral component was more posteriorly positioned on the tibia in posterior stabilised designs compared to their cruciate retaining counterparts when kneeling at maximal flexion. Furthermore, the bicruciate-stabilised fixed-bearing (BCS-FB) design appeared to achieve most flexion and the cruciate-retaining rotating-platform (CR-RP) design achieved the least, but both were from single studies with small sample sizes. Importantly, the heterogeneity for all the mean estimates was substantial.

The meta-analysis demonstrated some distinct differences in contact patterns during kneeling which were consistent with the current understanding of prosthetic kinematics. Both medial and lateral compartments for all designs translated more posteriorly at maximal flexion compared to 90°. However, posterior stabilised implants, whether fixed or rotating platform, were more posterior on the tibia at maximal flexion when compared to cruciate retaining. This result is unsurprising as the cam and post of posterior stabilised implants are designed to prevent anterior translation of the femur on the tibia and guide femoral rollback (Insall et al., 1982). Achieving posterior femoral translation mitigates against posterior impingement in higher flexion and is thought to be critical in restoring normal kinematics (Most et al., 2003). This meta-analysis of 638 participants supports this claim.

The meta-analysis indicates that external femoral rotation occurs in all designs. As the knee moves from 90° into maximal flexion, the lateral contact pattern translates more posteriorly than the medial resulting in apparent external femoral rotation. This evidence of external femoral rotation indicates that prosthetic knees behave like healthy knees during kneeling, with six-degree-of-freedom studies reporting rotations of between 10° and 20° (Galvin et al., 2018, 2019). Unfortunately, because contact-pattern data is two-dimensional, it is not possible

to directly compare the magnitude of rotation with the angular displacement data from of six-degree-of-freedom studies.

This review found that the BCS-FB design appeared to achieve the most flexion and the CR-RP design achieved the least. There did not appear to be any differences between any of the other designs. This finding contrasts with three previous systematic reviews which report greater flexion in posterior stabilised and rotating platform designs (Jacobs et al., 2004; Jiang et al., 2016; Verra et al., 2013). These reviews measured maximal flexion in non-kneeling positions, and this may have influenced the results. However, both the BCS-FB and CR-RP results are from single studies and in all designs the variability was high.

The meta-analyses revealed substantial within-design heterogeneity for most of the contact pattern data. The exception was the lateral to medial difference for the CS-FB designs at maximal flexion which was 0% (Figure 6-4). This is a surprising result since three different implants systems were included in this design. CS designs rely on geometry rather than ligamentous tethers or cam/post mechanisms to facilitate the kinematics. It is possible that these designs are more resilient to inter-individual differences, but this hypothesis would need to be tested.

The substantial heterogeneity in the other analyses could have been the result of implant geometry and the specifics of the task performed. Implant geometry has been shown to influence kinematics during gait and also flexion up to 90º (Ardestani et al., 2015; Bull et al., 2008; Schütz et al., 2019). Given that different prostheses were included within each design group, their varying geometries may have influenced the data. Kinematics are task specific (Galvin et al., 2018; McClelland et al., 2017) and kneeling was performed in different ways depending on the study. Rotation of the foot or the hip and whether the foot is free or constrained all influence the contact patterns. Yildirim *et al*. found that internally rotating the

foot increased the medial to lateral contact pattern difference (Yildirim et al., 2007). Hefzy *et al.* observed that the mechanical axis of the knee was a function of foot position relative to the hip (Hefzy et al., 1998) indicating that controlling the task is essential if data are to be compared. Three of the 26 studies reported bilateral kneeling. Two of those were comparable to unilateral kneeling in terms of maximal flexion angle and one was not. Niki *et al.* selected only patients who could achieve seiza kneeling (deep bilateral kneeling on feet) resulting in only 23 of a possible 371 patients included (Niki et al., 2013). It is important to differentiate between unilateral, bilateral and seiza kneeling cohorts because the kinematics may be fundamentally different.

There are some limitations in this meta-analysis. Most of the studies had small sample sizes, did not use consecutive patients, and did not have a comparison group. A comparison group is important because methods and technologies change rapidly making historical comparison-group data are obsolete. Other confounding factors include, differences in image acquisition strategies and instructions to participants, and inconsistent reporting of patellar resurfacing. It is also important to remark on the likelihood of selection bias in these cohorts. Of the 26 included studies only 27% reported consecutive selecting their cohort. Given that only 20% of TKR patients achieve kneeling (Wylde et al., 2019) it is likely that most of the patients included in these studies were high performing and selected for their kneeling ability.

The clinical implications of this study are twofold. First, in all designs there was evidence of posterior translation with apparent external femoral rotation. Second, the evidence to date lacks sufficient comparison data and is highly variable. Therefore, there is insufficient evidence to support any one implant design in terms of superior performance in high-flexion kneeling. Well-designed comparative trials are still required.

6.7 Conclusion

This meta-analysis revealed that the femoral component was consistently more posterior during high-flexion kneeling in posterior stabilised designs compared to their cruciate retaining counterparts. However, there was substantial heterogeneity between studies indicating a lack of clarity in this field. There remains a need for a high quality prospective comparative trials for reliable evidence and clinical utility.

7 The Influence of Total Knee Replacement Design on Kneeling Kinematics: A Prospective Randomised Clinical Trial

Statement of Contribution

This thesis is submitted as a Thesis by Compilation in accordance with

https://policies.anu.edu.au/ppl/document/ANUP_003405

I declare that the research presented in this Thesis represents original work that I carried out during my candidature at the Australian National University, except for contributions to multi-author papers incorporated in the Thesis where my contributions are specified in this Statement of Contribution.

Title: The influence of total knee replacement design on kneeling kinematics: A prospective randomised clinical trial
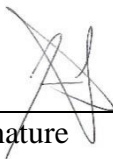
Authors: Joseph T Lynch, Diana M. Perriman, Jennie M Scarvell, Catherine R Galvin, Mark R Pickering, Terry Neeman, Paul N Smith,

Publication outlet: *Bone and Joint Journal*
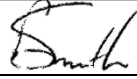
Current status of paper: *Accepted*
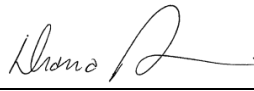
Contribution to paper: JTL: research design, acquisition, analysis and interpretation of data, drafting and critically revising the paper; DMP: research design, analysis and interpretation of data, critically revising the paper; JMS: research design, analysis and interpretation of data, drafting and critically revising the paper; MRP: research design, analysis and interpretation of data, critically revising the paper; CRG: acquisition, analysis and interpretation of data, drafting and critically revising the paper; TN: development of statistical plan; interpretation of data, drafting and critically revising the paper; PNS: research design, interpretation of data, drafting and critically revising the paper. All authors have read and approved the final submitted manuscript.

Senior author or collaborating authors endorsement: _____

Joseph Lynch		25/06/20
Candidate – Print Name	Signature	Date

Paul N Smith		25/06/20
Primary Supervisor – Print Name	Signature	Date

Dr Diana Perriman		25/06/20
Delegated Authority – Print Name	Signature	Date

7.1 Context

The systematic review with meta-analysis in chapter six highlighted a paucity of high-quality randomised trials which examined the influence of total knee replacement design on kneeling kinematics. Studies included in the review typically had small numbers, variable implant geometries, and different ways to achieve kneeling. As such, there was high heterogeneity and variability between studies making it difficult to draw any firm conclusions from the data. Therefore, a need for high quality prospective trial was identified. This chapter presents the results of our prospective randomised clinical trial of three different implant designs from one implant family (ZimmerBiomet Vanguard Knee System) which took place over five years. The results of this study will help inform surgeon choice for which implant to use and provide information regarding patient expectations around kneeling. This research was funded by ZimmerBiomet

7.2 Abstract

Modern total knee replacement prostheses are designed to restore healthy kinematics including high flexion. Kneeling is a high flexion, kinematically demanding activity after TKR. The debate about design choice has not yet been informed by 6-DoF *in-vivo* kinematics. This prospective randomised clinical trial compared kneeling kinematics in three TKR designs. 68 patients were randomised to either a posterior stabilized (PS-FB), cruciate retaining (CR-FB) or rotating platform (CR-RP) design. Sixty-four of these patients completed a minimum 1-year follow-up. Patients completed full-flexion kneeling while being imaged using single-plane fluoroscopy. Kinematics were calculated by registering the 3D implant models onto 2D-dynamic fluoroscopic images and exported for analysis. CR-FB designs had significantly lower maximal flexion compared to CR-RP and PS-FB. The PS-FB design displayed a more posteriorly positioned femur throughout flexion. Furthermore, the CR-RP femur was more externally rotated throughout kneeling. Finally, kinematics variability was high within all designs. The increased maximal flexion found in the PS-FB and CR-RP designs were likely achieved in different ways. The PS-FB design uses a cam-post to hold the femur more posteriorly preventing posterior impingement. The external rotation within the CR-RP design was surprising and hasn't previously been reported. It is likely due to the polyethylene bearing being decoupled from flexion. The findings of this study provide insights into the function of knee replacement designs in the context during deep kneeling. They also provide clinicians with a more kinematically informed choice for implant selection and provide better management of patient's functional expectations.

7.3   Introduction

In total knee replacement (TKR), high flexion is an important indicator of success. A well performing TKR normally achieves 110-120° of flexion (Verra et al., 2013) but higher flexion is considered a more desirable outcome. Deep kneeling in native knees requires up to 165° of flexion, which is greater than other high-flexion activities (Hefzy et al., 1998). Therefore, deep kneeling is demanding after TKR, but it is also highly desirable (Wylde et al., 2019). Understanding the kinematics of deep kneeling is the fundamental step in facilitating kneeling for future TKR recipients.

Implant choice is dictated, not only by implant survival and surgeon preference, but also by kinematic performance (Vertullo et al., 2017). However, the debate over which implant to use is still unresolved. According to the Australian Joint Registry, the two most commonly used designs are posterior cruciate retaining (CR), and posterior stabilised (PS), with both having fixed- and rotating-platform tibial insert variants (Australian Orthopaedic Association National Joint Replacement Registry (AOANJRR), 2019). The CR design retains the posterior cruciate ligament (PCL) and relies on it to mimic native femoral rollback in deep flexion. In the PS design, a cam and post replaces the PCL thereby preventing anterior translation and facilitating rollback of the femoral condyles on the tibial bearing (Insall et al., 1982). The rotating tibial platform was designed to reduce contact stresses on the polyethylene bearing through higher articular conformity and greater contact area (McEwen et al., 2005; Walker & Sathasivam, 2000). Additionally, this design theoretically promotes axial rotation (Sawaguchi et al., 2010). While there are minimal differences between implants in terms of pain and clinical outcomes (Verra et al., 2013), the CR design has a slightly lower revision rate at 18 years compared to PS (8.2% vs 9.5%) as do fixed-bearing designs compared to mobile bearings (8.3% vs 9.6%) (Australian Orthopaedic Association National Joint Replacement Registry (AOANJRR), 2019). However, in terms of function, the

posterior-stabilised design has been reported to confer greater maximal knee flexion (Verra et al., 2013), possibly providing more potential for deep kneeling after TKR.

The different TKR designs achieve deep kneeling using unique mechanisms. The PS design appears to facilitate a more posterior femoral position throughout flexion when compared to CR designs (Insall et al., 1982; Victor & Bellemans, 2006). The CR design uses the PCL to drive posterior femoral translation and its implant geometry to control axial rotation(Most et al., 2003). However, the kinematic data underpinning our assumptions about these designs may be flawed because: they are typically derived from retrospective single cohorts; are biased towards high-performing patients and; compare designs with different tibiofemoral and polyethylene geometries (Lynch et al., 2020). These deficiencies limit our understanding of the influence of design on six-degree-of-freedom kneeling kinematics.

The purpose of this study was to prospectively compare the six-degree-of-freedom kinematics of posterior-stabilised fixed-bearing (PS-FB), cruciate-retaining fixed-bearing (CR-FB) and cruciate-retaining rotating-platform (CR-RP) designs during deep kneeling. We hypothesized that 1) PS-FB designs will have greater maximal flexion angle than CR-FB and CR-RP. 2) The femoral component of PS-FB designs will be more posterior on the tibia throughout flexion compared to CR-FB and CR-RP designs.

7.4 Methods

This was a single-centre, prospective, longitudinal, parallel group, randomized clinical trial (International Standard Randomized Controlled Trials Number: 75076749). Ethics approval for the study was obtained from local ethical committees.

Eligible participants were aged over 18 years, had knee osteoarthritis, and were awaiting TKR. Full inclusion/exclusion criteria are reported in Table 7-1. All participants provided written informed consent to participate.

Table 7-1: Inclusion and exclusion criteria

Inclusion Criteria
X-ray confirmation of osteoarthritis
On surgical list for total knee replacement
Exclusion criteria
Lateral compartment osteoarthritis only
BMI > 38
Wholly inactive or severely restricted to the minimum of activities of daily living.
Knee flexion < 90° (can you position your foot under your knee while sitting?)
A psychosocial reason not to be able to consent or complete the requirements of the study
Metastatic disease
Pathological fracture
Revision knee replacement
Poor understanding and is unable to provide informed consent
Pregnancy

Between December 2013 and January 2016, 124 participants were recruited. Forty-five participants were excluded for not meeting the inclusion criteria and 11 were not randomised leaving 68 enrolled in the trial (Figure 7-1). All participants were blinded to the implant design.

A permuted-block randomization design with a block size of six, stratified by sex was used to allocate each subject to one of the three implant designs. Allocation was achieved using consecutively numbered envelopes according to the order dictated by a random number generator. These envelopes were held in a separate location by an administrator who was

blind to the randomization and design allocation and not involved in the study in any way

except to inform the team of the random allocation for each participant.
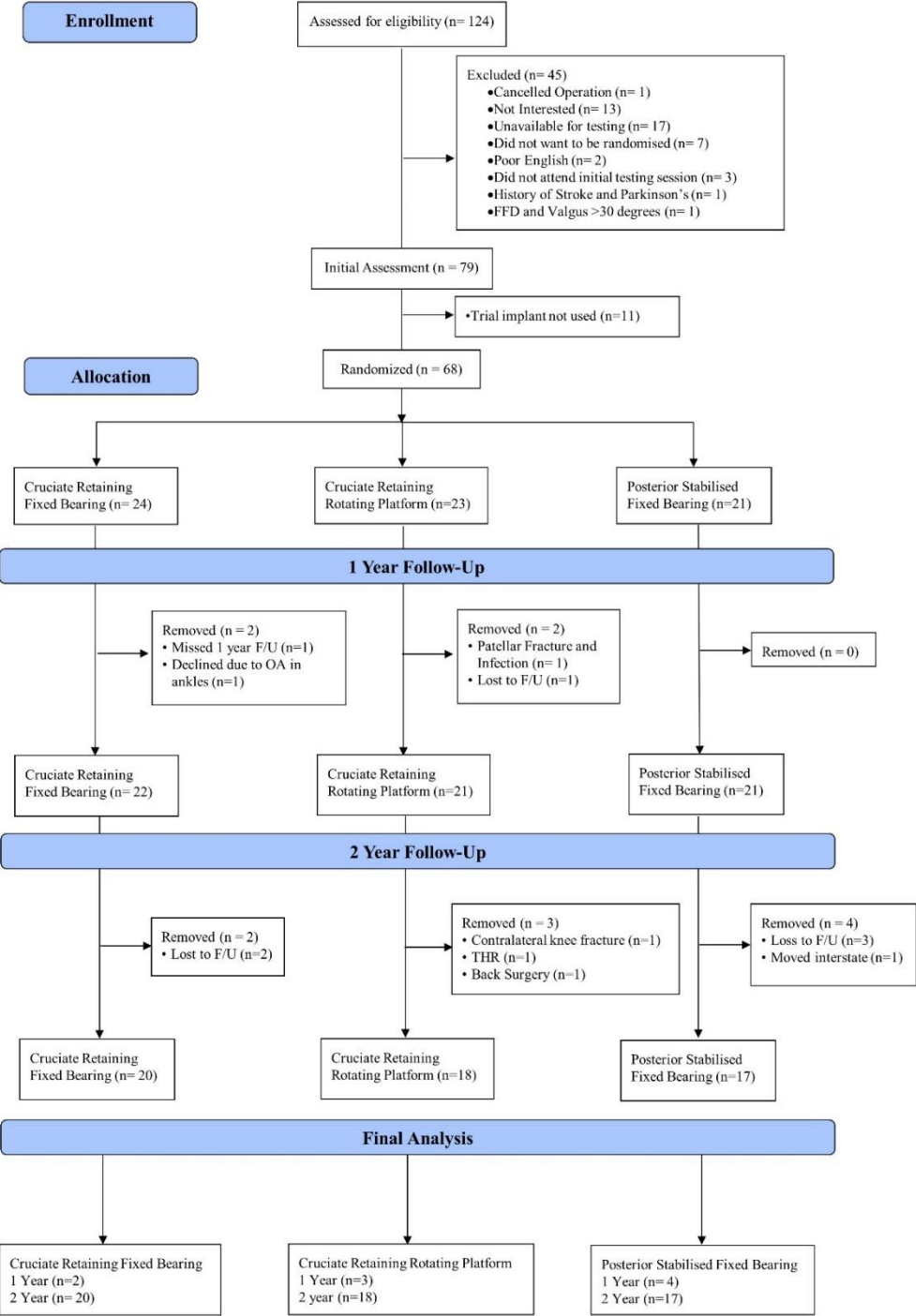
Figure 7-1: Consort flowchart illustrating patient selection for the trial.

One-year data was included for those participants who did not return for their two-year

follow-up

All surgeries were performed by a knee fellowship trained surgeon. All participants received one of three cemented Vanguard® TKR designs (Vanguard Knee System, ZimmerBiomet, Warsaw, Indiana) between January 2014 and October 2016. All designs had consistent femoral geometry. Participants received a general anaesthetic combined with a local spinal anaesthetic prior to inflation of the tourniquet. A midline incision with a medial parapatellar approach was used. Standard extra- and intra-medullary instrumentation was used in all knees. A standard technique was used with the aim of placing the components in neutral alignment relative to the mechanical axis.

Testing was conducted 12- and 24-months post-surgery and occurred between December 2013 to November 2018. Patient reported outcome measures (PROMs) included Oxford Knee Score (OKS), and 100-point visual analogue scales (VAS, 0-100 best to worse) for pain and satisfaction were collected to assess subjective performance.

Participants were asked to perform a unilateral deep-kneeling movement on a padded box with the foot hanging and the other leg behind the box so as not to obscure the knee of interest. All participants were initially positioned with their knee at approximately 90° and asked to bend until full flexion was achieved. Movement was recorded using single-plane fluoroscopy (Axiom Artis, Siemens, Munich, Germany) placed for a sagittal view of the knee, sampling images at 30Hz with 1024x1024-pixel spatial resolution and 12 bits/pixel. Calibration was achieved using a 350 mm x 350 mm perspex box implanted with an array of 1mm tantalum beads spaced at 20 mm intervals. The box enabled correction of the pin-cushion distortion present in the fluoroscopy image.

Kinematic data were generated by registering the femoral and tibial computer-aided design (CAD) models for each of the TKR designs to the fluoroscopic images using bespoke software Orthovis© (MathWorks, Natick, MA). The precision of Orthovis was previously

reported for in-plane (sagittal) registration as 0.2 mm for translation and 0.3° for rotation, while the out-of-plane precision was 0.9 mm and 0.5° (Akter et al., 2014a; Scarvell et al., 2010).

Orthogonal axes for femoral and tibial implants were adapted from the convention developed by Grood and Suntay (Grood & Suntay, 1983) and Guan *et al.*(Guan et al., 2017). The six-degree-of-freedom kinematics were then exported for analysis and reported as a function of flexion. Flexion, adduction, internal femoral rotation and anterior, medial and superior translations were described as positive (Figure 7-2).
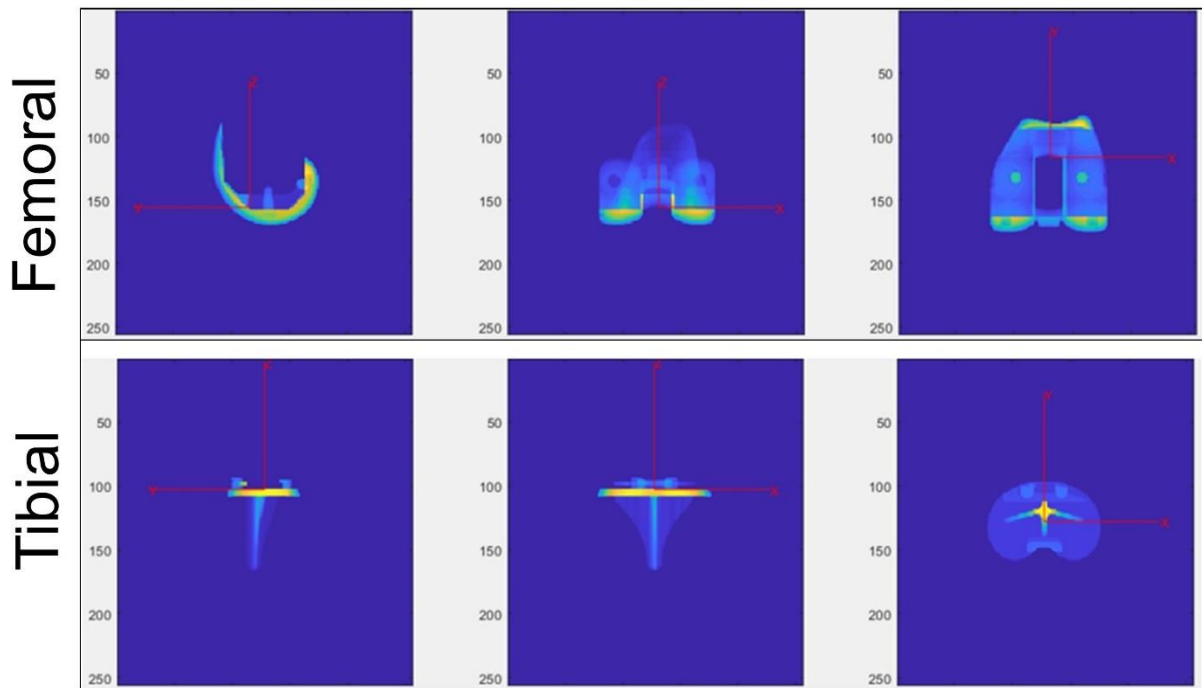
Figure 7-2. Femoral and Tibial Axes Definitions

Top: Axes definitions for the femoral and tibial components of the knee prostheses. The origin of the femoral axial system was identified in three planes. Left: Sagittal view - The most anterior position of the floor of the femoral component. Middle: Coronal - At the mid-point of the intercondylar notch. Right: Axial - The midpoint of the most anterior point of the intercondylar notch. The x-axis for the femoral component was parallel to the transverse surface of the most anterior point of intercondylar notch being positive in the medial direction and negative in the lateral direction. The z-axis was perpendicular to the x-axis being positive in the rostral/superior direction and negative in the caudal/inferior direction. The y-axis was perpendicular to both the x-and z-axes being positive in the anterior/ventral direction and negative in the posterior/dorsal direction.

Bottom: The origin of the tibial axial system was identified in three planes. Left: Sagittal view - At the middle of the horizontal line connecting the centres of the medial and lateral condyles on the polyethylene spacer. Middle: Coronal – Middle of the top surface of the tibial baseplate. Right: Axial – Top surface of the tibial baseplate. The x-axis of the tibial component was parallel to the transverse flat surface of the tibial baseplate with the medial direction being positive and the lateral direction being negative. The z-axis of the tibial component was perpendicular to the transverse flat surface of the tibial baseplate and the x-axis with the superior/rostral direction being positive and inferior/caudal direction being negative. The y-axis was perpendicular to both the x-axis and the z-axis with the anterior/ventral direction being positive and the posterior/dorsal direction being negative.

There were 36 participants who did not start the kneeling task at 90° of knee flexion and so backward extrapolation of this missing kinematic data was required to have a dataset that could be compared. This was achieved using the travelling salesman problem (TSP) algorithm (Lawler et al., 1985). This algorithm used the kinematic curves with complete data (*i.e.* curves which contained kinematic values starting at 90°) to predict the missing values at 5° flexion intervals for the curves that were missing data (Supplementary).

Sample size was determined by an *a-priori* power calculation. With a study power of 80% and statistical significance at less than 0.05 (two-sided $p < 0.05$), the sample size required for this study was 60 participants divided equally into the three TKR designs. The primary outcome was anterior-posterior translation range (difference from the mean 90° value and maximal flexion angle) because it is strongly associated with high flexion, stability of the knee, and replication of healthy knee kinematics during knee flexion. The clinically important difference of anterior-posterior translation was defined as 4.1mm, and we assumed a within-group standard deviation of 4.5 mm (Scarvell et al., 2007).

A detailed statistical plan was completed *a-priori*. An independent statistician blinded to the group assignments performed all the analyses. All analyses used the intention-to-treat principle where unavailable 2-year follow-up data were replaced by 1-year follow-up data.

Continuous baseline demographic data, as well as baseline PROMs for each design, were summarised using means ± standard deviation or errors. Categorical baseline data were summarised using frequencies and percentages within each design. Differences between designs for kinematic ranges (90°-maximal flexion), kinematics at maximal flexion and PROMs were estimated using multivariate-linear models, with design as the factor of interest, adjusted for BMI, sex and age. Average tibiofemoral positions and angles throughout flexion

were compared using mixed-effect-linear models, with flexion*design, BMI, sex and age as fixed effects and ID as the random effect. Mean differences between the TKR designs were described as marginal means with 95% confidence intervals. P-values for post-hoc pairwise comparisons were adjusted using the Tukey method for all analyses. All analyses were undertaken using R v3.6.1 (R Development Core Team, 2019).

7.5 Results

Of the 124 participants approached for the study, 68 were randomised, 64 returned for 1-year follow-up and 55 returned at 2 years. 6 were lost to follow up (CR-FB=2; PS-FB=3; CR-RP=1) (Figure 7-1). This resulted in 22 CR-FB, 21 CR-RP, and 21 PS-FB participants included in the final analyses (Figure 7-1). No prostheses were revised in the study period but one patient was removed because of a patellar fracture and subsequent infection prior to their one-year assessment (Table 7-2). There were no design differences for clinical outcomes at either baseline or follow-up (Table 7-3 and Table 7-4).

Table 7-2: Post-operative complications

		Cruciate Retaining-Fixed Bearing	Cruciate Retaining-Rotating Platform	Posterior Stabilised-Fixed Bearing
Manipulation under anaesthetic		2	-	1
Infection		-	-	-
	Skin	-	1	1
	Deep	1	1	-
Deep vein thrombosis		1	1	2
Pulmonary embolism		-	1	1
Patellar fracture		-	1	-

Table 7-3: Baseline characteristics for participants included in final analysis. Results displayed as mean ± standard deviation

	Cruciate Retaining-Fixed Bearing	Cruciate Retaining-Rotating Platform	Posterior Stabilised-Fixed Bearing
N	22	21	21
Sex (male; female)	11: 11	10: 11	8: 13
Age (years)	70.3 ± 7.4	70.0 ± 8.3	70.1 ± 7.1
Operated side (left; right)	15: 7	6: 15	13: 8
Mass (kg)	96.3 ± 16.20	88.0 ± 18.20	84.6 ± 19.00
Height (cm)	170.0 ± 9.3	168.2 ± 8.9	167.7 ± 8.8
BMI (kg m^{-2})	33.4 ± 5.4	30.9 ± 5.9	30.0 ± 6.2
Oxford Knee Score (/48)	23.7 ± 5.4	26.3 ± 9.1	26.0 ± 7.0
VAS Pain (/100)	52.3 ± 25.3	42.3 ± 30.2	50.1 ± 21.5

Note: Data are mean ± standard deviation

BMI – Body Mass Index

VAS – Visual Analogue Scale

Table 7-4: Summary of follow-up clinical results included in final analysis.
Where 2-year follow-up data was not present, 1-year follow-up data was brought forward.
Results displayed as mean ± standard error (95% confidence intervals) p = 0.05

	Cruciate Retaining-Fixed Bearing	Cruciate Retaining-Rotating Platform	Posterior Stabilised-Fixed Bearing
Follow-up Time (months)	22 ± 1.1 (20.3 to 24.5)	23 ± 1.1 (21.0 to 25.2)	23 ± 1.1 (20.0 to 24.3)
Maximal Flexion Angle (°)	**117 ± 1.8*^ (113.9 to 121.0)**	**123 ± 1.9* 120.0 to 127.2)**	**125 ± 1.9^ (121.3 to 128.7)**
Oxford Knee Score (/48)	37 ± 2.1 (32.7 to 40.8)	39 ± 2.0 (35.5 to 43.15)	41 ± 2.1 (37.4 to 45.5)
VAS Pain (/100)	19 ± 4.4 (10.2 to 27.5)	11 ± 4.2 (2.2 to 18.8)	11 ± 4.4 (2.6 to 20.0)
VAS Satisfaction (/100)	19 ± 5.3 (9.1 to 20.7)	11 ± 5.0 (1.2 to 21.0)	11 ± 5.3 (1.1 to 21.9)

VAS – Visual Analogue Scale: 0 is the best score and 100 is the worst

* CR-FB significantly different to CR-RP

¥ CR-RP significantly different to PS-FB

^ CR-FB significantly different to PS-FB

The CR-RP (123 ± 1.6) and PS-FB (125 ± 2.1) designs achieved higher maximal flexion than CR-FB (116 ± 2.1) (p=0.002) (Table 7-4). There were no design differences for anterior-posterior translation range (primary outcome) (Table 7-5). However, posterior-stabilised designs were more posterior at each flexion angle compared to both cruciate-retaining designs (Figure 7-3A).

Table 7-5: Total rotation and translation range between 90° to maximal flexion by prosthesis design.

Data reported as adjusted marginal means ± Standard error (upper and lower confidence intervals) with p values for between design differences (p).

Kinematic Variable	Cruciate Retaining-Fixed Bearing	Cruciate Retaining-Rotating Platform	Posterior Stabilised-Fixed Bearing	Group difference p-value
Anterior-Posterior (mm)	-15.6 ± 1.42 (-18.5 to -12.8)	-18.9 ± 1.43 (-21.8 to -16)	-19.8 ± 1.47 (-22.7 to -16.8)	P = 0.12
Internal/External (°)	1.4 ± 0.56 (0.3 to 2.5)	2.0 ± 1.38 (0.3 to 2.5)	0.5 ± 0.57 (-0.6 to 1.7)	P =0.44
Ab/Adduction (°)	-0.7 ± 0.29 (-1.2 to -0.1)	0.1 ± 0.29 (-0.5 to 0.6)	0.1 ± 0.29 (-0.5 to 0.7)	P = 0.14
Superior-Inferior (mm)	4.4 ± 0.28 (3.8 to 4.9)	3.9 ± 0.28 (3.4 to 4.5)	3.9 ± 0.29 (3.4 to 4.5)	P = 0.48
Mediolateral (mm)	0.0 ± 0.28 (-0.5 to 0.6)*	-1.0 ± 0.28 (-1.6 to -0.5) ¥	0.1 ± 0.28 (-0.5 to 0.6)	**p = 0.01**

Note: Between design differences:

* CR-FB significantly different to CR-RP

¥ CR-RP significantly different to PS-FB

^ CR-FB significantly different to from PS-FB

The CR-RP design displayed more external-femoral rotation at each angle throughout flexion when compared to the other designs (Figure 7-3B and Table 7-6). In contrast, CR-FB were less externally rotated at 130° of flexion compared to PS-FB and CR-RP. The total rotation range between 90° to maximal flexion did not differ between designs (Table 7-5). Visually, the CR-RP had highly variable starting position but 76% remained within ±3° of that position (Figure 7-4). However, there was substantial variability between patients for all designs.

Table 7-6: Kinematics at maximal flexion angle by prosthesis design.
Data are reported as adjusted marginal means ± Standard error (upper and lower confidence intervals) with p values for between-design differences.

Kinematics Variable	Cruciate Retaining-Fixed Bearing	Cruciate Retaining-Rotating Platform	Posterior Stabilised-Fixed Bearing	Group difference p-value
Anterior-Posterior (mm)	-0.3 ± 1.41 (-3.1 to 2.5)	-3.2 ± 1.41 (-6.0 to -0.4) ¥	-14.3 ± 1.45 (-17.2 to -11.4)^	p< 0.001
Internal/External (°)	1.0 ± 1.05 (-1.1 to 3.2)*	-3.1 ± 1.05 (-5.2 to -1.0)	0.3 ± 1.08 (-1.9 to 2.5)	p= 0.02
Ab/Adduction (°)	-0.6 ± 0.36 (-1.3 to 0.1)	-0.2 ± 0.36 (-0.9 to 0.5)	-0.2 ± 0.37 (-0.9 to 0.5)	p= 0.69
Superior-Inferior (mm)	54.9 ± 0.64 (53.6 to 56.2)	57.0 ± 0.64 (55.7 to 58.3)	55.2 ± 0.66 (53.9 to 56.5)	p= 0.05
Mediolateral (mm)	0.5 ± 0.76 (-1.0 to 2.0)	0.8 ± 0.78 (-0.7 to 2.4)	0.8 ± 0.78 (-0.7 to 2.4)	p= 0.44

Note: Between design differences:

* CR-FB significantly different to CR-RP

¥ CR-RP significantly different to PS-FB

^ CR-FB significantly different to from PS-FB

Abduction-Adduction angles were relatively small and there was no difference between designs. The coronal alignment remained close to the mechanical axis from 90° to 110° of flexion. CR-FB moved into slight abduction at both 120° and 130° of flexion while the PS-FB and CR-RP remained close to zero (Figure 7-3C). Visually, CR-RP had the most variable starting position but 90% remained within ±2° of that position. Similar to internal-external rotation, there was substantial between-patient variability with CR-RP demonstrating the most, but all rotational patterns were observed in the three groups (Figure 7-4). However, there was substantial between-patient variability for all designs.

There were no between-design differences in superior-inferior position (Table 7-5, Table 7-6, Figure 7-3D).
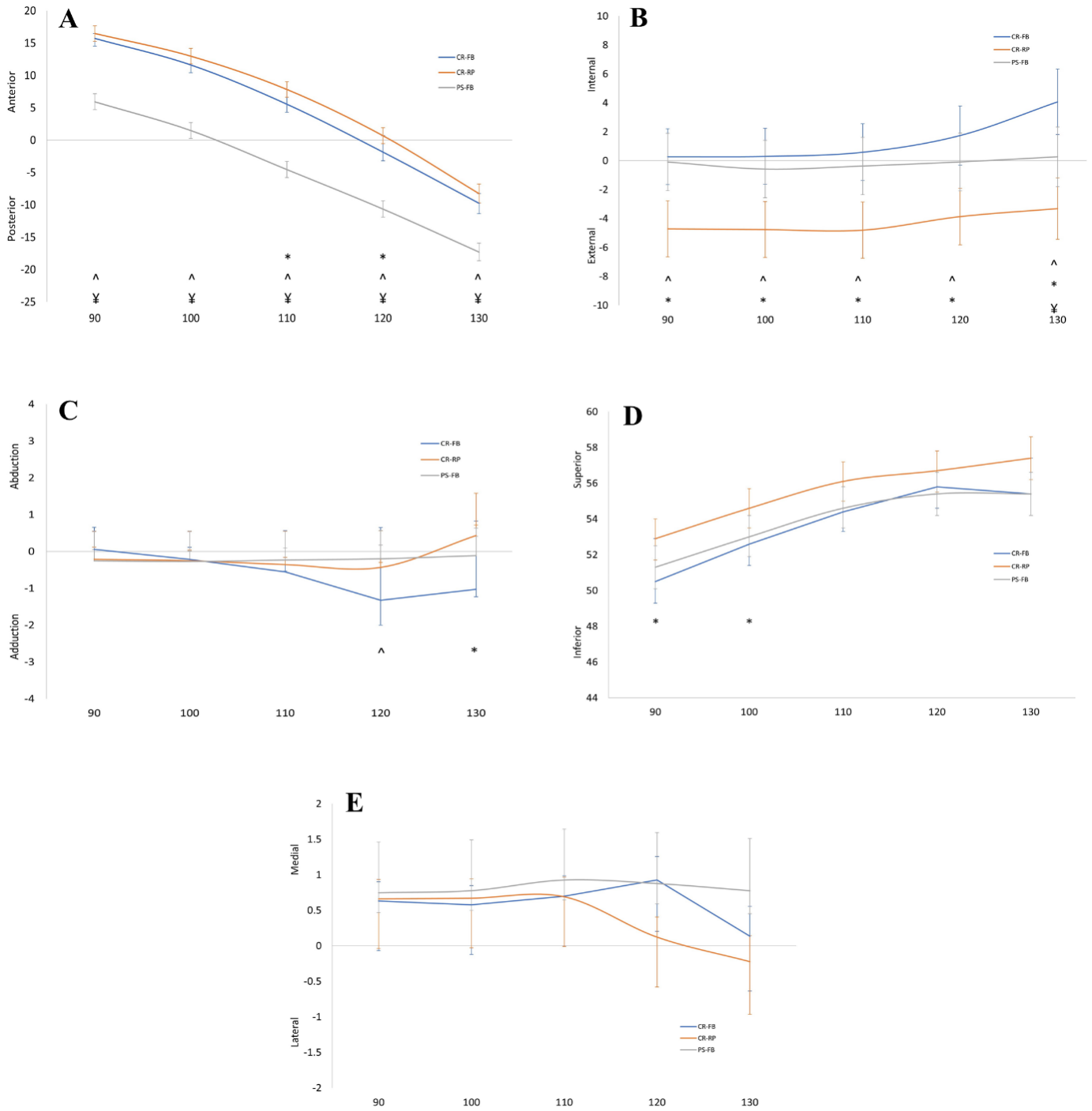
Figure 7-3: Output from the mixed effect linear models for kneeling kinematics from 90° to 130° of flexion
A) Anterior Posterior Position (mm); B) Internal External Rotation (º); C) Ab/Adduction (º); D) Superior-Inferior Position (mm) and; E) Mediolateral Position (mm), for the three prosthesis designs. Data reported as adjusted marginal means with upper and lower confidence intervals

Note CR-FB: —Cruciate Retaining Fixed Bearing; CR-RP: —Cruciate Retaining Rotating Platform; PS-FB: —Posterior Stabilized Fixed Bearing

* CR-FB significantly different to CR-RP; ¥ Group CR-RP significantly different to PS-FB; ^ Group CR-FB significantly different to from PS-FB

	Cruciate Retaining-Fixed Bearing	Cruciate Retaining-Rotating Platform	Posterior Stabilised-Fixed Bearing
Internal	6 (27%)	4 (19%)	3 (14%)
External	2 (9%)	1 (5%)	3 (14%)
+/- 3° Rotation	14 (64%)	16 (76%)	15 (71%)
Abduction	4 (18%)	1 (5%)	4 (18%)
Adduction	1 (5%)	1 (5%)	1 (5%)
+/- 2° Rotation	17 (77%)	19 (90%)	17 (76%)
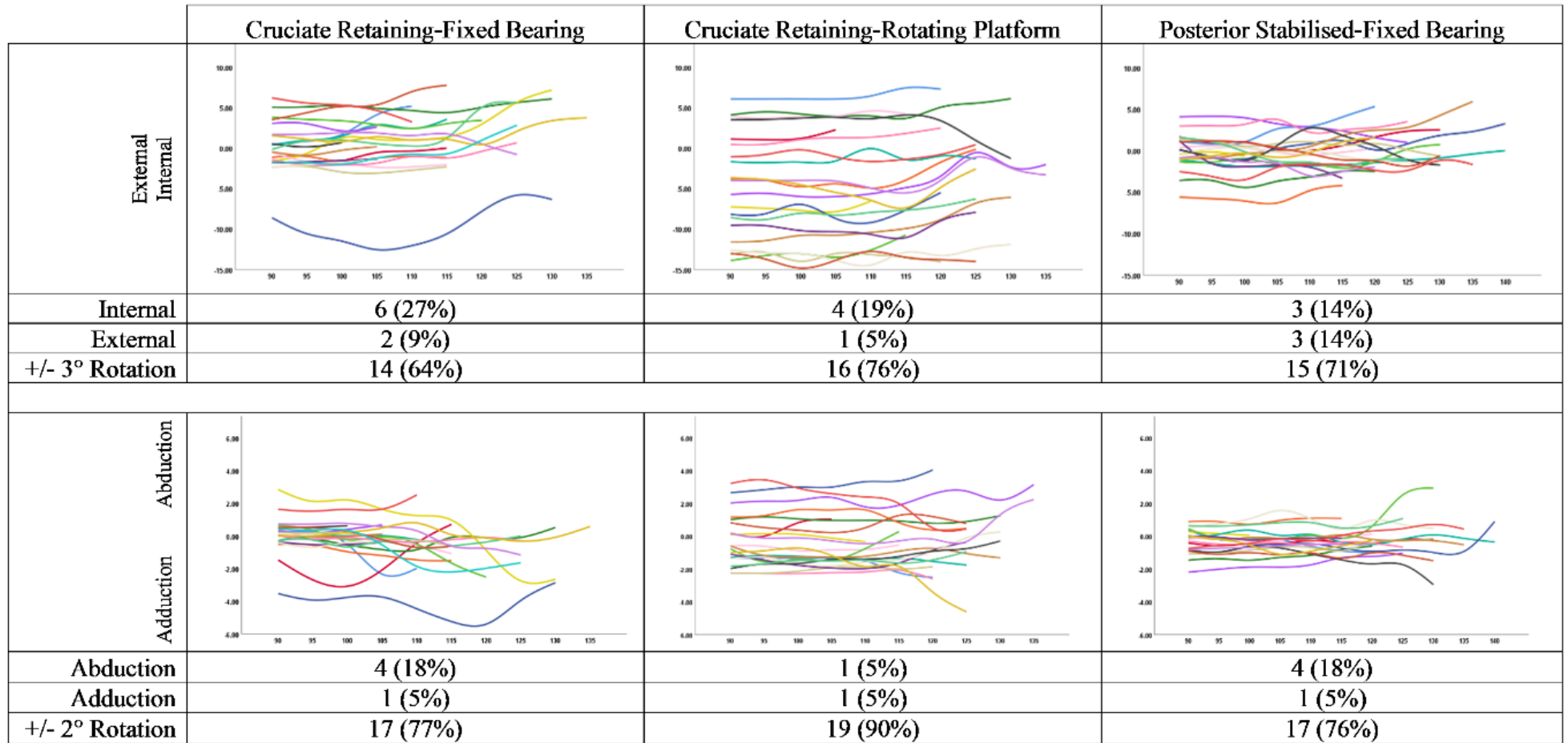
Figure 7-4: Individual kinematic curves for all three designs for internal-external rotation and abduction-adduction.

Top: Individual internal-external rotational patterns for all designs. Number and percentage of patients within each design who displayed an external (< -3°), internal (>3°), or no rotation (+/- 3°) pattern from 90° to maximal flexion

Bottom: Individual Add/Abduction patterns for all designs. Number and percentage of patients within each design who displayed an adduction (< -2°), abduction (>2°) or no rotation (+/- 2°) pattern from 90° to maximal flexion

7.6 Discussion

This study found that the femur on tibia position was more posterior in the PS-FB design throughout the flexion arc during deep kneeling. However, there were no differences between the designs for range of posterior translation. Additionally, the CR-RP design mediated a more externally rotated femur at each angle throughout flexion, but the range of rotation was not different to the other designs. Finally, both the PS-FB and CR-RP achieved a greater maximal flexion angle compared to CR-FB.

The femoral component of the PS-FB design began and remained more posteriorly located throughout flexion and PS-FB achieved more flexion than CR-FB. This finding was not unexpected as PS-FB are designed to do this via the cam-post mechanism (Incavo et al., 2004; Verra et al., 2005). Interestingly, there were no differences in the range of anterior-posterior translation between designs. Therefore, while the femoral component posteriorly translated equally for all designs, the advantage of the PS-FB design is that it starts and finishes more posteriorly. This is presumably the mechanism by which the PS-FB design achieved more flexion during kneeling than CR-FB (Insall et al., 1982). A more posterior position allows the femoral component to clear the back of the knee in higher flexion thereby reducing the likelihood of impingement of the posterior soft-tissue on the polyethylene bearing (Bellemans et al., 2002). While the cam-post mechanism is reported to engage before 90°, which would promote a more posterior starting position for deep kneeling, patient-specific engagement can be quite variable, which may partially explain the variability in our data (Khasian et al., 2019). Increased posterior femoral translation is also associated with reduced patellofemoral loading (Clary et al., 2013; Heyse et al., 2010). This is important in a kneeling context where joint contact pressures are reported to be up to 245% higher compared to an unloaded condition (Wilkens et al., 2007). Interestingly, these joint pressures are reduced at flexion

angles greater than 120° indicating a potential benefit for designs that can regularly achieve higher flexion ranges (Lee, 2014; Wilkens et al., 2007).

The CR-RP design also achieved greater flexion than CR-FB during deep kneeling. The CR-RP femurs were consistently more externally rotated, starting and finishing more externally rotated than both of the fixed bearing designs. Mobile platform TKRs are designed for better tibiofemoral conformity with lower contact stresses and low rotational constraint (McEwen et al., 2005; Walker & Sathasivam, 2000) but there is no evidence for a high flexion advantage (Jacobs et al., 2004). However, the results of this study indicate that higher flexion may be mediated by a more externally rotated femur throughout deep flexion. We are unsure whether this position resulted in less posterior impingement.

At terminal flexion, on average, all designs moved into relative internal rotation (Figure 7-3). This apparent paradoxical movement in deep flexion has been previously reported. Our data indicates that 27% of participants externally rotated between 90° and maximal flexion compared to up to 50% reported by others (Kitagawa et al., 2010; Meccia et al., 2014). Therefore, while not typically reported, this is not an uncommon feature in deep flexion.

Prosthesis design doesn't appear to influence either abduction-adduction or superior-inferior position. Our results agree with previous reports of deep flexion kinematics which reported a neutral pattern of abduction/adduction or superior/inferior kinematics through flexion (Watanabe et al., 2013, 2016). Interestingly, Howell *et al*, reported abd/adduction angles of 2° over the flexion cycle, but this may be the result of their cohort being kinematically aligned (Howell et al., 2009). Our group was mechanically aligned and well-balanced and we would therefore expect a neutral position.

Normal kinematics were not completely restored by any implant design. Our group recently published a series of papers showing that the healthy knee externally rotates and slightly

adducts throughout deep kneeling (Galvin, 2019; Scarvell et al., 2019). These patterns were not observed in this study. However, anterior-posterior and superior-inferior translations were similar to healthy kneeling although the magnitudes cannot be compared because the axis set for the native knee is not the same as the prosthetic knee.

High between-patient variability was observed in all designs. The kinematics of deep flexion can be influenced by several factors including: the type of activity (McClelland et al., 2017), tibiofemoral geometry (Ardestani et al., 2015; Clary et al., 2013), ethnicity (Leszko et al., 2011), and early thigh-calf contact as a result of soft tissue opposition (Kingston & Acker, 2019). Many of our participants had high BMIs (>30kg m^{-2}), and thigh-calf contact will have occurred at lower flexion ranges resulting in changes to the knee centre of rotation producing a first class lever at the knee with the pivot around the opposing tissues (Kingston & Acker, 2019). Both the hip and the foot were not constrainedand differences in tibial rotation, hip rotation and adduction are known to influence deep flexion kinematics (Hefzy et al., 1998; Yildirim et al., 2007). Therefore, the combination of an unconstrained hip and ankle/foot along with soft tissue impingement may have led to the employment of unique stratagies to achieve maximal flexion (Hemmerich et al., 2006).

The results of this study need to be interpreted in light of its limitations. We did not capture patellar kinematics which might have influenced tibiofemoral kinematics. Additionally, we did not grade PCL integrity. While the surgeon inspected the ligaments interoperatively, they were not quantitativly graded, and therefore it is possible that not all participants with a CR design had a functional PCL.

In conclusion, we found that implant design influenced kneeling kinematics but we observed a lot of inter-individual variation within designs. Specifically, PS-FB femurs were more posterior on the tibia throughout flexion; and CR-RP femurs were more externally rotated.

Both of these designs achieved more flexion during kneeling. The findings of this study provide insights into the performance of common knee replacement designs in the context of deep kneeling. They also provide clinicians with a more kinematically informed choice for implant selection and information for management of functional expectations.

7.7 Supplementary – Travelling Salesman Algorithm

The TSP algorithm achieves the most likely interpolation of the missing data by determining the best fit for the data-deficient curve within the dataset. The TSP algorithm essentially orders the curves so that the difference in root-mean-squared errors (RMSE) between each successive curve is minimized and then the missing data can be imputed from the two successive curves which are most similar.

A leave-one-out (LOO) cross-validation was performed to assess the ability of the TSP algorithm to predict the kinematic values of a new participant from outside of the training set. In each of the iterations, one curve containing complete data for one participant was left out from the development model. The model, based on the remaining curves, was then used to predict the kinematic values for the left-out participant. Separate TSP algorithms were performed for each variable. Results for each TSP model, comparing the actual and predicted data, were reported in terms of RMSE for 5 incrementally increasing intervals starting at 90° to 124° (Table 7-7).

Table 7-7: Prediction errors from the Travelling Salesman Problem Algorithm for 5 missing flexion intervals from 90°.
Errors are reported as root-mean-square error (RMSE). The number of participants who were missing data in each interval are reported

Flexion Interval Missing (°)	Number of Participants	Abd/Adduction (°)	Internal-External Rotation (°)	Superior-Inferior Position (mm)	Mediolateral Position (mm)	Anterior-Posterior Position (mm)
5	14	0.30	0.58	0.42	0.33	0.80
10	11	0.35	0.68	0.4	0.42	1.30
15	8	0.40	0.95	0.39	0.63	1.17
20	1	0.48	1.42	0.48	0.75	1.17
25	1	0.64	1.40	0.70	0.87	1.31

8 Discussion and Conclusions

The aim of this thesis was to examine the relationship between knee shape and knee kinematics during deep knee flexion in people with knee osteoarthritis (OA). Most previous studies have examined gait or early flexion activities, since that is the traditional biomechanical paradigm for exploring functional abnormalities. However, these activities do not always challenge the knee at the extremes of range, such as kneeling does. Kneeling is challenging for people with knee OA and following total knee replacement (TKR). Although, the inability to kneel does not impact western societies as much as gait impairment does, it is still reported as one of the most important activities people undergoing TKR would like to achieve (Weiss et al., 2002). In the worst-case scenario, it can render people unable to get up from the floor after a fall which can be life threatening.

The thesis had two parts. Firstly, we explored how OA changes the shape of the knee and how that shape change affects knee motion at the joint surface – the kinematics. These questions have been explored previously but we employed very precise technologies and novel statistical methods to provide more precision and to answer previously unexplored questions. Secondly, we examined the effect of implant design on kinematics after joint replacement.

The thesis has been presented as a compilation of papers and so each set of findings has been discussed previously; but, in this final chapter we will summarize the important findings and how they collectively contribute to the understanding of knee kinematics in health, osteoarthritis, and after prosthetic replacement.

8.1   Summary of important findings

In study one (Chapter four) we used statistical shape modelling to compare the bony shape of participants with end-stage OA to healthy controls in order to determine which features best distinguished between the two groups. Before understanding whether bony shape could

predict kinematics, it was important to explore the tibiofemoral joint's main shape features by developing a statistical shape model. We found that the shape features captured within our model could distinguish between healthy and OA knee shapes with an accuracy of 94.8%. The specific shape features that emerged were that OA knees displayed large bony expansions at the periphery of the tibial and femoral cartilage plates which were up to 10 mm (190%) larger than healthy controls. Furthermore, we found an area of increased bony expansion on the posteromedial tibial tubercle which corresponded to a large expansion on the posterior-medial femoral condyle. To our knowledge, this is the first time this bony tubercle has been explicitly reported in the literature. The corresponding bony expansions seen on the femur and tibia indicate that there is likely an impingement that occurs between these structures resulting in adaptation due to altered loading patterns (Neogi, 2012). These bony changes may explain why some people with knee OA have difficulty achieving full flexion and explain their altered kinematic profile.

In study two (Chapter five), we examined the association between tibiofemoral joint shape and kinematics during deep kneeling in participants with and without OA. We used the statistical shape modelling developed in study one, to predict the kneeling kinematics. The kinematics were generated using image registration and described using a novel technique called bivariate function principal component analysis (bfPCA) which, like SSM, describes the variability within the entire dataset in terms of principal components. This was the first time these two techniques have been combined to understand the associations between shape and kinematics. We found that variations in tibiofemoral bony shape were only weakly associated with the kinematics of deep knee flexion. While all of the random forest models contained different shape features that could predict kinematics, both group (OA or healthy) and BMI were found to be more important. Even so, these models only explained a small amount of the variation within the kinematic data and exhibited high prediction errors,

indicating that other predictors must be more important. Knee shape has been considered as an important driver for normal movement. However, the results of this study indicate that other factors, such as soft-tissue shape, might be more influential in driving the kinematics of deep kneeling. Furthermore, the random forest models indicated that the bfPCs of OA and healthy participants are different, indicating that OA knees exhibit a different kinematic pattern to healthy knees. These results have implications for the clinical understanding of the primary drivers of kneeling kinematics. They allude to the importance of factors such as soft tissue shape or neuromuscular adaptations to the pain of OA. Discovery of the primary drivers are likely to affect both the operative and non-operative management of knee OA and should be a focus for future investigation.

In order to understand the influence of knee replacement design on kneeling kinematics we first undertook a systematic review and meta-analysis of the published literature (study three - Chapter six). Quality-adjusted meta-analyses showed that all included design types demonstrated posterior-femoral translation and external rotation during kneeling but, posterior-stabilised (PS) designs were more posterior at maximal flexion when compared to cruciate-retaining (CR). The systematic review did not reveal any important systemic differences between designs. But that was not necessarily because none were present. The heterogeneity was very high reflecting significant inconsistency in the way the studies were conducted. These included: variable kneeling methods (single versus bilateral knees), differing condylar radii within design type. The results of this review indicated that there remains a need for high quality prospective comparative studies to directly compare designs using a common method.

In study four (Chapter seven) we conducted a randomised clinical trial which compared the six-degree-of-freedom kinematics of posterior-stabilised fixed-bearing (PS-FB), cruciate-retaining fixed-bearing (CR-FB) and cruciate-retaining rotating-platform (CR-RP) designs

during deep kneeling. In this study the method was identical for all three designs and the implants were all made by the same company and so had the same geometry (Zimmer Biomet). We found that the posterior stabilized-fixed bearing design maintained a more posterior femoral position on the tibia throughout flexion which accorded with the systematic review findings from Chapter six. However, there were no differences between any of the designs for any of the kinematic rotation and translation ranges between 90° and maximal flexion. The femoral component of the cruciate retaining-rotating platform design was more externally rotated throughout flexion, but again there were no differences in the range between 90° and maximal flexion. However, there was substantial between-patient variability which was likely due to a combination of soft tissue properties and unique patient-specific strategies to achieve maximal flexion. Investigating the relative kinematics of deep kneeling after knee replacement is new. The ability to kneel is more important to some patients than others. Restoration of a normal range of motion in the replaced knee is not predictably achievable for a number of reasons. These include patient factors, such as pain perception, the formation of restrictive scar tissue, and adherence to rehabilitation protocols (Wylde et al., 2019). All implant designs potentially allow a full range of knee motion. In our study we found that the PS and RP designs allowed greater flexion range. Therefore, the trade-off between design longevity and functional capacity in this respect will doubtless be a function of patient age, patient preference and clinician skill. These results provide clinicians with a more kinematically informed choice for implant selection and provides the ability to better manage patient's functional expectations. Furthermore, there is an opportunity to explore the effect of post-surgical programs which focus on kneeling.

8.2 Implications

This thesis highlights a number of femoral and tibial features which distinguish OA from healthy knees. While most of these differences are similar to those reported in the literature, a surprising finding was that of a large bony tubercle on the posterior-medial plateau of the osteoarthritic tibia (Barr et al., 2016; Bowes et al., 2015; Neogi et al., 2013). While Bowes *et al.,* reported widespread bony increase across the whole plateau, with more prominent enlargement around the edges, they did not specifically mention the tubercle (Bowes et al., 2015). A statistical shape model developed by Neogi and colleagues seems to include this tubercle, but the authors did not comment on its existence nor significance (Neogi et al., 2013). The fact that it is not commonly reported in relation to OA knee shape is interesting but may be due to it being occluded on 2D x-ray or missed in MRI slice selection. Furthermore, this region is difficult to access intraoperatively, making visual inspection difficult. This tubercle appears to lie under the posterior horn of the medial meniscus. Incidence of tears to this structure are related to higher osteoarthritis grades and increased cartilage degradation in this region (Bhattacharyya et al., 2003; Choi & Park, 2015; Kan et al., 2010). These tears likely increase contact stresses present in the medial compartment resulting in the observed bony changes in the underlying bone (Lau et al., 2018; Thambyah et al., 2005). The development of this tubercle may be an important 'sign in the development of OA and warrants further investigation.

The findings contained in this thesis highlight the complexity of kneeling kinematics. The major finding is that neither native bone shape, nor implant design, could fully explain the kinematics of deep kneeling. Shape has been thought to be a main driver of kinematics (Freeman & Pinskerova, 2005; Iwaki, Pinskerova, & Freeman, 2000; Martelli & Pinskerova, 2002). Indeed, knee shape is associated with the kinematics of gait and simulated flexion from 0 to 90° (Clouthier et al., 2019; Smoger et al., 2015). However, bony and prosthetic shape had

limited influence on kneeling kinematics. Deep kneeling is a demanding activity as it requires people to achieve the extremes of flexion. The participants in this thesis were required to flex their knee as far as possible in a loaded position which likely resulted in the impingement of the posterior structures of the knee. A recent finite element analysis (FEA) knee modelling study highlighted the importance of including posterior soft tissue structures in a model to achieve accurate kinematic predictions (Beidokhti, Janssen, Van De Groes, & Verdonschot, 2018). They also reported that resection of these structures resulted in a change of knee joint kinematics in early to mid-flexion but did deep flexion was not described. Furthermore, in OA, and subsequent TKR, the soft tissues of the knee are affected in a number of ways. In OA, the menisci are typically torn, resulting increased medial extrusion and altered joint mechanics (Scholes, Houghton, Lee, & Lustig, 2015). Additionally, there is scarring and thickening of the joint capsule (Hettinga, 1980; Loeser, Goldring, Scanzello, & Goldring, 2012). These changes possibly alter the mechanical properties of the knee joint due to increased collagenous and adipose tissues hindering its ability to achieve high flexion activities (Campbell, Trudel, & Laneuville, 2015).Therefore, the soft-tissue changes that accompany the bony shape changes seen in OA and TKR, may all contribute to altered kinematics.

Neuromuscular control will likely influence kneeling kinematics. There are ten muscles that cross the knee joint (Drake, Vogl, & Mitchell, 2020). These muscles act both in an agonist and antagonist capacity depending on the activity (Shapiro et al., 2005). Various muscle recruitment strategies will result in different force production and therefore different moments around the knee joint (Pandy, 2005). Furthermore, OA can lead to significant muscle impairment and weakness (Alnahdi et al., 2012) which can lead to decreased force production. Finally, ligaments and bones produce forces that act on the knee to influence kinematics (Pandy, 2005; Sakane, 1996). The altered muscle recruitment patterns and force

development may result in subtle kinematic changes which abnormally load the joint leading to progression of the disease. Many current musculoskeletal modelling approaches which utilise forward dynamics predict the corresponding kinematics based on muscle and other internal forces as inputs to the modelling equations (Otten, 2003; Pandy, 2005). Neuromuscular control is altered in the presence of pain (Sterling et al., 2001). In knee OA, increased pain is associated with altered neuromuscular and biomechanical patterns during gait and reduced knee flexion (Astephen Wilson, Deluzio, Dunbar, Caldwell, & Hubley-Kozey, 2011; Boyer & Hafer, 2019). Additionally, kinesiophobia has also been reported to reduce passive maximal knee flexion angle in patients following total knee replacement. (Brown et al., 2016; Brown et al., 2020). However, in a group of patients with patellofemoral pain, while increased kinesiophobia significantly reduced cadence and peak knee flexion during gait, it was not associated with isometric, concentric or eccentric knee extensor strength (de Oliveira Silva et al., 2019). Therefore, muscle recruitment strategies, force production, variable pain kinesiophobia levels that are reported in OA and TKR, may all contribute to altered kinematics.

Inter-individual anthropometric measurements possibly influenced kneeling kinematics. Thigh-calf contact as a result of soft tissue opposition is reported to occur between 100 and 124° of flexion but is dependent on thigh and shank circumference, and BMI (Kingston & Acker, 2018, 2019; Wu et al., 2019). As the participants described in this thesis had a BMI greater than 30 kg/m², it is likely that their thigh-calf contact occurred at lower flexion ranges. Modelling thigh and calf anthropometric measures might improve kinematic predictions.

Inter-individual kneeling strategies also likely influenced kinematic outcomes. The activity examined in this thesis involved kneeling with both the foot and hip unconstrained. This likely resulted in unique kinematic strategies that influenced the kneeling kinematics. Both foot and hip position can influence knee kinematics during deep flexion. Specifically,

increased ankle plantarflexion reduces external rotation and abduction when compared to dorsiflexion during kneeling (Hemmerich, Brown, Smith, Marthandam, & Wyss, 2006) and maximal flexion angle appears to be higher in participants with a neutrally positioned hip compared to when it is internally rotated (Hefzy, Kelly, & Cooke, 1998). Therefore, in order to properly assess factors which drive knee kinematics, understanding the relative positions of the hip and ankle/foot is important.

Two novel techniques (SSM and bfPCA) were used to describe the variability of the shape and kinematic data. These techniques could be applied to the problem of predicting disease progression and also responses to therapy. Both shape and kinematic data is inherently complex and traditionally has been difficult to describe. The use of principal component analysis reduces the dimensionality of these complex datasets and allows them to be characterized, and subsequently visualised, using a small number of principal components.

The work in this thesis identified unique shape features which distinguish osteoarthritic from healthy knees. These findings add to the growing body of literature which highlight the importance of bony shape in the development and progression of OA (Bowes, Vincent, Wolstenholme, & Conaghan, 2015; Bredbenner et al., 2010; Gregory et al., 2020; Hunter et al., 2015). SSM offers the opportunity for the identification of important features in OA, possibly creating biomarkers to more accurately monitor disease progression, and response to therapies (Bowes et al., 2015; Bredbenner et al., 2010; Gregory et al., 2020; Hunter et al., 2015; Neogi & Felson, 2016). Further investigation of bone shape might provide a potentially more sensitive and responsive biomarker to the treatment and progression of OA.

Functional data analysis, including bfPCA used in this thesis, has the potential to detect small, but important, differences in kinematic performance. bfPCA can extract information contained in functions like time-series or angle-angle data, that are not normally available

through traditional statistical methods (Ullah & Finch, 2013). Previously, bfPCA has been shown to distinguish OA from healthy knee kinematics in gait, but this is the first time that different patterns were observed in kneeling (Deluzio & Astephen, 2007; Deluzio, Wyss, Costigan, Sorbie, & Zee, 1999; Deluzio, Wyss, Zee, Costigan, & Sorbie, 1997). This technique has recently been proposed as a tool for monitoring performance and injury risk in a sporting context (Stephens, Chapman, Tate, & Warmenhoven, 2020; Warmenhoven et al., 2019). There is also an opportunity to extend this technique to monitoring the progress of rehabilitation programs. Indeed, this technique has been effectively used to compare the success of two different rehabilitation programs (Luz Sánchez-Sánchez et al., 2014). In this study, an ANOVA did not detect differences in functional recovery when measured using tradition methods, but by characterising the dynamics of recovery, fPCA did. The application of this technique to detect performance changes over time in OA is an enticing opportunity.

8.3   Limitations

The results described in this thesis should be considered in light of its methodological limitations. Firstly, the Orthovis technology was developed for use with single-plane fluoroscopy. Single-plane fluoroscopy has the advantage of delivering less ionizing radiation compared to bi-planar, but compromises accuracy in out-of-plane motions. Orthovis results in out-of-plane errors up to 0.9 mm and 0.6° (Scarvell et al., 2010). Using biplanar fluoroscopy would have reduced out-of-plane measurement error to up to 0.5 mm and 0.6° (Anderst, Zauel, Bishop, Demps, & Tashman, 2009; Guan, Gray, Keynejad, & Pandy, 2016; Miranda et al., 2011), but it would have doubled the radiation dose. In addition, the field of view would have been more limited making complete motion capture more challenging. Our method utilized a clinical environment and so the fluoroscopy was fixed. Moving systems which are mounted on gantries have been recently developed to allow for a more diverse set of activities

(Guan et al., 2016; List et al., 2017). However, they are not accessible in a clinical environment.

Secondly, using CT to generate our 3D models meant that we only captured the bony shape of the knee and were unable to analyse the cartilage or soft tissue. CT captures bony edges very clearly, but its ability to accurately capture soft tissue is limited. Changes in cartilage morphology commonly seen in OA will influence the articular knee shape and possibly the associated joint kinematics. Previous research which examined the associations between knee shape and function during gait and mid-flexion activities, incorporated cartilage morphology in the shape model (Clouthier et al., 2019; Smoger et al., 2015). Models including this data might have resulted in stronger associations than the ones found in this thesis. Future research should incorporate MRI data to provide accurate visualisation of soft tissue and cartilage. The use of MRI would remove the exposure to ionizing radiation.

Thirdly, we did not capture patellar shape or kinematics. The patella undergoes osteoarthritic changes and possibly may have influenced the shape changes in the trochlear region of the femur (Neogi et al., 2009). Deep flexion kinematics of both the patellofemoral and tibiofemoral joint are altered in the presence of osteoarthritis (Farrokhi et al., 2015; Galvin, 2019; Ohnishi et al., 2015; Scarvell, Galvin, Perriman, Lynch, & van Deursen, 2018). It is possible that some of the variability in the tibiofemoral kinematics might be attributed to the changes in patellofemoral joint. An exploration of the relationship between patellar shape and patellofemoral and tibiofemoral kneeling kinematics would be an important extension to this study of tibiofemoral shape and kinematics.

Another limitation to consider is that the studies comparing OA to healthy participants were cross-sectional. Therefore, we were unable to track the onset of OA or determine any causal

relationships. Specifically, we do not have data on how our participants shape and kinematics patterns are influenced by their pre-arthritic joint shape and kinematics.

Finally, the TKR axes system that was designed for this study relied solely on computer-aided design (CAD) model geometry because that is what was visible in the fluoroscopy images. While the axes were similar to that described by Guan *et al.*, it did not take in account the native bony landmarks (Guan et al., 2017). As a result, some of the kinematic variability might have been a result of intraoperative implant positioning and not implant design. However, this axes system does not require any additional three-dimensional imaging to capture joint kinematics and therefore can be used if only post-operative imaging is available. Future research will seek to include native anatomy in combination with CAD geometry.

8.4 Future Work

There are several directions in which the work presented in this thesis could be further developed. The role of bony shape has been examined but it is clear that the kinematics of kneeling are a complex result of more than bony shape alone. It is clearly important that the role of passive soft tissue structures of the knee are better understood (i.e. cartilage, ligaments, adipose tissue). Future research should aim to build all of these tissues into the 3D knee models to provide more accurate kinematic predictions and comparisons. Furthermore, exploring the neuromuscular control involved in kneeling is an important area for future research. Information from the shape models could be integrated into computational frameworks such as the Musculoskeletal Atlas Project (Zhang et al., 2014) and used to create accurate musculoskeletal models. This data would contribute to the development of more accurate prediction of joint centres and muscle attachment sites for an osteoarthritic population. Osteoarthritic shape changes will theoretically lead to altered attachment points

for muscles which will in turn change their lines of action and moment arms. While there has been no research which directly measures how osteoarthritic shape changes alter muscle lines of action and associated moment arms, a recent modelling study has determined that shape changes increased joint contact force, articular cartilage loading, and ligament loading (Clouthier et al., 2019). These results point to adaptations in muscle mechanics as a result of the shape changes. However, further investigation is required in this area. In chapter five we described our kneeling kinematics in terms of bfPCA's. This technique could be applied to identify different kinematics patterns for the TKR designs we reported in chapter seven. We reported the comparative kinematics in chapter seven using traditional methods in order to communicate with a clinical audience; but bfPCA is a promising way of interpreting this data which may lead to discoveries that we have been unable to access using current methods. Finally, this thesis does not address the influence of preoperative characteristics on total knee replacement kinematics. Future research should examine the influence of preoperative shape and kinematics in predicting post-operative function.

8.5   Conclusion

In conclusion, this thesis examined the role of knee shape on kneeling kinematics before and following total knee replacement. We found distinct shape differences between healthy and osteoarthritic tibiofemoral joints, most notably in the posterior medial aspects of the femur and tibia. Furthermore, we found weak associations between these shapes and kneeling kinematics. Finally, we demonstrated design specific kinematic patterns in TKR kneeling kinematics. However, variability was high in both osteoarthritic and TKR cohorts indicating that factors other than shape and design influence kinematics. These findings contribute new insights about the interaction between knee shape and motion in deep kneeling and provide some directions for future research. The message for surgeons and other clinicians is that

bony shape and TKR design are not the primary drivers of functional performance and that

kneeling should be on their radar as an activity to which their patients should aspire.

9 Bibliography

Abhishek, A., & Doherty, M. (2013). Diagnosis and Clinical Presentation of Osteoarthritis. *Rheumatic Disease Clinics of North America*, *39*(1), 45–66.

Acker, S. M., Cockburn, R. A., Krevolin, J., Li, R. M., Tarabichi, S., & Wyss, U. P. (2011). Knee Kinematics of High-Flexion Activities of Daily Living Performed by Male Muslims in the Middle East. *Journal of Arthroplasty*, *26*(2), 319–327.

Agricola, R., Leyland, K. M., Bierma-Zeinstra, S. M. A., Thomas, G. E., Emans, P. J., Spector, T. D., Weinans, H., Waarsing, J. H., & Arden, N. K. (2015). Validation of statistical shape modelling to predict hip osteoarthritis in females: data from two prospective cohort studies (Cohort Hip and Cohort Knee and Chingford). *Rheumatology*, *54*(54), 2033–2041.

Akter, M., Lambert, A. J., Pickering, M. R., Scarvell, J. M., & Smith, P. N. (2014a). 3D CT to 2D low dose single-plane fluoroscopy registration algorithm for in-vivo knee motion analysis. *36th Annual International Conference of the IEEE Engineering in Medicine and Biology Society*, 5121–5124.

Akter, M., Lambert, A. J., Pickering, M. R., Scarvell, J. M., & Smith, P. N. (2014b). Robust initialisation for single-plane 3D CT to 2D fluoroscopy image registration. *Computer Methods in Biomechanics and Biomedical Engineering: Imaging & Visualization*, 1–25.

Alnahdi, A. H., Zeni, J. A., & Snyder-Mackler, L. (2012). Muscle Impairments in Patients With Knee Osteoarthritis. *Sports Health*, *4*(4), 284–292.

Altman, R., Asch, E., Bloch, D., Bole, G., Borenstein, D., Brandt, K., Christy, W., Cooke, T. D., Greenwald, R., Hochberg, M., Howell, D., Kaplan, D., Koopman, W., Longley, S., Mankin, H., McShane, D. J., Medsger, T., Meenan, R., Mikkelsen, W., … Wolfe, F. (1986). Development of criteria for the classification and reporting of osteoarthritis: Classification of osteoarthritis of the knee. *Arthritis & Rheumatism*, *29*(8), 1039–1049.

Andriacchi, T. P., Dyrby, C. O., & Johnson, T. S. (2003). The use of functional analysis in evaluating knee kinematics. *Clinical Orthopaedics and Related Research*, *410*, 44–53.

Angerame, M. R., Holst, D. C., Jennings, J. M., Komistek, R., & Dennis, D. A. (2019). Systematic Review & Meta-Analysis Total Knee Arthroplasty Kinematics. *Journal of Arthroplasty*, *34*(10), 2502–2510.

Ardestani, M. M., Moazen, M., & Jin, Z. (2015). Contribution of geometric design parameters to knee implant performance: Conflicting impact of conformity on kinematics and contact mechanics. *Knee*, *22*(3), 217–224.

Argenson, J.-N. A., Scuderi, G. R., Komistek, R., Scott, W. N., Kelly, M. A., & Aubaniac, J.-M. (2005). In vivo kinematic evaluation and design considerations related to high flexion in total knee arthroplasty. *Journal of Biomechanics*, *38*(2), 277–284.

Arthritis Australia. (2014). *Time to Move: Osteoarthritis A national strategy to reduce a costly burden TIME TO MOVE: ARTHRITIS*.

Astephen, J. L., Deluzio, K. J., Caldwell, G. E., & Dunbar, M. J. (2008). Biomechanical changes at the hip, knee, and ankle joints during gait are associated with knee osteoarthritis severity. *Journal of Orthopaedic Research*, *26*(3), 332–341.

Australian Commission on Safety and Quality in Health Care. (2017). *Osteoarthritis of the Knee: Clinical Care Standard*. https://www.safetyandquality.gov.au/standards/clinical-care-standards/osteoarthritis-knee-clinical-care-standard

Australian Institute of Health and Welfare. (2019). *Osteoarthritis, What is osteoarthritis? - Australian Institute of Health and Welfare*. https://www.aihw.gov.au/reports/chronic-musculoskeletal-conditions/osteoarthritis/contents/what-is-osteoarthritis

Australian Orthopaedic Association National Joint Replacement Registry (AOANJRR).

(2019). *Hip, Knee and Shoulder Arthroplasty*.

https://aoanjrr.sahmri.com/documents/10180/397736/Hip%2C Knee %26 Shoulder

Arthroplasty

Baert, I. A. C., Jonkers, I., Staes, F., Luyten, F. P., Truijen, S., Verweijen, S., & Verschueren, S. M. P. (2012). Changes in gait kinematics and kinetics associated with structural joint degeneration in knee osteoarthritis. *Gait & Posture*, *36*, S89–S90.

Bahl, J. S., Zhang, J., Killen, B. A., Taylor, M., Solomon, L. B., Arnold, J. B., Lloyd, D. G., Besier, T. F., & Thewlis, D. (2019). Statistical shape modelling versus linear scaling: Effects on predictions of hip joint centre location and muscle moment arms in people with hip osteoarthritis. *Journal of Biomechanics*, *85*, 164–172.

Baka, N., Kaptein, B. L., de Bruijne, M., van Walsum, T., Giphart, J. E., Niessen, W. J., & Lelieveldt, B. P. F. (2011). 2D-3D shape reconstruction of the distal femur from stereo X-ray imaging using statistical shape models. *Medical Image Analysis*, *15*(6), 840–850.

Banks, S. A., & Hodge, W. A. (2004). 2003 Hap Paul Award paper of the International Society for Technology in Arthroplasty: Design and activity dependence of kinematics in fixed and mobile-bearing knee arthroplasties. *Journal of Arthroplasty*, *19*(7), 809–816.

Barnes, C. L., Sharma, A., David Blaha, J., Nambu, S. N., & Carroll, M. E. (2011). Kneeling Is Safe for Patients Implanted With Medial-Pivot Total Knee Arthroplasty Designs. *Journal of Arthroplasty*, *26*, 549–554.

Barr, A. J., Campbell, M. T., Hopkinson, D., Kingsbury, S. R., Bowes, M. A., & Conaghan, P. G. (2015). A systematic review of the relationship between subchondral bone features, pain and structural pathology in peripheral joint osteoarthritis. *Arthritis Research & Therapy*, *17*(1), 228.

Barr, A. J., Dube, B., Hensor, E. M. A., Kingsbury, S. R., Peat, G., Bowes, M. A., &

   Conaghan, P. G. (2014). The relationship between clinical characteristics, radiographic

   osteoarthritis and 3D bone area: data from the Osteoarthritis Initiative. *Osteoarthritis*

   and Cartilage, *22*, 1703–1709.

Barr, A. J., Dube, B., Hensor, E. M. A., Kingsbury, S. R., Peat, G., Bowes, M. A., Sharples,

   L. D., & Conaghan, P. G. (2016). The relationship between three-dimensional knee MRI

   bone shape and total knee replacement—a case control study: data from the

   Osteoarthritis Initiative. *Rheumatology*, *55*(9), 1585–1593.

Beidokhti, H. N., Janssen, D., Van De Groes, S., & Verdonschot, N. (2018). The peripheral

   soft tissues should not be ignored in the finite element models of the human knee joint.

   Medical & Biological Engineering & Computing, *56*, 1189–1199.

Bellemans, J., Banks, S. A., Victor, J., Vandenneucker, H., & Moemans, A. (2002).

   Fluoroscopic analysis of the kinematics of deep flexion in total knee arthroplasty.

   Influence of posterior condylar offset. *Journal of Bone and Joint Surgery British*, *84*(1),

   50–53.

Bercik, M. J., Joshi, A., & Parvizi, J. (2013). Posterior cruciate-retaining versus posterior-

   stabilized total knee arthroplasty: a meta-analysis. *Journal of Arthroplasty*, *28*(3), 439–

   444.

Bhattacharyya, T., Gale, D., Dewire, P., Totterman, S., Gale, M. E., McLaughlin, S., Einhorn,

   T. A., & Felson, D. T. (2003). The clinical importance of meniscal tears demonstrated by

   magnetic resonance imaging in osteoarthritis of the knee. *Journal of Bone an Joint*

   Surgery American, *85*(1), 4–9.

Bonnin, M., Amendola, A., Bellemans, J., MacDonald, S., Ménétrey, J., Ranawat, A. S., &

   Ranawat, C. S. (2012). *The Knee Joint Surgical Techniques and Strategies* (1st ed.).

Springer.

Bourne, R. B., Chesworth, B. M., Davis, A. M., Mahomed, N. N., & Charron, K. D. (2010). Patient Satisfaction after Total Knee Arthroplasty: Who is Satisfied and Who is Not? *Clinical Orthopaedics and Related Research*, *468*(1), 57–63.

Bowes, M. A., Vincent, G. R., Wolstenholme, C. B., & Conaghan, P. G. (2015). A novel method for bone area measurement provides new insights into osteoarthritis and its progression. *Annals of the Rheumatic Diseases*, *74*(3), 519–525.

Brand, R., & Claes, L. (1989). The law of bone remodelling. *Journal of Biomechanics*, *22*(2), 185–187.

Bredbenner, T. L., Eliason, T. D., Potter, R. S., Mason, R. L., Havill, L. M., & Nicolella, D. P. (2010). Statistical shape modeling describes variation in tibia and femur surface geometry between Control and Incidence groups from the Osteoarthritis Initiative database. *Journal of Biomechanics*, *43*, 1780–1786.

Breiman, L. (2001). Random Forests. *Machine Learning*, *45*, 5–32.

Brown, M. L., Plate, J. F., Von Thaer, S., Fino, N. F., Smith, B. P., Seyler, T. M., & Lang, J. E. (2016). Decreased Range of Motion After Total Knee Arthroplasty Is Predicted by the Tampa Scale of Kinesiophobia. *Journal of Arthroplasty*, *31*(4), 793–797.

Brown, O. S., Hu, L., Demetriou, C., Smith, T. O., & Hing, C. B. (2020). The effects of kinesiophobia on outcome following total knee replacement: a systematic review. *Archives of Orthopaedic and Trauma Surgery*, *1*, 1–14.

Bryan, S., Goldsmith, L. J., Davis, J. C., Hejazi, S., Macdonald, V., Mcallister, P., Randall, E., Suryaprakash, N., Wu, A. D., & Sawatzky, R. (2018). Revisiting patient satisfaction following total knee arthroplasty: a longitudinal observational study. *BMC*

Musculoskeletal Disorders, *19*(423), 1–8.

Bull, A. M. J., Kessler, O., Alam, M., & Amis, A. A. (2008). Changes in Knee Kinematics Reflect the Articular Geometry after Arthroplasty. *Clinical Orthopaedics and Related Research*, *466*, 2491–2499.

Bytyqi, D., Shabani, B., Lustig, S., Cheze, L., Karahoda Gjurgjeala, N., & Neyret, P. (2014). Gait knee kinematic alterations in medial osteoarthritis: three dimensional assessment. *International Orthopaedics*, *38*, 1191–1198.

Chan, W. P., Lang, P., Stevens, M. P., Sack, K., Majumdar, S., Stoller, D. W., Basch, C., & Genant, H. K. (1991). Osteoarthritis of the knee: comparison of radiography, CT, and MR imaging to assess extent and severity. *American Journal of Roentgenology*, *157*(4), 799–806.

Chaudhry, A., & Goyal, V. K. (2019). Fixed-bearing versus high-flexion RP total knee arthroplasty (TKA): midterm results of a randomized controlled trial. *Journal of Orthopaedic Traumatology*, *20*(2), 1–6.

Chen, C., Ma, Y., Geng, B., Tan, X., Zhang, B., Kumar Jayswal, C., Shahidur Khan, M., Meng, H., Ding, N., Jiang, J., Wu, M., Wang, J., & Xia, Y. (2016). Intercondylar Notch Stenosis of Knee Osteoarthritis and Relationship between Stenosis and Osteoarthritis Complicated with Anterior Cruciate Ligament Injury A Study in MRI. *Medicine*, *95*(17), 1–7.

Chen, D., Shen, J., Zhao, W., Wang, T., Han, L., Hamilton, J. L., & Im, H. J. (2017). Osteoarthritis: Toward a comprehensive understanding of pathological mechanism. In *Bone Research* (Vol. 5, p. 16044).

Choi, E.-S., & Park, S.-J. (2015). Introduction Clinical Evaluation of the Root Tear of the

Posterior Horn of the Medial Meniscus in Total Knee Arthroplasty for Osteoarthritis. *Knee Surg Relat Res*, *27*(2), 90–94.

Chokkhanchitchai, S., Tangarunsanti, T., Jaovisidha, S., Nantiruj, K., & Janwityanujit, S. (2010). The effect of religious practice on the prevalence of knee osteoarthritis. *Clinical Rheumatology*, *29*, 39–44.

Clary, C. W., Fitzpatrick, C. K., Maletsky, L. P., & Rullkoetter, P. J. (2013). The influence of total knee arthroplasty geometry on mid-flexion stability: An experimental and finite element study. *Journal of Biomechanics*, *46*(7), 1351–1357.

Clouthier, A. L., Smith, C. R., Vignos, M. F., Thelen, D. G., Deluzio, K. J., & Rainbow, M. J. (2019). The effect of articular geometry features identified using statistical shape modelling on knee biomechanics. *Medical Engineering & Physics*, *66*, 47–55.

Cootes, T. F., Cooper, D. H., Taylor, C. J., & Graham, J. (1992). Trainable method of parametric shape description. *Image and Vision Computing*, *10*(5), 289–294.

Coughlin, K. M., Incavo, S. J., Doohen, R. R., Gamada, K., Banks, S. A., & Beynnon, B. D. (2007). Kneeling Kinematics After Total Knee Arthroplasty: Anterior-Posterior Contact Position of a Standard and a High-Flex Tibial Insert Design. *Journal of Arthroplasty*, *22*(2), 160–165.

Creamer, P., & Hochberg, M. C. (1997). Osteoarthritis. *Lancet*, *350*(9076), 503–509.

Dai, Y., & Bischoff, J. E. (2013). Comprehensive assessment of tibial plateau morphology in total knee arthroplasty: Influence of shape and size on anthropometric variability. *Journal of Orthopaedic Research*, *31*(10), 1643–1652.

Dargel, J., Janna, A. E., Ae, F., Gotter, M., Dietmar, A. E., Ae, P., & Rgen Koebke, J. (2009). Side differences in the anatomy of human knee joints. *Knee Surgery Sports*

Traumatology Arthroscopy, *17*, 1368–1376.

Dawson, J., Fitzpatrick, R., Murray, D., & Carr, A. J. (1998). Questionnaire on the

perceptions of patients about total knee replacement. *The Journal of Bone and Joint

Surgery. British Volume*, *80-B*(1), 63–69.

de Oliveira Silva, D., Barton, C. J., Briani, R. V., Taborda, B., Ferreira, A. S., Pazzinatto, M.

F., & Azevedo, F. M. de. (2019). Kinesiophobia, but not strength is associated with

altered movement in women with patellofemoral pain. *Gait and Posture*, *68*, 1–5.

Delport, H. P., Banks, S. A., Schepper, J. De, Bellemans, J., & De Schepper, J. (2006). A

kinematic comparison of fixed-and mobile-bearing knee replacements. *Journal of Bone

and Joint Surgery British*, *88*(8), 1016–1021.

Deluzio, K. J., & Astephen, J. L. (2007). Biomechanical features of gait waveform data

associated with knee osteoarthritis. An application of principal component analysis. *Gait

and Posture*, *25*(1), 86–93.

Deluzio, Kevin J, Wyss, U. P., Zee, B., Costigan, P. A., & Sorbie, C. (1997). Principal

component models of knee kinematics and kinetics: Normal vs. pathological gait

patterns. *Human Movement Science*, *16*, 201–217.

Dennis, D. A., Komistek, R., Hoff, W. A., & Gabriel, S. M. (1996). In vivo knee kinematics

derived using an inverse perspective technique. *Clinical Orthopaedics and Related

Research*, *331*, 107–117.

Devers, B. N., Conditt, M. A., Jamieson, M. L., Driscoll, M. D., Noble, P. C., & Parsley, B. S.

(2011). Does Greater Knee Flexion Increase Patient Function and Satisfaction After

Total Knee Arthroplasty? *Journal of Arthroplasty*, *26*(2), 178–186.

Dieppe, P., Cushnaghan, J., Young, P., Kirwan, J., Dieppe, P., Cushnaghan, J., Young, P., &

Kirwan, J. (1993). Prediction of the progression of joint space narrowing in osteoarthritis of the knee by bone scintigraphy. *Annals of the Rheumatic Diseases*, *52*, 557–563.

Ding, C., Cicuttini, F. M., & Jones, G. M. D. (2007). Tibial subchondral bone size and knee cartilage defects: relevance to knee osteoarthritis. *Osteoarthritis and Cartilage*, *15*, 479–486.

Doi, S. A. R., Barendregt, J. J., Khan, S., Thalib, L., & Williams, G. M. (2015). Advances in the meta-analysis of heterogeneous clinical trials II: The quality effects model. *Contemporary Clinical Trials*, *45*, 123–129.

Donell, S. (2019). Subchondral bone remodelling in osteoarthritis. *EFORT Open Reviews*, *4*(6), 221–229.

Dryden, I. L., & Mardia, K. V. (1998). *Statistical shape analysis*. John Wiley & Sons.

Dunbar, M. J. (2001). Subjective outcomes after knee arthroplasty. *Acta Orthopaedica Scandinavica*, *72*(301), 1–63.

Dunbar, M. J., & Haddad, F. S. (2014). Patient satisfaction after total knee replacement: New inroads. *Bone and Joint Journal*, *96B*(10), 1285–1286.

Dunbar, M., Richardson, G., & Robrtsson, O. (2013). I can't get no satisfaction after my total knee replacement. *Bone and Joint Journal*, *95*, 148–152.

Elias, S. G., Freeman, M. A. R., & Gokcay, E. I. (1990). A correlative study of the geometry and anatomy of the distal femur. *Clinical Orthopaedics and Related Research*, *260*, 98–103.

Ersoz, M., & Ergun, S. (2003). Relationship between knee range of motion and Kellgren-Lawrence radiographic scores in knee osteoarthritis. *American Journal of Physical Medicine & Rehabilitation*, *82*(2), 110–115.

Fairbank, T. J. (1948). Knee joint changes after meniscectomy. *Journal of Bone and Joint Surgery British*, *30B*(4), 664–670.

Felson, D. T., Lawrence, R. C., Dieppe, P. A., Hirsch, R., Helmick, C. G., Jordan, J. M., Kington, R. S., Lane, N. E., Nevitt, M. C., Zhang, Y., Sowers, M., McAlindon, T., Spector, T. D., Poole, A. R., Yanovski, S. Z., Ateshian, G., Sharma, L., Buckwalter, J. A., Brandt, K. D., & Fries, J. F. (2000). Osteoarthritis: New Insights. Part 1: The Disease and Its Risk Factors. *Annals of Internal Medicine*, *133*(8), 635–646.

Foroughi, N., Smith, R., & Vanwanseele, B. (2009). The association of external knee adduction moment with biomechanical variables in osteoarthritis: A systematic review. *Knee*, *16*(5), 303–309.

Freeman, M. A. R., & Pinskerova, V. (2005). The movement of the normal tibio-femoral joint. *Journal of Biomechanics*, *38*(2), 197–208.

Galvin, C. R. (2019). *Healthy and Osteoarthritic Knee Kinematics. A 3D/2D Image-Registration Study of Kneeling.* University of Canberra.

Galvin, C. R., Perriman, D. M., Lynch, J. T., Pickering, M. R., Newman, P., Smith, P. N., & Scarvell, J. M. (2019). Age has a minimal effect on knee kinematics: A cross-sectional 3D/2D image-registration study of kneeling. *Knee*, *25*(5), 988–1002.

Galvin, C. R., Perriman, D. M., Newman, P. M., Lynch, J. T., Smith, P. N., & Scarvell, J. M. (2018). Squatting, lunging and kneeling provided similar kinematic profiles in healthy knees—A systematic review and meta-analysis of the literature on deep knee flexion kinematics. *Knee*, *25*(4), 514–530.

Gamada, K., Jayasekera, N., Kashif, F., Fennema, P., Schmotzer, H., & Banks, S. A. (2008). Does ligament balancing technique affect kinematics in rotating platform, PCL retaining

knee arthroplasties? *Knee Surgery Sports Traumatology Arthroscopy*, *16*(2), 160–166.

Garratt, A. M., Brealey, S., & Gillespie, W. J. (2004). Patient-assessed health instruments for the knee: a structured review. *British Society for Rheumatology*, *43*(11), 1414–1423.

Ginsel, B. L., Banks, S. A., Verdonschot, N., & Hodge, W. A. (2009). Improving maximum flexion with a posterior cruciate retaining total knee arthroplasty: A fluoroscopic study. *Acta Orthopaedica Belgica*, *75*(6), 801–807.

Gluck, T. (1891). Referat über die durch das moderne chirurgische Experiment gewonnenen positiven Resultate, betreffend die Naht und den Ersatz von Defecten höherer Gewebe, sowie über die Verwethung resorbirbarer und lebendiger Tampons in der Chirurgie. *Arch Klin Chir*, *41*, 187–239.

Gower, J. (1975). Generalized Procrustes Analysis. *Psychometrika*, *40*(1), 33–51.

Gray, H., & Carter, H. (1919). Anatomy of the Human Body. *The American Journal of Physical Medicine*.

Gregory, J. S., Barr, A. J., Yoshida, K., Alesci, S., Reid, D. M., & Aspden, R. M. (2020). Statistical shape modelling provides a responsive measure of morphological change in knee osteoarthritis over 12 months. *Rheumatology*, *In Press*.

Grood, E. S., & Suntay, W. J. (1983). A joint coordinate system for the clinical description of three-dimensional motions: application to the knee. *Journal of Biomechanical Engineering*, *105*(2), 136–144.

Guan, S., Gray, H. A., Schache, A. G., Feller, J., de Steiger, R., & Pandy, M. G. (2017). In vivo six-degree-of-freedom knee-joint kinematics in overground and treadmill walking following total knee arthroplasty. *Journal of Orthopaedic Research*, *35*(8), 1634–1643.

Guilak, F. (2011). Biomechanical factors in osteoarthritis. *Best Practice and Research*

Clinical Rheumatology, *25*(6), 815–823.

Hamai, S., Miura, H., Higaki, H., Matsuda, S., Shimoto, T., Sasaki, K., Yoshizumi, M.,
Okazaki, K., Tsukamoto, N., & Iwamoto, Y. (2008). Kinematic analysis of kneeling in
cruciate-retaining and posterior-stabilized total knee arthroplasties. *Journal of
Orthopaedic Research*, *26*(4), 435–442.

Hanson, G. R., Park, S. E., Suggs, J. F., Moynihan, A. L., Nha, K. W., Freiberg, A. a, & Li,
G. (2007). In vivo kneeling biomechanics after posterior stabilized total knee
arthroplasty. *Journal of Orthopaedic Science*, *12*(5), 476–483.

Haque, M. N., Pickering, M. R., Al Muhit, A., Frater, M. R., Scarvell, J. M., & Smith, P. N.
(2014). A fast and robust technique for 3D–2D registration of CT to single plane X-ray
fluoroscopy. *Computer Methods in Biomechanics and Biomedical Engineering: Imaging
and Visualization*, *2*(2), 76–89.

Harding, G. T., Hubley-Kozey, C. L., Dunbar, M. J., Stanish, W. D., & Wilson, J. L. A.
(2012). Body mass index affects knee joint mechanics during gait differently with and
without moderate knee osteoarthritis. *Osteoarthritis and Cartilage*, *20*, 1234–1242.

Harris, I. A., Harris, A. M., Naylor, J. M., Adie, S., Mittal, R., & Dao, A. T. (2013).
Discordance between patient and surgeon satisfaction after total joint arthroplasty.
Journal of Arthroplasty, *28*(5).

Harrison, A. J., Ryan, W., & Hayes, K. (2007). Functional data analysis of joint coordination
in the development of vertical jump performance. *Sports Biomechanics*, *6*(2), 199–214.

Haverkamp, D. J., Schiphof, D., Bierma-Zeinstra, S. M. A., Weinans, H., & Waarsing, J. H.
(2011). Variation in joint shape of osteoarthritic knees. *Arthritis & Rheumatism*, *63*(11),
3401–3407.

Hefzy, M. S., Kelly, B. P., & Cooke, T. D. V. (1998). Kinematics of the knee joint in deep flexion: a radiographic assessment. *Medical Engineering & Physics*, *20*(4), 302–307.

Heimann, T., & Meinzer, H.-P. (2009). Statistical shape models for 3D medical image segmentation: A review. *Medical Image Analysis*, *13*(4), 543–563.

Hemmerich, A., Brown, H., Smith, S., Marthandam, S. S. K., & Wyss, U. P. (2006). Hip, Knee, and Ankle Kinematics of High Range of Motion Activities of Daily Living. *Journal of Orthopaedic Research*, *24*(4), 770–781.

Heyse, T. J., Becher, C., Kron, N., Ostermeier, S., Hurschler, C., Schofer, M. D., Tibesku, C. O., & Fuchs-Winkelmann. (2010). Patellofemoral pressure after TKA in vitro: highly conforming vs. posterior stabilized inlays. *Arch Orthop Trauma Surg*, *130*, 191–196.

Higgins, J., Thomas, J., Chandler, J., Cumpston, M., Li, T., Page, M., & Welch, V. (Eds.). (2019). *Cochrane Handbook for Systematic Reviews of Interventions* (6.0). Cochrane. www.training.cochrane.org/handbook

Hilfiker, R., Jüni, P., Nüesch, E., Dieppe, P. A., & Reichenbach, S. (2015). Association of radiographic osteoarthritis, pain on passive movement and knee range of motion: A cross-sectional study. *Manual Therapy*, *20*(2), 361–365.

Hill, P. F., Vedi, V., Williams, A., Iwaki, F. H., Pinskerova, V., & Freeman, M. A. R. (2000). Tibiofemoral movement 2: the loaded and unloaded living knee studied by MRI. *Journal of Bone and Joint Surgery British*, *82*(8), 1196–1198.

Holla, J. F. M., Steultjens, M., Van Der Leeden, M., Roorda, L. D., Bierma-Zeinstra, S. M. A., Den Broeder, A. A., & Dekker, J. (2011). Determinants of range of joint motion in patients with early symptomatic osteoarthritis of the hip and/or knee: an exploratory study in the CHECK cohort. *Osteoarthritis and Cartilage*, *19*, 411–419.

Hoshino, Y., Wang, J. H., Lorenz, S., Fu, F. H., & Tashman, S. (2012). The effect of distal

   femur bony morphology on in vivo knee translational and rotational kinematics. *Knee*

   Surgery Sports Traumatology Arthroscopy, *20*(7), 1331–1338.

Howell, S. M., Hodapp, E. E., Kuznik, K., & Hull, M. L. (2009). In Vivo Adduction and

   Reverse Axial Rotation (External) of the Tibial Component Can Be Minimized.

   Orthopaedics, *32*(5), 319–326.

Howell, S. M., Hodapp, E. E., Vernace, J. V., Hull, M. L., & Meade, T. D. (2013). Are

   undesirable contact kinematics minimized after kinematically aligned total knee

   arthroplasty? An intersurgeon analysis of consecutive patients. *Knee Surgery Sports*

   Traumatology Arthroscopy, *21*(10), 2281–2287.

Howells, N., Murray, J., Wylde, V., Dieppe, P., & Blom, A. (2016). Persistent pain after knee

   replacement: do factors associated with pain vary with degree of patient dissatisfaction?

   Osteoarthritis and Cartilage, *24*(12), 2061–2068.

Huddleston, J. I., Moxley Scarborough, D., Goldvasser, D., Freiberg, A. A., & Malchau, H.

   (2009). How Often Do Patients with High-Flex Total Knee Arthroplasty Use High

   Flexion? *Clinical Orthopaedics and Related Research*, *467*(7), 1898–1906.

Hudelmaier, M., & Wirth, W. (2016). Differences in subchondral bone size after one year in

   osteoarthritic and healthy knees. *Osteoarthritis and Cartilage*, *24*, 623–630.

Hunter, D., Nevitt, M., Lynch, J., Kraus, V. B., Katz, J. N., Collins, J. E., Bowes, M. A.,

   Guermazi, A., Roemer, F. W., & Losina, E. (2015). Longitudinal validation of

   periarticular bone area and 3D shape as biomarkers for knee OA progression? Data from

   the FNIH OA Biomarkers Consortium. *Annals of Rheumatic Disease*, *0*, 1–8.

Hunter, D J, Guermazi, A., Lo, G. H., Grainger, A. J., Conaghan, P. G., Boudreau, R. M., &

Roemer, F. W. (2011). Evolution of semi-quantitative whole joint assessment of knee OA: MOAKS (MRI Osteoarthritis Knee Score). *Osteoarthritis and Cartilage*, *19*, 990–1002.

Hunter, D J, Guermazi, A., Roemer, F., Zhang, Y., & Neogi, T. (2013). Structural correlates of pain in joints with osteoarthritis. *Osteoarthritis and Cartilage*, *21*, 1170–1178.

Hunter, David J. (2011). Lower extremity osteoarthritis management needs a paradigm shift. *British Journal of Sports Medicine*, *45*(4), 283–288.

Iacono, F., Raspugli, G. F., Bruni, D., Filardo, G., Zaffagnini, S., Luetzow, W. F., Lo Presti, M., Akkawi, I., Muccioli, G. M., & Marcacci, M. (2014). The adductor tubercle as an important landmark to determine the joint line level in total knee arthroplasty: from radiographs to surgical theatre. *Knee Surgery Sports Traumatology Arthroscopy*, *22*, 3034–3038.

Incavo, S. J., Mullins, E. R., Coughlin, K. M., Banks, S. A., Banks, A., & Beynnon, B. D. (2004). Tibiofemoral kinematic analysis of kneeling after total knee arthroplasty. *Journal of Arthroplasty*, *19*(7), 906–910.

Insall, J. N., Lachiewicz, P. F., & Burstein, A. H. (1982). The posterior stabilized condylar prosthesis: a modification of the total condylar design. Two to four-year clinical experience. *Journal of Bone and Joint Surgery American*, *64*(9), 1317–1323.

Isaacson, J., & Brotto, M. (2014). Physiology of Mechanotransduction: How Do Muscle and Bone "Talk" to One Another? *Clinical Reviews in Bone and Mineral Metabolism*, *12*(2), 77–85.

Iwaki, H., Pinskerova, V., & Freeman, M. A. R. (2000). Tibiofemoral movement 1: the shapes and relative movements of the femur and tibia in the unloaded cadaver knee.

Journal of Bone and Joint Surgery British, *82*(8), 1189–1195.

Jacobs, W., Anderson, P., Limbeek, J., & Wymenga, A. (2004). Mobile bearing vs fixed bearing prostheses for total knee arthroplasty for post-operative functional status in patients with osteoarthritis and rheumatoid arthritis. *Cochrane Database of Systematic Reviews*, *2*, 1–91.

Jain, S., Pathak, A. C., Kanniyan, K., Kulkarni, S., Tawar, S., & Mane, P. (2013). What Is the High Flexion Knee Prosthesis? High-Flexion Posterior-Stabilized Total Knee Prosthesis: Is It Worth the Hype? Why Is the High Flexion Knee Prosthesis Needed? *Knee Surgery Related Research*, *25*(3), 100–105.

Jeong, Y., Heo, S., Lee, G., & Park, W. (2018). Pre-obesity and obesity impacts on passive joint range of motion. *Ergonomics*, *61*(9), 1223–1231.

Jiang, C., Liu, Z., Wang, Y., Bian, Y., Feng, B., & Weng, X. (2016). Posterior Cruciate Ligament Retention versus Posterior Stabilization for Total Knee Arthroplasty: A Meta-Analysis. *PLoS One*, *11*(1), 1–15.

Kan, A., Oshida, M., Oshida, S., Imada, M., Nakagawa, T., & Okinaga, S. (2010). Anatomical significance of a posterior horn of medial meniscus: the relationship between its radial tear and cartilage degradation of joint surface. *Sports Medicine, Arthroscopy, Rehabilitation, Therapy Technology*, *2*(1), 1–4.

Kanekasu, K., Banks, S. A., Honjo, S., Nakata, O., & Kato, H. (2004). Fluoroscopic analysis of knee arthroplasty kinematics during deep flexion kneeling. *Journal of Arthroplasty*, *19*(8), 998–1003.

Kawashima, K., Tomita, T., Tamaki, M., Murase, T., Yoshikawa, H., & Sugamoto, K. (2013). In vivo three-dimensional motion analysis of osteoarthritic knees. *Modern*

Rheumatology, *23*(4), 646–652.

Kellgren, J. H., & Lawrence, J. S. (1957). Radiological assessment of osteoarthrosis. *Annals of Rheumatic Disease*, *16*, 494–502.

Khasian, M., Sharma, A., Fehring, T. K., Griffin, W. L., Mason, J. B., & Komistek, R. (2019). Kinematic Performance of Gradually Variable Radius Posterior-Stabilized Primary TKA During Various Activities: An In Vivo Study Using Fluoroscopy. *Journal of Arthroplasty*, *35*(4), 1101–1108.

Kim, Y.-H., Park, J.-W., & Kim, J.-S. (2018). Comparison of High-Flexion Fixed-Bearing and High-Flexion Mobile-Bearing Total Knee Arthroplasties—A Prospective Randomized Study. *Journal of Arthroplasty*, *33*(1), 130–135.

Kingsley, C., & Patel, S. (2017). Patient-reported outcome measures and patient-reported experience measures What are PROMs and PREMs? *British Journal of Anaesthesia: Education*, *17*(4), 137–144.

Kingston, D. C., & Acker, S. M. (2018). Thigh-calf contact parameters for six high knee flexion postures: Onset, maximum angle, total force, contact area, and center of force. *Journal of Biomechanics*, *67*, 46–54.

Kingston, D. C., & Acker, S. M. (2019). Prediction of thigh-calf contact parameters from anthropometric regression. *Proceedings of the Institution of Mechanical Engineers, Part H: Journal of Engineering in Medicine*, *233*(4), 414–423.

Kitagawa, A., Tsumura, N., Chin, T., Gamada, K., Banks, S. A., & Kurosaka, M. (2010). In vivo comparison of knee kinematics before and after high-flexion posterior cruciate-retaining total knee arthroplasty. *Journal of Arthroplasty*, *25*(6), 964–969.

Kohn, M. D., Sassoon, A. A., & Fernando, N. D. (2016). Classifications in Brief: Kellgren-

Lawrence Classification of Osteoarthritis. *Clinical Orthopaedics and Related Research*, *474*(8), 1886–1893.

Kuroyanagi, Y., Mu, S., Hamai, S., Robb, W. J., & Banks, S. A. (2012). In vivo knee kinematics during stair and deep flexion activities in patients with bicruciate substituting total knee arthroplasty. *Journal of Arthroplasty*, *27*(1), 122–128.

Ladd, A. L., Crisco, J. J., Hagert, E., Rose, J., & Weiss, A.-P. C. (2014). The 2014 ABJS Nicolas Andry Award: The Puzzle of the Thumb: Mobility, Stability, and Demands in Opposition. *Clinical Orthopaedics and Related Research*, *472*, 3605–3622.

Lansdown, D. A., Pedoia, V., Zaid, M., Amano, K., Souza, R. B., Li, X., & Ma, C. B. (2017). Variations in Knee Kinematics After ACL Injury and After Reconstruction Are Correlated With Bone Shape Differences. *Clinical Orthopaedics and Related Research*, *10*, 2427–2435.

Lau, B. C., Conway, D., Mulvihill, J., Zhang, A. L., & Feeley, B. T. (2018). Biomechanical consequences of meniscal tear, partial meniscectomy, and meniscal repair in the knee. *Journal of Bone and Joint Surgery Reviews*, *6*(4).

Lawler, E. L., Lenstra, J. K., Rinnooy Kan, A. H. G., & Shmoys, D. B. (1985). *The Traveling salesman problem: a guided tour of combinatorial optimization*. John Wiley & Sons Ltd.

Laxafoss, E., Jacobsen, S., Gosvig, K. K., & Sonne-Holm, S. (2013). The alignment of the knee joint in relationship to age and osteoarthritis: The Copenhagen Osteoarthritis Study. *Skeletal Radiology*, *42*(4), 531–540.

Lee, T. Q. (2014). Biomechanics of Hyperflexion and Kneeling before and after Total Knee Arthroplasty. *Clinics in Orthopedic Surgery*, *6*(2), 117–126.

Leszko, F., Hovinga, K. R., Lerner, A. L., Komistek, R., & Mahfouz, M. R. (2011). In vivo

normal knee kinematics: Is ethnicity or gender an influencing factor? *Clinical Orthopaedics and Related Research*, *469*(1), 95–106.

Li, J.-S., Tsai, T.-Y., Felson, D. T., Li, G., & Lewis, C. L. (2017). Six degree-of-freedom knee joint kinematics in obese individuals with knee pain during gait. *PLoS One*, *12*(3), 1–11.

Li, N., Tan, Y., Deng, Y., & Chen, L. (2014). Posterior cruciate-retaining versus posterior stabilized total knee arthroplasty: a meta-analysis of randomized controlled trials. *Knee Surgery Sports Traumatology Arthroscopy*, *22*, 556–564.

Liao, C.-D., Huang, Y.-C., Chiu, Y.-S., & Liou, T.-H. (2017). Effect of body mass index on knee function outcomes following continuous passive motion in patients with osteoarthritis after total knee replacement: a retrospective study. *Physiotherapy*, *103*(3), 266–275.

Loeser, R. F., Goldring, S. R., Scanzello, C. R., & Goldring, M. B. (2012). Osteoarthritis A Disease of the Joint as an Organ. *Arthritis & Rheumatism*, *64*(6), 1697–1707.

Lynch, J. T., Scarvell, J. M., Galvin, C. R., Smith, P. N., & Perriman, D. M. (2020). Influence of component design on in vivo tibiofemoral contact patterns during kneeling after total knee arthroplasty: a systematic review and meta-analysis. *Knee Surgery, Sports Traumatology, Arthroscopy*.

Lynch, J. T., Schneider, M. T. Y., Perriman, D. M., Scarvell, J. M., Pickering, M. R., Asikuzzaman, M., Galvin, C. R., Besier, T. F., & Smith, P. N. (2019). Statistical shape modelling reveals large and distinct subchondral bony differences in osteoarthritic knees. *Journal of Biomechanics*, *93*, 177–184.

Mahoney, O. M., Kinsey, T. L., Banks, A. Z., & Banks, S. A. (2009). Rotational Kinematics

of a Modern Fixed-Bearing Posterior Stabilized Total Knee Arthroplasty. *Journal of Arthroplasty*, *24*(4), 641–645.

Manninen, P., Riihimäki, H., Heliövaara, M., & Mäkelä, P. (1996). Overweight, gender and knee osteoarthritis. *International Journal of Obesity and Related Metabolic Disorders*, *20*(6), 595–597.

Maratt, J. D., Lee, Y., Lyman, S., & Westrich, G. H. (2015). Predictors of Satisfaction Following Total Knee Arthroplasty. *Journal of Arthroplasty*, *30*(7), 1142–1145.

Martelli, S., & Pinskerova, V. (2002). The shapes of the tibial and femoral articular surfaces in relation to tibiofemoral movement. *Journal of Bone and Joint Surgery British*, *84*(4), 607–613.

Masouros, S. D., Bull, A. M. J., & Amis, A. A. (2010). Biomechanics of the knee joint. *Orthopaedics and Trauma*, *24*(2), 84–91.

Matsuda, S, Miura, H., Nagamine, R., Urabe, K., Ikenoue, T., Okazaki, K., & Iwamoto, Y. (1999). Posterior tibial slope in the normal and varus knee. *The American Journal of Knee Surgery*, *12*(3), 165–168.

Matsuda, Shuichi, Miura, H., Nagamine, R., Mawatari, T., Tokunaga, M., Nabeyama, R., & Iwamoto, Y. (2004). Anatomical analysis of the femoral condyle in normal and osteoarthritic knees. *Journal of Orthopaedic Research*, *22*(1), 104–109.

McAlindon, T. E., Bannuru, R. R., Sullivan, M. C., Arden, N. K., Berenbaum, F., Bierma-Zeinstra, S. M. A., Hawker, G. A., Henrotin, Y., Hunter, D. J., Kawaguchi, H., Kwoh, K., Lohmander, S., Rannou, F., Roos, E. M., & Underwood, M. (2014). OARSI guidelines for the non-surgical management of knee osteoarthritis. *Osteoarthritis and Cartilage*, *22*, 363–388.

McClelland, J. A., Feller, J. A., Menz, H. B., & Webster, K. E. (2017). Patients with total knee arthroplasty do not use all of their available range of knee flexion during functional activities. *Clinical Biomechanics*, *43*, 74–78.

McCormack, H. M., De L. Horne, D. J., & Sheather, S. (2020). Clinical applications of visual analogue scales: a critical review. *Psychological Medicine*, *18*, 1007–1019.

McEwen, H. M. J., Barnett, P. I., Bell, C. J., Farrar, R., Auger, D. D., Stone, M. H., & Fisher, J. (2005). The influence of design, materials and kinematics on the in vitro wear of total knee replacements. *Journal of Biomechanics*, *38*(2), 357–365.

Meccia, B., Komistek, R., Mahfouz, M., & Dennis, D. A. (2014). Abnormal Axial Rotations in TKA Contribute to Reduced Weightbearing Flexion. *Clinical Orthopaedics and Related Research*, *472*(1), 248–253.

Medical Advisory Secretariat. (2005). Total knee replacement: an evidence-based analysis. *Ontario Health Technology Assessment Series*, *5*(9), 1–51.

Mellon, S. J., & Tanner, K. E. (2012). Bone and its adaptation to mechanical loading: A review. *International Materials Reviews*, *57*(5), 235–255.

Mezghani, N., Ouakrim, Y., Fuentes, A., Mitiche, A., Hagemeister, N., Vendittoli, P.-A., & De Guise, J. A. (2017). Mechanical biomarkers of medial compartment knee osteoarthritis diagnosis and severity grading: Discovery phase. *Journal of Biomechanics*, *52*, 106–112.

Mikashima, Y., Tomatsu, T., Horikoshi, M., Nakatani, T., Saito, S., Momohara, S., & Banks, S. A. (2010). In vivo deep-flexion kinematics in patients with posterior-cruciate retaining and anterior-cruciate substituting total knee arthroplasty. *Clinical Biomechanics*, *25*(1), 83–87.

Mills, K., Hunt, M. A., & Ferber, R. (2013). Biomechanical deviations during level walking associated with knee osteoarthritis: a systematic review and meta-analysis. *Arthritis Care & Research*, *65*(10), 1643–1665.

Mochizuki, T., Sato, T., Tanifuji, O., Kobayashi, K., Koga, Y., Yamagiwa, H., Omori, G., & Endo, N. (2013). In vivo pre- and postoperative three-dimensional knee kinematics in unicompartmental knee arthroplasty. *Journal of Orthopaedic Science*, *18*(1), 54–60.

Moonot, P., Mu, S., Railton, G. T., Field, R. E., & Banks, S. A. (2009). Tibiofemoral kinematic analysis of knee flexion for a medial pivot knee. *Knee Surgery Sports Traumatology Arthroscopy*, *17*, 927–934.

Moro-oka, T., Muenchinger, M., Canciani, J.-P., & Banks, S. A. (2007). Comparing in vivo kinematics of anterior cruciate-retaining and posterior cruciate-retaining total knee arthroplasty. *Knee Surgery Sports Traumatology Arthroscopy*, *15*(1), 93–99.

Moschi, A., & Zingoni, G. (1977). Biomechanics of the Knee. *Italian Journal of Orthopaedics and Traumatology. Supplementum*, *3*.

Most, E., Zayontz, S., Li, G., Otterberg, E., Sabbag, K., & Rubash, H. E. (2003). Femoral Rollback After Cruciate-Retaining and Stabilizing Total Knee Arthroplasty. *Clinical Orthopaedics and Related Research*, *410*, 101–113.

Muhit, A. A., Pickering, M. R., Ward, T., Scarvell, J. M., & Smith, P. N. (2010). A comparison of the 3D kinematic measurements obtained by single-plane 2D-3D image registration and RSA. *IEEE Engineering in Medicine and Biology Society*, *March*, 6288–6291.

Mulholland, S. J., & Wyss, U. P. (2001). Activities of daily living in non-Western cultures: range of motion. *International Journal of Rehabilitation Research*, *24*(3), 191–198.

Murray, D. W., Fitzpatrick, R., Rogers, K., Pandit, H., Beard, D. J., Carr, A. J., & Dawson, J. (2007). The use of the Oxford hip and knee scores. *Journal of Bone and Joint Surgery British*, *89*(8), 1010–1014.

Nagano, Y., Naito, K., Saho, Y., Torii, S., Ogata, T., Nakazawa, K., Akai, M., & Fukubayashi, T. (2012). Association between in vivo knee kinematics during gait and the severity of knee osteoarthritis. *Knee*, *19*, 628–632.

Naili, J. E., Lindgren, V., Iversen, M. D., Hedström, M., & Broström, E. W. (2017). Improved knee biomechanics among patients reporting a good outcome in knee-related quality of life one year after total knee arthroplasty. *BMC Musculoskeletal Disorders*, *18*(122), 1–11.

Nakamura, E., Banks, S. A., Tanaka, A., Sei, A., & Mizuta, H. (2009). Three-Dimensional Tibiofemoral Kinematics During Deep Flexion Kneeling in a Mobile-Bearing Total Knee Arthroplasty. *Journal of Arthroplasty*, *24*(7), 1120–1124.

Nakamura, M., Sumen, Y., Sakaridani, K., Exham, H., & Ochi, M. (2006). Relationship between the shape of tibial spurs on X-ray and meniscal changes on MRI in early osteoarthritis of the knee. *Magnetic Resonance Imaging*, *24*(9), 1143–1148.

Nakamura, S., Ito, H., Yoshitomi, H., Kuriyama, S., Komistek, R., & Matsuda, S. (2015). Analysis of the Flexion Gap on In Vivo Knee Kinematics Using Fluoroscopy. *Journal of Arthroplasty*, *30*(7), 1237–1342.

Nakamura, S., Sharma, A., Kobayashi, M., Ito, H., Nakamura, K., Zingde, S. M., Nakamura, T., & Komistek, R. (2014). 3D in vivo femoro-tibial kinematics of tri-condylar total knee arthroplasty during kneeling activities. *Knee*, *21*(1), 162–167.

Neogi, T. (2012). Clinical significance of bone changes in osteoarthritis. *Therapeutic*

Advances in Musculoskeletal Disease, *4*(4), 259–267.

Neogi, T., Bowes, M. A., Niu, J., De Souza, K. M., Vincent, G. R., Goggins, J., Zhang, Y., & Felson, D. T. (2013). Magnetic Resonance Imaging-Based Three-Dimensional Bone Shape of the Knee Predicts Onset of Knee Osteoarthritis: Data From the Osteoarthritis Initiative. *Arthritis & Rheumatism*, *65*(8), 2048–2058.

Neogi, T., & Felson, D. T. (2016). Bone as an imaging biomarker and treatment target in OA. *Nature Reviews Rheumatology*, *12*(9).

Niki, Y., Takeda, Y., Udagawa, K., Enomoto, H., Toyama, Y., & Suda, Y. (2013). Is greater than 145° of deep knee flexion under weight-bearing conditions safe after total knee arthroplasty? A fluoroscopic analysis of Japanese-style deep knee flexion. *Bone and Joint Journal*, *95-B*(6), 782–787.

Noble, P. C., Conditt, M. A., Cook, K. F., & Mathis, K. B. (2006). The John Insall Award: Patient Expectations Affect Satisfaction with Total Knee Arthroplasty. *Clinical Orthopaedics and Related Research*, *452*, 35–43.

Nunley, R. M., Nam, D., Johnson, S. R., & Barnes, C. L. (2014). Extreme Variability in Posterior Slope of The Proximal Tibia: Measurements on 2,395 CT Scans of Patients Undergoing UKA? *Journal of Arthroplasty*, *29*(8), 1677–1680.

Okamoto, N., Breslauer, L., Hedley, A. K., Mizuta, H., & Banks, S. A. (2011). In Vivo Knee Kinematics in Patients With Bilateral Total Knee Arthroplasty of 2 Designs. *Journal of Arthroplasty*, *26*(6), 914–918.

Ozdemir, F., Ozlem, A., Ae, T., Kokino, S., & Turan, F. N. (2006). How do marginal osteophytes, joint space narrowing and range of motion affect each other in patients with knee osteoarthritis. *Rheumatology International*, *26*(516), 1–7.

Park, J., Seeley, M. K., Francom, D., Reese, S., & Hopkins, J. T. (2017). Functional vs. Traditional Analysis in Biomechanical Gait Data: An Alternative Statistical Approach. *Journal of Human Kinetics*, *60*, 39–49.

Parrette, S., Flecher, X., Ollivier, M., Aubaniac, J.-M., & Argenson, J.-N. A. (2011). Role of Knee Flexion in the Quality of Life of Patients Implanted With Primary TKA. *Techniques in Knee Sugery*, *10*(2), 73–76.

Pauwels, F. (1980). Biomechanics of the Locomotor Apparatus. In *Biomechanics of the Locomotor Apparatus*. Springer-Verlag.

Pavlova, A. V., Saunders, F. R., Muthuri, S. G., Gregory, J. S., Barr, R. J., Martin, K. R., Hardy, R. J., Cooper, R., Adams, J. E., Kuh, D., & Aspden, R. M. (2017). Statistical shape modelling of hip and lumbar spine morphology and their relationship in the MRC National Survey of Health and Development. *Journal of Anatomy*, *231*(2), 248–259.

Peters, A., Galna, B., Sangeux, M., Morris, M., & Baker, R. (2010). Quantification of soft tissue artifact in lower limb human motion analysis: A systematic review. *Gait & Posture*, *31*(1), 1–8.

Pinskerova, V., Samuelson, K. M., Stammers, J., Maruthainar, K., Sosna, A., & Freeman, M. A. R. (2009). The knee in full flexion: An Anatomical Study. *Journal of Bone and Joint Surgery British*, *91*(6), 830–834.

Price, D. D., McGrath, P. A., Rafii, A., & Buckingham, B. (1983). The validation of visual analogue scales as ratio scale measures for chronic and experimental pain. *Pain*, *17*(1), 45–56.

R Core Team. (2018). *R: A language and Environment for Statistical Computing*. R Foundation for Statistical Computing. https://www.r-project.org/

Robertsson, O., Dunbar, M. J., Pehrsson, T., Knutson, K., & Lidgren, L. (2000). Patient satisfaction after knee arthroplasty: A report on 27,372 knees operated on between 1981 and 1995 in Sweden. *Acta Orthopaedica Scandinavica*, *71*(3), 262–267.

Rodríguez-Merchán, E. C., & Oussedik, S. (Eds.). (2015). *Total Knee Arthroplasty: A Comprehensive Guide*. Springer International Publishing.

Rowe, P. J., Myles, C. M., Walker, C., & Nutton, R. (2000). Knee joint kinematics in gait and other functional activities measured using flexible electrogoniometry: How much knee motion is sufficient for normal daily life? *Gait & Posture*, *12*(2), 143–155.

Saadat, S., Pickering, M. R., Perriman, D., Scarvell, J. M., & Smith, P. N. (2017). Fast and Robust Multi-Modal Image Registration for 3D Knee Kinematics. *2017 International Conference on Digital Image Computing: Techniques and Applications (DICTA)*, 1–5.

Saffarini, M., Demey, G., Nover, L., & Dejour, D. (2016). Evolution of trochlear compartment geometry in total knee arthroplasty. *Annals of Translational Medicine*, *4*(1), 1–6.

Sasho, T., Akagi, R., Tahara, M., Katsuragi, J., Nakagawa, R., Enomoto, T., Yusuke, S., Kimura, S., Yamaguchi, S., & Watanabe, A. (2017). Osteophyte formation on medial wall of the intercondylar notch of femur is an early sign of osteoarthritic knee development using osteoarthritis initiative data. *Osteoarthritis and Cartilage*, *25*, S84.

Sawaguchi, N., Majima, T., Ishigaki, T., Mori, N., Terashima, T., & Minami, A. (2010). Mobile-bearing total knee arthroplasty improves patellar tracking and patellofemoral contact stress. In vivo measurements in the same patients. *Journal of Arthroplasty*, *25*(6), 920–925.

Scarvell, Jennie M, Galvin, C. R., Perriman, D. M., Lynch, J. T., & van Deursen, R. W.

(2018). Kinematics of knees with osteoarthritis show reduced lateral femoral roll-back and maintain an adducted position. A systematic review of research using medical imaging. *Journal of Biomechanics*, *75*, 108–122.

Scarvell, Jennie M, Hribar, N., Galvin, C. R., Pickering, M. R., Perriman, D. M., Lynch, J. T., & Smith, P. N. (2019). Analysis of Kneeling by Medical Imaging Shows the Femur Moves Back to the Posterior Rim of the Tibial Plateau, Prompting Review of the Concave-Convex Rule. *Physical Therapy*, *99*(3), 311–318. https://doi.org/10.1093/ptj/pzy144

Scarvell, Jennifer M., Pickering, M. R., & Smith, P. N. (2010). New registration algorithm for determining 3D knee kinematics using CT and single-plane fluoroscopy with improved out-of-plane translation accuracy. *Journal of Orthopaedic Research*, *28*(3), 334–340.

Scarvell, Jennifer M., Smith, P. N., Refshauge, K. M., & Galloway, H. R. (2007). Magnetic Resonance Imaging Analysis of Kinematics in Osteoarthritic Knees. *Journal of Arthroplasty*, *22*(3), 383–393.

Schneider, M. T. Y., Zhang, J., Crisco, J. J., Weiss, A.-P. C., Ladd, A. L., Mithraratne, K., Nielsen, P., & Besier, T. (2017). Trapeziometacarpal joint contact varies between men and women during three isometric functional tasks. *Medical Engineering & Physics*, *50*, 43–49.

Schneider, M., Zhang, J., Crisco, J. J., Weiss, A. P. C., Ladd, A. L., Nielsen, P., & Besier, T. (2015). Men and women have similarly shaped carpometacarpal joint bones. *Journal of Biomechanics*, *48*, 3420–3426.

Schneider, M., Zhang, J., Walker, C., Crisco, J., Weiss, A.-P., Ladd, A., Nielsen, P., & Besier, T. (2018). Early morphologic changes in trapeziometacarpal joint bones with osteoarthritis. *Osteoarthritis and Cartilage*, *26*(10), 1338–1344.

Schnurr, C., Jarrous, M., Güdden, I., Eysel, P., & Pierre König, D. (2013). Pre-operative arthritis severity as a predictor for total knee arthroplasty patients' satisfaction. *International Orthopaedics*, *37*, 1257–1261.

Scholes, C., Houghton, E. R., Lee, M., & Lustig, S. (2015). Meniscal translation during knee flexion: what do we really know? *Knee Surgery Sports Traumatology Arthroscopy*, *23*, 32–40.

Schütz, P., Taylor, W. R., Postolka, B., Fucentese, S. F., Koch, P. P., Freeman, M. A. R., Pinskerova, V., & List, R. (2019). Kinematic Evaluation of the GMK Sphere Implant During Gait Activities: A Dynamic Videofluoroscopy Study. *Journal of Orthopaedic Research*, *37*(11), 2337–2347.

Scott, C. E. H., Bugler, K. E., Clement, N. D., MacDonald, D., Howie, C. R., & Biant, L. C. (2012). Patient expectations of arthroplasty of the hip and knee. *Journal of Bone and Joint Surgery British*, *94-B*(7), 974–981.

Scott, G., Imam, M. A. A., Eifert, A., Freeman, M. A. R., Pinskerova, V., Field, R. E. E., Skinner, J., & Banks, S. A. (2016). Can a total knee arthroplasty be both rotationally unconstrained and anteroposteriorly stabilised? *Bone and Joint Research*, *5*(3), 80–86.

Shapiro, M. B., Prodoehl, J., Corcos, D. M., & Gottlieb, G. L. (2005). Muscle activation is different when the same muscle acts as an agonist or an antagonist during voluntary movement. *Journal of Motor Behavior*, *37*(2), 135–145.

Shepstone, L., Rogers, J., Kirwan, J. R., & Silverman, B. W. (2001). Shape of the intercondylar notch of the human femur: a comparison of osteoarthritic and non-osteoarthritic bones from a skeletal sample. *Annals of Rheumatic Disease*, *60*, 968–73.

Skou, S. T., Roos, E. M., Laursen, M. B., Rathleff, M. S., Arendt-Nielsen, L., Simonsen, O.,

& Rasmussen, S. (2015). A Randomized, Controlled Trial of Total Knee Replacement. *New England Journal of Medicine*, *373*(17), 1597–1606.

Slim, K., Nini, E., Forestier, D., Kwiatkowski, F., Panis, Y., & Chipponi, J. (2003). Methodological index for non-randomized studies (MINORS): development and validation of a new instrument. *ANZ Journal of Surgery Surg*, *73*(9), 712–716.

Smith, P. N., Refshauge, K. M., & Scarvell, J. M. (2003). Development of the Concepts of Knee Kinematics. *Archives of Physical Medicine and Rehabilitation*, *84*(12), 1895–1902.

Smoger, L. M. (2016). *Statistical Modeling to Investigate Anatomy and Function of the Knee*. Denver University.

Smoger, L. M., Fitzpatrick, C. K., Clary, C. W., Cyr, A. J., Maletsky, L. P., Rullkoetter, P. J., & Laz, P. J. (2015). Statistical modeling to characterize relationships between knee anatomy and kinematics. *Journal of Orthopaedic Research*, *33*(11), 1620–1630.

Stagni, R., Fantozzi, S., Cappello, A., & Leardini, A. (2005). Quantification of soft tissue artefact in motion analysis by combining 3D fluoroscopy and stereophotogrammetry: A study on two subjects. *Clinical Biomechanics*, *20*(3), 320–329.

Sterling, M., Jull, G., & Wright, A. (2001). The effect of musculoskeletal pain on motor activity and control. *Journal of Pain*, *2*(3), 135–145.

Steultjens, M. P. M., Dekker, J., van Baar, M. E., Oostendorp, R. A. B., & Bijlsma, J. W. J. (2000). Range of joint motion and disability in patients with osteoarthritis of the knee or hip. *Rheumatology*, *39*(9), 955–961.

Stoddard, J. E., Deehan, D. J., Bull, A. M. J., McCaskie, A. W., & Amis, A. A. (2013). The kinematics and stability of single-radius versus multi-radius femoral components related to mid-range instability after TKA. *Journal of Orthopaedic Research*, *31*(1), 53–58.

Sullivan, L. H. (1896). The Tall Office Building Artistically Considered. *Lippincott's Monthly Magazine*, 403–409.

Tanaka, A., Nakamura, E., Okamoto, N., Banks, S. A., & Mizuta, H. (2011). Three-dimensional kinematics during deep-flexion kneeling in mobile-bearing total knee arthroplasty. *Knee*, *18*(6), 412–416.

Tanamas, S. K., Wluka, A. E., Pelletier, J.-P., Pelletier, J. M., Abram, F., Berry, P. A., Wang, Y., Jones, G., & Cicuttini, F. M. (2010). Bone marrow lesions in people with knee osteoarthritis predict progression of disease and joint replacement: a longitudinal study. *Rheumatology*, *49*(12), 2413–2419.

Thambyah, A., Goh, J. C. H., & De, S. Das. (2005). Contact stresses in the knee joint in deep flexion. *Medical Engineering & Physics*, *27*(4), 329–335.

The Royal Australian College of General Practitioners. (2018). *Guideline for the management of knee and hip osteoarthritis Second edition*.

Theis, K. A., Murphy, L., Hootman, J. M., & Wilkie, R. (2013). Social participation restriction among us adults with arthritis: A population-based study using the international classification of functioning, disability and health. *Arthritis Care and Research*, *65*(7), 1059–1069.

Todo, S., Kadoya, Y., Moilanen, T., Kobayashi, A., Yamano, Y., Iwaki, H., & Freeman, M. A. R. (1999). Anteroposterior and rotational movement of femur during knee flexion. *Clinical Orthopaedics and Related Research*, *362*, 162–170.

Ullah, S., & Finch, C. F. (2013). Applications of functional data analysis: A systematic review. In *BMC Medical Research Methodology* (Vol. 13, Issue 43, pp. 1–12).

van Manen, M. D., Nace, J., & Mont, M. A. (2012). Management of primary knee

osteoarthritis and indications for total knee arthroplasty for general practitioners. *The Journal of the American Osteopathic Association*, *112*(11), 709–715.

Verra, W. C., van den Boom, L. G., Jacobs, W., Clement, D. J., Wymenga, A. A., & Nelissen, R. G. (2013). Retention versus sacrifice of the posterior cruciate ligament in total knee arthroplasty for treating osteoarthritis. *Cochrane Database of Systematic Reviews*, *10*.

Verra, W., Van-den-Boom, L., Jacobs, W., Clement, D., Wymenga, A., & Nelissen, R. (2005). Retention versus sacrifice of the posterior cruciate ligament in total knee replacement for treatment of osteoarthritis and rheumatoid arthritis. *Cochrane Database of Systematic Reviews*, *10*, 1–105.

Vertullo, C. J., Grimbeek, P. M., Graves, S. E., & Lewis, P. L. (2017). Surgeon's Preference in Total Knee Replacement: A Quantitative Examination of Attributes, Reasons for Alteration, and Barriers to Change. *Journal of Arthroplasty*, *32*, 2980–2989.

Victor, J., Banks, S. A., & Bellemans, J. (2005). Kinematics of posterior cruciate ligament-retaining and -substituting total knee arthroplasty. *Journal of Bone and Joint Surgery British*, *87-B*(5), 646–655.

Victor, J., & Bellemans, J. (2006). Physiologic kinematics as a concept for better flexion in TKA. *Clinical Orthopaedics and Related Research*, *452*, 53–58.

Victor, J., Mueller, J. K. P., Komistek, R., Sharma, A., Nadaud, M. C., & Bellemans, J. (2010). In vivo kinematics after a cruciate-substituting TKA. *Clinical Orthopaedics and Related Research*, *468*(3), 807–814.

Walker, P. S., & Hajek, J. V. (1972). The load-bearing area in the knee joint. *Journal of Biomechanics*, *5*(6), 581–589.

Walker, P. S., & Sathasivam, S. (2000). Design forms of total knee replacement. *Proceedings*

of the Institution of Mechanical Engineers, Part H: Journal of Engineering in Medicine, *214*(1), 101–119.

Wang, Y., Wluka, A. E., & Cicuttini, F. M. (2005). The determinants of change in tibial plateau bone area in osteoarthritic knees: a cohort study. *Arthritis Research & Therapy*, *7*(3), 687–693.

Warmenhoven, J., Cobley, S., Draper, C., Harrison, A., Bargary, N., & Smith, R. (2019a). Bivariate functional principal components analysis: considerations for use with multivariate movement signatures in sports biomechanics. *Sports Biomechanics*, *18*(1), 10–27.

Warmenhoven, J., Cobley, S., Draper, C., Harrison, A., Bargary, N., & Smith, R. (2019b). Considerations for the use of functional principal components analysis in sports biomechanics: examples from on-water rowing. *Sports Biomechanics*, *18*(3), 317–341.

Warmenhoven, J., Cobley, S., Draper, C., Harrison, A. J., Bargary, N., & Smith, R. (2017). Assessment of propulsive pin force and oar angle time-series using functional data analysis in on-water rowing. *Scandinavian Journal of Medicine and Science in Sports*, *27*(12), 1688–1696.

Watanabe, T, Muneta, T., Sekiya, I., & Banks, S. A. (2015). Intraoperative joint gaps and mediolateral balance affect postoperative knee kinematics in posterior-stabilized total knee arthroplasty. *Knee*, *22*(6), 527–534.

Watanabe, Toshifumi, Ishizuki, M., Muneta, T., & Banks, S. A. (2013). Knee kinematics in anterior cruciate ligament-substituting arthroplasty with or without the posterior cruciate ligament. *Journal of Arthroplasty*, *28*(4), 548–552.

Watanabe, Toshifumi, Muneta, T., Koga, H., Horie, M., Nakamura, T., Otabe, K., Nakagawa,

Y., Katakura, M., & Sekiya, I. (2016). In-vivo kinematics of high-flex posterior-stabilized total knee prosthesis designed for Asian populations. *International Orthopaedics*, *40*(11), 2295–2302.

Weber, W., & Weber, F. (1836). *Mechanik der menschlichen, Gehwerkzeuge: Mechanics of the Human Walking Apparatus. Section 4: On the Knee.* 75.

Weidow, J., Pak, J., & Kärrholm, J. (2002). Different patterns of cartilage wear in medial and lateral gonarthrosis. *Acta Orthopaedica Scandinavica*, *73*(3), 326–329.

Weiss, J M, Noble, P. C., Conditt, M. A., Kohl, H. W., Roberts, S., Cook, K. F., Gordon, M. J., & Mathis, K. B. (2002). What functional activities are important to patients with knee replacements? *Clinical Orthopaedics and Related Research*, *404*, 172–188.

Weiss, Jennifer M., Noble, P. C., Conditt, M. A., Kohl, H. W., Roberts, S., Cook, K. F., Gordon, M. J., & Mathis, K. B. (2002). What Functional Activities Are Important to Patients With Knee Replacements? *Clinical Orthopaedics and Related Research*, *404*, 172–188.

Wilkens, K. J., Duong, L. V., McGarry, M. H., Kim, W. C., & Lee, T. Q. (2007). Biomechanical Effects of Kneeling After Total Knee Arthroplasty. *Journal of Bone an Joint Surgery American*, *89*(12), 2745–2751.

Willing, R., & Kim, I. Y. (2011). Design optimization of a total knee replacement for improved constraint and flexion kinematics. *Journal of Biomechanics*, *44*(6), 1014–1020.

Wluka, A. E., Wang, Y., Davis, S. R., & Cicuttini, F. M. (2005). Tibial plateau size is related to grade of joint space narrowing and osteophytes in healthy women and in women with osteoarthritis. *Annals of Rheumatic Disease*, *64*(7), 1033–1037.

Wolff, J. (1986). The Law of Bone Remodelling. In *The Law of Bone Remodelling*. Springer-Verlang.

World Health Organization. (2015). *WHO global disability action plan 2014-2021. Better health for all people with disability.* https://www.who.int/disabilities/actionplan/en/

World Health Organization. (2018). *Healthy settings for older people are healthy settings for all: the experience of Friuli-Venezia Giulia, Italy.* http://www.euro.who.int/__data/assets/pdf_file/0005/373280/healty-ageing-report-eng.pdf

Wright, R. W., & The MARS Group. (2014). Osteoarthritis Classification Scales: Interobserver Reliability and Arthroscopic Correlation. *Journal of Bone and Joint Surgery American*, *96*(14), 1145–1151.

Wu, G., Siegler, S., Allard, P., Kirtley, C., Leardini, A., Rosenbaum, D., Whittle, M., D'Lima, D. D., Cristofolini, L., Witte, H., Schmid, O., Stokes, I., & Standardization and Terminology Committee of the International Society of Biomechanics. (2002). ISB recommendation on definitions of joint coordinate system of various joints for the reporting of human joint motion—part I: ankle, hip, and spine. *Journal of Biomechanics*, *35*(4), 543–548.

Wu, G., Van Der Helm, F. C. T., Makhsous, M., Roy, P. Van, Anglin, C., Nagels, J., Karduna, A. R., Mcquade, K., Wang, X., Werner, F. W., & Buchholz, B. (2005). ISB recommendation on definitions of joint coordinate systems of various joints for the reporting of human joint motion-Part II: shoulder, elbow, wrist and hand. *Journal of Biomechanics*, *38*, 981–992.

Wylde, V., Artz, N., Howells, N., & Blom, A. W. (2019). Kneeling ability after total knee replacement. *EFORT Open Reviews*, *4*(7), 460–467.

Yang, B., Yu, J.-K., Zheng, Z.-Z., Lu, Z.-H., Zhang, J.-Y., & Reilly, G. (2014). Comparative Study of Sex Differences in Distal Femur Morphology in Osteoarthritic Knees in a Chinese Population. *PLoS One*, *9*(2), e89394.

Yildirim, G., Walker, P. S., Sussman-Fort, J., Aggarwal, G., White, B., & Klein, G. R. (2007). The contact locations in the knee during high flexion. *Knee*, *14*(5), 379–384.

Zeighami, A., Dumas, R., Kanhonou, M., Hagemeister, N., Lavoie, F., De Guise, J. A., & Aissaoui, R. (2017). Tibio-femoral joint contact in healthy and osteoarthritic knees during quasi-static squat: A bi-planar X-ray analysis. *Journal of Biomechanics*, *53*, 178–184.

Zelle, J., Barink, M., De Waal Malefijt, M., & Verdonschot, N. (2009). Thigh-calf contact: Does it affect the loading of the knee in the high-flexion range? *Journal of Biomechanics*, *42*(5), 587–593.

Zelle, J., Barink, M., Loeffen, R., De Waal Malefijt, M., & Verdonschot, N. (2007). Thigh-calf contact force measurements in deep knee flexion. *Clinical Biomechanics*, *22*, 821–826.

Zeller, I. M., Sharma, A., Kurtz, W. B., Anderle, M. R., & Komistek, R. (2017). Customized versus Patient-Sized Cruciate-Retaining Total Knee Arthroplasty: An In Vivo Kinematics Study Using Mobile Fluoroscopy. *Journal of Arthroplasty*, *32*(4), 1344–1350.

Zeng, X., Ma, L., Lin, Z., Huang, W., Huang, Z., Zhang, Y., & Mao, C. (2017). Relationship between Kellgren- Lawrence score and 3D kinematic gait analysis of patients with medial knee osteoarthritis using a new gait system. *Nature Scientific Reports*, *7*(4080), 1–8.

Zhang, J., Ackland, D., & Fernandez, J. (2018). Point-cloud registration using adaptive radial basis functions. *Computer Methods in Biomechanics and Biomedical Engineering*, *21*(7), 498–502.

Zhang, J., & Besier, T. F. (2017). Accuracy of femur reconstruction from sparse geometric data using a statistical shape model. *Computer Methods in Biomechanics and Biomedical Engineering*, *20*(5), 566–576.

Zhang, J., Fernandez, J., Hislop-Jambrich, J., & Besier, T. F. (2016). Lower limb estimation from sparse landmarks using an articulated shape model. *Journal of Biomechanics*, *49*, 3875–3881.

Zhang, J., Malcolm, D., Hislop-Jambrich, J., Thomas, C. D. L., & Nielsen, P. M. F. (2014). An anatomical region-based statistical shape model of the human femur. *Computer Methods in Biomechanics and Biomedical Engineering: Imaging & Visualization*, *2*(3), 176–185.

10 Appendices

10.1 Ethical Approval

10.1.1 ACT Health

ACT Government Health Directorate
Human Research Ethics Committee

Associate Professor Paul Smith
Trauma and Orthopaedic Research
Building 6 Level 1
Canberra Hospital
Garran ACT 2605

Dear Associate Professor Smith,

Re: ETH.4.11.071

The ACT Health Human Research Ethics Committee considered the proposed:

PICKLeS: A Prospective imaging study of cruciate retaining and substituting knee replacement, in osteoarthritis and healthy aging at its meeting of 2 May 2011.

I am pleased to advise you that the study has been approved out of session.

Approval includes:

- Ethics Application
- Protocol version 1 dated 24 March 2011
- Participant information brochure, version received May 2011
- Participant consent form, version received May 2011

I confirm that the ACT Health Human Research Ethics Committee is constituted according to the National Health and Medical Research Council Guidelines and operates in compliance with applicable regulatory requirements and the International Conference on Harmonization Guidelines on Good Clinical Practice.

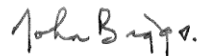I attach for your records an Outcome of Consideration of Protocol form.

A copy of your application will be sent to ACT Insurance Authority for consideration. Please note that this may take up to four weeks for more complex matters.

The study cannot commence until you receive written approval from the Insurance and Legal Liaison Manager, Mr Simon Fenton, who can be contacted on (02) 620 50928.

Page **1** of **3**

Any enquiries regarding insurance matters must be addressed to Mr Fenton.

Yours sincerely

Professor John SG Biggs MA MD
FRCOG FRANZCOG DHMSA
Chairman
ACT Health Human Research Ethics Committee

22 July 2011

10.1.2 Australian National University

-----Original Message-----
From: aries@anu.edu.au [mailto:aries@anu.edu.au]
Sent: Thursday, 20 July 2017 2:52 PM
To: Joseph Lynch <u6212993@anu.edu.au>
Cc: Human.Ethics.Officer@anu.edu.au; diana.perriman@act.gov.au
Subject: Human Ethics Protocol 2017/354 - Approval

THIS IS A SYSTEM-GENERATED E-MAIL. PLEASE DO NOT REPLY. SEE BELOW FOR E-MAIL
CONTACT DETAILS.

Dear Mr Joseph Lynch,

Protocol: 2017/354
PICKLeS Study: A Prospective imaging study of cruciate retaining, substituting and rotating
platform knee replacements and osteoarthric and healthy aging

I am pleased to advise you that your Human Ethics application received approval by the Chair on
the 20/07/2017.

For your information:

1. Under the NHMRC/AVCC National Statement on Ethical Conduct in Human Research we are
required to follow up research that we have approved.
Once a year (or sooner for short projects) we shall request a brief report on any ethical issues
which may have arisen during your research or whether it proceeded according to the plan
outlined in the above protocol.

2. Please notify the committee of any changes to your protocol in the course of your research,
and when you complete or cease working on the project.

3. Please notify the Committee immediately if any unforeseen events occur that might affect
continued ethical acceptability of the research work.

4. Please advise the HREC if you receive any complaints about the research work.

5. The validity of the current approval is five years' maximum from the date shown approved.
For longer projects you are required to seek renewed approval from the Committee.

All the best with your research,

Human Ethics Officer
Research Integrity & Compliance

10.2 Patient Consent Form

Consent Form to Participate in a Research Project

The Pickles Study - A Prospective Imaging study of Cruciate Retaining, Cruciate Substituting and Rotating Platform Knee Replacement and osteoarthritis and healthy aging.

Before reading and signing this consent form please read the patient information pamphlet.

I, _____
            (name of participant)

of _____ _____ _____
        (street)   (suburb/town)   (state & postcode)

I have read the Patient Information Pamphlet and I understand that:

1. This study has been approved by ACT Health Human Research Ethics Committee.

2. The aim of the project is to compare the motion and function of three different types of total knee replacements, with healthy motion, and healthy aging.

3. The procedure will involve one (healthy knee group) or three (Knee replacement group) visits at which there will be:
    - Physical examination of my knee
    - Questionnaires to complete
    - Images including a CT lying still, and a fluoroscopy while doing some activities

    Participants having a total knee replacement will be randomized to receive either: a posterior stabilized, a posterior cruciate retaining or a rotating platform total knee replacement.

4. Risks of participating in this study include exposure to a small amount of ionizing radiation used in medical imaging, described in the Patient Information Sheet, and the standard risks of having a total knee replacement, which I have discussed with my surgeon as part of my surgical consent.

5. The results obtained from the study are unlikely to benefit to my medical management, but may assist patients in the future.

6. I may refuse to participate or request to withdraw from this project at any time and for any reason of my own, without affecting my medical care

7. Should I have any problems or queries about the way in which the study is conducted, and I do not feel comfortable contacting the research staff I may contact the ACT Health Ethics Committee on 6174 7968, or in person at Level 6, Building 10, Canberra Hospital, Garran.

8. Participation in this project will not result in any extra medical or hospital costs to me.

9. I understand that when this research is published my identity will not be revealed.

10. In giving my consent, I acknowledge that the relevant research staff involved in the study may examine my medical records in so far as they relate to this project.

I also state that I have/have not participated in any other research project in the past 3 months. If I have, the details are as follows:

_____

Participant: **Investigator's Signature:**

_____   _____
    (Name)

_____
    (Signature)

_____/ _____/
_____

10.3 Patient Reported Outcome Measures

10.3.1 Oxford Knee Score

During the past 4 weeks……..

1. How would you describe the pain you usually have in your knee?
   - o None   4
   - o Very Mild   3
   - o Mild   2
   - o Moderate   1
   - o Severe   0

2. How much has pain from your knee interfered with your usual work? (including housework)
   - o Not at all
   - o A little bit
   - o Moderately
   - o Greatly
   - o Totally

3. Have you felt that your knee might suddenly 'give way' or let you down?
   - o Rarely/Never
   - o Sometimes or just at first
   - o Often, not at first
   - o Most of the time
   - o All of the time

4. Have you been troubled by pain in your knee at night in bed?
   - o No nights
   - o Only one or two nights
   - o Some nights
   - o Most nights
   - o Every night

5. Could you kneel down and get up again afterwards?
   - o Yes easily
   - o With little or no difficulty
   - o With moderate difficulty
   - o With extreme difficulty
   - o No, impossible

6. For how long are you able to walk before the pain in your knee becomes severe.
   - o No pain for 30 minutes
   - o 16 -30 minutes
   - o 5 – 15 minutes
   - o Around the house only
   - o Not at all – severe on walking

7. After a meal (sat at a table), how painful has it been for you to stand up from a chair because of your knee?
   - o Not at all painful
   - o Slightly painful
   - o Moderately painful
   - o Very painful
   - o Unbearable

8. Could you walk down a flight of stairs?
   - o Yes, easily
   - o With little difficulty
   - o With moderate difficulty
   - o With extreme difficulty
   - o No, impossible

9. Have you been limping when walking, because of your knee?
   - o Rarely/never
   - o Sometimes or just at first
   - o Often, not just at first
   - o Most of the time
   - o All of the time

10. Have you had any trouble washing and drying yourself (all over) because of your knee?
    - o No trouble at all
    - o Very little trouble
    - o Moderate trouble
    - o Extreme difficulty
    - o Impossible to do

11. Have you had any trouble getting in and out of a car or using public transport because of you knee?
    - o No trouble at all
    - o Very little trouble
    - o Moderate trouble
    - o Extreme difficulty
    - o Impossible to do

12. Could you do household shopping on your own?
    - o Yes easily
    - o With little difficulty
    - o With moderate difficulty
    - o With extreme difficulty
    - o No, impossible

10.3.2 Visual Analogue Scales for Pain and Satisfaction

How much pain have you felt in your knee in the past week?

No pain   Extreme pain

TKR Participants only

How satisfied are you with your knee surgery?   (not with the surgeon, just with the result of the operation)

Completely satisfied   Extremely dissatisfied.

How much does your knee feel like a normal knee?

Completely normal   Not at all normal

10.3.3 Phase Determination R Code

```
# Read in the data
setwd()
datAll=read.csv("Data", header=T)

# Only keep registered data
ww=which(datAll$ortho=="Reg"); datAll=datAll[ww,]; rm(ww)

# Get a sorted list of Patient IDs. The Patient IDs are stored as a factor; we
# get the sorted levels of the factor into the vector "subject".
subjects=sort(levels(datAll$ID))

# MAIN LOOP
# The charts are all going into one PDF file which we open here:
pdf("flexionFramePhases.pdf", width=11)
# We loop through all the patients in "subjects"
for (subj in subjects) {
  dat=datAll[datAll$ID==subj,] # just get the data for the current patient "subj" into "dat"
  dat=dat[complete.cases(cbind(dat$flexion,dat$frame)),] # Get rid of data rows with missing flexion or
frame data
  if (dim(dat)[1] < 1) {next} # exit the main loop if there is no data (< 1 row) for this subject

  ss1=smooth.spline(dat$frame,dat$flexion) # Fit a smooth spline to flexion~frame
  ss1d=predict(ss1, deriv=1) # Get its first derivative as a set of x-y coords
  ss1dl=lowess(ss1d, f=.094) # Fit a lowess line of best fit to the 1st
  # derivative. f=.094 has been found by trial and error.
  inflPoints=numeric(length(ss1dl$y)) # inflPoints is a vector of 0s, one for each row of ss1dl
  # This for loop detects when ss1dl crosses zero, i.e. an inflection point,
  # and stores the frame number in inflPoints
  for (i in 1:(length(ss1dl$y)-1))
  {
    if ( ss1dl$y[i]==0 || ss1dl$y[i] <= 0 && ss1dl$y[i+1] >= 0 ||ss1dl$y[i] >= 0 && ss1dl$y[i+1] <= 0) {
      if(ss1dl$y[i]==0) {inflPoints[i]=i} else {
        inflPoints[i]=(i+1)
      }
    }
  }

  # Delete members of the inflPoints vector that don't contain inflection points
  ww=which(inflPoints==0); inflPoints=inflPoints[-ww]
  # Add 1 to the beginning of inflPoints and the number of frames to the end of inflPoints.
  # This helps detect the phases when there is no inflection point near the
  # beginning of phase 1 or the end of phase 2
  inflPoints=c(1,inflPoints)
  inflPoints=c(inflPoints,length(ss1dl$y))

  # Now we construct a matrix m which contains the beginning and end point for
  # the phases. It has 2 columns and 3 rows.  There are two cases. Case 1 is
  # where there are more than 3 inflection points. For this case we use the
  # kmeans algorithm to find 3 clusters of inflection points.  We then use
  # boxplot.stats() to find the upper and lower whiskers of the frame numbers for
  # these clusters. These determine the boundaries of the phases. Case 2 is
  # where there are exactly 3 inflection points. These points are the
```

```
  # boundaries of the two phases.
  m=matrix(0,ncol=2,nrow=3)
  if(length(inflPoints) > 3) { # Case 1
    k=kmeans(dist(inflPoints), nstart=1000, 3)$cluster
    print(k)
    m[1,]=boxplot.stats(inflPoints[k==1])$stats[c(1,5)]
    m[2,]=boxplot.stats(inflPoints[k==2])$stats[c(1,5)]
    m[3,]=boxplot.stats(inflPoints[k==3])$stats[c(1,5)]
  } else
    if (length(inflPoints)==3) { # Case 2
      m[1,2]=inflPoints[1]
      m[2,1]=inflPoints[2]-1
      m[2,2]=inflPoints[2]
      m[3,1]=inflPoints[3]
    } else { # Case 3 - less than three inflection points
      next; # Jump out of the main loop (this is a kludge)
    }


  oo=order(m[,1]); m=m[oo,] # Sort the rows of the matrix m
  phase1idx=m[1,2]:m[2,1] # Get the row numbers of the phases into phase1idx and phase2idx
  phase2idx=m[2,2]:m[3,1]
  phase1=dat[phase1idx,] # Get the data for the phases into phase1 and phase2
  phase2=dat[phase2idx,]

  # Set up a vector of plot colours: 2 (red) for outside the phases, and blue and green for the phases
  colours=rep(2,length(ss1$x))
  colours[phase1idx]=4
  colours[phase2idx]=3

  #Plots
  par(mfrow=c(1,2)) # Set up plot device for 1 row 2 columns of plots
  # Plot ss1
  plot(ss1, xlab="Frame", ylab="Flexion", sub="Blue: Phase 1; Green: Phase 2", col=colours, main=subj)
  # Plot ss1d
  plot(ss1d, xlab="Frame", ylab="1st Derivative of Flexion", main=subj)
  # Scale flexion to fit on the ss1d plot, and plot as a set of red points
  flexionScaled=dat$flexion*max(ss1d$y)/max(dat$flexion)
  points(flexionScaled, col="red", pch=20, cex=.2)
  # Add a line for ss1dl, the lowess smoothed derivative of ss1
  lines(ss1dl, col="orange")
  # Add vertical purple lines for inflection points and a horizontal gray line at 0 on the y axis
  abline(v=inflPoints, col="purple")
  abline(h=0, col="gray")

} # End of main loop

# Close the PDF file
dev.off()
```

10.3.4 Travelling Salesman Problem Extrapolation Matlab Code

```matlab
%% Travelling Salesman Problem
% Adapted from the TSP Example, Matlab Optimization Toolbox
(https://mathworks.com/help/optim/ug/travelling-salesman-problem.html)
% by Santhanakrishnan Narayanan (n.santhanakrishnan@gmail.com)

% Use this code to solve both symmetrical and asymmetrical TSPs based on binary integer programming.
% Required inputs: Distance matrix file
% Place the file in the same folder as the script
% Enter the file name along with extension like .csv/.xls
% The matrix file should be a square matrix
% Distance between (i,i) should be zero. Also the values for non-existing routes should be zero.
% Copyright 2014 The MathWorks, Inc.

%reading distanceMatrix from csv file
% distanceMatrixFile = input('Enter name of the file containing distance matrix (include extension like
.csv/.xls): ','s');
% distanceMatrix = readmatrix(distanceMatrixFile);
% distanceMatrix = distanceMatrix(:,2:end);

load distance_matrix Md
distanceMatrix = Md.^2;

%creating city pairs and converting distance square matrix to distance
%column vector
fprintf('Creating city pairs\n');
numberOfCities = size(distanceMatrix,1); %number of cities
c=1;
for count = 1:numberOfCities:(numberOfCities*numberOfCities)
    cityPairs(count:numberOfCities*c, 1) = c;
    cityPairs(count:numberOfCities*c, 2) = 1:numberOfCities;
    distanceVector(count:numberOfCities*c, 1) = distanceMatrix(c,:)';
    c=c+1;
end
lengthDistanceVector = length(distanceVector);


 %% Equality Constraints
fprintf('Creating equality constraints\n');
%Number of trips = number of cityPairs
Aeq = spones(1:length(cityPairs));
beq = numberOfCities;

%Number of trips to a city = 1 and from a city = 1
Aeq = [Aeq;spalloc(2*numberOfCities,length(cityPairs),2*numberOfCities*(numberOfCities+numberOfCities-
1))]; %allocate a sparse matrix to preallocate memory for the equality constraints;
c=1;
for count = 1:2:((2*numberOfCities)-1)
    columnSum = sparse(cityPairs(:,2)==c);
    Aeq(count+1,:) = columnSum'; % include in the constraint matrix
    rowSum = cityPairs(:,1)==c;
    Aeq(count+2,:) = rowSum';
    c=c+1;
end
beq = [beq; ones(2*numberOfCities,1)];
```

```matlab
%Non-existing routes
nonExists = sparse(distanceVector == 0);
Aeq(2*c,:) = nonExists';
beq = [beq; 0];



%% Binary Bounds
%Setting the decision variables as binary variables
intcon = 1:lengthDistanceVector;
lb = zeros(lengthDistanceVector,1);
ub = ones(lengthDistanceVector,1);

%% Optimize Using intlinprog
fprintf('Solving the problem\n');
opts = optimoptions('intlinprog','CutGeneration','Advanced','NodeSelection','mininfeas','Display','off');
[decisionVariables,optimumCost,exitflag,output] = intlinprog(distanceVector,intcon,[],[],Aeq,beq,lb,ub,opts);

%% Subtour Detection
tours = detectSubtours(decisionVariables,cityPairs);
numberOfTours = length(tours);
fprintf('Number of subtours: %d\n',numberOfTours);

%% Subtour Constraints
A = spalloc(0,lengthDistanceVector,0); % creating sparse inequality constraint matrix
b = [];
while numberOfTours > 1 % repeat until there is just one subtour
  b = [b;zeros(numberOfTours,1)]; % entering inequality constraints RHS
  A = [A;spalloc(numberOfTours,lengthDistanceVector,numberOfCities)]; % entering inequality constraints
LHS
  for count = 1:numberOfTours
    inequalityConstraintNumber = size(A,1)+1;
    subTourId = tours{count}; % Extracting subtour one by one

    % adding subtour constraints (inequality constraints)
    subTourPairs = nchoosek(1:length(subTourId),2);
    for jj = 1:size(subTourPairs,1) % Finding variables associated with the current sub tour
      subTourVariable = (sum(cityPairs==subTourId(subTourPairs(jj,1)),2)) & ...
            (sum(cityPairs==subTourId(subTourPairs(jj,2)),2));
      A(inequalityConstraintNumber,subTourVariable) = 1;
    end
    b(inequalityConstraintNumber) = length(subTourId)-1; % reducing number of trips allowed by One Ex.,
A-B-A: 2 -> 1
  end

  % Optimize again
  fprintf('\nsolving the problem again eliminating subtours\n');
  [decisionVariables,optimumCost,exitflag,output] =
intlinprog(distanceVector,intcon,A,b,Aeq,beq,lb,ub,opts);

  % Check for subtours again
  fprintf('Checking again for subtours\n');
  tours = detectSubtours(decisionVariables,cityPairs);
  numberOfTours = length(tours);
  fprintf('Number of subtours: %d\n',numberOfTours);
end
```

```
%% Solution Quality
%smaller the value better the solution
fprintf('\nSolution Quality: %f (lesser the better)\n',output.absolutegap);
fprintf('Optimized tour route:');
celldisp(tours);
fprintf('Note: The numbers correspond to order of cities in the input file\n');
fprintf('Total distance of the optimal route: %d\n', optimumCost);
```